PROBING STRONGLY COUPLED ANISOTROPIC QUARK-GLUON PLASMA VIA HOLOGRAPHY

BY

SOMDEB CHAKRABORTY

ENROLLMENT NUMBER: PHYS05200804006

SAHA INSTITUTE OF NUCLEAR PHYSICS, KOLKATA

A thesis submitted to the
Board of Studies in Physical Sciences

In Partial Fulfillment of Requirements
for the Degree of

DOCTOR OF PHILOSOPHY

of

HOMI BHABHA NATIONAL INSTITUTE

OCTOBER, 2014

Homi Bhabha National Institute

Recommendations of the Viva Voce Board

As members of the Viva Voce Board, we certify that we have read the dissertation prepared by **SOMDEB CHAKRABORTY** entitled **Probing Strongly Coupled Anisotropic Quark-Gluon Plasma via Holography** and recommend that it may be accepted as fulfilling the dissertation requirement for the Degree of Doctor of Philosophy.

______________________ Date: 17/04/2015

Chairman - Prof. Munshi Golam Mustafa

Shibaji Roy ______________________ Date: 17/4/15

Guide/Convener - Prof. Shibaji Roy

Gautam ______________________ Date: 17.4.15

External Examiner - Prof. Gautam Mandal

______________________ Date: 17.4.15

Member 1 - Prof. Harvendra Singh

______________________ Date: 17/4/2015

Member 2 - Prof. Asit K. De

Final approval and acceptance of this dissertation is contingent upon the candidate's submission of the final copies of the dissertation to HBNI.

I hereby certify that I have read this dissertation prepared under my direction and recommend that it may be accepted as fulfilling the dissertation requirement.

Date:

Place: 17/4/15, Kolkata

Guide: Shibaji Roy

Prof. Shibaji Roy

STATEMENT BY THE AUTHOR

This dissertation has been submitted in partial fulfillment of requirements for an advanced degree at Homi Bhabha National Institute (HBNI) and is deposited in the Library to be made available to borrowers under the rules of HBNI.

Brief quotations from this dissertation are allowed without special permission, provided that accurate acknowledgement of the source is made. Requests for permission for extended quotation(s) from or reproduction of this manuscript in whole or in part may be granted by the Competent Authority of HBNI when in his or her judgment the proposed use of the material is in the interests of scholarship. In all other instances, however, permission must be obtained from the author.

Somdeb Chakraborty 14/4/15.

Somdeb Chakraborty

DECLARATION

I, hereby declare that the investigation presented in the thesis has been carried out by me. The work is original and has not been submitted earlier as a whole or in part for a degree / diploma at this or any other Institution / University.

Somdeb Chakraborty

Somdeb Chakraborty

LIST OF PUBLICATIONS ARISING FROM THE THESIS

Journal

1. Brownian motion in strongly coupled, anisotropic Yang-Mills plasma: A holographic approach.
   Shankhadeep Chakrabortty, Somdeb Chakraborty and Najmul Haque;
   Phys. Rev. D 89 066013 (2014) [arXiv:1311.5023]

2. Holographic quark-antiquark potential in hot, anisotropic plasma.
   Somdeb Chakraborty and Najmul Haque;
   Nucl. Phys. B 874 (2013) 821-851 [arXiv:1212.2769]

3. Wilson loops in noncommutative Yang-Mills theory using gauge/gravity duality.
   Somdeb Chakraborty, Najmul Haque and Shibaji Roy;
   Nucl. Phys. B 862 (2012) 650-670 [arXiv:1201.0129]

4. Calculating the jet quenching parameter in the plasma of noncommutative Yang-Mills theory from gauge/gravity duality.

Somdeb Chakraborty and Shibaji Roy;

Phys. Rev. D 85 046006 (2012) [arXiv:1105.3384]

5. Wilson loops in $(p+1)$-dimensional Yang-Mills theories using gravity/gauge theory correspondence.

   Somdeb Chakraborty and Shibaji Roy;

   Nucl. Phys. B 850 (2011) 463-476 [arXiv:1103.1248]

Chapters in Books and Lecture Notes

None

Conferences

None

Others

None

Somdeb Chakraborty

Somdeb Chakraborty

ACKNOWLEDGEMENTS

As I reminisce the years spent at the Saha Institute of Nuclear Physics, I feel my indebtedness to a lot many people. The journey that commenced with admission to the Post M.Sc. course at SINP and culminated in writing this doctoral thesis, has not been a smooth one, marked by moments of success and punctuated by longer periods of struggle. It was possible only due to the sincere help and support from various directions. First and foremost, I thank my supervisor Prof. Shibaji Roy for introducing me to the fascinating subject of AdS/QGP. I convey my sincere thanks to all my collaborators - Najmul, Shankhadeep and Parijat. I must single out Najmul for his unflagging zeal and taking time out of his hectic schedule in helping me out with numerics whenever required. I avail this opportunity to record my heart-felt gratitude to Munshi Golam Mustafa. Whatever I have learned about quark-gluon plasma has been from the fruitful discussions with him. The light-hearted chats with him during our daily tea-sessions will be fondly cherished. The acknowledgement section would not be complete without a mention of Pratik Khastgir, who has been like a "friend, philosopher and guide" since my IIT days. He has been a true mentor, always there with his valuable advice regarding academics and life, in general. Research at "363" would not have been enjoyable without the unending gossips with Lab, Chapa, Pratyay, Avirup and the *khokas* - Mainak and Anirban. This is not to forget my other colleagues - Sovan da, Srijit da, Aminul, Dipankar, Aritra and Sourav with whom I had shared office at some time or the other. Nilu, Boldu, Pishi and Bishu provided enough memories to be savored in years to come. Last but not the least, I thank my parents who have always motivated me to pursue higher studies and my wife for her support and patience during the difficult times.

Contents

Page

SYNOPSIS

The anti-de Sitter space/conformal field theory correspondence or AdS/CFT correspondence for short, offers a novel approach to access the strong coupling regime of a wide spectrum of quantum field theories. The basic recipe of the correspondence is to map (in an appropriate sense) the strongly coupled gauge theory to a weakly coupled string dual or classical gravity, that is amenable to perturbative treatment. Recent years have witnessed a deluge of interest in exploiting the correspondence to unravel salient features of the plasma phase of such theories. Besides the generic theoretical interests, the phenomenology of ultra-relativistic heavy ion collisions has also acted as a catalyst for undertaking such studies. In fact, inspiration has acted the other way too, and insights from theoretical studies using the correspondence has helped open up new vistas of explorations in the colliders.

Experiments at the Relativistic Heavy Ion Collider (RHIC) and the Large Hadron Collider (LHC) have provided fascinating insights into the properties of quantum chromodynamics (QCD) matter at extreme high temperature and/or energy density. Experimental signatures suggest that in the energy scale accessed at the colliders, QCD matter appears in a new state - “quark-gluon plasma” (QGP). This new state of matter comes into being after a phase transition from the hadronic state to a deconfined state of quarks and gluons. Experimental evidence further indicates that the QGP formed does not behave as a weakly coupled gas of quarks and gluons but is dominated by strong coupling effects. To cite one instance, while computing the ratio of the shear viscosity η to the entropy density s, weak and strong coupling results differ not only quantitatively but also parametrically, and experimental data suggests the accuracy of the strong coupling result. Thus, it is very crucial that we have at our disposal a suitable machinery to explain the wealth of experimental data from a theoretical standpoint. A theoretical explanation of any strongly coupled phenomenon is always a challenging assignment since the strong coupling casts a question mark upon the reliability of the time-tested tools of conventional perturbative field theory. Lattice field theory has emerged as a viable alternative to explore such strongly coupled phenomena in a non-perturbative framework, but not without its own baggage of shortcomings. Indeed, it has successfully explained a multitude of thermodynamic properties of hot and dense QCD matter like critical temperature, nature of phase transition, equation of state, etc., but the very premises upon which it is formulated, make it incapable of handling real-time dynamics and it encounters problems - both conceptual and computational. It is thus highly desirable that one seeks alternative avenues to investigate gauge theories with large couplings. The AdS/CFT correspondence has been immensely successful in explaining a plethora of strongly coupled phenomena across a diverse range of fields and energy scales, be it QCD, QGP, condensed matter physics, or even fluid dynamics.

The correspondence, in its basic incarnation, advocated a duality between type IIB string theory living on $AdS_5 \times S^5$ and $\mathcal{N} = 4$, SU(N_c) super Yang-Mills (SYM) theory, with N_c being the number of colors, living on the 4-dimensional boundary of AdS_5. Since then, the duality has been generalized to embrace a wider variety of gauge theories under its ambit and is now more appropriately called the gauge/string duality or the holographic duality. The generalizations enable us to study less symmetric and hence, more realistic physical systems, making the duality more potent.

Having said so, it must be borne in mind, that the exact dual to real world QCD has still eluded us. Presently, various "toy" gauge theories with known string duals are used to carry out the dual computations, and most intriguingly, the results obtained, in many instances, agree with those of QCD. The computed quantities are also in good qualitative agreement with experimental data. In fact, many of the results exhibit a kind of universality among the different theories pointing to the existence of a universality class. Further, in spite of the limitations, the results are all obtained from first principle calculations in non-Abelian field theories at non-zero temperature. This makes it worthwhile to pursue this complimentary avenue further and understand various facets of strongly coupled gauge theories.

By now there is a large body of literature which calculates different quantities of experimental interest in QCD-like gauge theories in the deconfined phase using the duality. However, most of these works concern QGP that is locally isotropic.

The primary aim of the thesis is to use holographic ideas to elicit lessons about strongly coupled QGP when effects of anisotropy might be dominant. While a study of how anisotropy affects quantities of experimental relevance is interesting in its own right, what makes it more appealing is that the presence of anisotropy is one of the hallmarks of the plasma during its early stage right after its birth. Thus, a proper understanding of anisotropy-induced modifications is absolutely imperative in our endeavor to understand better the early-time dynamics of QGP.

The plasma, just after its creation in heavy ion collisions, is locally anisotropic and far away from equilibrium for a time $t < \tau_{out}$. It settles down in an isotropic state only after time $\tau_{iso} > \tau_{out}$, so that the standard hydrodynamic description of the plasma makes sense only if we want to probe the plasma at time scale $t > \tau_{iso}$. One would, of course, like to make progress and study the plasma in the time scale $t < \tau_{out}$ when it is far away from equilibrium. However, it turns out to be a really challenging task. Instead, we shall focus on an intermediate window $\tau_{out} < t < \tau_{iso}$, where the plasma is in equilibrium but yet to attain isotropy. To probe the plasma in this time domain, it is imperative that one takes into account the inherent anisotropy. It has been proposed that an inherently anisotropic hydrodynamic description, which involves a derivative expansion around an anisotropic state, can be used to study the plasma in this regime. Motivated by the field-theoretic computations, there has been a surge in interest in investigating the anisotropic plasma in the spirit of the gauge/string duality.

In the thesis, we consider two specific toy models of anisotropic plasma in the framework of the duality to compute different quantities related to heavy probe quarks that are of direct relevance to collider experiments. While there are many such quantities, we focus specifically on those quantities, where there is a promise of significant interplay between experimental data and insights obtained via the gauge/string duality. One of the quantities we compute is the bound state quark-antiquark potential $V(\ell)$ as a function of the quark-antiquark separation (ℓ). This provides information regarding the suppression of quarkonium production (like J/Ψ) which, in turn sheds light upon the temperature of the matter and the degree to which the presence of matter screens the interaction between the color particles. An alternative mode to explore the extent to which these color particles are screened is simply to compute the screening length L_{max}, the distance beyond which the bound states melt into the plasma. Another quantity of experimental interest is the jet quenching parameter $\hat{q}$. Jet quenching refers to the set of experiments that brings forth what happens when a very energetic quark or gluon, (with momentum much greater than the temperature of the thermal bath) plows through the strongly coupled plasma. While some measurements quantify how the energetic parton loses energy others attempt to observe how the plasma in turn is affected by the parton that passes through it. There is a single all-inclusive parameter $\hat{q}$ that measures the radiative energy loss of the energetic parton. Another coefficient μ, the drag coefficient, quantifies the amount of collisional energy loss undergone by the parton. We shall try to compute these quantities at various stages of the thesis.

Before considering the anisotropic cases, we set the stage by studying the isotropic, strongly coupled, thermal $\mathcal{N} = 4$ SYM plasma in various space dimensions. We compute holographically the expectation values of certain time-like Wilson loops in the plasma and hence, extract the velocity-dependent quark-antiquark potential $V(\ell)$ and the screening length L_{max}. We further consider light-like Wilson loops which are related to the jet quenching parameter $\hat{q}$.

Having set the stage, we consider the anisotropic models next. The anisotropic models we study are essentially toy models having different sources of anisotropy, far removed from the realistic hot and dense plasma. Nevertheless, by studying these models we hope to capture the telltale signs of anisotropy at least at the qualitative level.

The first model we consider is the thermal non-commutative Yang-Mills theory (NCYM) in $(3+1)$-dimensions. The motivation for studying NCYM plasma is primarily three-fold. Firstly, in NCYM plasma the presence of non-commutativity reduces the symmetry of the theory from $SO(3)$ to $SO(2)$ rendering the theory anisotropic. Hence, NCYM can serve as an interesting playground for exploring the effects of anisotropy. Secondly, NCYM is interesting in its own right since it arises quite naturally in string theory and M-theory and it is of interest to see how non-commutativity affects the different observables. Thirdly, a consistent gauge theory can indeed be formulated in non-commutative space-time. Even though, so far, its existence has not been detected in low energy, one cannot rule out the possibility that its effect may be manifested at extremely high energy scale, where the fabric of space-time itself may be modified. The experimental lower bound on the non-commutativity scale reported in the literature usually gives a very small effect and is hard to detect. So, it is desirable to search for its effect in alternative channels. High energy heavy ion collision offers one such arena and it may be worthwhile to look whether it can provide a better window for the effect of non-commutativity to be observed. Driven by these motivations we perform a similar type of computation of Wilson loops in NCYM. We find out the potential of heavy quarkonia using holographic techniques with the velocity v and the non-commutativity θ as parameters. The results are compared with the known commutative case. An analytic expression for the screening length is obtained in a restricted domain of the parameter space. The limit $v \to 1$ is considered from which the expression for the jet quenching parameter $\hat{q}$ is extracted. The effects of non-commutativity upon $\hat{q}$ are studied for both small and large values of θ and attempt is made to connect the results to the recent collider data by giving some numerical estimates.

In the next stage we use holographic principles to study the second anisotropic toy model - a topologically deformed SYM where the deformation parameter depends upon one of the space coordinates thereby injecting anisotropy into the theory. To have analytical handle over our computations, we confine ourselves only to small values of anisotropy whence the metric components and the other relevant fields can be written analytically (perturbatively). While investigating the properties of massive quark probes in this model is interesting by itself, we were driven by the inspiration to seek whether the quantities computed in NCYM bear any resemblance to their counterparts in the deformed SYM, that is to see whether the effects of anisotropy are generic enough and one can speak of a universality class. The interaction potential and the screening length of mesonic bound states are found out for different orientations of the dipole in the plasma and the effects of anisotropy on the dissociation of the mesons explored. The general observation is that in a weakly anisotropic plasma, the screening length decreases and the potential becomes weaker so that the dipole becomes more susceptible to dissociation. The findings are compared with those obtained in other anisotropic models. In particular, results for the static dipole potential obtained are different from those found using Hard Thermal Loop (HTL) approach in field theory. On the other hand, all our results are remarkably similar with those obtained for hot NCYM pointing to the suggestion that there may indeed be some universal class of anisotropic plasma. This notion is further strengthened in the analysis of the Brownian motion of a non-relativistic heavy probe quark in weakly anisotropic hot plasma. The concomitant Langevin equation supplies information regarding the drag force, the random force auto-correlator and the relaxation time. The validity of the fluctuation-dissipation theorem in anisotropic plasma is verified from a holographic perspective. To study the Langevin equation in the gravity dual a probe string is considered and its fluctuations around the classical solution quantized, all the while confining only to the low frequency, weak anisotropy domain to have analytical control over the calculations. An interesting qualitative agreement of the results with their NCYM cousins is noticed. It is important to check the validity of this comparison for arbitrary strength of anisotropy. However, this is beyond the scope of analytic computation and would make an interesting course of future study. Another potential avenue will be to investigate Brownian motion in more general scenarios, like in the relativistic setting and for fluctuations of any frequency. What transpires from the above investigations is that although the source of anisotropy in the two models discussed are drastically different we observe qualitatively similar effects on diverse experimentally pertinent observables. This leads us to speculate on a more general note, that since the computations hinge upon the coupling of the string to the background metric, any source of anisotropy leading to similar types of background will lead to qualitatively similar effect upon the heavy quark observables.

List of Figures

CHAPTER 1

PROLOGUE

1.1 Overview

One of the spectacular developments in string theory has been the conjectured duality between a conformal field theory (CFT) and a theory of gravity in anti-de Sitter (AdS) space-time, which goes by the name of the “Anti de-Sitter space/Conformal Field Theory correspondence” in string theory parlance, or the “AdS/CFT correspondence” [1–3]* in short. The correspondence offers an innovative approach to access the strong coupling regime of a wide class of quantum field theories, that are otherwise inaccessible by standard field-theoretic techniques. The essence of the correspondence is to establish a mapping in an well-defined sense between a gauge theory respecting conformal invariance and a string theory in AdS space-time. It can be shown that under certain conditions a strongly coupled gauge theory can be mapped to a weakly coupled string theory, which reduces to classical gravity thereby, permitting a perturbative analysis. This is what makes the correspondence

*A comprehensive review of the correspondence can be found in [4].

so appealing - one just solves the problem perturbatively in the weakly coupled string dual and reverts back to the strongly coupled gauge theory of interest! In the process one invokes the so-called "AdS/CFT dictionary" that relates gauge-theoretic quantities to their string theory counterparts. In recent years, a considerable effort has been directed towards exploiting this remarkable correspondence to unravel the salient features of the plasma phase of gauge theories that admit a dual string description. Apart from generic theoretical interests, the phenomenology of ultra-relativistic heavy ion collisions, i.e., collisions of atomic nuclei where the center-of-mass energy per nucleon far exceeds the nucleon rest mass, has also acted as a catalyst for undertaking such studies. In fact, inspiration has acted the other way too, and precious insights gained from theoretical studies using the correspondence have paved way for exploring uncharted frontiers in the collider experiments. It is this thriving symbiotic relationship between heavy ion phenomenology and the AdS/CFT correspondence that will be the underlying theme of the thesis.

Experiments currently underway at the Relativistic Heavy Ion Collider (RHIC) at the Brookhaven National Laboratory and the Large Hadron Collider (LHC) at the European Organization for Nuclear Research (CERN) have provided fascinating insights into properties of Quantum Chromodynamics (QCD) matter at extreme high temperature and/or energy density. Experimental signatures suggest that in the energy scale accessed at the colliders, QCD matter appears in the guise of a new phase - "Quark-Gluon Plasma" (QGP) which emerges after a phase transition from the hadronic state to a deconfined state of quarks and gluons. Experimental evidence further indicates that the QGP formed does not behave as a weakly coupled gas of quarks and gluons but resembles a strongly coupled fluid [5–7]. For instance, while computing the ratio of the shear viscosity η to the entropy density s, weak and strong coupling results [8,9] are found to differ not only quantitatively but also parametrically, and experimental data [10] supports the strong coupling result.

Later this ratio was shown to be universal for all strongly coupled gauge theories in the limit of large number of colors and permitting a dual gravitational description [11]. In such a scenario one of the major questions confronting us is whether the perturbative framework suffices to explain the relevant physics issues at a temperature of few hundred MeV's (as attained in the colliders) or we should take recourse to a formalism that is robust at strong coupling. Although in a non-Abelian plasma weak coupling effects are distinctly different from strong coupling ones, *a priori* it is not apparent which observations and features owe their origin to weak coupling and which of them can be attributed to the strong coupling behavior. Hence, one of the exigent task at hand is to systematically disentangle the effects of strong coupling and weak coupling. Thus, in our endeavor to explain the wealth of experimental data accumulated from heavy ion collisions, a pressing requirement is a cross-fertilization of perturbative and non-perturbative ideas. Conventional field theory, which is essentially based on a perturbative framework, is well-suited to explain the weak coupling features. On the other hand, it is very crucial that we also have at our disposal a suitable machinery to explain the effects stemming from a large value of the coupling. A theoretical explanation of any strongly coupled phenomenon is always a challenging assignment since strong coupling imposes severe restrictions upon the applicability of the time-tested tools of traditional perturbative field theory. Lattice field theory has emerged as a viable alternative to investigate systems bearing the stamp of strong coupling effects, in a non-perturbative framework, but not without its own baggage of shortcomings. Indeed, it has successfully explained a multitude of thermodynamic properties of hot and dense QCD matter like critical temperature, nature of phase transition, equation of state, etc., but the very premises upon which it is formulated, make it incapable of handling real-time dynamics that are of relevance to QGP physics. It is thus highly desirable that one seeks alternative avenues to investigate gauge theories characterized by high values of the coupling parameter. This makes us turn our attention to the AdS/CFT correspondence which has been immensely successful in explaining a plethora of strongly coupled phenomena across a diverse range of fields and energy scales, be it QCD, QGP, condensed matter physics, or even fluid dynamics.

The correspondence, in its primitive incarnation [1], conjectured a bold duality between type IIB string theory living on $AdS_5 \times S^5$ and $\mathcal{N} = 4$, $SU(N_c)$ super Yang-Mills (SYM) theory, with N_c being the number of colors, living on the 4-dimensional boundary of AdS_5. Since then, the duality has been the subject of intense theoretical investigations and generalized to encompass a wider variety of gauge theories under its ambit and is now more appropriately called the *gauge/string duality* or the *holographic duality* (since it relates a field theory to a theory of gravity in one higher dimension). The generalizations empower us to study less symmetric and hence, more realistic physical systems, making the duality even more potent.

Having said so, it must be admitted, that this approach is plagued by its own limitations. The duality does not provide precision tools for QCD physics and can at best be considered a complementary toolkit offering a semi-quantitative insight into the strong coupling regime of QCD. In spite of intense efforts the exact dual to QCD has remained elusive. But the duality does hold for a large class of solvable models that share many features with QCD. In the absence of any well-controlled machinery, the duality remains our best bet for deciphering the rich structure underlying QCD physics. Presently, various "toy" gauge theories admitting string duals are engaged to carry out the dual computations, and most intriguingly, the results extracted, in many instances, agree with those of QCD predictions and experimental observations (at least qualitatively). In fact, many of the results exhibit a kind of universality among the different theories hinting at the existence of a universality class. Further, in spite of the limitations, the results are all obtained from first principle calculations in non-Abelian field theories. This makes it worthwhile to pursue this complementary path further and try to obtain a better understanding of strongly coupled gauge theories.

By now there is a vast literature computing, holographically, different quantities of experimental interest in QCD-like gauge theories in the deconfined phase. However, most of the works concern QGP that is locally isotropic. The primary aim of the thesis is to use holographic ideas to elicit lessons about *strongly coupled* QGP when effects of *anisotropy* might be dominant. While a study of how anisotropy affects quantities of experimental relevance is interesting in its own right, what makes it more appealing is that anisotropy is one of the hallmarks of the plasma during its early stage right after its birth. Thus, a proper understanding of anisotropy-induced modifications is absolutely imperative in our endeavor to understand better the early-time dynamics of QGP.

In collisions with a non-zero impact parameter, i.e., when the nuclei do not collide head-on, anisotropic pressure gradient develops in the overlapping region of two colliding nuclei, transforming the initial coordinate-space anisotropy into an observed momentum-space anisotropy, through interactions between the produced particles, leading to an anisotropic particle distribution. The early success of relativistic ideal hydrodynamics in explaining various results at RHIC provided empirical evidence in favor of fast thermalization and isotropization - at time scales $\tau_{iso} \sim 0.5$ fm. In an attempt to make better agreement with experimental results this was subsequently generalized to relativistic viscous hydrodynamics, which, however, predicted the presence of a sizable pressure anisotropy. It was found that the transverse pressure exceeds the longitudinal (along the beam direction) one with the difference being the largest for time ≤ 2 fm. Thus viscous hydrodynamical simulations suggest that isotropization may occur as late as $\tau_{iso} \sim 2$ fm. Currently, the question of the degree of momentum-space anisotropy in QGP is open to intense theoretical debate and is deemed worthy of an in-depth study. Recent studies [12,13] suggest that large momentum-space anisotropies may be present for most part of the time evolution both at weak and strong coupling.

The plasma, just after its birth in relativistic heavy ion collisions, is locally anisotropic and far away from equilibrium for a time $t < \tau_{out}$. It settles down in an isotropic state only after time $\tau_{iso} > \tau_{out}$, so that the standard hydrodynamic description of the plasma makes sense only if we want to probe the plasma at time scale $t > \tau_{iso}$. One would, of course, like to make progress and study the plasma in the time scale $t < \tau_{out}$ when it is far away from equilibrium. However, in the present state of development, studying the far-from-equilibrium dynamics of the hot plasma and its temporal evolution to an equilibrium state, is a rather difficult task. Instead, we focus our attention upon an intermediate temporal window $\tau_{out} < t < \tau_{iso}$, where the plasma is in equilibrium but yet to attain isotropy, and which is much more accessible *via* our current theoretical tools. To probe the plasma in this time domain, it is essential that one takes into account the inherent anisotropy present in the system. It is suspected that the magnitude of this momentum-space anisotropy can be so high that it may even violate the central assumption of canonical viscous hydrodynamical treatments - which is to linearize around an isotropic background. It has been shown that large linear corrections result in unphysical results such as negative particle pressures, negative one-particle distribution functions, etc. [14]. Another closely related aspect of the same problem is that microscopic models of the early stages of relativistic heavy ion collisions indicate that the produced system is highly anisotropic [15]. In the theory of the Color Glass Condensate (CGC), at very early proper times, $\tau \ll 1/Q_s$, where Q_s is the saturation scale, the classical gluon fields lead to an energy-momentum tensor of the form $T_{\mu\nu} = \mathrm{diag}(\varepsilon, \varepsilon, \varepsilon, -\varepsilon)$ [16,17] implying a negative value of the longitudinal pressure with the transverse pressure equal to the energy density. At later proper times, $\tau \gg 1/Q_s$, both analytical perturbative approaches [18] and full numerical simulations [19] furnish the form $T_{\mu\nu} = \text{diag}(\varepsilon, \varepsilon/2, \varepsilon/2, 0)$ showing that the longitudinal pressure is zero. Consequently, proper matching of the results of the microscopic models with the hydrodynamic description (where the energy-momentum tensor should be close to the isotropic form) is not easy. Another vital issue is that physically one expects entropy production to vanish in two limits: the ideal hydrodynamical limit (vanishing shear viscosity) and the free streaming limit (infinite shear viscosity). However, within the realm of viscous hydrodynamics, entropy production is a monotonically increasing function of the shear viscosity. In the large shear viscosity limit, viscous hydrodynamics becomes a poor approximation and one has to seek an alternative framework. The afore-mentioned difficulties spurred the development of a reorganization of viscous hydrodynamics in which one incorporates the possibility of large momentum-space anisotropies at the leading order. The inclusion of large anisotropies also allows for direct matching with theories such as CGC. This framework has been dubbed anisotropic hydrodynamics [20–26]. Motivated by these field-theoretic developments, there has also been a surge in interest in investigating anisotropic plasma in the spirit of the gauge/string duality.

In the thesis, we consider two specific holographic toy models of anisotropic plasma to compute different quantities related to heavy probe quarks that are of direct relevance to collider experiments. While there are many such quantities, we focus specifically on those quantities, where there is a promise of significant cross-fertilization between experimental data and insights obtained *via* the gauge/string duality. One of the quantities we compute is the bound state quark-antiquark (Q-$\bar{Q}$) potential $E(L)^{\dagger}$ as a function of the quark-antiquark separation (L). This provides information regarding the suppression of quarkonium production (like J/Ψ states) which, in turn, sheds light upon the temperature of the matter and

†We shall also denote the bound state potential by $V(L)$ interchangeably.

the degree of color screening. An alternative mode to explore this screening is simply to compute the screening length L_{max}, the distance beyond which the bound states melt into the plasma. Other quantities that we evaluate include the jet quenching parameter $\hat{q}$ that measures the radiative energy loss of an energetic parton plowing through the plasma and the drag coefficient γ, which encodes the amount of collisional energy loss undergone by a probe quark as it executes stochastic motion in the plasma. The drag coefficient is, in turn, related to the relaxation time, t_{relax}, which is a characteristic time scale beyond which the plasma thermalizes. We shall try to compute these quantities at various stages of the thesis and observe how they carry the imprint of anisotropy. In this context let us also issue the caveat that since all the computations will be performed using "toy" models, one should exercise utmost care in attempting to connect our results to realistic QCD plasma. Nevertheless, it is a fruitful undertaking since many of the toy models belong to the same universality class as QCD and hence, provide precious qualitative insights into the rich dynamics that underlies QCD. In fact, remarkably, we find that the stamp of anisotropy on many of the quantities that we compute are qualitatively very similar.

1.2 Plan of the Thesis

To help the reader navigate through the thesis, we provide here a short description of the ensuing chapters and their contents. Chapter 2 aims to provide a concise overview of aspects of QCD and QGP relevant to our purpose and to heavy ion phenomenology. This is followed by a lightning review of the AdS/CFT correspondence. We further establish the relevance of the gauge/string duality in the context of QGP. In chapter 3 we discuss holographic computation of Wilson loops in strongly coupled thermal $\mathcal{N} = 4$ SYM plasma following well-defined prescription in the literature and learn how to extract various heavy quark observables from the expectation values of different Wilson loops. Thereby we set the stage for the computations to be carried out in the more general scenarios of anisotropic plasma in the subsequent chapters. Chapter 4 concerns the first of our anisotropic models - the finite temperature, strongly coupled, non-commutative Yang-Mills (NCYM) plasma. To start with we compute the jet quenching parameter $\hat{q}_{\mathrm{NCYM}}$ from a light-like Wilson loop and working in light-cone coordinates right from the outset. Then we compute the dipole[‡] potential $E(L)$ as a function of the dipole length L when the dipole is moving along the commutative direction. We show numerically how $E(L)$ varies with L with the dipole velocity v and the non-commutativity θ as parameters. We are also able to arrive at an analytical expression for the screening length in a restricted domain of the parameter space of v and θ. Finally, for the sake of completeness, by taking the limit $v \to 1$ we recompute the expectation value of a light-like Wilson loop to extract the expression for $\hat{q}_{\mathrm{NCYM}}$ that matches with the expression found out earlier. We consider the effect of non-commutativity upon $\hat{q}_{\mathrm{NCYM}}$ for both small and large values of θ and attempt to connect our results with recent collider data by giving some numerical estimates using benchmark values of θ available in the literature. Chapter 5 deals with different aspects of massive probe quarks in a topologically deformed SYM theory - the second of our anisotropic models, where the deformation parameter depends upon one of the space coordinates thereby injecting anisotropy into the theory. To have analytical handle over our computations, we confine ourselves only to small values of anisotropy whence the metric components and the other relevant fields can be written analytically (perturbatively). The interaction potential and the screening length of mesonic bound states are found out for different orientations of the dipole in the plasma and the effect of anisotropy on the dissociation of mesons is discussed. The findings are compared with those obtained in other anisotropic models. We further analyze the

[‡]We shall frequently refer to a heavy quark-antiquark pair as a dipole.

Brownian motion of a non-relativistic heavy probe quark in the plasma. The concomitant Langevin equation supplies information regarding the drag force, the random force auto-correlator and the relaxation time. The validity of the fluctuation-dissipation theorem in an anisotropic medium is verified from a holographic perspective. Finally, we conclude in chapter 6 with a summary of the work done. We also outline potential future avenues along which the work done in the thesis can be advanced further to know more about anisotropy-induced modifications in hot and dense strongly coupled QGP.

Chapter 2

QGP and AdS/CFT - A Guide for the Beginners

2.1 Overview

This chapter aims to present a concise overview of the various collateral ideas that will be relevant to the rest of the thesis. In §2.2 we briefly outline aspects of QCD and QGP*, that will be required to appreciate the contents of the thesis, in particular, focusing on the energy loss of heavy quarks in §2.2.1 and the phenomenon of quarkonium suppression in §2.2.2. §2.3 provides a crash course on the AdS/CFT correspondence. We skim through the basics of string theory in §2.3.1 and motivate the correspondence in §2.3.2. In §2.4 we attempt to uncover the interplay between the gauge/string duality and QGP. Finally, we conclude in §2.5 and lay down the path to be followed in the rest of the thesis.

*Our discussion is, by no means, complete. For a more insightful discussion the reader is referred to [27], from which we draw heavily.

2.2 A Primer on Heavy Ion Phenomenology

Four decades since the discovery of asymptotic freedom [28, 29], QCD - the theory strong interactions, continues to fascinate us with its vast array of unsolved mysteries and unanswered questions. While considerable advancement has been made to unravel the intricacies of QCD, much progress remains to be achieved [30].

QCD predicts that at a certain temperature (or energy density) hadronic matter undergoes a phase transition to a deconfined state of quarks and gluons, or QGP. Subsequently, lattice calculations have confirmed this transition to be not a true phase transition, but rather a rapid crossover occurring around a temperature $T_c \sim 160$ MeV. This novel state of matter is believed to have existed during the nascent stages of the evolution of the Universe [31] and presently, in high density astrophysical objects like neutron stars [32]. Thus a comprehensive understanding of strongly interacting matter under extreme conditions is essential not only in nuclear physics but also in astrophysics. Experimentally, heavy ion collision provides us access to explore bulk QCD matter within the realms of a laboratory. Different collider facilities have helped us enrich our understanding of the QCD phase transition by probing different regimes of temperature and baryon number density in the phase diagram. At peak RHIC and LHC energies, the produced matter is marked by weak baryon densities and high temperatures, while upcoming programs at the Facility for Antiproton Ion Research at the Gesellschaft für Schwerionenforschung, Germany and the Neuclotron-based Ion Collider fAcility at the Joint Institute of Nuclear Research, Russia are poised to scan the phase diagram at high baryon chemical potential and low temperature. Results from heavy ion experiments have unveiled a multitude of remarkable features of bulk QCD that can not be explained by a naive extrapolation of results of proton-proton collisions. It was inferred from CERN Super Proton Synchrotron [33] results that in the energy window accessed there, a new state of matter is created that bears some of the most crucial theoretically predicted signatures of QGP like thermalization, chiral symmetry restoration, deconfinement, etc. This notion is further corroborated by RHIC data [5–7] which indicates the creation of strongly coupled QGP. The strong coupling feature came as a surprise since asymptotic freedom forbids any strong interaction at sufficiently high temperature. This entails that any analysis of strongly coupled QGP should be based on a formalism that is faithful and robust at strong coupling. Presently, it is the turn of LHC to probe further this exotic state of matter in higher energy regime and luminosity and with increased precision. Among the issues that the ongoing collider experiments aim to address are [30]:

1. Dynamical quantities like the jet quenching parameter, the diffusion coefficient of heavy quark, the coefficient of drag, etc.

2. Melting of heavy quark bound states in thermal QGP due to color screening.

We emphasize upon these two issues since in both the cases there is the prospect of significant and fruitful interplay between results garnered from analyzing experimental data and those obtained from employing the gauge/string duality. In the following we briefly discuss these two issues.

2.2.1 Energy loss - radiative and collisional

The basic program in a heavy ion collision is to collide large nuclei, such as gold (at RHIC) or lead (at LHC) against each other at an ultra-relativistic center-of-mass energy $\sqrt{s}$. The purpose of using heavy ions is that it enables one to create a large volume of matter at high energy density. This provides the best opportunity to observe phenomena related to macroscopic amount of strongly interacting matter. Earlier experiments involved electron-positron or proton-proton (pp) collisions that produced many hadrons in the final state. But the origin of these hadrons were attributed to the few partons in the initial stage that subsequently disintegrated, rather than to the presence of bulk matter. Thus, at heavy ion colliders one expects to capture the vast array of rich phenomena associated with bulk interacting matter that were so far unobserved in the more elementary electron-positron or pp collisions. Heavy ion physicists have devised elaborate machinery to analyze collective phenomena associated with collisions of heavy nuclei. Generically, these tools quantify deviations from benchmark measurements (obtained in pp collisions) where such collective phenomena are not present.

Jet quenching is one such experimental phenomena, which reveals what transpires when a very energetic parton (quark or gluon) moves through the matter with a momentum much greater than the temperature of the thermal bath. It should be noted that these energetic partons are not external probes of QGP. Rather, they are produced within the plasma itself. In a tiny fraction of pp collisions with $\sqrt{s} \sim 200$ GeV, partons from incident protons scatter with large momentum transfer (which is referred to as a hard process) producing back-to-back partons in the final stage that carry transverse momenta ~ 10 GeV. The occurrence of such a hard process is a rarity, but nevertheless, there is no dearth of experimental data so that these processes are well-studied. Concomitantly, there also exists elaborate field-theoretic framework that provides well-controlled calculations for the rates of these hard processes. Experimental data along with theoretical tools provide a solid foundation that enables us to study departures from benchmark values when such hard processes occur in high density thermal medium. The characteristic feature of heavy ion collision is that once an energetic parton is created, unless it is produced right at the edge of the fireball, it has to traverse a small distance ~ 10 fm through the hot and dense medium created in the collision. Hence, these partons can be used to probe the plasma which produces them.

The presence of the medium ensures that the parton suffers energy loss and alters direction as it moves. This alteration in the direction of its momentum is what we refer to as the "transverse momentum broadening". "Transverse" implies direction perpendicular to the original direction of the parton.

It is well-known from electromagnetism that *bremsstrahlung* is the dominant mode of energy loss of an electron moving through matter in the high energy limit. The same holds true in calculations of QCD parton energy loss in the high energy limit [34–36]. The hard parton suffers multiple inelastic interactions with the spatially extended medium, which induces gluon *bremsstrahlung*. In this context, by high parton energy limit we mean the set of limits

$$E \gg \omega \gg |\mathbf{k}|, |\mathbf{q}| \equiv \Big|\Sigma_i \mathbf{q}_i\Big| \gg T, \Lambda_{QCD} \tag{2.1}$$

where E is the energy of the high energy projectile parton, ω and $\mathbf{k}$ are the typical energy and the momentum of the gluons radiated in the elementary radiative processes $q \to qg$ or $g \to gg$, and $\mathbf{q}$ is the transverse momentum (transverse to its initial direction) accumulated by the projectile parton through many radiative interactions in the medium. T and Λ_{QCD} represent any energy scales that characterize the properties of the medium itself. This set of approximations underlies all analytical calculations of radiative parton energy loss to date [34, 35, 37–39].

The analysis of energy loss has its roots in the eikonal formalism. So here we briefly review the essence of this formalism. From the point of view of the projectile, the target appears to have a finite spatial extension and width but is Lorentz-contracted. So viewed from the projectile rest frame, it passes through the target in a very short time interval during which its transverse position does not change appreciably. So, at ultra-relativistic energies, the primary impact of the target on the projectile is a "rotation" of the parton's color due to the color field of the target. These rotation phases are given by Wilson lines along the (straight line) trajectories of the propagating projectile:

$$W(\mathbf{x}) = \mathcal{P}\text{exp}\left[i\int dz^- T^a A_a^+(\mathbf{x}, z^-)\right]. \tag{2.2}$$

Here **x** denotes the transverse position of the projectile, which remains unchanged as the projectile moves at the speed of light along the $z^- \equiv (z-t)/\sqrt{2}$ light-like direction. A^+ is the large component of the target color field and T^a is the generator of the $SU(N_c)$ in the representation of the projectile, i.e., fundamental if the parton is a quark or adjoint if it is a gluon. In the eikonal approach to scattering it is assumed that the projectile impinges on the target from outside. Analyzing the problem one finally arrives at the number $N(\mathbf{k})$ of radiated gluons with momentum **k**,

$$\begin{aligned} N(\mathbf{k}) &= \frac{\alpha_S C_F}{2\pi}\int d\mathbf{x}d\mathbf{y}e^{i\mathbf{k}.(\mathbf{x}-\mathbf{y})}\frac{\mathbf{x}.\mathbf{y}}{\mathbf{x}^2\mathbf{y}^2}\left[1-\frac{1}{N^2-1}\langle\text{Tr}\left[W^{A\dagger}(\mathbf{x})W^A(\mathbf{0})\right]\rangle\right. \\ &\left. -\frac{1}{N^2-1}\langle\text{Tr}\left[W^{A\dagger}(\mathbf{y})W^A(\mathbf{0})\right]\rangle+\frac{1}{N^2-1}\langle\text{Tr}\left[W^{A\dagger}(\mathbf{y})W^A(\mathbf{x})\right]\rangle\right] \end{aligned} \tag{2.3}$$

where the C_F prefactor is for the case when the projectile is a quark in the fundamental representation. The projectile is located at transverse position **0**, and the $\langle ... \rangle$ denotes averaging over the gluon fields of the target. If the target is in thermal equilibrium, these are thermal averages. Although Eq. 2.3 is not applicable to the physically relevant case, nevertheless, we can obtain valuable insights from this relation. For one, we see that the entire medium-dependence is captured in the target expectation values of the form $\langle\text{Tr}\left[W^{A\dagger}(\mathbf{y})W^A(\mathbf{x})\right]\rangle$ of two eikonal Wilson lines. The *jet quenching parameter* $\hat{q}$ defines the fall-off properties of this two-point correlator in the transverse direction $L \equiv |\mathbf{x}-\mathbf{y}|$

$$\boxed{\langle \text{Tr}\left[W^A(\mathcal{C}_{\text{light-like}})\right]\rangle \approx \exp\left[-\frac{1}{4\sqrt{2}}\hat{q}L^-L^2\right]} \tag{2.4}$$

in the limit of small L. We have boxed the equation to emphasize that we are going to use it extensively during the course of the thesis. Let us also take this opportunity to clarify the symbols used. L^- denotes the light-cone length of the Wilson lines or the extent of the target along the light-like z^- direction, **x** and **y** denote the transverse positions of the gluon amplitude and the complex conjugate amplitude respectively. $\mathcal{C}$ is a contour that spans a distance L^- along the light-cone direction z^- and finally returns at transverse position **y**. These two long straight light-like lines are connected by short transverse segments located at $z^- = \pm L^-/2$, far outside the target. Also it is evident from Eq. 2.3 that L is conjugate to the momentum $|\mathbf{k}|$. We have also made the assumption that $L^- \gg L$. Eq. 2.3 reveals that all the information regarding the medium is encoded in the quantity $\hat{q}$ which we designate as the jet quenching parameter. Making use of Eq. 2.4 in Eq. 2.3 we find that $\mathbf{k}^2 \sim \hat{q}L^-$. This suggests that $\hat{q}$ can be interpreted as the transverse momentum squared picked up by the parton per unit distance L^-. In fact, this intuitive idea can be rigorously established *via* other approaches [40, 41] and it can be shown that

$$\hat{q} = \frac{\langle \mathbf{k}^2 \rangle}{L^-} = \frac{1}{L^-}\int \frac{d\mathbf{k}}{(2\pi)^2}\mathbf{k}^2\mathcal{P}_{\mathbf{k}} \tag{2.5}$$

where $\mathcal{P}_{\mathbf{k}}$, the probability that the gluon picks up a transverse momentum **k** while traversing a distance L^- through the medium is suitably normalized as,

$$\int \frac{d\mathbf{k}}{(2\pi)^2}\mathcal{P}_{\mathbf{k}} = 1. \tag{2.6}$$

It is to be noted that the way we have defined $\hat{q}$ in Eq. 2.5, it depends upon transverse momentum broadening only. Notions of radiation and energy loss do not enter the definition directly. We remark that instead of viewing Eq. 2.4 as an approximation, we shall, henceforth, treat it as the non-perturbative definition of $\hat{q}$ to be used subsequently in the thesis. Thus all one has to do is just find an expression for the expectation value of the light-like Wilson loop $\langle W^A(\mathcal{C}_{\text{light-like}})\rangle$ and from there extract $\hat{q}$ *via* Eq. 2.4.

The reason that the eikonal formalism as outlined here cannot be applied straight away to the problem of parton energy loss in heavy ion collisions is that the high energy partons do not impinge on the target from some distant production site. Rather they are produced within the same collision that produces the medium whose properties they subsequently probe. As a consequence, they are produced with significant virtuality implying that even if there were no medium present, they would radiate copiously and would fragment in a parton shower. The analysis of medium-induced parton energy loss then requires understanding the interference between radiation in vacuum and the medium-induced *bremsstrahlung* radiation and the problem goes beyond the eikonal approximation. In this case the eikonal Wilson lines are replaced by retarded Green's functions. However, it turns out that even after the Wilson lines have been replaced by the Green's functions the only attribute of the medium that enters the analysis of parton energy loss is the jet quenching parameter, defined in Eq. 2.4, and which already appeared in the eikonal approximation.

The preceding discussion only focused upon the radiative energy loss suffered by a parton. In passing let us mention that although this is the dominant mode of energy dissipation in the high energy regime, there exists yet another mechanism - the collisional energy loss. A massive quark, when immersed in QGP, interacts with the constituents of the medium and undergoes a chaotic motion which can be captured through the Langevin equation and in the process undergoes collisional energy loss. The resulting phenomenon is well-known as the Brownian motion of the test particle. The energy loss is proportional to the quark's momentum, the proportionality factor being called the *drag coefficient* γ, which measures the extent of collisional energy loss. We shall discuss in chapter 5 how to compute the drag coefficient from an analysis of Langevin dynamics of a heavy quark invoking the principles of the gauge/string duality.

2.2.2 Quarkonium suppression

Next we focus upon the issue of quarkonium suppression. As mentioned earlier, QCD matter undergoes a crossover to a deconfined state of quarks and gluons at a temperature $T_c \sim 160$ MeV. Creation of the deconfined phase implies that a bound state of quarks no longer exists. It is then only natural to moot the question - "what prevents the formation of such bound states in QGP?" An intuitive answer is that in QGP, the attractive force that holds a meson together is screened by the presence of the medium. Intuitively, we also expect the degree of screening to increase with the separation distance between the constituent quarks in the meson. Thus, one anticipates the existence of a critical separation L_{max} up to which the attractive force is sufficient to bind the meson. We shall, henceforth, designate L_{max} as the *screening length*. One can then ponder, how close should the quark and the antiquark be such that the attractive force between them is the same as that when they are in vacuum? It was suggested by Matsui and Satz [42] that measurements of quarkonia production in heavy ion collisions can lead us to the answer to this question.

The generic term *quarkonium* refers to the charm-anticharm (c-$\bar{c}$) or charmonium mesons (J/Ψ, Ψ', χ_c, ...) and the bottom-antibottom (b-$\bar{b}$) or bottomonium mesons (Υ, Υ', ...). The first quarkonium state to be discovered was J/Ψ, the $1s$ state of c-$\bar{c}$ bound system. It measures about half the size of a typical meson like ρ. The bottomonium state Υ is still smaller by a factor of two. Hence, if the temperature of the QGP is steadily increased, we expect the J/Ψ mesons to survive as a bound state up to a high temperature $T > T_c$. This is because, by definition, T_c indicates the temperature at which normal mesons and baryons made up of light quarks dissociate. Going by the proposal of Matsui and Satz, if the temperature of the QGP is high enough, color screening will prevent charm and anticharm quarks from forming a bound state and consequently, the number of J/Ψ mesons produced in the collision will be suppressed. However, one expects the Υ's to survive up to a still higher temperature on account of their small size, until the attractive force is screened even on the short length scale corresponding to their size. Till now, this proposal by Matsui and Satz remains the most direct signature of the formation of deconfined matter. Generically, one expects the attraction that binds a meson to decrease with rise in temperature T. One can give a heuristic argument to justify this behavior. Typical momentum scale in QGP will be $\sim T$ so that if the separation between the quark and the antiquark is less than $1/T$ then the medium is incapable of resolving them and the pair exists as a bound state. On the other hand, if the distance exceeds $1/T$ then the medium is able to resolve the separation and the color charge on the quark and the antiquark is screened by the medium. Thus in a QGP at a temperature T, only those quarkonia will be formed whose radii is smaller than $1/T$. These arguments, though not rigorous, nevertheless, support the idea that quarkonia production rates can be taken to be a measuring yardstick of whether QGP has been formed and, if formed, at what temperature.

Lattice methods are presently capable of computing the free energy $F_{Q\bar{Q}}(r)$ of a heavy quark-antiquark pair. At zero temperature, lattice results for $F_{Q\bar{Q}}(r)$ in QCD without dynamical quarks are well approximated by the ansatz

$$F_{Q\bar{Q}}(r) = \sigma r - \frac{\alpha}{r} \tag{2.7}$$

where the linear term is dominant at large distance. At short distance the perturbative Coulombic attraction is more significant. The string tension $\sigma \sim 0.2$ GeV^2. If now one introduces the pair in a thermal medium, the free energy ansatz is modified as [43, 44]

$$F_{Q\bar{Q}}(r) = -\frac{\alpha}{r} + \sigma r \left(\frac{1 - e^{-m_D r}}{m_D r} \right) \tag{2.8}$$

where $m_D \equiv m_D(T)$ is interpreted at high temperatures as the temperature-dependent Debye screening mass. By taking the form of $F_{Q\bar{Q}}(r)$ as the potential in the Schrödinger equation it is possible to determine which bound states in this potential survive as the potential is weakened with increasing temperature. Studies using such potential models have been successful in predicting the dissociation temperature T_d of various quarkonia. For example, it is found that $T_d(J/\Psi) \simeq 2.1T_c$, whereas, for the more loosely bound and larger $2s$ state Ψ', one has $T_d(\Psi') \simeq 1.1T_c$. For the $1s$ state of the bottomonium family it is estimated that $T_d(\Upsilon(1s)) > 4T_c$. For the corresponding $2s$ and $3s$ states estimates suggest $T_d(\Upsilon(2s)) \simeq 1.6T_c$ and $T_d(\Upsilon(3s)) \simeq 1.2T_c$ respectively [43, 44]. Thus we find that the estimates obtained by using the potential model fits well with the heuristic argument given earlier supporting that deeply bound quarkonia ($1s$ states) survive to higher temperatures compared to their loosely bound sisters. It must be admitted that the potential model does lack rigor and thus it is even difficult to predict the uncertainties associated with the above estimates. Nevertheless, in conjunction with lattice QCD results, it still provides strong qualitative support to the central idea of Matsui and Satz that quarkonium mesons melt in hot QGP and that this melting process takes place *sequentially*, with smaller quarkonia living up to higher temperatures.

Thus we find that an analysis of quarkonia potential and how it is screened in presence of the medium provides a handle to understand quarkonia suppression. Motivated by this, we shall evaluate the quark-antiquark potential in thermal SYM plasma (both isotropic and anisotropic) employing the ideas of the AdS/CFT correspondence.

To summarize, in this section we have discussed at length two salient features associated with heavy ion collisions, namely energy loss (both collisional and radiative) and quarkonium suppression. Of course, there are other important issues that need to be addressed but we have focused specifically on these two features since there is a possibility of considerable overlap between experimental observations and theoretical predictions extracted from the gauge/string duality with the phenomenological modeling acting as a bridge between the two. In the ensuing sections, we discuss, albeit very briefly, the most important aspects of string theory and try to motivate the remarkable gauge/string duality that will form the backbone of all our calculations.

2.3 AdS/CFT for the Layman

In this section we discuss the basics of the gauge/string duality. We begin our little tour of the underlying concepts of string theory, commencing with a discussion of D-branes and gauge theories and culminating in establishing the AdS/CFT correspondence from a heuristic point of view.

2.3.1 A little tour of string theory

Contrary to ordinary quantum field theory that describes the dynamics of point particles, the fundamental constituents of string theory are one-dimensional objects called *strings*. Strings have a characteristic length, which is the Planck length $l_P = 1.6 \times 10^{-33}$ cm. This is, of course, much smaller than the smallest length scale we can resolve in present day experiments. That is why, in the energy scale accessed in these experiments, strings will behave effectively as point-like objects and quantum field theory works so well. Strings are characterized by the string tension T_{string} and by a dimensionless coupling constant g_s, that controls the strength of all interactions. The string tension can be written in terms of the string length l_s as,

$$T_{\text{string}} \equiv \frac{1}{2\pi\alpha'} \qquad\qquad \alpha' \equiv l_s^2. \tag{2.9}$$

Just as a point particle describes a world-line in space-time, similarly a string sweeps out a two-dimensional world-sheet. For a closed string, a world-sheet will have no boundary. Mimicking the action for a point particle which is simply the length of its world-line, we shall postulate that the action for a string is given by the area of its world-sheet. We parametrize the two-dimensional string world-sheet by coordinates τ and σ which we collectively designate as ξ^α with $\alpha = 0, 1$ respectively for τ and σ. We assume that the string propagates in a D-dimensional space-time described by coordinates x^M, $\{M = 0, 1, ..., D-1\}$. The trajectory of the string is then described by specifying the functions $x^M = x^M(\xi)$. The two-dimensional metric induced on the string world-sheet is,

$$\boxed{g_{\alpha\beta} = G_{MN}\frac{\partial x^M}{\partial \xi^\alpha}\frac{\partial x^N}{\partial \xi^\beta}} \tag{2.10}$$

where G_{MN} describes the D-dimensional space-time metric. The string action (also called the Nambu-Goto action) is then given by,

$$\boxed{\mathcal{S} = \frac{1}{2\pi\alpha'}\int d\tau d\sigma\sqrt{-\text{det}g_{\alpha\beta}}.} \tag{2.11}$$

We will have to fall back on these two boxed equations time and again through the thesis. Quantization of the above action yields the quantum states of a single string. It turns out that the quantization process imposes severe constraint on the space-time dimension in which the string propagates - not all space-time dimensions allow for a consistent string propagation. For example, if we start with a D-dimensional Minkowski space-time then one must have $D = 26$. Physically, different states in the string spectrum are nothing but different vibration modes of the string. From the perspective of the background space-time each of these modes corresponds to a particle with a specific mass m and spin s. The spectrum typically consists of a finite number of massless modes and an infinite tower of massive modes with masses of the order of $m_s \equiv l_s^{-1}$. Quite remarkably, it turns out that the closed string spectrum always consists of a particle with $m = 0$ and $s = 2$, which we interpret as the graviton. This is why, string theory is referred to as a quantum theory of gravity. The graviton describes small fluctuations of the space-time metric signifying that the space-time that we initially started with is actually dynamical.

It is possible to construct other string theories by incorporating more degrees of freedom to the string world-sheet. In this thesis, we shall be primarily talking about the supersymmetric theory of strings, the so-called type IIB superstring theory [45, 46] which is obtained by adding two-dimensional world-sheet fermions to the above action. Although, at the end of the day, we shall be interested in breaking this supersymmetry to get as near to QCD as possible, existence of this symmetry is necessary to ensure stability of the construction. In case of superstring theories it turns out that ruling out negative norm states requires that we fix the space-time dimension $D = 10$. Apart from the graviton, the spectrum of type IIB superstring theory also contains two scalars, a number of antisymmetric tensor fields, and various fermionic partners as dictated by supersymmetry. At low energy $E \ll m_s$, one may integrate out the massive modes so that it is possible to write down an effective action involving only the massless modes. Since the massless string spectrum always contains the graviton, the low energy effective action, to second order in derivatives, has the form of

Einstein gravity coupled to other massless modes,

$$\mathcal{S}_{low} = \frac{1}{16\pi G_D} \int d^D x \sqrt{-\text{det}G}\mathcal{R} + ... \tag{2.12}$$

where $\mathcal{R}$ is the Ricci scalar in D-dimensional space-time and the "..." stands for additional terms containing other massless modes. One of the scalars, the dilaton ϕ will play a vital role in our discussion later. g_s, the string coupling, is given by the expectation value of the dilaton, $g_s = e^{\phi}$. As such g_s may vary over space and time. In such a scenario, we may still, however, speak of a coupling constant implying the asymptotic value of the dilaton at infinity, i.e., $g_s = e^{\phi_\infty}$.

The fermions in the closed string spectrum can have either left-handed chirality (left moving) or right-handed chirality (right moving). Further, they can enjoy either periodic (Ramond sector) or antiperiodic (Neveu-Schwarz sector) boundary conditions. Depending upon the handedness and the nature of the boundary conditions one can distinguish between four different sectors: R-R, NS-NS, R-NS and NS-R. The R-R and the NS-NS sectors give space-time bosons while the R-NS and the NS-R sectors give space-time fermions. The NS-NS sector contains the graviton G_{MN}, the two-form field B_{MN} and the dilaton ϕ whereas the R-R sector contains the $(p+1)$-form field A_{p+1} in the massless sector. Depending upon whether p is even or odd we accordingly have type IIA or IIB string theory.

D-branes and gauge theories

Perturbatively, string theory is a theory of strings. Non-perturbatively, string theory also contains higher-dimensional solitonic objects called D-branes [47]. A Dp-brane is a $(p+1)$-dimensional object in $(9+1)$-dimensional space-time with which strings can interact. A closed string can break on a Dp-brane whereas an open string can end on a Dp-brane. The end-points of open strings can move freely along the $(p+1)$ directions of the Dp-brane but can not leave it and move along the transverse directions. Thus the open string satisfies Neumann boundary conditions along the $(p+1)$ D-brane directions and Dirichlet boundary conditions along the $(9-p)$ directions transverse to the Dp-brane. A Dp-brane spans a $(p+1)$-dimensional world-volume in space-time. D0-branes are particle-like objects, D1-branes are string-like, D2-branes are membrane-like and so on.

Introduction of Dp-branes enriches the structure of string theory vastly. As we had mentioned earlier, a closed string can break by encountering a Dp-brane and turn into an open string. Just as the quantization of the closed string resulted in dynamical fluctuations of the space-time, a similar quantization of open strings culminates in a spectrum that contains fluctuations of the Dp-brane. The open string spectrum comprises of a finite number of massless modes and an infinite tower of massive modes with masses $\sim m_s = l_s^{-1}$. For the case of a single Dp-brane the massless spectrum contains an Abelian gauge field $A_\mu(x), \{\mu = 0, 1, ..., p\}, (9-p)$ scalar fields $\phi^i(x), \{i = 1, 2, ..., (9-p)\}$, and their superpartners. Since the fields are supported on the D-brane they depend only upon the world-volume coordinates of the Dp-brane and not on the directions transverse to the D-brane. The $(9-p)$ scalars describe fluctuations of the D-brane in the transverse directions that include possible deformations of the D-brane as also linear motion. The Dp-branes are also charged under the $(p+1)$-form field, A_{p+1} coming from the R-R sector of type II string theory. A very peculiar property of D-branes is the appearance of a non-Abelian gauge field when multiple D-branes are brought close to each other. Apart from the degrees of freedom pertaining to each brane, now there arise new degrees of freedom from strings that stretch from one brane to another. As a specific example, we can consider two parallel branes separated by a distance d. Now, there can be four types of strings depending upon the brane on which the end-points of the strings lie as seen from Figure 2.1. The strings

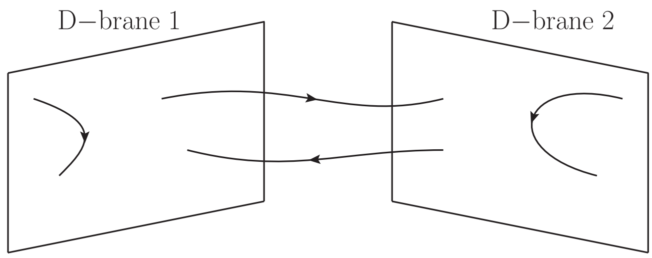

Figure 2.1: Parallel set of D-branes supporting open strings

with both end-points lying on the same brane give rise to massless gauge fields as discussed earlier. Let us denote these gauge fields as $(A_\mu)^1{}_1$ and $(A_\mu)^2{}_2$. Here the upper (lower) index denotes the brane on which the string starts (ends). Now, we have the additional possibility that a string can start from brane $1(2)$ and end on $2(1)$. These strings give birth to two more vector fields which we call $(A_\mu)^1{}_2$ and $(A_\mu)^2{}_1$. These are massive fields with mass given by $m = d/2\pi\alpha'$. Now let us consider the case when the two D-branes are put on top of each other, i.e., we make their separation $d = 0$. This implies that the vector fields $(A_\mu)^2{}_1$ and $(A_\mu)^1{}_2$ become massless in this limit. So, now the spectrum consists of four massless vector fields which we denote as $(A_\mu)^a{}_b$ with $a, b = 1, 2$. Now this is exactly the gauge field of a non-Abelian $U(2)$ gauge group. Similarly, the $(9-p)$ massless scalars also become 2×2 matrices $(\phi^i)^a{}_b$ which transform in the adjoint representation of the $U(2)$ gauge group. Having got the basic intuition, it is straight forward to generalize the notion when N_c branes are stacked together. We have a $U(N_c)$ multiplet of non-Abelian gauge field with the $(9-p)$ scalars transforming in the adjoint representation of $U(N_c)$. The low energy dynamics can be obtained by integrating out the massive modes and it turns out that it is governed by a non-Abelian gauge theory [48]. Let us now take a concrete example. We consider N_c D3-branes in type IIB superstring theory. The massless spectrum is now made up of a gauge field A_μ, six scalar fields ϕ_i, $\{i = 1, 2, ..., 6\}$, and four Weyl fermions, all transforming in the adjoint representation of $U(N_c)$. It was shown in [48] that if we confine ourselves only to theories with at most second derivative then the low energy effective action for these massless modes is exactly that of $\mathcal{N}=4$ SYM theory in $(3+1)$-dimensions with gauge group $U(N_c)$ [49, 50]. The bosonic part of the Lagrangian is

$$\mathcal{L}_{\text{boson}} = -\frac{1}{g_{\text{YM}}}\text{Tr}\left(\frac{1}{4}F^{\mu\nu}F_{\mu\nu} + \frac{1}{2}D_\mu\phi^i D^\mu\phi^i + [\phi^i,\phi^j]^2\right) \tag{2.13}$$

where the Yang-Mills coupling constant is,

$$g_{\text{YM}}^2 = 4\pi g_s. \tag{2.14}$$

Eq. 2.13 is the bosonic part of the most general renormalizable Lagrangian consistent with $\mathcal{N}=4$ global supersymmetry. Due to the high degree of supersymmetry the theory enjoys many interesting features. For example, the β-function vanishes, so that the coupling constant is independent of scale and the theory respects conformal invariance. Another notable aspect of the Lagrangian is that the $U(1)$ part is free and can be decoupled. Physically, this can be understood as follows. Excitations of the overall diagonal $U(1)$ subgroup of $U(N_c)$ describe the center-of-mass motion of the whole system of branes. Owing to the overall translational invariance this symmetry decouples itself from the remnant $SU(N_c) \subset U(N_c)$, which is a symmetry of the motion of the branes relative to one another. The Lagrangian (Eq. 2.13) also receives higher order correction suppressed by $\alpha' E^2$. For a single Dp-brane with constant $F_{\mu\nu}$ and $\partial_\mu\phi^i$, all the higher order correction terms can be resummed exactly in the Dirac-Born-Infeld action [51],

$$\mathcal{S}_{\text{DBI}} = -T_{\text{D}p}\int d^{p+1}x e^{-\phi}\sqrt{-\det\left(g_{\mu\nu} + 2\pi l_s^2 F_{\mu\nu}\right)} \tag{2.15}$$

where $T_{\mathrm{D}p}$ is the Dp-brane tension, the mass per unit spatial volume given as,

$$T_{\mathrm{D}p} = \frac{1}{(2\pi)^p g_s l_s^{p+1}}. \tag{2.16}$$

Here ϕ is the dilaton and $g_{\mu\nu}$ is the metric induced on the Dp-brane. Owing to their infinite extent D-branes are infinitely massive. However, the mass per unit volume is finite as seen above. The dependence of the tension on the string length is dictated by considerations of dimensional analysis. As is typical in field theory, the tension depends inversely upon g_s. However, contrary to solitons in field theory where the tension varies with coupling as $1/g^2$ here the tension varies as $1/g_s$. In the limit of vanishing coupling, $g_s \to 0$, the tension becomes extremely large, and the D-brane decouples from the spectrum.

D-branes and space-time geometry

Since D-branes are massive objects they distort space-time in their vicinity. The space-time metric sourced by N_c Dp-branes is found out by solving the supergravity equations of motion. The low energy effective action of type II supergravity is given by (in the Einstein frame) [52],

$$\mathcal{S} = \frac{1}{16\pi G_{10}} \int d^{10}x \sqrt{-\mathrm{det}G} \left(\mathcal{R} - \frac{1}{2} G_{MN} \partial^M \phi \partial^N \phi - \frac{1}{2} \sum_n \frac{1}{n!} e^{a_n \phi} F_n^2 + \ldots \right) \tag{2.17}$$

with $a_n = -\frac{1}{2}(n-5)$ and G_{MN} denoting the ten-dimensional space-time metric. Here the "..." represents the fermionic term and the NS-NS three-form field strength term. The n-form field strengths we have used belong to the R-R sector. For type IIA (IIB) theory n is even (odd). In type IIB theory for $n = 5$ the form field F_5 is self-dual. The equations of motion following from the above action are [53–55]

$$\begin{aligned}
\mathcal{R}^M_N &= \frac{1}{2}\partial^M\phi\partial_N\phi + \frac{1}{2n!}e^{a\phi}\left[nF^{MK_2\ldots K_n}F_{NK_2\ldots K_n} - \frac{n-1}{8}\delta^M_N F_n^2\right], \\
\nabla^2\phi &= \frac{1}{\sqrt{G}}\partial_M\left(\sqrt{G}\partial_N\phi G^{MN}\right) = \frac{a}{2n!}F_n^2, \\
&\partial_M(\sqrt{G}e^{a\phi}F^{MK_2\ldots K_n}) = 0.
\end{aligned} \tag{2.18}$$

This is supplemented by the Bianchi identity,

$$\partial_{[K_1}F_{K_2\ldots K_n]} = 0. \tag{2.19}$$

Also for the sake of simplicity we have assumed that F_n exists only for one value of n and write $a_n \equiv a$. After solving the equations of motion it is possible to find out the space-time metric sourced by the Dp-branes. In particular, it can be shown that for the metric to reduce to the familiar form $AdS_q \times S^{10-q}$ one must require the coupling with the dilaton to vanish. This happens when the dilaton is a constant, in particular, zero and $n = 5$. In this case, we obtain the metric corresponding to D3-brane

$$ds^2 = H^{-1/2}\left(-dt^2 + dx_1^2 + dx_2^2 + dx_3^2\right) + H^{1/2}\left(dr^2 + r^2 d\Omega_5^2\right) \tag{2.20}$$

where,

$$H(r) = 1 + \frac{R^4}{r^4} \tag{2.21}$$

and

$$R^4 = 4\pi g_s N_c l_s^4. \tag{2.22}$$

Here $\{t, x_1, x_2, x_3\}$ are the world-volume coordinates on the D3-brane and y_i, $\{i = 1, 2, ..., 6\}$ are the coordinates transverse to the D3-brane with

$$r^2 = \sum_{i=1}^{6} y_i^2. \tag{2.23}$$

To have a feel of the geometry induced by the D3-brane, let us consider its limit in two different regimes. In the limit $r \gg R$, $H \to 1$ and the metric tends to that of flat Minkowski space-time $\mathbb{R}^{1,9}$. In the other limit $r \ll R$ the metric would at first appear to be singular. This is often referred to as the *throat* geometry. However, a clever redefinition of the coordinates circumvents the difficulty. We define a new coordinate,

$$U = \frac{r}{l_s^2} \tag{2.24}$$

and consider the limit $l_s^2 \to 0$ in conjunction with $r \to 0$ such that U remains a meaningful variable. In the new coordinate, the metric reads,

$$\begin{aligned} ds^2 &= l_s^2 \left(\frac{U^2 dx_{(4)}^2}{\sqrt{4\pi g_s N_c}} + \sqrt{4\pi g_s N_c} \left(\frac{dU^2}{U^2} + d\Omega_5^2 \right) \right) \\ &= \frac{U^2}{R^2} d\tilde{x}_{(4)}^2 + \frac{R^2}{U^2} dU^2 + R^2 d\Omega_5^2 \end{aligned} \tag{2.25}$$

where we have defined

$$dx_{(4)}^2 = -dt^2 + \sum_{i=1}^{3} (dx^i)^2 \tag{2.26}$$

and $\tilde{x} \equiv l_s^2(t, x^1, x^2, x^3)$. The metric, written in this form, is manifestly in the form of a product geometry. One component is S^5 with metric $R^2 d\Omega_5^2$ and the remaining component is AdS_5. As we shall see shortly, in the Maldacena conjecture we are required to take the "near-horizon limit" which amounts to taking $l_s \to 0$. In that case, for U to remain a meaningful coordinate, we must also let $r \to 0$. Thus we consider a region very close to the surface of the D3-brane. In this region, we only need to consider the $AdS_5 \times S^5$ structure whereas the dynamics in the asymptotically flat space-time decouples from the theory. So this also goes by the name of the decoupling limit.

2.3.2 The AdS/CFT correspondence

In the preceding subsection we had prepared the groundwork for discussing the AdS/CFT correspondence. In this section we shall try to motivate the AdS/CFT correspondence [1–3] (see [4] for a comprehensive review) by studying string theory in the presence of D-branes from two different perspectives. To start with we consider type IIB string theory in ten-dimensional Minkowski space-time and a set of N_c parallel D3-branes. String theory in this background comprises of two types of excitations: closed strings and open strings. Closed strings are excitations of empty space whereas open strings encode excitations of D-branes. If we confine our attention to a study of this theory in the low energy regime then only the massless string states will survive. It is then possible to write down an effective Lagrangian describing the string interactions. The closed string spectrum gives a gravity supermultiplet in ten dimensions and the corresponding low energy Lagrangian is that of type IIB supergravity (as discussed in the previous section). On the other hand, we found that the open string massless states give a $\mathcal{N} = 4$ supermultiplet and is described by the low energy effective Lagrangian of $\mathcal{N} = 4$ SYM theory.

The complete effective action of the massless modes can be written as,

$$\mathcal{S}_{eff} = \mathcal{S}_{bulk} + \mathcal{S}_{brane} + \mathcal{S}_{int}. \tag{2.27}$$

$\mathcal{S}_{bulk}$ denotes the action of ten-dimensional gravity with some higher derivative corrections. The brane action $\mathcal{S}_{brane}$, which is defined on the D3-brane world-volume, contains the $\mathcal{N} = 4$ SYM theory plus some higher derivative corrections. Lastly, $\mathcal{S}_{int}$ stands for the interaction between the brane modes and the bulk modes. The bulk action can be expanded as a free quadratic part describing the propagation of free massless modes (including graviton) plus some interactions within the bulk. Upon taking the low energy limit, all the interaction terms and also the higher derivative terms cease to make any contribution. So what we are left with is just the pure $\mathcal{N} = 4$ SYM theory in $(3 + 1)$-dimensions and a free theory of gravity in the bulk.

We shall now look at the same problem, albeit from a slightly different perspective. In the preceding section, we saw how D-branes arise as solutions of type II supergravity. We now wish to focus on the low energy sector in this description. This implies looking at those excitations that have arbitrarily small energy with respect to an observer in asymptotically Minkowski space-time. We can distinguish between two distinct sets of excitations. One is the set of massless excitations propagating in the bulk. Another is the set of excitations in the throat region. For such excitations, we can allow for any value of proper energy. This is because to an observer sitting at asymptotic Minkowski space-time, the energy E is measured to be

$$E = \sqrt{-G_{tt}}E_p = H^{-1/4}E_p \tag{2.28}$$

where E_p is the energy measured at a point P located at a radial coordinate r. Now as we approach the throat $r \to 0$, and for fixed E_p, the energy measured by the observer, i.e., E approaches zero. Thus even the massive modes living in the throat region will appear to be massless. If we consider only the low energy domain, these modes are pushed deeper into the throat and ultimately decouple from the massless modes populating the bulk. Thus the

low energy regime consists of two decoupled pieces: a theory of free gravity in the bulk and the other is the near-horizon geometry which corresponds to $AdS_5 \times S^5$.
We note that from both points of view we have two decoupled theories in the low energy limit. Of these, the theory of gravity is common to both the views. It is then only natural to identify the remaining sectors. Thus we are led to the equivalence of two theories

- type IIB string theory on $AdS_5 \times S^5$ where both the subspaces have a common radius R and the string coupling is g_s.
- $\mathcal{N} = 4$ SYM theory in $(3+1)$-dimensions with gauge group $SU(N_c)$ and Yang-Mills coupling constant g_{YM}, which is known to be a conformally-invariant theory.

For two theories to be equivalent a reasonable demand is that they should have the same symmetries. So let us now discuss the symmetries of these two theories. AdS_5 can be viewed as embedded in a six-dimensional flat space-time $\mathbb{R}^{2,4}$ which has a symmetry group $SO(2,4)$. In fact, this is the same symmetry group as the conformal symmetry in $(3+1)$-dimensions. In the bulk there also exists a $SO(6)$ symmetry corresponding to the five-sphere S^5. So the total symmetry is $SO(2,4) \times SO(6)$. However, since spinors are involved, the relevant groups are the covering groups $SU(4)$ of $SO(6)$ and $SU(2,2)$ of $SO(2,4)$ so that we speak of a $SU(4) \times SU(2,2)$ symmetry. But the thirty-two Majorana spinor supercharges of type IIB theory transform in such a way that the full symmetry group is the Lie supergroup $SU(2,2|4)$. On the gauge theory side, the $SO(6)$ symmetry is realized as the R-symmetry of the theory under which the non-Abelian gauge fields transform as singlets, the complex Majoranas as $\{\mathbf{4}\}$ and $\{\bar{\mathbf{4}}\}$ of $SU(4)$ and the scalars as $\{\mathbf{6}\}$ of the $SO(6)$ or as antisymmetric tensors of rank two under $SU(4)$. On the other hand, $\mathcal{N} = 4$ SYM, being a scale-invariant theory, also enjoys a $SO(2,4) \sim SU(2,2)$ space-time symmetry. This, in the presence of supersymmetry, leads to a larger symmetry group with sixteen new fermionic generators. Altogether, on the gauge theory side too the symmetry is $SU(2,2|4)$.

We have also seen how the coupling constant in the two theories are related in Eq. 2.14. N_c is the rank of the gauge group and also equals the number of D3-branes stacked upon each other on the string theory side. The common radius R is given by Eq. 2.22. We define the 't Hooft coupling λ as

$$\lambda \equiv g_{\mathrm{YM}}^2 N_c \tag{2.29}$$

so that Eq. 2.22 can be recast as

$$R^4 = g_{\mathrm{YM}}^2 N_c l_s^4 = \lambda l_s^4. \tag{2.30}$$

By "equivalence" of the two theories we mean a matching between the states and the fields on the superstring side and the local gauge-invariant operators on the $\mathcal{N} = 4$ SYM side and also a correspondence between the correlators of the two theories. The correspondence we have stated here is said to be in its *strong* form. In this form it holds for all values of N_c and g_s. However, at present string quantization on curved space is a rather complicated task. In such a scenario, we seek special limits in which the conjecture becomes more tractable but at the same time reveals useful information, which we are going to discuss now.

't Hooft limit

In the 't Hooft limit we keep λ fixed but allow $N_c \to \infty$. On the gauge theory side this limit is well-defined in perturbation theory and corresponds to a $1/N_c$ expansion of the field theory's Feynman diagrams. On the string theory side, a large N_c implies that the string coupling $g_s \sim \lambda/N_c \to 0$. We can thus do calculations in the string theory side simply by restricting ourselves to tree-level diagrams without the need to do any loop calculations.

The full quantum non-perturbative description of $\mathcal{N} = 4$ SYM theory is then obtained from this classical theory of strings in the large N_c limit.

Large λ limit

In the next stage we impose the further condition that λ must be very large. We can make use of Eq. 2.30 to fully appreciate the significance of imposing this constraint. If we keep R, the common radius fixed, then this limit means that $l_s^2 \to 0$ so that we are in the low energy limit whence classical string theory reduces to classical supergravity. Alternatively, we may fix l_s. In that case a large λ ensures that $R \to \infty$. Then all curvatures are small and quantum gravity corrections can be ignored so that classical supergravity is sufficient to capture the essential physics. Either way we observe that taking λ to be large ensures that classical string theory simplifies to classical supergravity that is much easier to access. On the contrary, for perturbation theory to be valid on the gauge theory side in the large N_c limit, we require g_{YM} to be small which is evident from Eq. 2.29. Thus we find that the two descriptions - perturbative gauge theory and string theory on $AdS_5 \times S^5$ are valid in two different regimes. It is in this sense that the two theories are said to be dual to each other.

2.4 AdS/CFT in Quark-Gluon Plasma

In the previous section we have conjectured an equivalence between string theory and $\mathcal{N} = 4$ SYM theory at *zero temperature*, since we had considered the stack of N_c D3-branes to be in their ground state. On the supergravity side this corresponds to the so-called extremal solutions. A very natural generalization is to consider the case when the gauge theory has a non-zero temperature, which will be of more interest to us. Correspondingly, we need to excite the degrees of freedom on the D-branes to a finite temperature. This yields the non-extremal solutions in supergravity [56, 57]. It is found that the effect of incorporating a non-zero temperature is to only modify the AdS_5 part of the metric as,

$$ds^2 = \frac{r^2}{R^2}\left(-f dt^2 + dx_1^2 + dx_2^2 + dx_3^2\right) + \frac{R^2}{r^2 f} dr^2 + R^2 d\Omega_5^2 \tag{2.31}$$

with

$$f(r) = 1 - \frac{r_0^4}{r^4}. \tag{2.32}$$

Note that by setting $r_0 = 0$ we recover the familiar $AdS_5 \times S^5$ space-time,

$$ds^2 = ds^2_{AdS_5} + R^2 d\Omega_5^2 \tag{2.33}$$

with

$$ds^2_{AdS_5} = \frac{r^2}{R^2}\eta_{\mu\nu} dx^\mu dx^\nu + \frac{R^2}{r^2} dr^2, \qquad\qquad r \in (0, \infty). \tag{2.34}$$

Here $\{x^\mu\}$ refers to the coordinates of the Minkowski space-time or the gauge theory co-ordinates. It can be easily seen from Eq. 2.34 that for a r = constant slice, the metric reduces to the familiar Minkowski space-time up to a conformal factor of $\frac{r^2}{R^2}$. As $r \to \infty$ we approach the "boundary" of the space-time. This is a boundary in the conformal sense, not in the topological sense since the scale factor $\frac{r^2}{R^2}$ blows up near the boundary. However, we shall not go into such subtleties and simply refer to the $r \to \infty$ limit as the boundary.

It is customary to define the new coordinate $z = R^2/r \in (0, \infty)$ in terms of which the AdS_5 metric assumes the form,

$$ds^2_{AdS_5} = \frac{R^2}{z^2}\left(-dt^2 + dx_1^2 + dx_2^2 + dx_3^2 + dz^2\right). \tag{2.35}$$

Here the boundary theory lives at $z \to 0$. Introducing finite temperature the AdS_5-black hole metric is written as,

$$ds^2 = \frac{R^2}{z^2}\left(-f dt^2 + dx_1^2 + dx_2^2 + dx_3^2 + \frac{dz^2}{f}\right) \qquad z \in (0, z_0) \tag{2.36}$$

now with,

$$f(z) = 1 - \frac{z^4}{z_0^4} \tag{2.37}$$

with the event horizon at $z_0 = 1/r_0$.

String theory in this background is dual to $\mathcal{N} = 4$ SYM theory at *finite temperature*. In the thesis we shall be concerned with various deformations of the thermal SYM theory.

The Hawking temperature of the black D3-brane can be computed in the standard procedure [58] of demanding that the Euclidean continuation of the metric (Eq. 2.36) obtained *via* the substitution $t \to -it_E$,

$$ds^2 = \frac{R^2}{z^2}\left(f dt_E^2 + dx_1^2 + dx_2^2 + dx_3^2 + \frac{dz^2}{f}\right) \tag{2.38}$$

be regular at $z = z_0$. This requires that t_E be identified with a period β given as

$$\beta = \frac{1}{T} = \pi z_0. \tag{2.39}$$

This temperature is, in turn, identified with the temperature of the $\mathcal{N} = 4$ SYM theory on the boundary. This is reasonable, since t_E corresponds to precisely the Euclidean time coordinate in the boundary theory. Having generalized the speculated equivalence to the finite temperature case, we can make some further generalizations. For example, one can introduce a chemical potential μ into our theory. For a boundary theory enjoying a $U(1)$

symmetry like the $\mathcal{N} = 4$ SYM, it is possible to incorporate a chemical potential μ corresponding to the $U(1)$ charge. If we represent the boundary current by J_μ then by the AdS/CFT dictionary the bulk gauge field A_μ is related to this current respecting the boundary condition,

$$\lim_{z\to 0} A_t = \mu. \tag{2.40}$$

This condition, complemented by the requirement that the gauge field is well-behaved at the horizon, effectively means that there is an electric field in the bulk, i.e., the black hole is now charged. We shall not consider charged black holes and their gauge theory duals in details here. The interested reader is referred to [59–64] for more details. It is also possible to generalize the correspondence in other directions. For instance, keeping in mind realistic QCD, theories with lesser number of supersymmetries or theories which are not scale-invariant have been studied *via* their string duals. In particular, the two models of thermal SYM theory that we shall explore in this thesis both violate conformal invariance.

Wilson loops

Let us now turn to a discussion of Wilson loops. In course of the thesis we shall have occasions to compute the expectation values of various types of Wilson loops in different contexts. Hence, it is worthwhile to devote some space to an elaborate discussion of Wilson loops and their computation in the holographic context.

The expectation values of Wilson loops,

$$W(\mathcal{C}) = \mathrm{Tr}\, \mathcal{P} \exp\left[i \int_{\mathcal{C}} dx^\mu A_\mu(x)\right] \tag{2.41}$$

form an important class of non-local observables in any gauge theory. The expectation values of Wilson loops contain a wealth of information about the non-perturbative physics of

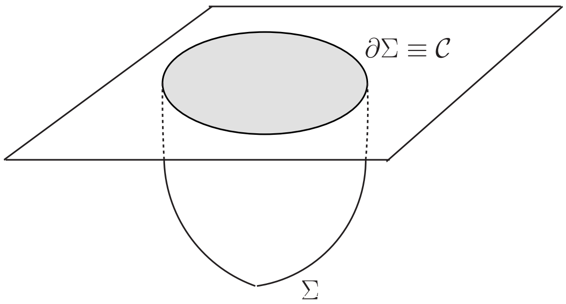

Figure 2.2: String world-sheet and Wilson Loop

non-Abelian gauge theories. For example, they find applications in studying confinement, thermal phase transitions, quark screening, etc. In many of the applications it is useful to take $\mathcal{C}$ to be the path traversed by a quark. We shall here describe how to compute the expectation values of Wilson loops in strongly coupled non-Abelian gauge theories using the dual string description. For the sake of definiteness, we shall talk about $\mathcal{N} = 4$ SYM theory as the prototype gauge theory. Let us recall that the field content of $\mathcal{N} = 4$ SYM theory includes six scalar fields ϕ^i in the adjoint representation. This allows us to slightly generalize Eq. 2.41 to [65, 66],

$$W(\mathcal{C}) = \frac{1}{N_c} \mathrm{Tr}\, \mathcal{P} \exp \left[i \oint_{\mathcal{C}} ds \left(A_\mu \dot{x}^\mu + \vec{n} \cdot \vec{\phi} \sqrt{\dot{x}^2} \right) \right] \tag{2.42}$$

with $\vec{\phi} = \{\phi^1, \phi^2, ..., \phi^6\}$, $\vec{n}$ a unit vector in $\mathbb{R}^6$ that parametrizes a path in this space (in S^5) just as $x^\mu(s)$ parametrizes a path in $\mathbb{R}^{1,3}$. The factor $\sqrt{\dot{x}^2}$ is necessary to make the second term a density under world-line parametrizations. The quantity in Eq. 2.42 can be interpreted in terms of the string world-sheet. We take $\mathcal{C}$ to be the path traced out by a quark. Although we have seen that the field content of $\mathcal{N} = 4$ SYM has no quark, it is possible to include quarks in our theory by introducing open strings attached to a D-brane located at some radial coordinate $r = r_m$. The mass of the quark so introduced is then proportional to r_m. The end-point of the open string that terminates on the D-brane is the holographic dual of a quark in the gauge theory. It is then natural to speculate that the boundary $\partial\Sigma$ of the string world-sheet Σ must be the path $\mathcal{C}$ of the quark, i.e., we are led to the identification, $\partial\Sigma \equiv \mathcal{C}$ as depicted in Figure 2.2. We then identify the expectation value of the Wilson loop operator, which furnishes the partition function or the amplitude of the quark traversing $\mathcal{C}$, with the partition function of the dual string world-sheet Σ,

$$\langle W(\mathcal{C})\rangle = Z_{\text{string}}[\partial\Sigma = \mathcal{C}]. \tag{2.43}$$

Also, to keep things simple we shall consider only infinitely heavy, i.e., non-dynamical quarks. In the gravity picture this is equivalent to the statement that the D-brane is located at infinite radial position, i.e., $r_m \to \infty$. This essentially ensures that the boundary of the string world-sheet $(\partial\Sigma)$ lies in the boundary of AdS. Now recall that the string end-point couples to the fields living on the D-brane, i.e., it couples with both the gauge field A_μ and the scalars. The coupling with the scalars reflects that the string pulls the D-brane and distorts its shape. The pull is orthogonal to the directions spanned by the D-brane and we indicate this direction by $\vec{n}$. The coupling to the gauge field indicates that the string end-point behaves as a point particle charged under this gauge field. Thus we see that the correct Wilson loop operator dual to the string world-sheet should be Eq. 2.42 rather than Eq. 2.41. Note that the two operators match only when the Wilson loop is light-like and $\dot{x}$ vanishes.

In the limit when the number of colors N_c is very large and also the 't Hooft coupling is large the string partition function simplifies greatly and takes the form,

$$Z_{\text{string}}[\partial\Sigma = \mathcal{C}] = e^{i\mathcal{S}(\mathcal{C})} \tag{2.44}$$

which relates the Wilson loop operator to the classical string action as

$$\langle W(\mathcal{C})\rangle = e^{i\mathcal{S}(\mathcal{C})}. \tag{2.45}$$

Evaluating the expectation value of the Wilson loop thus boils down to finding the classical action $\mathcal{S}(\mathcal{C})$, which, in turn, is obtained by extremizing the Nambu-Goto action and imposing the proper boundary condition that the string ends on the curve $\mathcal{C}$.

It is important to be able to appreciate that both the large N_c limit and the large λ limit are essential for Eq. 2.44 to hold. Taking $N_c \to \infty$ at fixed λ ensures that $g_s \to 0$ which allows us to ignore the possibility of strings breaking off from the string world-sheet and forming loops. Moreover, $\lambda \to \infty$ guarantees that the string tension becomes very large and we can rule out fluctuations of the string so that the string assumes its classical configuration.

Let us now compute holographically a prototype Wilson loop in a simple case for illustrative purpose. We consider an infinitely heavy static quark, which implies that $\mathcal{C}$ is now just a straight line of length $\mathcal{T}$ along the time direction. On the field theory side, we expect,

$$\langle W(\mathcal{C})\rangle = e^{iM\mathcal{T}} \tag{2.46}$$

where M is the quark mass. Symmetry suggests that on the string theory side, the corresponding string world-sheet will also be a straight line with the string hanging straight down from the boundary to the horizon and translating along the time direction. The action for such a world-sheet will be infinite since the proper distance of the boundary from the AdS center is, in fact, infinite. This is consistent with the gauge theory picture where we have taken the quark to be infinitely massive. To obtain a finite value for the quark mass, we introduce a regulator in the bulk so that now the boundary is effectively at $z = \epsilon$ instead of at $z = 0$. On the field theory side this corresponds to introducing a short distance cut-off. To explicitly evaluate the world-sheet action we require to suitably parametrize the world-sheet. We choose $\xi^0 \equiv \tau = t$ and $\xi^1 \equiv \sigma = z$. For a static quark we further have $x^i =$ constant. The induced metric on the two-dimensional string world-sheet is given by,

$$ds^2 = \frac{R^2}{\sigma^2}\left(-d\tau^2 + d\sigma^2\right). \tag{2.47}$$

This yields the desired solution,

$$\mathcal{S} = \frac{\mathcal{T}R^2}{2\pi\alpha'}\int_{\epsilon}^{\infty}\frac{dz}{z^2} = \frac{\sqrt{\lambda}}{2\pi\epsilon}\mathcal{T}. \tag{2.48}$$

In the process we have called into action the AdS/CFT dictionary $R^2/\alpha' = \sqrt{\lambda}$. Combining Eqs. 2.45 and 2.46 we finally obtain the expression for the quark mass M as

$$M = \frac{\sqrt{\lambda}}{2\pi\epsilon}. \tag{2.49}$$

Note that as $\epsilon \to 0$, the quark mass M becomes very large, which is consistent with what we started with - massive non-dynamical quark at rest in the boundary theory.

2.5 Summary

In this chapter we have outlined the essential features pertaining to QGP and AdS/CFT that are relevant for our purpose. In particular, we skimmed through the basics of string theory and motivated the conjectured equivalence between $\mathcal{N} = 4, SU(N_c)$ SYM theory and type IIB string theory on $AdS_5 \times S^5$. We further got a feel of computing Wilson loops in gauge theories employing holographic techniques. Armed with these prerequisites we now proceed to compute expectation values of Wilson loops in more general scenarios. In the next chapter, we shall perform such computations in the context of $\mathcal{N} = 4$ SYM theories at finite temperature and in $(p+1)$-dimensions whose gravity dual is given by black Dp-branes. We shall also relate the expectation values so obtained to various heavy quark observables in the deconfined (high temperature) phase of $\mathcal{N} = 4$ SYM plasma. Subsequently, we shall see more of Wilson loops when we investigate the two models of anisotropic plasma in chapters 4 and 5 and extract information about various heavy quark observables from expectation values of such loops.

CHAPTER 3

WILSON LOOPS IN HOT YANG-MILLS THEORY IN $(p+1)$-DIMENSIONS

3.1 Overview

In the present chapter we set the stage for the anisotropic models to be investigated later, by considering heavy probe quarks in the background of isotropic $\mathcal{N}=4, SU(N_c)$ SYM theory at finite temperature. Following the well-defined recipe available in the literature and discussed in chapter 2, we evaluate expectation values of certain Wilson loops in thermal SYM plasma in various dimensions in the limit of large 't Hooft coupling and large number of colors *via* holography and relate them to various heavy quark observables that are of relevance to the recent collider experiments at RHIC and LHC*.

We compute the expectation value of a special time-like Wilson loop to extract the static quark-antiquark potential [68] in a flowing strongly coupled quark-gluon plasma. In a

*The present chapter is based on [67].

similar vein, the expectation value of a particular light-like Wilson loop furnishes the expression of the jet quenching parameter [69]. The velocity-dependent interaction potential E of a quarkonium bound state moving with an arbitrary velocity v through hot QGP, the screening length L_{max} [70–73] as well as the jet quenching parameter $\hat{q}$ [74,75]† have been calculated in $(3+1)$-dimensional $\mathcal{N}=4$ SYM plasma using the AdS/CFT correspondence. Here we follow the footsteps and generalize the computations to other dimensions. In space-time dimensions other than $(3+1)$, the gauge theory does no longer respect conformal invariance and it is thus an added motivation to see how the lack of conformal invariance affects the heavy quark observables‡.

Starting from non-extremal Dp-brane solution [54], a particular decoupling limit [76] of which defines the gravity dual of $(p+1)$-dimensional $SU(N_c)$ SYM theory at large N_c we apply the fundamental string probe approach to compute the Nambu-Goto world-sheet action for this background. As discussed earlier, the expectation value of the required Wilson loop corresponds to the minimal area of the string world-sheet whose boundary is the loop in question [65]. In §3.2 we consider time-like Wilson loop when the velocity v of the bound state Q-$\bar{Q}$ pair (which we shall frequently refer to as the "dipole") is $0<v<1$ and obtain the potential E of a dipole moving through $(p+1)$-dimensional SYM plasma with v as a parameter. Next we extract expressions for the screening length of the dipole§ in various dimensions. §3.3 concerns the calculation of $\hat{q}$ from light-like Wilson loop, i.e., by taking the $v \to 1$ limit of the previous calculation. $\hat{q}$ has been calculated earlier in [74] for $p=3$. Here we follow their method to generalize the results for any p. Finally, we conclude in §3.4 with a summary of the results obtained and future program.

†Also see [27] for a recent review.

‡Non-conformal theories have also been considered, among other things, in [71] and we thank Makoto Natsuume for bringing this reference to our attention.

§Screening length of a dipole moving with velocity v has been calculated in [71] at the leading order.

3.2 Q-$\bar{Q}$ Potential and Screening Length

Using the AdS/CFT correspondence, we calculate in this section expectation values of time-like Wilson loops in $(p+1)$-dimensional SYM theory by calculating the Nambu-Goto action of a fundamental string in the background of a non-extremal Dp-brane in a particular decoupling limit. From this we obtain the velocity-dependent Q-$\bar{Q}$ potential E and the screening length L_{max} of the heavy quark bound state.

3.2.1 Supergravity dual

Let us first try to understand the holographic dual to thermal $SU(N_c)$ SYM theory in $(p+1)$-dimensions. The metric (given in string frame), the dilaton and the form field of the non-extremal Dp-brane solution of type II supergravity are given as [54],

$$\begin{aligned} ds^2 &= H^{-\frac{1}{2}}\left(-f dt^2 + \sum_{i=1}^{p}(dx^i)^2\right) + H^{\frac{1}{2}}\left(\frac{dr^2}{f} + r^2 d\Omega_{8-p}^2\right) \\ e^{2(\phi-\phi_0)} &= H^{\frac{3-p}{2}}, \qquad F_{[p+2]} = \coth\alpha\, dH^{-1}\wedge dt \wedge dx^1 \wedge \ldots \wedge dx^p \end{aligned} \tag{3.1}$$

where,

$$H(r) = 1 + \frac{r_0^{7-p}\sinh^2\alpha}{r^{7-p}}, \qquad f(r) = 1 - \frac{r_0^{7-p}}{r^{7-p}} \tag{3.2}$$

with r_0 and α being two parameters related to the mass and the charge of the black Dp-brane. There is an event horizon at $r = r_0$ and $e^{\phi_0} = g_s$ is the string coupling constant where ϕ_0 is the asymptotic value of the dilaton ϕ. The form field $F_{[p+2]}$ has to be made self-dual for $p = 3$. In the decoupling limit we zoom into the region,

$$r_0^{7-p} < r^{7-p} \ll r_0^{7-p}\sinh^2\alpha \tag{3.3}$$

so that α is a very large angle and

$$H(r) \approx \frac{r_0^{7-p} \sinh^2 \alpha}{r^{7-p}} \tag{3.4}$$

and the metric now takes the form,

$$ds^2 = \frac{r^{\frac{7-p}{2}}}{r_0^{\frac{7-p}{2}} \sinh \alpha} \left(-f dt^2 + \sum_{i=1}^{p} (dx^i)^2 \right) + \frac{r_0^{\frac{7-p}{2}} \sinh \alpha}{r^{\frac{7-p}{2}}} \frac{dr^2}{f} + \frac{r_0^{\frac{7-p}{2}} \sinh \alpha}{r^{\frac{3-p}{2}}} d\Omega_{8-p}^2. \tag{3.5}$$

Along with the other field configurations this is the gravity dual of $(p+1)$-dimensional finite temperature $SU(N_c)$ SYM theory [76]. We shall use this as the background in the following for computing Wilson loops.

3.2.2 Q-$\bar{Q}$ potential

Let us recall that the $\mathcal{N}=4$ SYM theory spectrum does not include any quark. Hence, to compute the Q-$\bar{Q}$ interaction potential we need to introduce these quarks from the outside. On the gravity side this amounts to introducing open strings attached to D-branes. However, it must also be remembered that in heavy ion collision these quarks are not introduced externally but are rather produced in the collision itself. These quarks act as probes of the plasma. Going by the standard custom, we shall also assume the quarks to be infinitely heavy which ensures that the D-branes to which the open strings are attached are pushed all the way to the boundary of the space-time. On the gravity side, the open string acts as a probe implying that we ignore any back-reaction that the string (or the D-brane to which it is attached) may have upon the space-time sourced by the N_c Dp-branes. The string starts from a D-brane, hangs downwards along the radial direction, reaches a turning point from where it again rises upwards to terminate on the D-brane. The end-points of the string on the D-brane correspond to a quark and an antiquark in the fundamental representation. Let the line joining the end-points of the open string along the D-brane, i.e., the dipole lie along the x^1 direction and move with an arbitrary velocity $0 < v < 1$ along the x^p direction. Since the dipole lies perpendicular to its direction of propagation, p must be greater than one. Since we are interested in computing the potential of a moving mesonic bound state it turns out to be convenient to go to the rest frame of the Q-$\bar{Q}$ pair. This explicitly introduces the velocity parameter v into our calculations. To go to the rest frame $(t',\, x^{p\,\prime})$, we inflict a boost as,

$$\begin{aligned} dt &= \cosh\eta\, dt' - \sinh\eta\, (dx^p)' \\ dx^p &= -\sinh\eta\, dt' + \cosh\eta\, (dx^p)' \end{aligned} \tag{3.6}$$

where the boost parameter η is related to the dipole velocity v as $\tanh\eta = v$. Viewed from this frame the meson is static and the QGP is flowing with velocity v in the negative x^p direction. The Wilson loop lies in the t'-$x^{1\,\prime}$ plane and we denote the lengths as $\mathcal{T}$ and L respectively in those directions. We further assume $\mathcal{T} \gg L$ such that the string world-sheet is time-translation invariant. Using Eq. 3.6 in the metric of Eq. 3.5 we get,

$$\begin{aligned} ds^2 &= -A(r)dt^2 - 2B(r)dtdx^p + C(r)(dx^p)^2 + \frac{r^{\frac{7-p}{2}}}{r_0^{\frac{7-p}{2}}\sinh\alpha}\sum_{i=1}^{p-1}(dx^i)^2 \\ &\qquad + \frac{r_0^{\frac{7-p}{2}}\sinh\alpha}{r^{\frac{7-p}{2}}}\frac{dr^2}{f} + \frac{r_0^{\frac{7-p}{2}}\sinh\alpha}{r^{\frac{3-p}{2}}}d\Omega_{8-p}^2 \\ &\equiv G_{MN}dx^M dx^N \end{aligned} \tag{3.7}$$

where M, N are ten-dimensional space-time indices. We have also defined,

$$\begin{aligned}
A(r) &= \frac{r^{\frac{7-p}{2}}}{r_0^{\frac{7-p}{2}}\sinh\alpha}\left(1-\frac{r_0^{7-p}\cosh^2\eta}{r^{7-p}}\right),\\
B(r) &= \frac{r_0^{\frac{7-p}{2}}}{r^{\frac{7-p}{2}}\sinh\alpha}\sinh\eta\cosh\eta,\\
C(r) &= \frac{r^{\frac{7-p}{2}}}{r_0^{\frac{7-p}{2}}\sinh\alpha}\left(1+\frac{r_0^{7-p}\sinh^2\eta}{r^{7-p}}\right).
\end{aligned}$$

Also note that since we will be using the primed coordinates from now on, we have dropped the 'prime' in writing Eq. 3.7 for brevity. We will evaluate the world-sheet action (Eq. 2.11) using Eq. 2.10, with the static gauge condition $\tau = t$, $\sigma = x^1$, where $-L/2 \leq x^1 \leq L/2$ and $r = r(\sigma)$ and the x^i's $(i = 2, ..., p)$ are constants. $r(\sigma)$ is the string embedding we want to determine with the boundary condition, $r(\pm\frac{L}{2}) = r_0\Lambda$ where $r_0\Lambda$ denotes the location of the boundary. With the above gauge choice we have,

$$\mathcal{S} = \frac{\mathcal{T}}{2\pi\alpha'}\int_{-L/2}^{L/2} d\sigma\left[A(r)\left(\frac{r^{\frac{7-p}{2}}}{r_0^{\frac{7-p}{2}}\sinh\alpha} + \frac{r_0^{\frac{7-p}{2}}\sinh\alpha}{r^{\frac{7-p}{2}}}\frac{(\partial_\sigma r)^2}{f}\right)\right]^{\frac{1}{2}}. \tag{3.8}$$

At this point, we introduce new dimensionless quantities $y = r/r_0, \tilde{\sigma} = \sigma/(r_0\sinh\alpha)$, and $\ell = L/(r_0\sinh\alpha) = 4\pi LT/(7-p)$, where T is the Hawking temperature that can be obtained from the non-extremal Dp-brane metric in Eq. 3.1 as $T = (7-p)/(4\pi r_0\sinh\alpha)$ to recast Eq. 3.8 as,

$$\mathcal{S} = \frac{\mathcal{T}r_0}{\pi\alpha'}\int_0^{\ell/2} d\tilde{\sigma}\mathcal{L} = \frac{\mathcal{T}d_p^{\frac{1}{5-p}}\lambda^{\frac{1}{5-p}}(4\pi T)^{\frac{2}{5-p}}}{\pi(7-p)^{\frac{2}{5-p}}}\int_0^{\ell/2} d\sigma\mathcal{L} \tag{3.9}$$

where

$$\mathcal{L} = \sqrt{\left(y^{7-p}-\cosh^2\eta\right)\left(1+\frac{y'^2}{y^{7-p}-1}\right)} \tag{3.10}$$

with $y' = \partial y/\partial\sigma$. Here we exploited the fact that y is an even function of σ by symmetry. In the second expression in Eq. 3.9, we have omitted the 'tilde' in σ for brevity and invoked the AdS/CFT dictionary [76],

$$\begin{aligned} r_0^{7-p}\sinh^2\alpha &= d_p g_{\rm YM}^2 N_c \alpha'^{5-p} = d_p\lambda\alpha'^{5-p} \\ r_0\sinh\alpha &= \frac{7-p}{4\pi T} \end{aligned} \tag{3.11}$$

where $d_p = 2^{7-2p}\pi^{(9-3p)/2}\Gamma((7-p)/2)$ and we have taken $p < 5$¶. $y(\sigma)$ is determined by extremizing Eq. 3.9. Since the Lagrangian density in Eq. 3.10 does not depend explicitly on σ, it at once leads us to a conserved quantity

$$\mathcal{H} = \mathcal{L} - y'\frac{\partial\mathcal{L}}{\partial y'} = \frac{y^{7-p}-\cosh^2\eta}{\sqrt{\left(y^{7-p}-\cosh^2\eta\right)\left(1+\frac{y'^2}{y^{7-p}-1}\right)}} = \text{constant}. \tag{3.12}$$

In the following we distinguish between two cases: (i) $\cosh^{\frac{2}{7-p}}\eta < \Lambda$, whence, the action is real and the Wilson loop is time-like leading us to the Q-$\bar{Q}$ potential and the screening length. This will be the content of this section. (ii) $\cosh^{\frac{2}{7-p}}\eta > \Lambda$ so that the action is imaginary and the Wilson loop is light-like. From this case we compute $\hat{q}$. This case will be attended to in the next section. For $\cosh^{\frac{2}{7-p}}\eta < \Lambda$, let us denote the constant of motion in Eq. 3.12 as q and solve for y' as,

$$y' = \frac{1}{q}\sqrt{\left(y^{7-p}-1\right)\left(y^{7-p}-y_c^{7-p}\right)} \tag{3.13}$$

where $y_c^{7-p} = \cosh^2\eta + q^2 > 1$, denotes the largest turning point where y' vanishes. Integrating Eq. 3.13 at once yields the expression for the Q-$\bar{Q}$ separation in terms of the

¶We will mention about the cases $p = 5$ and 6 later.

integration constant q

$$2\int_0^{\ell/2} d\sigma = \ell(q) = 2q\int_{y_c}^{\infty} \frac{dy}{\sqrt{(y^{7-p}-1)\left(y^{7-p}-y_c^{7-p}\right)}} \tag{3.14}$$

where we have taken the boundary $\Lambda \to \infty$. In general, it is not possible to perform the above integration analytically and provide an analytical expression for $\ell(q)$. However, as we shall see shortly, for large rapidity η or large y_c, it is possible to analytically evaluate the above integral and obtain the form of L_{max}. Substituting y' from Eq. 3.13 into Eq. 3.9 along with Eq. 3.10 and inflicting a change of variables from σ to y, we have,

$$\mathcal{S}(\ell) = \frac{\mathcal{T} d_p^{\frac{1}{5-p}} \lambda^{\frac{1}{5-p}} (4\pi T)^{\frac{2}{5-p}}}{\pi(7-p)^{\frac{2}{5-p}}} \int_{y_c}^{\infty} dy \frac{y^{7-p}-\cosh^2\eta}{\sqrt{(y^{7-p}-1)\left(y^{7-p}-y_c^{7-p}\right)}} \tag{3.15}$$

where we have expressed $\mathcal{S}$ completely in terms of gauge theory parameters by invoking the gauge/string dictionary. A cursory glance reveals that the above action is divergent. In the dual gauge theory this implies that the bound state energy diverges. The reason for this divergence is, in fact, not far to seek. The bound state potential $E_{\text{tot}}(\ell)$ has two contributions. One, $E(\ell)$, arising due to the interaction between the quark and the antiquark while the other contribution stems from the self-energy terms, E_{self}, of the quark and the antiquark, which diverge. Since we are interested in finding out the interaction energy, we shall make use of the AdS/CFT dictionary,

$$e^{i(\mathcal{S}(\mathcal{C})-\mathcal{S}_0)} = \langle W(\mathcal{C})\rangle = e^{i\mathcal{T}(E_{\text{tot}}(\ell)-2E_{\text{self}})}. \tag{3.16}$$

Hence, to calculate $E(\ell)$ we must subtract from $\mathcal{S}$ the self-energy of the free quark-antiquark pair which, in the dual string picture translates to the action $\mathcal{S}_0$ corresponding to two disjoint strings hanging down radially,

$$\boxed{E(\ell) = \frac{\mathcal{S}(\ell) - \mathcal{S}_0}{\mathcal{T}}.} \tag{3.17}$$

To compute $\mathcal{S}_0$, we consider an open string along the radial direction, i.e., a single quark and use the static gauge condition $\tau = t$, $\sigma = r$, $x^p = x^p(\sigma)$ and $x^i =$ constant $(i = 2, ..., p)$. With these we evaluate the world-sheet action and multiply by 2 to get the contribution for two strings. From Eq. 2.11 we get in this case,

$$\mathcal{S}_0 = \frac{2\mathcal{T}}{2\pi\alpha'} \int_{r_0}^{\infty} dr \sqrt{\frac{r_0^{\frac{7-p}{2}} \sinh\alpha}{r^{\frac{7-p}{2}}} \frac{A(r)}{f} + \left(A(r)C(r) + B(r)^2\right).(x^{p\,\prime})^2}. \tag{3.18}$$

Note that the string stretches all the way up to the horizon r_0. Introducing new dimensionless variables as before $y = r/r_0$ and $z = x^p/(r_0 \sinh\alpha)$ and substituting r_0/α' in terms of the parameters of the gauge theory we get from Eq. 3.18,

$$\mathcal{S}_0 = \frac{\mathcal{T} d_p^{\frac{1}{5-p}} \lambda^{\frac{1}{5-p}} (4\pi T)^{\frac{2}{5-p}}}{\pi(7-p)^{\frac{2}{5-p}}} \int_1^{\infty} dy \sqrt{\frac{y^{7-p} - \cosh^2\eta}{y^{7-p} - 1} + \left(y^{7-p} - 1\right)\left(\frac{\partial z}{\partial y}\right)^2}. \tag{3.19}$$

which yields the equation of motion (with $\tilde{q}$ being a constant)

$$\left(\frac{\partial z}{\partial y}\right)^2 = \tilde{q}^2 \frac{y^{7-p} - \cosh^2\eta}{\left(y^{7-p} - 1\right)^2 \left(y^{7-p} - \tilde{q}^2 - 1\right)}. \tag{3.20}$$

Since y varies from 1 to ∞, the R.H.S. can, in general, be negative and unphysical for arbitrary values of η and $\tilde{q}$. Hence, to get physical solution we constrain the value of the constant as $\tilde{q} = \sinh\eta$ whence,

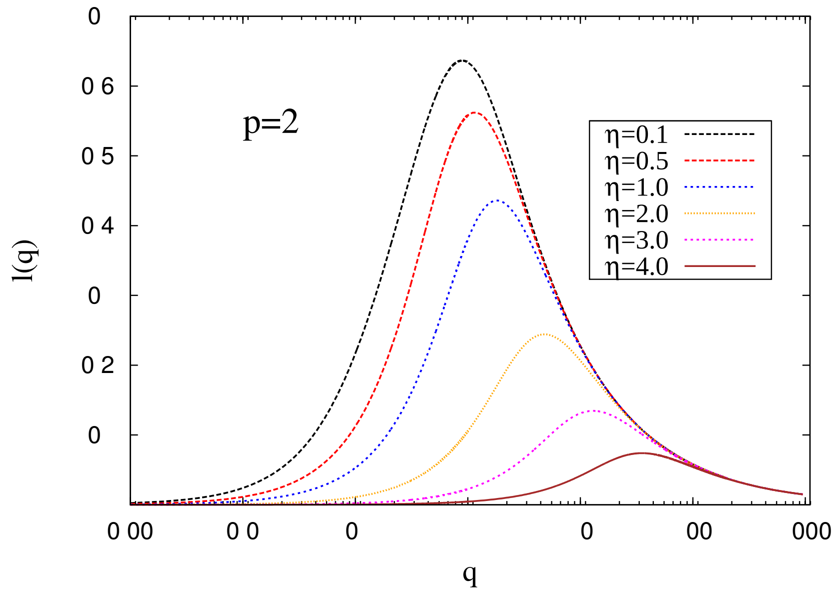

Figure 3.1: Q-$\bar{Q}$ separation ℓ as a function of q for $p=2$ at different rapidities η of the dipole

$$\frac{\partial z}{\partial y} = \frac{\sinh\eta}{(y^{7-p}-1)} \quad \Rightarrow \quad z(y) = \text{constant} - y\sinh\eta\ {}_2F_1\left(1, \frac{1}{7-p}, \frac{8-p}{7-p}; y^{7-p}\right) \tag{3.21}$$

where ${}_2F_1$ is the hypergeometric function. Plugging in $\partial z/\partial y$ into Eq. 3.19 we get

$$\mathcal{S}_0 = \frac{\mathcal{T} d_p^{\frac{1}{5-p}} \lambda^{\frac{1}{5-p}} (4\pi T)^{\frac{2}{5-p}}}{\pi(7-p)^{\frac{2}{5-p}}} \int_1^\infty dy \tag{3.22}$$

So, the quarkonium bound state potential in Eq. 3.17 has the form,

$$E(\ell) = \frac{d_p^{\frac{1}{5-p}} \lambda^{\frac{1}{5-p}} (4\pi T)^{\frac{2}{5-p}}}{\pi(7-p)^{\frac{2}{5-p}}} \left[\int_{y_c}^\infty dy \left(\frac{y^{7-p} - \cosh^2\eta}{\sqrt{(y^{7-p}-1)(y^{7-p}-y_c^{7-p})}} - 1\right) + 1 - y_c\right]. \tag{3.23}$$

The integration appearing in Eq. 3.23 is not amenable to analytical handling. Hence, we

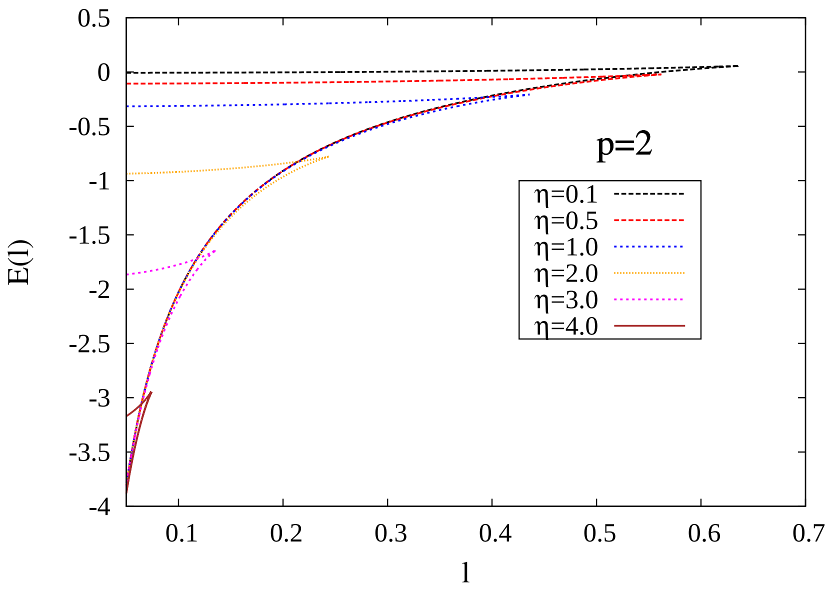

Figure 3.2: Normalized Q-$\bar{Q}$ potential $E(\ell)$ as a function of ℓ for $p = 2$ at the same set of rapidities (as in Figure 3.1)

first plot $\ell(q)$-q for fixed values of η from Eq. 3.14 which can then be numerically inverted to obtain q as a function of ℓ. Plugging in this in Eq. 3.23 we plot $E(\ell)$-ℓ. We provide the plots for $p = 2$, 4 and 5 in Figures 3.1-3.6 respectively. Also, for comparison among the different p's we give the plots of $\ell(q)$-q and $E(\ell)$-ℓ in Figures 3.7 and 3.8 respectively at $\eta = 1$ (which corresponds to $v = 0.76$). We have previously constrained p to be less than 5. This is because the constant (expressed in terms of the parameters of the gauge theory by Eq. 3.11) in front of the second expression in Eq. 3.9 is ill-defined for $p = 5$. But no such problem arises if we continue with r_0 and α'. This may be an indication that in this case complete decoupling does not occur. However, we can still plot $\ell(q)$-q and $E(\ell)$-ℓ keeping the constant in terms of the gravity parameters. For $p = 6$, it is known that the decoupling does not occur and so, we do not consider the $p = 6$ case here. The general features of the plots for $p = 2$ and 4 remain very similar (although the details, as shown in Figures 3.7 and 3.8, are quite different) to the $p = 3$ case discussed in [70, 74]. It is clear from Eq. 3.14 that as $q \to 0$, $\ell \sim q$ for all p, whereas for large q, we find $\ell \sim q^{-(5-p)/(7-p)}$ for $p < 5$. However, for $p = 5$, ℓ goes to a constant for large q. These can be seen in Figures 3.1-3.6. Also, for $p < 5$, the plots bear out that the Q-$\bar{Q}$ separation has a maximum ℓ_{max} beyond which there is no solution to Eq. 3.14. From Figures 3.1 and 3.3 we see that the peak of the $\ell(q)$ curve reduces and shifts towards right, i.e., towards a larger value of q as we increase η. From Figure 3.7, we see that at a fixed value of η, the peak reduces as we increase p and shifts towards left, i.e., towards a lower value of q. As $\ell(q)$ decreases from ℓ_{max}, there are two dipoles at a fixed ℓ for two different values of q. The Q-$\bar{Q}$ potential, in general, decreases with increasing values of η at each p and has two branches corresponding to the two values of q. The smaller value of q corresponds to the upper branch and has higher energy, whereas the larger value of q corresponds to the lower branch and has lower energy. So, the dipole with lower q will be metastable and will go to the state with higher q as it is energetically more favorable. Also, there exists a critical $\eta = \eta_c$ above which the whole upper branch of the $E(\ell)$ curve is negative. But for $\eta < \eta_c$ the $E(\ell)$ curve crosses zero at $\ell = \ell_c$, continues to rise till $\ell = \ell_{max}$ and turns back crossing zero again at $\ell = \ell'_c > \ell_c$. Below ℓ_c, the upper branch is metastable. A dipole on the upper branch on slight perturbation will come down to the lower branch. At $\ell = \ell_c$, the dipole in the upper branch and the two isolated string configurations (or dissociated quark and antiquark) have the same energy. So, both the states can coexist. However, with slight disturbance it will settle down to the dipole in the lower branch. In the regime $\ell_c < \ell < \ell'_c$ the upper branch has positive energy while the lower one has negative energy. So a dipole sitting on the upper branch, when perturbed, may either come down and settle in the lower branch or it may dissociate into a free quark-antiquark pair. At $\ell = \ell'_c$, the dipole in the lower branch and the two isolated string states (or dissociated quark and antiquark) can

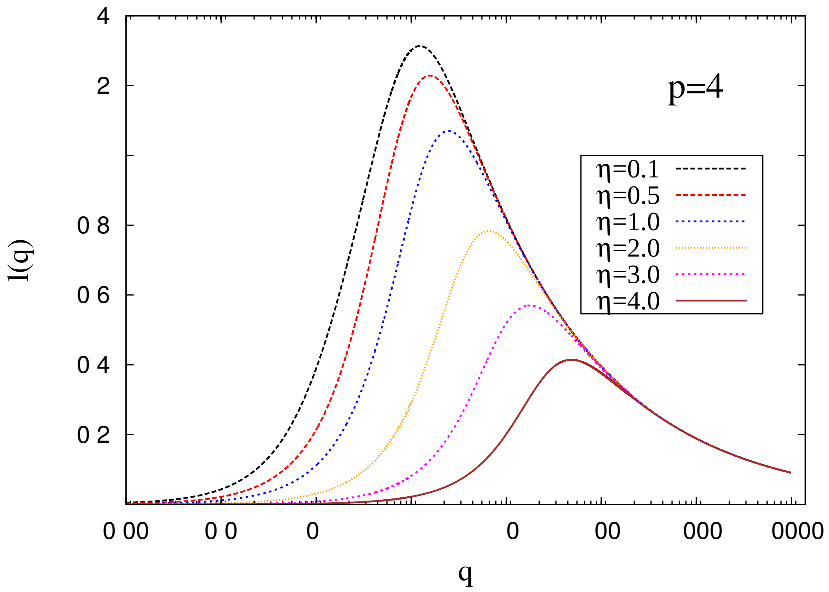

Figure 3.3: Q-$\bar{Q}$ separation ℓ as a function of q for $p = 4$ at different rapidities η of the dipole

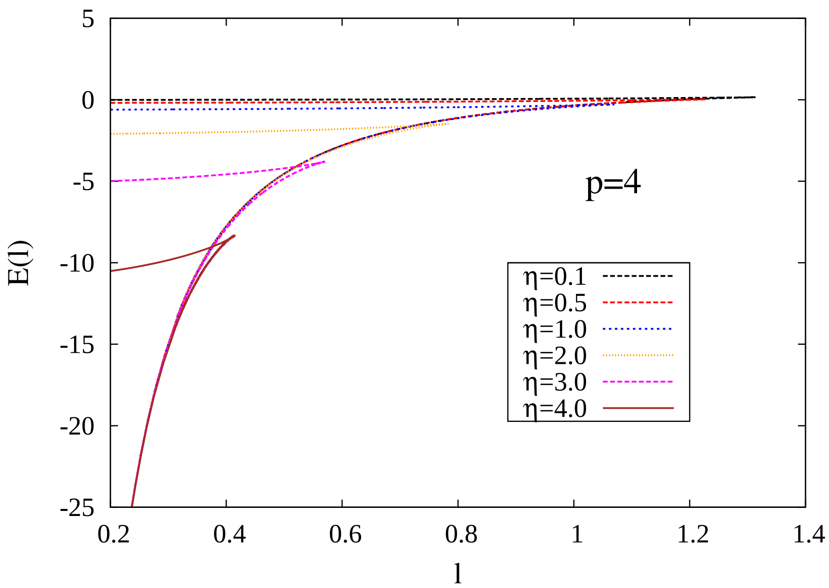

Figure 3.4: Normalized Q-$\bar{Q}$ potential $E(\ell)$ as a function of ℓ for $p = 4$ at the same set of rapidities (as in Figure 3.3)

coexist and both are stable configurations. In the domain $\ell_c' < \ell < \ell_{max}$ both the branches have positive energy and so a dipole sitting on either of them will dissociate when slightly disturbed. Beyond ℓ_{max} no dipole will be formed at all. Some of these features were mentioned in [70, 74] for $p = 3$, but here we find that these features continue to hold for the $p = 2$ and 4 cases as well. For $p = 5$, since there is no maximum for $\ell(q)$ plot, there is no lower branch in the $E(\ell)$-ℓ plot. The plot of $E(\ell)$ for different values of p are given in Figure 3.8 for comparison.

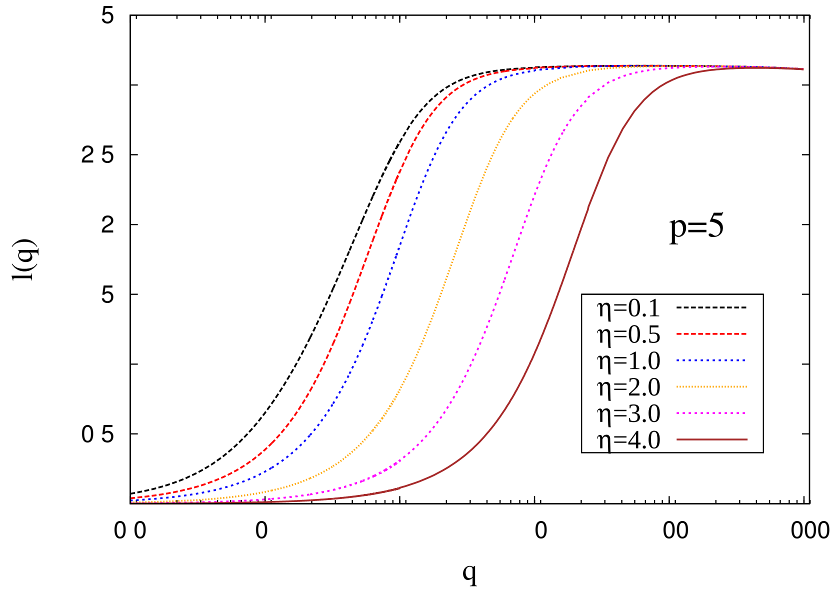

Figure 3.5: Q-$\bar{Q}$ separation ℓ as a function of q for $p = 5$ at different rapidities η of the dipole

We had mentioned that, in general, it is not feasible to arrive at an analytical expression for $\ell(q)$. However, for large η or large y_c, we can expand $\ell(q)$ in powers of $1/y_c$ as,

$$\begin{aligned}\ell(q) &= 2q\int_{y_c}^{\infty}\frac{dy}{y^{\frac{7-p}{2}}(y^{7-p}-y_c^{7-p})^{\frac{1}{2}}}+q\int_{y_c}^{\infty}\frac{dy}{y^{\frac{3(7-p)}{2}}(y^{7-p}-y_c^{7-p})^{\frac{1}{2}}}\\ &\quad+\frac{3q}{4}\int_{y_c}^{\infty}\frac{dy}{y^{\frac{5(7-p)}{2}}(y^{7-p}-y_c^{7-p})^{\frac{1}{2}}}+\cdots. \end{aligned} \tag{3.24}$$

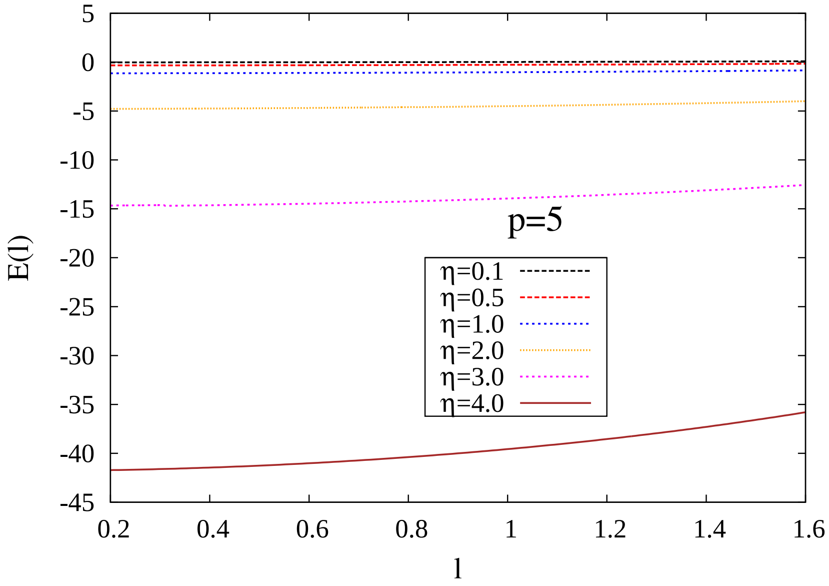

Figure 3.6: Normalized Q-$\bar{Q}$ potential $E(\ell)$ as a function of ℓ for $p = 5$ at the same set of rapidities (as in Figure 3.5)

The above integrations can be handled analytically, and we have the following expressions of $\ell(q)$ for $p = 2,\ 3$ and 4,

$$\ell(q)^{p=2} = \frac{2q\sqrt{\pi}}{5y_c^4}\left[\frac{\Gamma(\frac{4}{5})}{\Gamma(\frac{13}{10})} + \frac{\Gamma(\frac{9}{5})}{10\Gamma(\frac{23}{10})}\frac{1}{y_c^5} + \frac{3\Gamma(\frac{14}{5})}{8\Gamma(\frac{33}{10})}\frac{1}{y_c^{10}} + \cdots\right], \tag{3.25}$$

$$\ell(q)^{p=3} = \frac{2q\sqrt{\pi}}{y_c^3}\left[\frac{\Gamma(\frac{3}{4})}{\Gamma(\frac{1}{4})} + \frac{\Gamma(\frac{7}{4})}{8\Gamma(\frac{9}{4})}\frac{1}{y_c^4} + \frac{3\Gamma(\frac{11}{4})}{32\Gamma(\frac{13}{4})}\frac{1}{y_c^8} + \cdots\right], \tag{3.26}$$

$$\ell(q)^{p=4} = \frac{4q\sqrt{\pi}}{y_c^2}\left[\frac{\Gamma(\frac{2}{3})}{\Gamma(\frac{1}{6})} + \frac{\Gamma(\frac{5}{3})}{12\Gamma(\frac{13}{6})}\frac{1}{y_c^3} + \frac{\Gamma(\frac{8}{3})}{16\Gamma(\frac{19}{6})}\frac{1}{y_c^6} + \cdots\right]. \tag{3.27}$$

Truncating the series up to the second term we can calculate ℓ_{max} as,

$$\begin{aligned}\ell_{max}^{p=2} &= \frac{2\cdot 3^{3/10}\sqrt{\pi}\Gamma(\frac{4}{5})}{8^{4/5}\sqrt{5}\Gamma(\frac{13}{10})}\left[\frac{1}{\cosh^{\frac{3}{5}}\eta} + \frac{3}{130}\frac{1}{\cosh^{\frac{13}{5}}\eta} + \cdots\right] \qquad (3.28)\\ &= 0.54\left[\frac{1}{\cosh^{\frac{3}{5}}\eta} + \frac{3}{130}\frac{1}{\cosh^{\frac{13}{5}}\eta} + \cdots\right],\end{aligned}$$

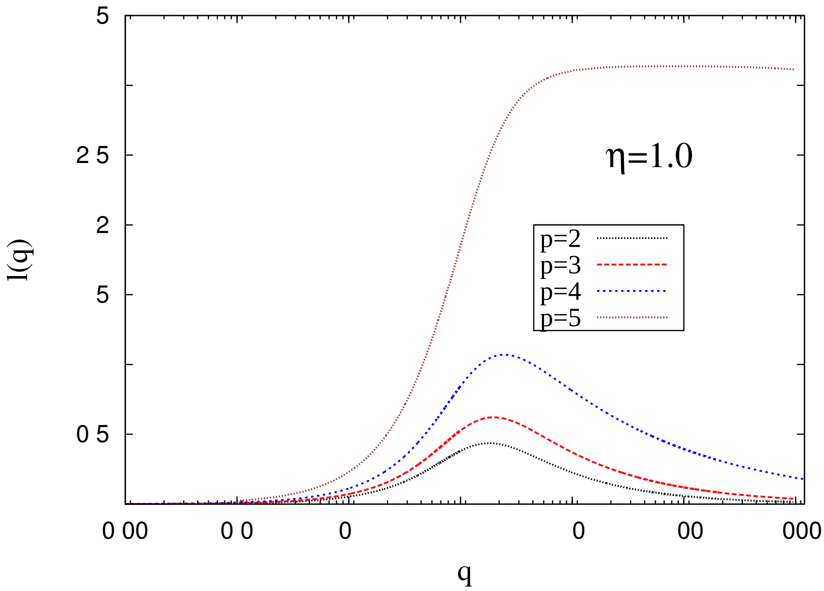

Figure 3.7: Q-$\bar{Q}$ separation ℓ as a function of q for different values of p at $\eta = 1.0$

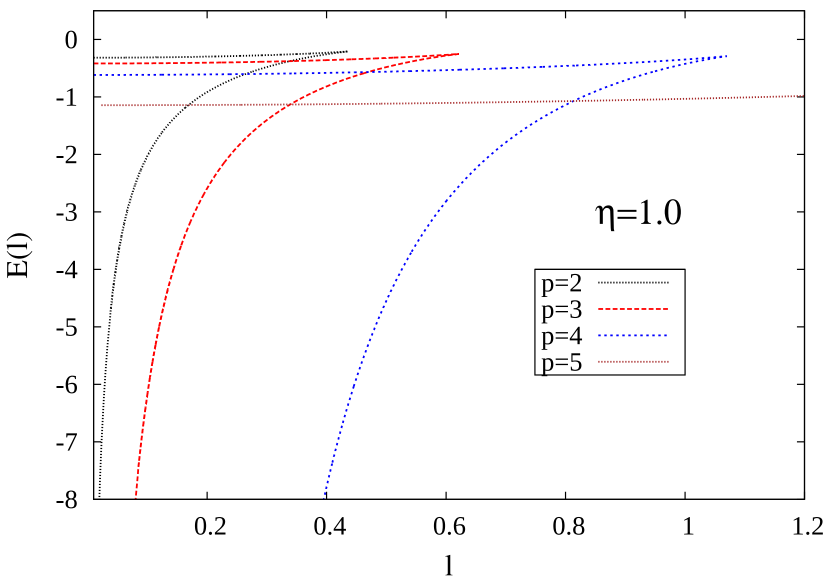

Figure 3.8: Q-$\bar{Q}$ potential as a function of ℓ for different values of p at $\eta = 1.0$

$$\begin{aligned}
\ell_{max}^{p=3} &= \frac{2\sqrt{2\pi}\Gamma(\frac{3}{4})}{3^{3/4}\Gamma(\frac{1}{4})}\left[\frac{1}{\cosh^{\frac{1}{2}}\eta}+\frac{1}{10}\frac{1}{\cosh^{\frac{5}{2}}\eta}+\cdots\right] \qquad (3.29)\\
&= 0.74\left[\frac{1}{\cosh^{\frac{1}{2}}\eta}+\frac{1}{10}\frac{1}{\cosh^{\frac{5}{2}}\eta}+\cdots\right],\\
\ell_{max}^{p=4} &= \frac{4^{1/3}\sqrt{3\pi}\Gamma(\frac{2}{3})}{\Gamma(\frac{1}{6})}\left[\frac{1}{\cosh^{\frac{1}{3}}\eta}+\frac{1}{14}\frac{1}{\cosh^{\frac{7}{3}}\eta}+\cdots\right] \qquad (3.30)\\
&= 1.18\left[\frac{1}{\cosh^{\frac{1}{3}}\eta}+\frac{1}{14}\frac{1}{\cosh^{\frac{7}{3}}\eta}+\cdots\right].
\end{aligned}$$

The quantity $L_{max} = (7-p)\ell_{max}/(4\pi T)$ can be thought of as the screening length of the dipole in the medium since this is the maximum value of L beyond which we have two dissociated quark and antiquark or two disjoint world-sheet corresponding to $E(L) = 0$. It has been pointed out in [70, 74] for $p = 3$ that if we set $\eta = 0$ in the above result, then Eq. 3.29, which was derived for large η, is not too far off from the actual result at $\eta = 0$ and so the screening length decreases with increasing velocity according to the scaling $L_{max}^{p=3}(v) \simeq L_{max}^{p=3}(0)/\cosh^{1/2}\eta = L_{max}^{p=3}(0)/\sqrt{\gamma}$, where $\gamma = 1/\sqrt{1-v^2}$. By looking at the similarity of the behavior of $\ell(q)$ and $E(\ell)$ for $p = 2,\ 4$, with $p = 3$, we may conclude that similar behavior will also hold true for $p = 2,\ 4$ as well. The velocity-dependence of the screening lengths thus assumes the following forms for different values of p,

$$\begin{aligned}
L_{max}^{p=2}(v) &\simeq \frac{L_{max}^{p=2}(0)}{\cosh^{\frac{3}{5}}\eta} = \frac{L_{max}^{p=2}(0)}{\gamma^{\frac{3}{5}}}, \qquad (3.31)\\
L_{max}^{p=3}(v) &\simeq \frac{L_{max}^{p=3}(0)}{\cosh^{\frac{1}{2}}\eta} = \frac{L_{max}^{p=3}(0)}{\gamma^{\frac{1}{2}}}, \qquad (3.32)\\
L_{max}^{p=4}(v) &\simeq \frac{L_{max}^{p=4}(0)}{\cosh^{\frac{1}{3}}\eta} = \frac{L_{max}^{p=4}(0)}{\gamma^{\frac{1}{3}}}. \qquad (3.33)
\end{aligned}$$

The velocity-scaling of the screening length as found out above does have significant phenomenological consequences. If such a scaling does really hold for QCD in heavy ion collisions then it should have qualitative bearing upon dissociation of quarkonia states like J/Ψ [70]. Let us elaborate on this with a specific illustration. Consider, for instance, the explanation of J/Ψ suppression observed in SPS and RHIC as proposed in [44, 77]. Lattice computations of Q-$\bar{Q}$ potential suggest that $J/\Psi(1s)$ dissociates at a temperature $T_d \sim 2.1T_c$ whereas the states $\chi_c(2p)$ and $\Psi'(2s)$ melt at $T_d \sim 1.2T_c$. Hence, if collisions at SPS and RHIC attain a temperature T such that $1.2T_c < T < 2.1T_c$ then the anomalous suppression of J/Ψ can be attributed to the complete loss of the "secondary" J/Ψ's that arise from the decay of excited states rather than the dissociation of the original J/Ψ themselves. Now for $p = 3$ we find that the screening length scales with velocity as $L_{max} \sim \gamma^{-\frac{1}{2}}$. Then, roughly speaking, the temperature T_d required to dissolve the bound state should also scale as $T_d \sim \gamma^{-\frac{1}{2}}$. This points to the fact that J/Ψ suppression may witness a sharp increase (from the melting of actual J/Ψ's themselves) for J/Ψ's with transverse momentum p_T that is at most ~ 9 GeV. If the temperature at RHIC reaches around $1.5T_c$ then the same suppression can be observed at a lower threshold of $p_T \sim 5$ GeV. This range of energy where such quarkonium suppression may take place lies well within the range of future runs at RHIC and will be studied intensely at LHC for both J/Ψ and Upsilon channels.

It was pointed out in [71] that in the large η limit one generically has,

$$L_{max} \propto \frac{1}{\epsilon(\eta)^{\nu}} \tag{3.34}$$

where $\epsilon(\eta) = \cosh^{\frac{1}{2}} \epsilon(0)$ is the boosted energy density. In particular, for any gauge theory that is dual to asymptotically AdS_5 geometry one finds $\nu = 4$. For non-conformal theories this scaling index can deviate from $1/4$. This is exactly what we find here for L_{max} for the cases $p = 2$ and 4. So the bottom line of the above computation is that when the heavy meson is moving with an ultra-relativistic velocity v then the screening length L_{max} decreases. The dependence of L_{max} upon v has been found out here in various space dimensions. The suppression in screening length points to the fact that when the quarkonium is moving through the plasma with a large momentum (which is most likely to be the case) then it is more prone to dissociation than when it is static and a marked increase in quarkonium suppression is expected.

3.3 Jet Quenching Parameter

So far in our discussion we assumed that the rapidity η is finite and $\cosh^{\frac{2}{7-p}} \eta < \Lambda$. So, the velocity of the string is in the range $0 < v < 1$ and the Wilson loop is time-like. Now we will consider case $\cosh^{\frac{2}{7-p}} \eta > \Lambda$. In order to extract the jet quenching parameter we take $\eta \to \infty$ or $v \to 1$, so that the Wilson loop is light-like and then take $\Lambda \to \infty^{\|}$. Note from Eq. 3.9 that since now $\cosh^{\frac{2}{7-p}} \eta > \Lambda$, the action is imaginary and we write the second expression in Eq. 3.9 as,

$$\mathcal{S} = i \frac{\mathcal{T} d_p^{\frac{1}{5-p}} \lambda^{\frac{1}{5-p}} (4\pi T)^{\frac{2}{5-p}}}{\pi (7-p)^{\frac{2}{5-p}}} \int_0^{\ell/2} d\sigma \mathcal{L} \tag{3.35}$$

where

$$\mathcal{L} = \sqrt{\left(\cosh^2 \eta - y^{7-p}\right) \left(1 + \frac{y'^2}{y^{7-p} - 1}\right)}. \tag{3.36}$$

$^{\|}$We will be brief here since the jet quenching parameter for $(p+1)$-dimensional Yang-Mills theory has already been given in [74, 75]. But here we obtain it by taking the $v \to 1$ limit of the time-like Wilson loop as was done there for the $p = 3$ case.

Absence of any explicit σ-dependence at once leads to

$$\mathcal{H} = \mathcal{L} - y'\frac{\partial \mathcal{L}}{\partial y'} = \text{constant} \quad \Rightarrow \quad \frac{\cosh^2\eta - y^{7-p}}{\sqrt{(\cosh^2\eta - y^{7-p})\left(1 + \frac{y'^2}{y^{7-p}-1}\right)}} = q_0 \tag{3.37}$$

where we have denoted the constant as q_0. Eq. 3.37 can be solved for y' as,

$$y' = \frac{1}{q_0}\sqrt{(y^{7-p}-1)(y_m^{7-p} - y^{7-p})} \tag{3.38}$$

where $y_m^{7-p} = \cosh^2\eta - q_0^2$. On integration Eq. 3.38 gives us,

$$\ell = 2q_0 \int_1^{\Lambda} \frac{dy}{\sqrt{(y_m^{7-p} - y^{7-p})(y^{7-p}-1)}}. \tag{3.39}$$

Substituting the value of y' from Eq. 3.38 into Eq. 3.35 we get,

$$\mathcal{S}(\ell) = i\frac{\mathcal{T} d_p^{\frac{1}{5-p}} \lambda^{\frac{1}{5-p}} (4\pi T)^{\frac{2}{5-p}}}{\pi(7-p)^{\frac{2}{5-p}}} \int_1^{\Lambda} dy \frac{\cosh^2\eta - y^{7-p}}{\sqrt{(y_m^{7-p} - y^{7-p})(y^{7-p}-1)}}. \tag{3.40}$$

When η is large, ℓ in Eq. 3.39 permits an expansion as follows,

$$\ell = \frac{2q_0}{\cosh\eta}\int_1^{\Lambda} \frac{dy}{\sqrt{y^{7-p}-1}} + \mathcal{O}\left(\frac{q_0^3}{\cosh^3\eta}, \frac{\Lambda^{7-p}}{\cosh^3\eta}\right). \tag{3.41}$$

Next, with $\eta \to \infty$, the second term in Eq. 3.41 drops out and taking $\Lambda \to \infty$ we get,

$$\ell = \frac{2q_0}{\cosh\eta} a_p, \qquad \text{with,} \quad a_p = \frac{2}{5-p}\sqrt{\pi}\frac{\Gamma\left(1 + \frac{5-p}{2(7-p)}\right)}{\Gamma\left(\frac{6-p}{7-p}\right)}. \tag{3.42}$$

Further, since L is much smaller than the other length dimensions of the problem, $\ell = (4\pi LT)/(7-p) \ll 1$ implying $q_0 = (\ell \cosh\eta)/(2a_p) \ll 1$. In this limit, $\mathcal{S}(\ell)$ in Eq. 3.40 can be expanded as,

$$\mathcal{S}(\ell) = \mathcal{S}^{(0)} + q_0^2 \mathcal{S}^{(1)} + \mathcal{O}(q_0^4) \tag{3.43}$$

where

$$\mathcal{S}^{(0)} = i\frac{\mathcal{T} d_p^{\frac{1}{5-p}} \lambda^{\frac{1}{5-p}} (4\pi T)^{\frac{2}{5-p}}}{\pi (7-p)^{\frac{2}{5-p}}} \int_1^{\Lambda} dy \frac{\cosh^2\eta - y^{7-p}}{\sqrt{y^{7-p}-1}} \tag{3.44}$$

$$\begin{aligned} q_0^2 \mathcal{S}^{(1)} &= i\frac{\mathcal{T} d_p^{\frac{1}{5-p}} \lambda^{\frac{1}{5-p}} (4\pi T)^{\frac{2}{5-p}}}{\pi (7-p)^{\frac{2}{5-p}}} q_0^2 \int_1^{\Lambda} \frac{dy}{\sqrt{(y^{7-p}-1)(\cosh^2\eta - y^{7-p})}} \\ &\simeq -i\frac{(\mathcal{T}\cosh\eta) d_p^{\frac{1}{5-p}} \lambda^{\frac{1}{5-p}} L^2}{8\pi a_p} \left(\frac{4\pi T}{7-p}\right)^{\frac{2(6-p)}{5-p}} . \end{aligned} \tag{3.45}$$

From physical expectation it has been argued in [74] that as ℓ or q_0 goes to zero, $\mathcal{S}^{(0)}$ is the self-energy of two dissociated quark and antiquark or the area of two disjoint world-sheet. $\mathcal{T}\cosh\eta$ in Eq. 3.45 can be identified as $L^-/\sqrt{2}$, where L^- is the length of the Wilson loop in the light-like direction. Invoking Eqs. 2.4 and 2.45 we obtain

$$\boxed{\langle W(\mathcal{C})\rangle = e^{2i(\mathcal{S}(\mathcal{C}) - \mathcal{S}_0)} = e^{-\frac{1}{4\sqrt{2}}\hat{q} L^- L^2}} \tag{3.46}$$

where the factor of two in the exponent in the second expression is due to the fact that for evaluating the jet quenching parameter we need to compute the expectation value of the adjoint Wilson loop, whereas, here we have actually found out the expectation value of a fundamental Wilson loop. The third expression is valid for $L \ll 1$[**]. Thus from Eq. 3.46 and using Eq. 3.45 we extract the value of the jet quenching parameter as,

$$\hat{q} = -i\frac{8\sqrt{2}\left(\mathcal{S}(\ell) - \mathcal{S}^{(0)}\right)}{L^- L^2} = \frac{d_p^{\frac{1}{5-p}} \lambda^{\frac{1}{5-p}}}{\pi a_p} \left(\frac{4\pi T}{7-p}\right)^{\frac{2(6-p)}{5-p}} . \tag{3.47}$$

Substituting the explicit values of a_p and d_p given earlier it takes the form,

$$\hat{q} = \frac{4T^2 \left[2^{7-2p}\pi^{\frac{9-3p}{2}}\Gamma\left(\frac{7-p}{2}\right)\right]^{\frac{1}{5-p}} (4\pi)^{\frac{7-p}{5-p}}\Gamma\left(\frac{6-p}{7-p}\right)}{\sqrt{\pi}\Gamma\left(\frac{5-p}{14-2p}\right)(7-p)^{\frac{7-p}{5-p}}} \left(T\sqrt{\lambda}\right)^{\frac{2}{5-p}} . \tag{3.48}$$

It can be easily verified that by defining an effective dimensionless coupling constant $\lambda_{\text{eff}} = \lambda T^{p-3}$ at temperature T, as given in [74], the above expression can be recast as,

$$\hat{q} = \frac{8\sqrt{\pi}\Gamma\left(\frac{6-p}{7-p}\right)}{\Gamma\left(\frac{5-p}{14-2p}\right)} b_p^{\frac{1}{2}} \lambda_{\text{eff}}^{\frac{p-3}{2(5-p)}}(T)\sqrt{\lambda_{\text{eff}}(T)}\,T^3 \equiv \sqrt{a(\lambda_{\text{eff}})}\,\sqrt{\lambda_{\text{eff}}}T^3 \tag{3.49}$$

where $b_p^{(5-p)/2} = [2^{16-3p}\pi^{(13-3p)/2}\Gamma((7-p)/2)]/[(7-p)^{7-p}]$ and $a(\lambda_{\text{eff}})$ characterizes the number of degrees of freedom at temperature T.

3.4 Conclusion

To conclude, in this chapter using the gauge/string duality and the Maldacena prescription we have computed expectation values of special Wilson loops in $(p+1)$-dimensional strongly coupled SYM theory and related them to observables of QGP obtained in heavy ion experiments. We have considered both time-like and light-like Wilson loops. From time-like Wilson loops we obtained the Q-$\bar{Q}$ separation (Eq. 3.14) and the velocity-

[**]This is automatically satisfied since in the limit $v \to 1$ for the constant q_0 to be finite L has to approach zero.

dependent Q-$\bar{Q}$ potential (Eq. 3.23) when the quarkonium moves through the plasma with an arbitrary velocity $v < 1$ and plotted the relevant functions in Figures 3.1-3.6. We further obtained the form of the screening length and its velocity-dependence in Eqs. 3.31-3.33. By taking the $v \to 1$ limit, the time-like Wilson loop reduces to a light-like one and from there we obtained the jet quenching parameter in $(p+1)$-dimensional SYM theory. In the next chapter we use these techniques to perform similar computations in the first of our anisotropic models - the non-commutative Yang-Mills theory at finite temperature and strong 't Hooft coupling and explore the effect of non-commutativity (or anisotropy) on the heavy quark observables.

CHAPTER 4

HEAVY QUARKS IN NON-COMMUTATIVE HOT SUPER YANG-MILLS PLASMA

4.1 Introduction

In the previous chapter we have learnt to compute expectation values of Wilson loops that contain a wealth of information about various properties of quark-gluon plasma. We have learnt to relate the expectation values to various heavy quark observables like the bound state interaction potential, the screening length and the jet quenching parameter. In this chapter, we examine the first of our anisotropic models - the thermal non-commutative Yang-Mills theory at strong 't Hooft coupling and large number of colors*. The purpose of studying non-commutative gauge theory is 3-fold†. Firstly, in NCYM plasma the presence

*The present chapter is based on [78, 79].

†Space-time non-commutativity is an old idea introduced first by Heisenberg and Pauli [80] in order to evade the infinities in quantum field theory before renormalization was successful. It was Snyder [81] and then Connes who took the idea seriously. Connes along with Chamseddine [82] even introduced non-commutative geometry as a generalization to Riemannian geometry and obtained gauge theory as a companion to general relativity giving rise to a true geometric unification. In this framework parameters of the

of non-commutativity reduces the symmetry of the theory from $SO(3)$ to $SO(2)$ rendering the theory anisotropic. Hence, NCYM theory can serve as an interesting playground for exploring the effects of anisotropy. The presence of non-commutativity singles out a particular direction in space respecting a remnant $SO(2)$ symmetry in the transverse, non-commutative plane. In the context of heavy ion collisions, this particular direction may be thought of as the beam direction. Secondly, NCYM is interesting in its own right since it arises quite naturally in string theory [83–85] and M-theory [86] and it is of interest to see how non-commutativity affects the different observables. Thirdly, a consistent gauge theory can indeed be formulated in non-commutative space-time. Even though, so far, its existence has not been detected in low energy, one can not rule out the possibility that its effect may be manifested at extremely high energy scale, where the fabric of space-time itself may be modified. The experimental lower bound on the non-commutativity scale reported in the literature [87] usually gives a very small effect and is hard to detect. So, it is desirable to search for its effect in alternative channels. High energy heavy ion collision offers one such arena and it may be worthwhile to look whether it can provide a better window for the effect of non-commutativity to be observed[‡]. Driven by these motivations we perform a similar type of computation of Wilson loops in thermal NCYM plasma. The plan of the present chapter is as follows: In §4.2 we explain the dual string theory background that we shall use for performing the computations. §4.3 is devoted to the computation of the jet quenching parameter $\hat{q}_{\rm NCYM}$ in strongly coupled NCYM plasma in $(3+1)$-dimensions using light-cone coordinates. The effects of non-commutativity upon $\hat{q}_{\rm NCYM}$ are studied

standard model appear as geometric invariants.

[‡]One might wonder how would space-time non-commutativity appear in heavy ion collision in the first place? It is known that one of the mechanisms for the appearance of spatial non-commutativity is the presence of an intense magnetic field in the background. It has been shown in both analytic calculations [88] and numerical simulations [89] that such an intense magnetic field is indeed possible in heavy ion collision in RHIC (or in LHC). So, it may be quite relevant to consider such a possibility in the present context.

for both small and large values of θ, the non-commutativity parameter, and attempt is made to connect the results to the recent collider data by giving some numerical estimates. In §4.4 we find out the potential of heavy quarkonia using holographic techniques with the velocity v and the non-commutativity θ as parameters. The results are compared with the known commutative case. An analytic expression for the screening length is obtained in a restricted domain of the parameter space. The limit $v \to 1$ is considered from which the expression for the jet quenching parameter $\hat{q}_{\rm NCYM}$ is extracted. Finally, we conclude in §4.5 with a summary of the results obtained.

4.2 Gravity Dual to Thermal NCYM Plasma

A particular form of anisotropy is manifested in non-commutative gauge theories. In this chapter we consider the 4-dimensional maximally supersymmetric $SU(N_c)$ Yang-Mills theory living on $\mathbb{R}^{1,1} \times \mathbb{R}^2_\theta$. The non-commutativity parameter is non-vanishing only in the $\mathbb{R}^2_\theta$-plane which defined by the Moyal algebra,

$$[x^2, x^3] = i\theta \tag{4.1}$$

where x^2, x^3 define the coordinates along the non-commutative gauge theory directions. The gravity dual to NCYM theory is given by a particular decoupling limit [84, 85] of non-extremal (D1,D3) bound state of type IIB string theory. (D1,D3) bound state [90, 91] contains a non-zero B-field that becomes asymptotically very large in the decoupling limit and sources space-space non-commutativity [83]. The non-extremal (D1,D3) bound state solution of type IIB string theory is given by the following metric (in the string frame), the dilaton ϕ, the NS-NS B-field and the R-R form fields [91],

$$\begin{aligned}
ds^2 &= H^{-\frac{1}{2}}\left(-f(dt)^2+(dx^1)^2+\frac{H}{F}\left((dx^2)^2+(dx^3)^2\right)\right)+H^{\frac{1}{2}}\left(\frac{dr^2}{f}+r^2d\Omega_5^2\right) \\
e^{2\phi} &= g_s^2\frac{H}{F}, \qquad B_{23}=\frac{\tan\alpha}{F} \\
A_{01} &= \frac{1}{g_s}(H^{-1}-1)\sin\alpha\coth\varphi, \qquad A_{0123}=\frac{1}{g_s}\frac{(1-H)}{F}\cos\alpha\coth\varphi+\mathrm{T.T.}
\end{aligned} \tag{4.2}$$

where the various functions appearing above are,

$$f=1-\frac{r_0^4}{r^4}, \qquad H=1+\frac{r_0^4\sinh^2\varphi}{r^4}, \qquad F=1+\frac{r_0^4\cos^2\alpha\sinh^2\varphi}{r^4}. \tag{4.3}$$

The D3-branes span x^1, x^2 and x^3 directions while the D1-branes lie along x^1. α measures the relative number of D1 and D3 branes through $\cos\alpha = N/\sqrt{N^2+M^2}$, with N being the number of D3-branes and M the number of D1-branes per unit codimension two surface transverse to D1-branes [92]. φ is the boost parameter, r_0 denotes the horizon of the non-extremal (D1,D3) bound state and g_s is the string coupling constant. A_{01} and A_{0123} are R-R form fields corresponding to D1-brane and D3-brane respectively. T.T. denotes a term, involving transverse part of the brane to make the field-strength self-dual, whose explicit form is not required for our discussion. B_{23} is the NS-NS form responsible for the appearance of non-commutativity in the decoupling limit. The NCYM decoupling limit is a low energy limit for which we zoom into the region [84],

$$r_0 < r \sim r_0\sqrt{\sinh\varphi\cos\alpha} \ll r_0\sqrt{\sinh\varphi}. \tag{4.4}$$

In this limit φ is a large parameter and α is close to $\pi/2$ so that,

$$H \approx \frac{r_0^4 \sinh^2 \varphi}{r^4}, \qquad \frac{H}{F} \approx \frac{1}{\cos^2 \alpha (1 + a^4 r^4)} \equiv \frac{h}{\cos^2 \alpha} \tag{4.5}$$

where we have defined

$$h \equiv \frac{1}{1 + a^4 r^4}, \qquad \text{with,} \quad a^4 \equiv \frac{1}{r_0^4 \sinh^2 \varphi \cos^2 \alpha}. \tag{4.6}$$

From Eq. 4.2 we notice that asymptotically the B-field becomes very large in the decoupling limit. The non-vanishing component of the B-field is B_{23} which gives rise to a magnetic field in the D3-brane world-volume and is responsible for making x^2 and x^3 directions non-commutative [93]. Using Eq. 4.5, we rewrite the metric in Eq. 4.2 as,

$$ds^2 = \frac{r^2}{r_0^2 \sinh \varphi} \left(-f dt^2 + (dx^1)^2 + h \left[(dx^2)^2 + (dx^3)^2 \right] \right) + \frac{r_0^2 \sinh \varphi}{r^2} \left(\frac{dr^2}{f} + r^2 d\Omega_5^2 \right). \tag{4.7}$$

where we have scaled $x^{2,3} \to \cos\alpha \, x^{2,3}$. The metric along with the other fields (Eq. 4.2) in the decoupling limit is the gravity dual of $(3+1)$-dimensional thermal NCYM theory. Before proceeding further, let us also make some comments about the geometry. First note that if we set $r_0 = 0$, the geometry reduces to the familiar $AdS_5 \times S^5$ case. With some hindsight let us also note that unlike the AdS_5 case, now the boundary (ultra-violet) is not located at $r \to \infty$ but rather at $r = r_0 \Lambda$ which is taken to be very large but finite. When we send $\Lambda \to \infty$, we have $h \to 0$ and the geometry degenerates. Hence, we need to impose $r < r_0 \Lambda$. Also note that the background above can be obtained as a chain of T-duality transformations on the $AdS_5 \times S^5$ geometry. The non-trivial B-field and the dilaton are generated due to this sequence of T-duality transformations. Thus, one can view the $\{x^2, x^3\}$ directions as a 2-torus $\mathbb{T}_\theta^2 \cong \mathbb{R}_\theta^2 / \mathbb{Z}_2$. The limit $\Lambda \to \infty$ can thus be considered as a degeneration of this 2-torus.

4.3 Jet Quenching Parameter in Thermal NCYM Plasma

In this section we first compute the jet quenching parameter, which measures the radiative energy loss of an energetic parton, in NCYM plasma. We have already seen in the previous chapter, that this is furnished by the expectation value of a light-like Wilson loop. Hence, it proves convenient to recast the space-time metric (Eq. 4.7) in light-cone coordinates,

$$\begin{aligned} ds^2 &= \frac{r^2}{r_0^2 \sinh\varphi}\Big[-(1+f)dx^+dx^- + \frac{1}{2}(1-f)\left[(dx^+)^2+(dx^-)^2\right] \\ &\qquad +h\left[(dx^2)^2+(dx^3)^2\right]\Big] + \frac{r_0^2\sinh\varphi}{r^2}\frac{dr^2}{f} + r_0^2\sinh\varphi d\Omega_5^2 \\ &\equiv G_{MN}dx^M dx^N \end{aligned} \tag{4.8}$$

where we have defined $x^\pm = (t \pm x^1)/\sqrt{2}$.

By the AdS/CFT dictionary, the light-like Wilson loop is related *via* Eq. 3.46 to the extremized action $\mathcal{S}(\mathcal{C})$ of the string world-sheet Σ whose boundary $\partial\Sigma$ is the mentioned loop $\mathcal{C}$ [74, 75]. The Nambu-Goto action is easily calculated from Eqs. 2.10 and 2.11 with G_{MN} obtained from Eq. 4.8. We set $\tau = x^-$ and $\sigma = x^2$. The length of the rectangular loop $\mathcal{C}$ along x^2 and x^- are L and L^- respectively and we assume $L^- \gg L$. As a result the surface is invariant under τ-translation and we have $x^M(\tau,\sigma) = x^M(\sigma)$. Furthermore, the Wilson loop lies at x^+ = constant and x^3 = constant. Note that one of the sides of the rectangular Wilson loop is chosen along a non-commutative direction (x^2) so that $\hat{q}_{\text{NCYM}}$ evaluated from this Wilson loop will carry the effect of non-commutativity. The radial coordinate $r(\sigma)$ gives the string embedding and we impose the condition that the world-sheet has $\mathcal{C}$ as its boundary, i.e., $r(\pm L/2) = r_0\Lambda$, for some finite Λ. The configuration is shown clearly in Fig. 4.1. The action (Eq. 2.11) now reduces to,

$$\mathcal{S} = \frac{\sqrt{2}L^-}{2\pi\alpha' \sinh\varphi} \int_0^{L/2} d\sigma \left[\frac{1}{1 + a^4 r^4} + \frac{r_0^4 \sinh^2\varphi}{r^4 - r_0^4} (r')^2 \right]^{\frac{1}{2}} \tag{4.9}$$

where $r' = \partial_\sigma r$. Defining new dimensionless variables $y = r/r_0$, $\tilde{\sigma} = \sigma/(r_0 \sinh\varphi)$ and $\ell = L/(r_0 \sinh\varphi)$, we can rewrite the action as,

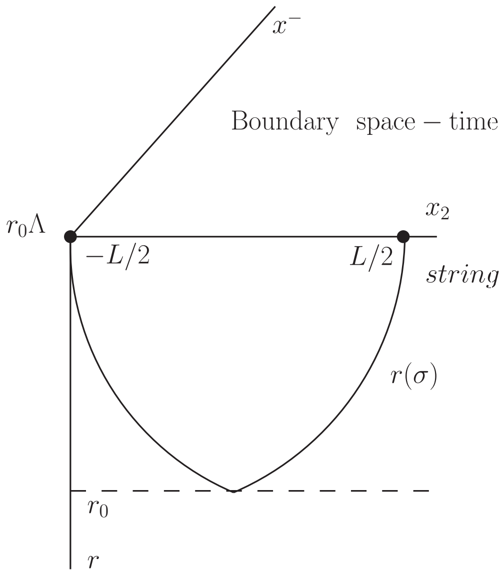

Figure 4.1: String configuration for evaluating $\hat{q}_{\rm NCYM}$

$$\mathcal{S} = \frac{\sqrt{2}L^- r_0}{2\pi\alpha'} \int_0^{\ell/2} d\sigma \left[\frac{1}{1 + a^4 r_0^4 y^4} + \frac{(y')^2}{y^4 - 1} \right]^{\frac{1}{2}}. \tag{4.10}$$

(Note that we have omitted the 'tilde' from σ) from which equation of motion follows,

$$y' = \left[1 - q_0^2(1 + a^4 r_0^4 y^4)\right]^{\frac{1}{2}} \frac{\sqrt{y^4 - 1}}{q_0(1 + a^4 r_0^4 y^4)} \tag{4.11}$$

where q_0 is an integration constant. From the first factor in Eq. 4.11 we have $q_0 < 1/(1 + a^4 r_0^4 y^4)^{\frac{1}{2}}$ for all values of y. In fact, q_0 has more stringent restriction to be mentioned later.

The above equation has a solution[§] where y starts from Λ coming all the way down to the turning point at $y = 1$ with $y' = 0$ and goes back again to Λ. Integration of Eq. 4.11 yields,

$$\ell = 2\int_0^{\ell/2} d\sigma = 2q_0 \int_1^{\Lambda} dy \frac{1 + a^4 r_0^4 y^4}{\sqrt{(y^4-1)\left[1 - q_0^2(1 + a^4 r_0^4 y^4)\right]}}. \tag{4.12}$$

Since $\ell = L/(r_0 \sinh\varphi)$ is very small compared to any other length scale of the problem, it implies from Eq. 4.12 that q_0 must be very small, i.e., $q_0 \ll 1/\sqrt{1 + a^4 r_0^4 \Lambda^4}$ and so, we can expand Eq. 4.12 in powers of q_0 and from there we formally obtain its value as,

$$q_0 = \frac{\ell}{2}\left[\int_1^{\Lambda} dy \frac{1 + a^4 r_0^4 y^4}{\sqrt{y^4 - 1}}\right]^{-1}. \tag{4.13}$$

Substituting Eq. 4.11 in Eq. 4.10 and expanding in powers of q_0, we obtain

$$\mathcal{S} - \mathcal{S}_0 = \frac{\sqrt{2}L^- r_0 q_0^2}{4\pi\alpha'}\int_1^{\Lambda} dy \frac{1 + a^4 r_0^4 y^4}{\sqrt{y^4 - 1}} = \frac{\sqrt{2}L^- r_0 \ell^2}{16\pi\alpha'}\left[\int_1^{\Lambda} dy \frac{1 + a^4 r_0^4 y^4}{\sqrt{y^4 - 1}}\right]^{-1} \tag{4.14}$$

where use has been made Eq. 4.13. $\mathcal{S}_0$ denotes the action for the world-sheet of two free strings (or the self-energy of the quark-antiquark pair). The integral in square brackets in Eq. 4.14 diverges if we take the boundary (Λ) where the NCYM theory lives, to ∞. The evaluation of the action here differs from the commutative case. In the commutative version the action, after subtracting the self-energy of the quarks, becomes finite. This is evident if we put $a^4 r_0^4$, which is a measure of non-commutativity (to be discussed later), to zero. However, for the non-commutative case, the action in Eq. 4.14 is still divergent if we put $\Lambda \to \infty$. This is because in the non-commutative case the gauge theory does not

[§]Here we discard another solution at UV corresponding to the surface at infinity. Since $\hat{q}$ is a property of the thermal medium and does not describe UV physics, the surface at infinity is not physically relevant [75].

live at $r = \infty$¶, the usual boundary of the AdS_5-space, but rather lives on a surface which is at a finite distance. Instead of directly evaluating this distance we shall, instead, first evaluate the integral in Eq. 4.14 for finite Λ and then subtract the divergent part obtained by letting $\Lambda \to \infty$. This way we regularize the integral in order to give any meaning to the extremized action‖. Once the subtraction is made the NCYM theory can be considered to be living effectively at $r = \infty$. So, we first evaluate the integral for finite Λ as follows,

$$\begin{aligned}\int_1^\Lambda dy \frac{1+a^4r_0^4y^4}{\sqrt{y^4-1}} &= -\Lambda\sqrt{\Lambda^4-1} + \frac{1}{3}(3+a^4r_0^4)\frac{\sqrt{\pi}\Gamma\left(\frac{5}{4}\right)}{\Gamma\left(\frac{3}{4}\right)} \\ &\quad + \frac{1}{3}(3+a^4r_0^4)\Lambda^3\,{}_2F_1\left(-\frac{3}{4},\frac{1}{2};\frac{1}{4};\frac{1}{\Lambda^4}\right)\end{aligned} \tag{4.15}$$

where ${}_2F_1(a,b;c;1/\Lambda^4)$ is a hypergeometric function. For large Λ it has an expansion

$${}_2F_1\left(a,b;c;\frac{1}{\Lambda^4}\right) = 1 + \frac{ab}{c}\frac{1}{\Lambda^4} + \frac{a(a+1)b(b+1)}{2c(c+1)}\frac{1}{\Lambda^8} + \cdots. \tag{4.16}$$

Using the above expansion in Eq. 4.15 and finally setting $\Lambda \to \infty$, we find that apart from a finite part the above integral has a single divergent piece of the form $(a^4r_0^4/3)\Lambda^3$ and all other terms vanish. So, removing the divergent part we get the regularized integral as,

$$\int_1^\infty dy \frac{1+a^4r_0^4y^4}{\sqrt{y^4-1}} = \left(1+\frac{a^4r_0^4}{3}\right)\frac{\sqrt{\pi}\Gamma\left(\frac{5}{4}\right)}{\Gamma\left(\frac{3}{4}\right)}. \tag{4.17}$$

¶This is implicit in the quark-antiquark potential calculation done in [84] (see also [94]). There it was not possible to fix the position of the string at infinity since a small perturbation would change it violently. So, the calculation was performed by going to a conjugate 'momentum' variable and the energy was found to be divergent. A finite answer was obtained only after subtracting the divergent part. This, in turn, implies that the boundary screen is not at infinity but at a finite radial distance [94].

‖There are two ways to describe the finiteness of the integral in the action (Eq. 4.14). Either we take Λ to be finite in which case the integral is obviously finite (in this case the integral can be evaluated only if we know the exact position of the boundary) or we take Λ to be infinite and subtract the unique divergent part (as explicitly calculated below) of the integral and obtain a finite result. In the former case the boundary is at a finite radial distance, but for the latter case it is at infinity. But, effectively, they describe the same thing. Here we have adopted the second approach.

Substituting Eq. 4.17 in Eq. 4.14 yields,

$$\mathcal{S}-\mathcal{S}_0=\frac{\sqrt{2}L^- r_0 \ell^2}{16\pi\alpha'}\frac{\Gamma\left(\frac{3}{4}\right)}{\sqrt{\pi}\Gamma\left(\frac{5}{4}\right)}\left(1+\frac{a^4 r_0^4}{3}\right)^{-1}. \tag{4.18}$$

Now to extract $\hat{q}_{\mathrm{NCYM}}$ we invoke Eq. 3.46 whence, we obtain

$$\hat{q}_{\mathrm{NCYM}}=\frac{r_0}{\pi\alpha' r_0^2\sinh^2\varphi}\frac{\Gamma\left(\frac{3}{4}\right)}{\sqrt{\pi}\Gamma\left(\frac{5}{4}\right)}\left(1+\frac{a^4 r_0^4}{3}\right)^{-1} \tag{4.19}$$

where we have reinserted $\ell = L/(r_0\sinh\varphi)$. Since $\hat{q}_{\mathrm{NCYM}}$ is a gauge-theoretic quantity, we replace all the parameters of string theory appearing in Eq. 4.19 by the corresponding gauge theory parameters making use of the gauge/string dictionary [84]. The temperature of the non-extremal (D1,D3) bound state, which by the gauge/string duality is the temperature of the NCYM theory, can be obtained from Eq. 4.2,

$$T=\frac{1}{\pi r_0\cosh\varphi}\approx\frac{1}{\pi r_0\sinh\varphi} \tag{4.20}$$

where in the last expression we have used the fact that in the decoupling limit (Eq. 4.4), φ is large. Also from the charge of the D3-brane we have

$$r_0^4\sinh^2\varphi = 2\hat{\lambda}\alpha'^2. \tag{4.21}$$

Here $\hat{\lambda}=\hat{g}_{\mathrm{YM}}^2 N_c$ is the 't Hooft coupling of NCYM theory and $\hat{g}_{\mathrm{YM}}$ is the NCYM coupling. The NCYM 't Hooft coupling is related to the ordinary 't Hooft coupling by $\lambda=(\alpha'/\theta)\hat{\lambda}$. Here θ is a finite parameter and in the decoupling limit as $\alpha'\to 0$, $\hat{\lambda}$ remains finite. Using Eqs. 4.20 and 4.21 we obtain,

$$\sinh\varphi = \frac{1}{\pi^2\sqrt{2\hat{\lambda}}\,T^2\alpha'}, \qquad \text{and} \qquad r_0 = \pi\sqrt{2\hat{\lambda}}\,T\alpha'. \tag{4.22}$$

Also we have

$$a^4r_0^4 = \frac{1}{\sinh^2\varphi\cos^2\alpha} = \pi^4(2\hat{\lambda})T^4\theta^2. \tag{4.23}$$

In the above we have used the decoupling limit $\cos\alpha = \alpha'/\theta$ and as $\alpha' \to 0$, $\alpha \to \pi/2$ as we mentioned earlier. Also, from Eq. 4.23 we notice that since $a^2r_0^2$ is proportional to θ, therefore, ar_0 is a measure of non-commutativity. Now using Eqs. 4.22 and 4.23 in Eq. 4.19 we find that for small non-commutativity ($a^2r_0^2 \sim \theta \ll 1$)

$$\hat{q}_{\text{NCYM}} = \frac{\pi^{\frac{3}{2}}\Gamma\left(\frac{3}{4}\right)}{\Gamma\left(\frac{5}{4}\right)}\sqrt{\hat{\lambda}}T^3\left[1 - \frac{\pi^4\hat{\lambda}T^4\theta^2}{3} + \mathcal{O}(\theta^4)\right]. \tag{4.24}$$

As expected, by setting $\theta = 0$, we recover the SYM result. In this case the NCYM 't Hooft coupling $\hat{\lambda}$ equals the ordinary 't Hooft coupling λ and also in writing Eq. 4.24 we have replaced $2\hat{\lambda}$ by $\hat{\lambda}$ to match the commutative results in [75]. This difference in a factor of 2 is just a convention as mentioned in [74]. In the presence of non-commutativity the jet quenching parameter gets reduced from its commutative value and the reduction gets enhanced with temperature as T^7, keeping other parameters fixed. This reduction in radiative energy loss for the non-commutative case can be intuitively understood as non-commutativity introduces a non-locality in space due to space uncertainty and there is no point-like interaction among the partons. So, the parton energy loss would be less in this case. We can try to estimate the correction (the second term in Eq. 4.24) arising due to non-commutativity from the experimental bound on the non-commutativity scale. In the literature various disparate experimental bounds on θ have been obtained from various physical considerations. The bound on θ has been claimed to be $\sim$ (1-10 TeV)$^{-2}$ in [87], whereas, it is $\sim$ (10^{12}-10^{13} GeV)$^{-2}$ in [95] or even stronger $\sim$ (10^{15} GeV)$^{-2}$ in [96]. In theories of gravity it can be of the order of Planck scale $\sim$ (10^{19} GeV)$^{-2}$ [97]. It is clear that in all these cases except the first one there is no hope of getting a significant correction due to non-commutativity in collider experiments. At RHIC collision energy $\sim$ 200 GeV where the temperature attained by QGP is $\sim$ 300 MeV, even the first case does not give a significant correction ($\pi^4\hat{\lambda}T^4\theta^2/3 \sim 4.96 \times 10^{-12}$ taking[**] $\hat{\lambda} = 6\pi$ and $T = 300$ MeV relevant for the Au-Au collision at RHIC and taking $\theta = 1$ TeV^{-2}) compared to the leading order term. At LHC where the collision energy would be much higher, the temperature of the QGP may rise and is expected to go up to 1-10 GeV. In that case the correction to the jet quenching due to non-commutativity can be estimated to be $\pi^4\hat{\lambda}T^4\theta^2/3 \sim (6.12\times 10^{-6}$-$6.12\times 10^{-10})$, still too low to be detected. Conversely, to get a 10% correction on the jet quenching parameter due to non-commutativity, the temperature of the plasma would have to be $T \sim 200$ GeV. For large non-commutativity ($ar_0 \sim \sqrt{\theta} \gg 1$), on the other hand, the jet quenching parameter in Eq. 4.19 takes the form,

$$\hat{q}_{\text{NCYM}} = \frac{3\Gamma\left(\frac{3}{4}\right)}{\pi^{\frac{5}{2}}\Gamma\left(\frac{5}{4}\right)}\frac{1}{\sqrt{\hat{\lambda}}\,T\theta^2}\left[1 - \frac{3}{\pi^4\hat{\lambda}T^4\theta^2} + \mathcal{O}\left(\frac{1}{\theta^4}\right)\right]. \tag{4.25}$$

We thus find that for large non-commutativity, the jet quenching varies inversely with temperature and also inversely with the square-root of the NCYM 't Hooft coupling.

As discussed earlier, the presence of non-commutativity singles out the x^1 direction so that all the space coordinates are no longer on equal footing. Introduction of non-commutativity alters the Minkowskian boundary space-time $\mathbb{R}^{1,3}$ to $\mathbb{R}^{1,1}\times\mathbb{R}^2_\theta$ where the non-commutativity parameter θ is non-vanishing only on the Moyal plane $\mathbb{R}^2_\theta$. Thus, we can think of non-

[**] We have taken the 't Hooft coupling of the NCYM theory to be the same as that of the commutative theory, although there is no concrete reason for this. This is taken just for the estimate. Actually these two couplings are related as given earlier and as $\alpha' \to 0$, $\lambda \to 0$, but $\hat{\lambda}$ remains finite. We have taken this finite value to be 6π for better comparison.

commutativity as the source of anisotropy in the gauge theory and treat θ as a measure of anisotropy. Our results suggest that the introduction of anisotropy leads to a suppression in jet quenching whose direct fallout will be a reduction in the suppression of quarkonium states like J/Ψ.

4.4 Q-$\bar{Q}$ Potential in Thermal NCYM Plasma

In this section we compute the quarkonium bound state potential in hot NCYM plasma in (3+1)-dimensions from gauge/string duality. Since we have already discussed the computation of Q-$\bar{Q}$ potential in the preceding chapter we shall be brief in our discussion here. Using a fundamental open string as a probe we consider its dynamics in the given background. The line joining the end-points of the string or the dipole lie along x^2, one of the non-commutative directions and move along x^1 with a velocity v where $0 < v < 1$ [††]. We boost to the rest frame $(t',\, x^{1\,\prime})$ of the dipole through the transformation,

$$
\begin{aligned}
dt &= \cosh\eta dt' - \sinh\eta dx^{1\,\prime} \\
dx^1 &= -\sinh\eta dt' + \cosh\eta dx^{1\,\prime}.
\end{aligned}
\tag{4.26}
$$

The rectangular Wilson loop lies along t' and x^2 directions and we denote the lengths along those directions as $\mathcal{T}$ and L respectively. Eq. 4.7 written in terms of the boosted

[††] There are various other possibilities one can consider, for example, the dipole lies along the commutative direction x^1 and moves along one of the non-commutative directions x^2 (say) or the dipole lies along one of the non-commutative directions x^2 and moves along the other non-commutative direction x^3. The dipole can even have an arbitrary orientation with respect to its motion and the motion can also be in arbitrary direction in the mixed commutative-non-commutative boundary. Here we consider only the simplest case to see the non-commutative effect.

coordinates assumes the form,

$$\begin{aligned} ds^2 &= -A(r)dt^2 - 2B(r)dtdx^1 + C(r)(dx^1)^2 + \frac{r^2 h}{r_0^2 \sinh\varphi}\left[(dx^2)^2 + (dx^3)^2\right] \\ &\quad + \frac{r_0^2 \sinh\varphi}{r^2}\frac{dr^2}{f} + r_0^2 \sinh\varphi d\Omega_5^2 \\ &\equiv \tilde{G}_{MN} dx^M dx^N \end{aligned} \tag{4.27}$$

where

$$\begin{aligned} A(r) &= \frac{r^2}{r_0^2 \sinh\varphi}\left(1 - \frac{r_0^4 \cosh^2\eta}{r^4}\right), \\ B(r) &= \frac{r_0^2 \sinh\eta\cosh\eta}{r^2 \sinh\varphi}, \\ C(r) &= \frac{r^2}{r_0^2 \sinh\varphi}\left(1 + \frac{r_0^4 \sinh^2\eta}{r^4}\right). \end{aligned} \tag{4.28}$$

Note that since we will be using the 'primed' coordinates from now on, we have dropped the prime for simplicity. Using the space-time metric defined in Eq. 4.27 we evaluate the Nambu-Goto action employing the static gauge $\tau = t$, $\sigma = x^2$, where $-L/2 \leq x^2 \leq L/2$ and $r = r(\sigma), x^1(\sigma), x^3(\sigma) = $ constant, to we get,

$$\mathcal{S} = \frac{\mathcal{T}}{2\pi\alpha'}\int_{-L/2}^{L/2} d\sigma \left[A(r)\left(\frac{r^2 h}{r_0^2 \sinh\varphi} + \frac{r_0^2 \sinh\varphi}{r^2}\frac{(\partial_\sigma r)^2}{f}\right)\right]^{\frac{1}{2}} \tag{4.29}$$

with $A(r)$ as given in Eq. 4.28. Introducing the dimensionless quantities $y = r/r_0$, $\tilde{\sigma} = \sigma/(r_0 \sinh\varphi)$ and $\ell = L/(r_0 \sinh\varphi)$, Eq. 4.29 can be rewritten as,

$$\mathcal{S} = \frac{\mathcal{T} r_0}{\pi\alpha'}\int_0^{\ell/2} d\sigma \mathcal{L} = \mathcal{T} T\sqrt{\hat{\lambda}}\int_0^{\ell/2} d\sigma \mathcal{L} \tag{4.30}$$

where

$$\mathcal{L} = \sqrt{\left(y^4 - \cosh^2\eta\right)\left(\frac{1}{1 + a^4 r_0^4 y^4} + \frac{y'^2}{y^4 - 1}\right)}. \tag{4.31}$$

We shall, henceforth, not use the 'tilde' on $\tilde{\sigma}$ anymore. Here $y' \equiv dy/d\sigma$ and we have used the fact that y is an even function of σ by symmetry. In writing the second expression in Eq. 4.30 we have made use of the standard gauge/string relations [84, 85], given in Eqs. 4.20, 4.21 and 4.23 now with $\hat{\lambda}$ replaced by $2\hat{\lambda}$. To find the string profile we will compute $y(\sigma)$ by extremizing the action in Eq. 4.30. Now since the Lagrangian density in Eq. 4.30 does not explicitly depend on σ, we have the following constant of motion,

$$\mathcal{H} = \mathcal{L} - y'\frac{\partial \mathcal{L}}{\partial y'} = \frac{y^4 - \cosh^2\eta}{(1 + a^4 r_0^4 y^4)\sqrt{\left(y^4 - \cosh^2\eta\right)\left(\frac{1}{1+a^4 r_0^4 y^4} + \frac{y'^2}{y^4-1}\right)}} = q = \text{constant}. \tag{4.32}$$

As in the commutative theory [74] discussed in chapter 3 we will consider two different regimes: (a) we take $\sqrt{\cosh\eta} < \Lambda$ and then take $\Lambda \to \infty$. The rapidity in this case remains finite, the Wilson loop is time-like and the action is real. We shall compute the Q-$\bar{Q}$ potential in this case and also provide an expression of the screening length in a specific case. (b) we take $\sqrt{\cosh\eta} > \Lambda$ and then take $\eta \to \infty$, keeping Λ finite. The Wilson loop in this case is light-like and the action is imaginary. We will take $\Lambda \to \infty$ in the end to obtain an expression for $\hat{q}_{\text{NCYM}}$ in hot NCYM plasma. As we shall shortly, this will match with the expression for the jet quenching parameter found out in the previous section. We consider case (a) in this section and postpone the discussion of case (b) to the next section. When $\sqrt{\cosh\eta} < \Lambda$, the action would be real and from Eq. 4.32 y' can be solved as,

$$y' = \frac{\sqrt{1 - a^4 r_0^4 q^2}}{q(1 + a^4 r_0^4 y^4)}\sqrt{\left(y^4 - 1\right)\left(y^4 - y_c^4\right)} \tag{4.33}$$

where $y_c^4 = (\cosh^2\eta + q^2)/(1 - a^4 r_0^4 q^2) > 1$ denotes the larger turning point where y' vanishes. Integrating Eq. 4.33 we obtain,

$$2\int_0^{\ell/2} d\sigma = \ell(q) = \frac{2q}{\sqrt{1 - a^4 r_0^4 q^2}} \int_{y_c}^{\Lambda} \frac{1 + a^4 r_0^4 y^4}{\sqrt{(y^4 - 1)(y^4 - y_c^4)}} dy. \tag{4.34}$$

Observe that if we naively take Λ, where the boundary theory is supposed to live, to ∞, the above integral diverges. Here ℓ is related to the dipole length L by $\ell = L/(r_0 \sinh\varphi) = \pi LT$ and so the divergence in $\ell(q)$ is physically meaningless. Note that $\ell(q)$ in the commutative theory is indeed finite as can be seen from Eq. 4.34 by putting $a^2 r_0^2 = 0$. However, for the non-commutative case $\ell(q)$ is divergent if we take $\Lambda \to \infty$. The reason why this divergence crops up is the same as that discussed in §4.3 in the discussion of $\hat{q}_{\text{NCYM}}$.

In the context of Wilson loop calculation, it has been noticed before [98] that the string end-points for a static string can not be fixed at a finite length at $\Lambda \to \infty$ in a non-commutative theory. Therefore, the dipole length L indeed diverges. The reason for this divergence has been argued to be the non-local interaction between the Q-$\bar{Q}$ pair in a magnetic field [99]. To be precise, the interaction point in terms of the center-of-mass coordinate gets shifted by a momentum-dependent term. Thus if the only non-zero component of the B-field is B_{23}, as in our case, then by placing the dipole along x^2, it automatically gets a momentum along x^3. So, if we keep the dipole static along x^3, the length will diverge at infinity. To compensate the momentum along x^3, the dipole must move along x^3 with a particular velocity [100]. In that case, the end-points of the string can be fixed at a finite length on the boundary at infinity and thus the divergence in the dipole length gets removed.

In the following, we, however, take recourse to the same strategy as in the preceding section in the evaluation of $\hat{q}_{\text{NCYM}}$ to get rid of the divergence, i.e., we first perform the integration for finite Λ and then identify the unique divergent part by allowing $\Lambda \to \infty$. Then we subtract this divergent piece from the integral to cure it of the divergence. After regularization, the non-commutative theory may be thought of as living at $\Lambda = \infty$. By inspection it can be seen that the divergent piece is of the form $2qa^4r_0^4\Lambda/\sqrt{1-a^4r_0^4q^2}$. Removing the divergent part the finite $\ell(q)$ can be written as,

$$\ell(q) = \frac{2q}{\sqrt{1-a^4r_0^4q^2}} \left[\int_{y_c}^{\Lambda} \frac{1+a^4r_0^4y^4}{\sqrt{(y^4-1)(y^4-y_c^4)}} dy - a^4r_0^4\Lambda \right] \Bigg|_{\Lambda\to\infty} . \tag{4.35}$$

The above equation, therefore, gives us the Q-$\bar{Q}$ separation $L(q) = \ell(q)/(\pi T)$ of the bound state as a function of the constant of motion q.

Substituting y' from Eq. 4.33 into the action (Eq. 4.30) results in,

$$\mathcal{S}(\ell) = \frac{\mathcal{T}T\sqrt{\hat{\lambda}}}{\sqrt{1-a^4r_0^4q^2}} \int_{y_c}^{\Lambda} \frac{y^4-\cosh^2\eta}{\sqrt{(y^4-1)(y^4-y_c^4)}} dy. \tag{4.36}$$

As in the commutative case, this action is divergent as it contains contribution from the Q-$\bar{Q}$ self-energy $\mathcal{S}_0$

$$\mathcal{S}_0 = \mathcal{T}T\sqrt{\hat{\lambda}} \int_1^{\Lambda} dy. \tag{4.37}$$

So, subtracting $\mathcal{S}_0$ from $\mathcal{S}(\ell)$ we get,

$$\begin{aligned} \mathcal{S}(\ell) - \mathcal{S}_0 \quad = \quad & \frac{\mathcal{T}T\sqrt{\hat{\lambda}}}{\sqrt{1-a^4r_0^4q^2}} \left[\int_{y_c}^{\Lambda} dy \left\{ \frac{y^4-\cosh^2\eta}{\sqrt{(y^4-1)(y^4-y_c^4)}} - \sqrt{1-a^4r_0^4q^2} \right\} \right. \\ & \left. - \sqrt{1-a^4r_0^4q^2}(y_c-1) \right] . \end{aligned} \tag{4.38}$$

However, owing to the fact that the NCYM theory does not live at $\Lambda \to \infty$ this action still diverges after regularization. Hence, to obtain a well-behaved action, we shall subtract the divergent term $\mathcal{S}_{\text{div}}$ from Eq. 4.38 and then take $\Lambda \to \infty$. Doing that we find the finite quark-antiquark potential in the quarkonium bound state as,

$$\begin{aligned} E(\ell) &= \frac{\mathcal{S}-\mathcal{S}_0-\mathcal{S}_{\text{div}}}{\mathcal{T}} \\ &= \frac{T\sqrt{\hat{\lambda}}}{\sqrt{1-a^4r_0^4q^2}}\left[\int_{y_c}^{\Lambda} dy\left\{\frac{y^4-\cosh^2\eta}{\sqrt{(y^4-1)(y^4-y_c^4)}}-\sqrt{1-a^4r_0^4q^2}\right\}\right. \\ &\left.\left. -\sqrt{1-a^4r_0^4q^2}(y_c-1)-\left(1-\sqrt{1a^4r_0^4q^2}\right)\Lambda\right]\right|_{\Lambda\to\infty} \end{aligned} \tag{4.39}$$

where in the above $\mathcal{S}_{\text{div}} = (1-\sqrt{1-a^4r_0^4q^2})\Lambda$ with $\Lambda \to \infty$. Here too it is not possible to perform the integration in Eq. 4.39 in a closed form. So, we will obtain the Q-$\bar{Q}$ potential numerically. We first plot $\ell(q)$-q using Eq. 4.35 and use it to plot $E(\ell)$-ℓ from Eq. 4.39 at different fixed values of η and ar_0. In the ensuing subsection we provide the various plots along with a discussion of the results.

4.4.1 Plots and discussion of the results

In this subsection we give and discuss the various plots of Q-$\bar{Q}$ separation $\ell(q)$ as a function of constant of motion q and the velocity-dependent Q-$\bar{Q}$ potential $E(\ell)$ as a function of the Q-$\bar{Q}$ separation length ℓ for various values of the rapidity η as well as the non-commutativity parameter $ar_0 \sim \sqrt{\theta}$.

In Figures 4.2-4.5, η is fixed at $\eta = 0.1$. In Figures 4.2 and 4.3 ar_0 takes small values starting from 0 (where there is no non-commutativity) to 1.0, whereas, in Figures 4.4 and 4.5 ar_0 takes fairly large values starting from 2.0 to 10.0. The main difference between the commutative results and the non-commutative results is that in the former case the constant of motion q can take arbitrarily large values, but in the latter case q can not exceed certain finite value (q_{max}) since beyond this value the Q-$\bar{Q}$ separation $\ell(q)$ becomes negative which is unphysical. The reason behind this cut-off is the regularization of the integral performed

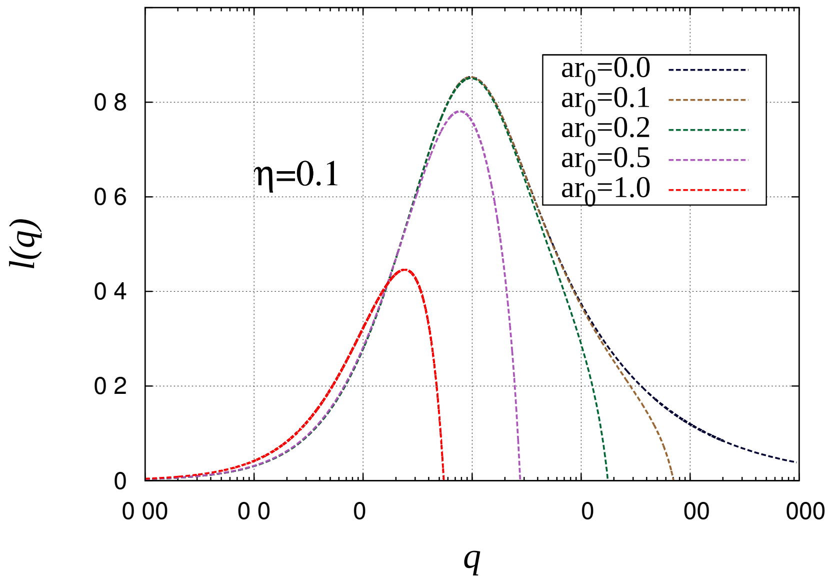

Figure 4.2: Q-$\bar{Q}$ separation $\ell(q)$ as a function of q for different values of ar_0 at $\eta = 0.1$

in Eq. 4.35 - the last term in Eq. 4.35 is subtracted to make $\ell(q)$ finite as $\Lambda \to \infty$. However, as q increases, y_c increases which makes the last term dominate over the integral and therefore, $\ell(q)$ becomes negative. Thus this effect is due to the non-commutativity of the underlying boundary theory. We see from Figure 4.2 that as ar_0 increases, $\ell(q)$ curve deviates more and more from the commutative curve, the maximum value of ℓ, i.e., ℓ_{max} falls and the peak shifts towards the left (i.e., the maximum occurs at a smaller value of q). In particular, the deviation from the commutative case becomes more pronounced after ℓ_{max} is reached. However this feature continues upto certain value of $ar_0 \sim 2.0$ and as it is increased further (see Figure 4.4) the $\ell(q)$ curve now deviates more from the commutative case throughout the allowed range of q, but the maximum value, ℓ_{max}, again starts rising and the peak as before shifts further towards left, i.e., towards smaller values of q. Figures 4.3 and 4.5 show the plot of the velocity-dependent Q-$\bar{Q}$ potential $E(\ell)$ with the Q-$\bar{Q}$ separation length ℓ for $\eta = 0.1$ with various values of ar_0. Each curve has two branches corresponding to the two dipole solutions obtained in Figures 4.2 and 4.4. The slight deviation of $\ell(q)$ from the commutative case for small values of q, i.e., below the value of q corresponding to $\ell(q) = \ell_{max}$, (see Figure 4.2) is reflected in the fact that in Figure 4.3 the upper branches almost merge with the commutative counterpart whereas the greater deviation in $\ell(q)$ after ℓ_{max} is reached leads to a rise in the lower branch of the $E(\ell)$ curve from the commutative case in Figure 4.3. However, as the non-commutativity parameter is increased the overall deviation (particularly in the lower branch) of the $E(\ell)$ curve is more pronounced from its commutative value. In contrast, in Figure 4.5 as the non-commutativity parameter is further increased, $E(\ell)$, in general, dips slightly for both the branches. The feature that the screening length ($\sim \ell_{max}$) initially drops and then rises and correspondingly the lower branch of the potential $E(\ell)$ rises and then drops as we go on increasing ar_0 (with the transition occurring at around $a_t r_0 \sim ar_0 = 2.0$), occurs only

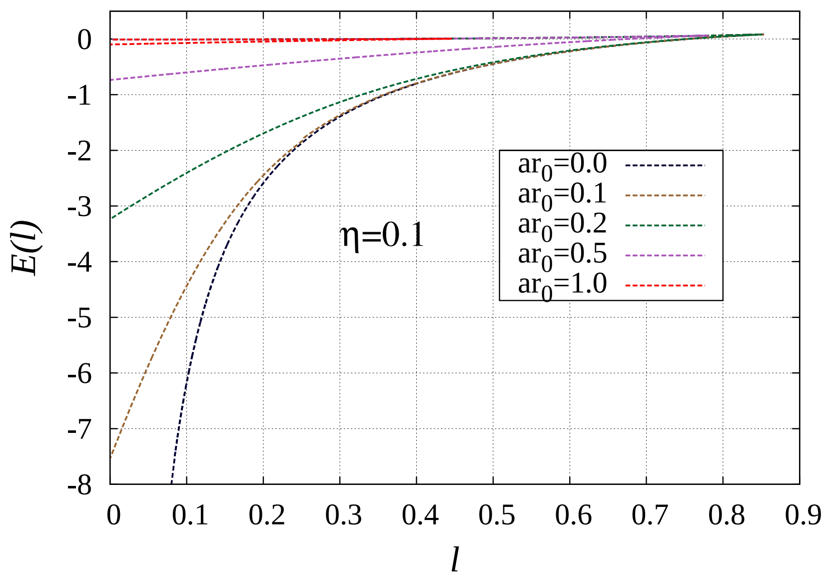

Figure 4.3: Normalized Q-$\bar{Q}$ potential $E(\ell)$ as a function of ℓ for the same set of ar_0 (as in Figure 4.2) at $\eta = 0.1$

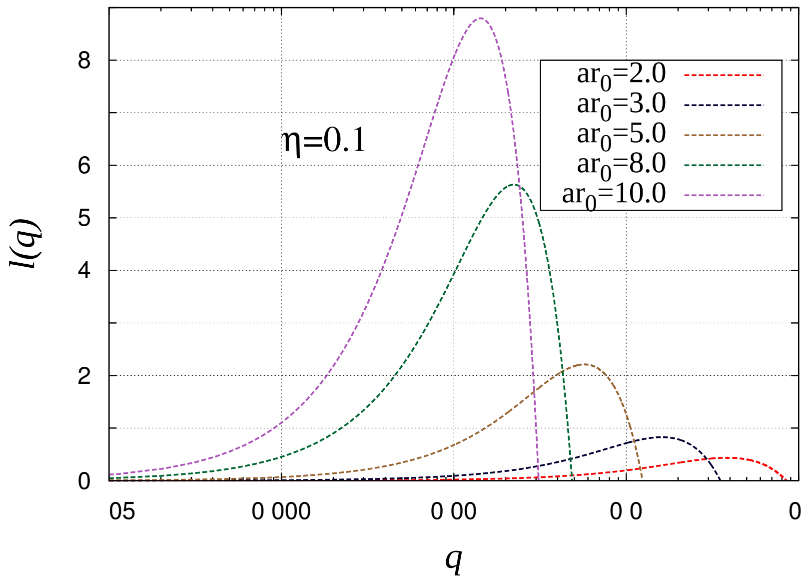

Figure 4.4: Q-$\bar{Q}$ separation $\ell(q)$ as a function of q for different large values of ar_0 at $\eta = 0.1$

for the smaller value of the rapidity, $\eta = 0.1$. There exists a critical value of $\eta = \eta_c$ above which this transition is not observed. As the rapidity becomes higher than η_c its effect starts to dominate and the transition (from falling ℓ_{max} to rising ℓ_{max} as the non-commutativity parameter is increased) is suppressed so that now the screening length continuously drops and the lower branch of the Q-$\bar{Q}$ potential continuously rises. We have seen this to happen for $\eta = 0.5$ and $\eta = 1.0$. That is why we have given those plots only for the smaller values of ar_0 in Figures 4.6-4.9. Although the details of these plots are different, the general features remain very similar to those of $\eta = 0.1$ (for small non-commutativity) and hence, we refrain from an elaborate discussion for these cases. Therefore, we shall take the $\eta = 0.1$ case as the prototype and discuss the generic features of the plots. We see from the plots in Figure 4.2 that ℓ_{max} drops as the non-commutativity is increased. This implies that with increase of non-commutativity, the quarkonia bound states will be more vulnerable to dissociation with the consequence that there will be an increase in J/Ψ

suppression [101]. On the other hand, from the plots in Figure 4.3 we observe that with increase of non-commutativity the Q-$\bar{Q}$ potential rises (the lower curves which correspond to the stable states) in value which means that the quark and the antiquark will be more and more loosely bound and eventually there will be no bound state formation. This may be expected since there is a fuzziness in the direction of the dipole due to non-commutativity. However, in Figure 4.4, when the non-commutativity is large (and the rapidity remains small) we see that around $ar_0 = 2.0$, ℓ_{max} starts rising again and so more dipoles can form, but from Figure 4.5 we see (from the lower curve) that in this case the quark-antiquark pair will be very very loosely bound. This does not happen when the rapidity is large (we have not shown the plots for this case with large non-commutativity). In contrast to Figures 4.2-4.9, where we plot $\ell(q)$-q and $E(\ell)$-ℓ for fixed values of η but with varying values of ar_0, in Figures 4.10-4.13, we plot the same functions for fixed values of ar_0, but varying

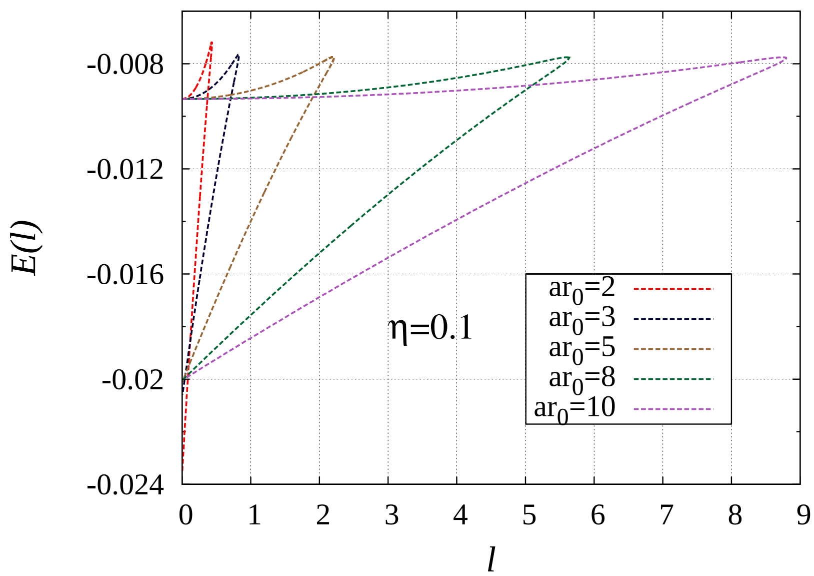

Figure 4.5: Normalized Q-$\bar{Q}$ potential $E(\ell)$ as a function of ℓ for the same set of ar_0 (as in Figure 4.4) at $\eta = 0.1$

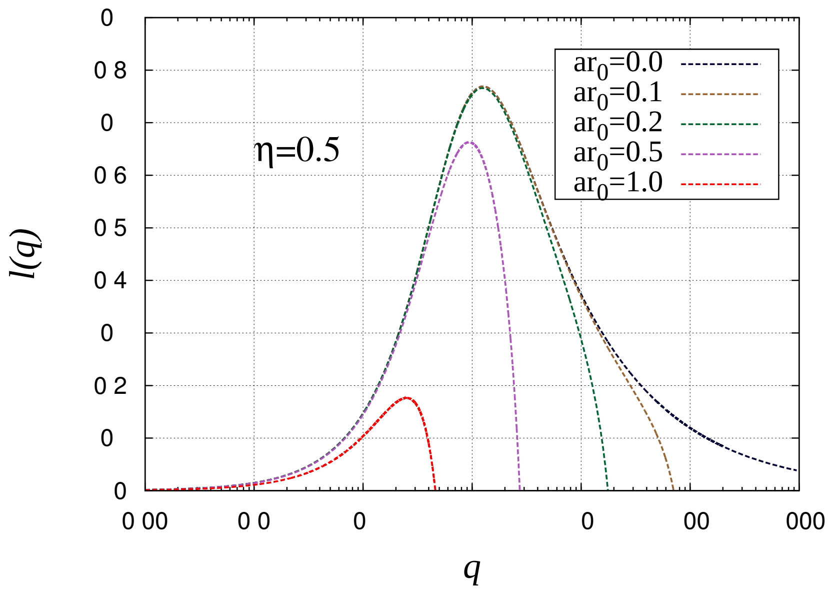

Figure 4.6: Q-$\bar{Q}$ separation $\ell(q)$ as a function of q for different values of ar_0 at $\eta = 0.5$

values of η. In Figures 4.10 and 4.11, ar_0 is fixed to a small value 0.1 whereas in Figures 4.12 and 4.13, it is fixed to a large value 10.0. In Figure 4.10 we find that as the rapidity increases the screening length decreases (which means there will be less dipole formation i.e., more J/Ψ suppression) and the peaks shift towards right, i.e., to a larger value of q. This is expected as in the commutative case also there is a decrease in screening length with increase in rapidity. Further note that for large q, $\ell(q)$ becomes independent of q. This is also manifest in the $E(\ell)$-ℓ plots in Figure 4.11, i.e., the lower branches of the curves merge. Contrast this to the case when ar_0 is changed (but still kept small) keeping η fixed, when the lower part of the $\ell(q)$ curve (i.e., small q) does not exhibit significant deviation, the peak shifts towards left and the upper branch of the $E(\ell)$ curves merge. So we can think of η and ar_0 as sort of having opposite effects. These features are also evident for large values of ar_0 given in Figures 4.12 and 4.13. In Figure 4.12 as the rapidity η increases the screening length decreases and the peaks shift towards right, but since now the scale of the

q-axis is very much enlarged this is not much visible (this is also due to the fact that η now changes by a very small amount). The independence of $\ell(q)$ with q for larger values of q is not evident in this case due to the differences in scale along the q-axis in Figures 4.10 and 4.12. Unlike in Figure 4.11, the lower branches of the $E(\ell)$ curves do not merge for different values of η as is evident from Figure 4.13. However, the spread is again due to the enlarged (compared to Figure 4.11) scale of the $E(\ell)$-axis which is chosen to show the two branches of the $E(\ell)$ curve distinctly.

So let us summarize our result about the bound state quarkonium potential in NCYM plasma at finite temperature. For our purpose, we can treat the non-commutativity parameter θ as a measure of anisotropy in the gauge theory. We can then distinguish between different regimes. Firstly, there exists a critical value η_c below which the screening length and the Q-$\bar{Q}$ potential exhibits interesting phenomena. For $\eta < \eta_c$ there is again two differ-

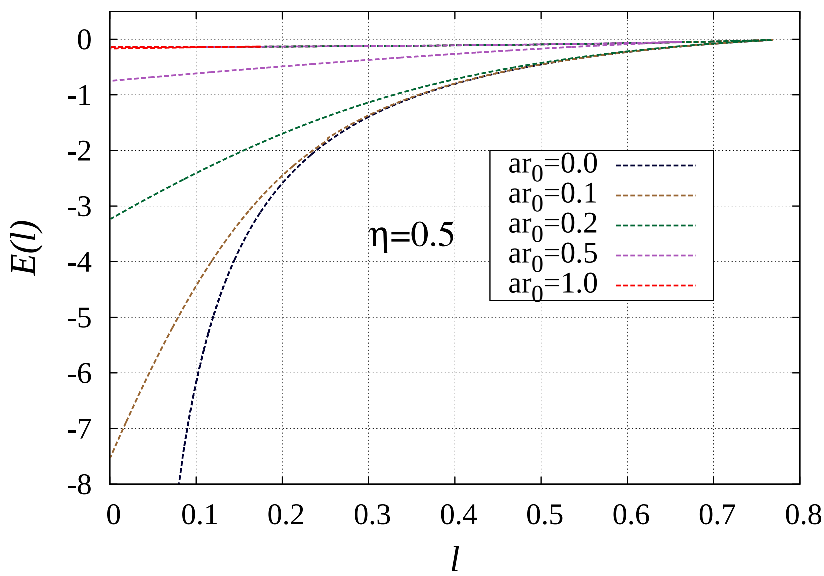

Figure 4.7: Normalized Q-$\bar{Q}$ potential $E(\ell)$ as a function of ℓ for the same set of ar_0 (as in Figure 4.6) at $\eta = 0.5$

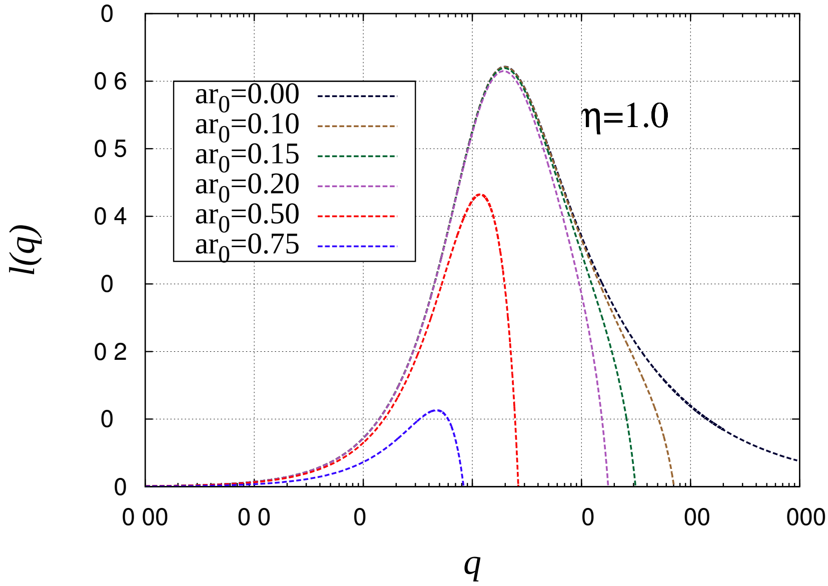

Figure 4.8: Q-$\bar{Q}$ separation $\ell(q)$ as a function of q for different values of ar_0 at $\eta = 1.0$

ent regimes depending upon $ar_0 \gtrless a_t r_0$. For $ar_0 < a_t r_0$ as the value of ar_0 is increased, the screening length steadily decreases and correspondingly, the potential rises showing that the bound state becomes more and more unstable. In the opposite regime where $ar_0 > a_t r_0$ as the non-commutativity parameter is increased, the screening now witnesses a marked rise while, on the other hand, the potential falls slightly with rising non-commutativity. But, the potential becomes almost flat so that the quark-antiquark pair is now very very loosely bound. On the other hand, in the regime $\eta > \eta_c$ the effect of rapidity dominates over that of anisotropy and as the anisotropy parameter rises, the screening length continually drops and the bound states become progressively loosely bound. Thus, the bottom line of our analysis is that for quarkonia with high momentum, the generic effect of anisotropy is to make the bound state more susceptible to melting which leads to suppression in the yield of various quarkonia that is measured in the collider experiments.

4.4.2 Screening length in a special case

In this section we find out an analytical expression for the screening length ℓ_{max} in a restricted regime of the parameter space of the rapidity η and the non-commutativity parameter θ. The expression for the regularized Q-$\bar{Q}$ separation length $\ell(q)$ as a function of the constant of motion q is given in Eq. 4.35. However, as we have mentioned, it is not possible to perform the integration, in general, and give an exact analytic expression for $\ell(q)$ which compelled us to resort to numerical means to solve Eq. 4.35 and plot $\ell(q)$ against q in the previous subsection. It must be realized that this has nothing to do with the non-commutativity of the underlying gauge theory and this happens also for the case of commutative theory. For the case of commutative theory it is possible to give an exact analytic expression of $\ell(q)$ only in the large velocity or large rapidity limit. Non-commutativity, on

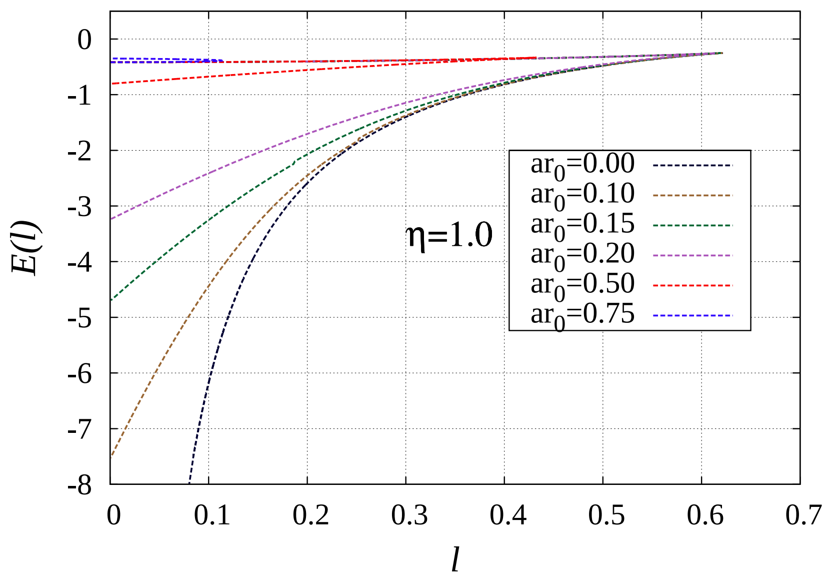

Figure 4.9: Normalized Q-$\bar{Q}$ potential $E(\ell)$ as a function of ℓ for the same set of ar_0 (as in Figure 4.8) at $\eta = 1.0$

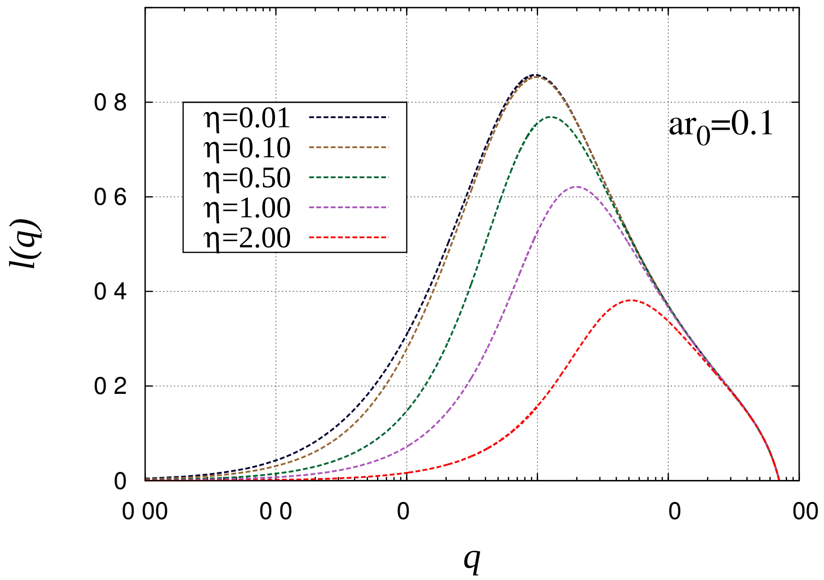

Figure 4.10: Q-$\bar{Q}$ separation $\ell(q)$ as a function of q for different values of η at $ar_0 = 0.1$

the other hand, makes the analysis a little bit more involved and in this case it is possible to obtain the analytic expression only when the rapidity is large and the non-commutativity is small with the product remaining small. For large η or large y_c, the expression for $\ell(q)$ in Eq. 4.35 can be expanded as follows,

$$\begin{aligned}\ell(q) \;=\; & \left[\frac{2q}{\sqrt{1-a^4r_0^4q^2}}\int_{y_c}^{\Lambda}\frac{1+a^4r_0^4y^4}{y^2\sqrt{y^4-y_c^4}}dy+\frac{q}{\sqrt{1-a^4r_0^4q^2}}\int_{y_c}^{\Lambda}\frac{1+a^4r_0^4y^4}{y^6\sqrt{y^4-y_c^4}}dy\right.\\ & \left.\left.+\frac{3q}{4\sqrt{1-a^4r_0^4q^2}}\int_{y_c}^{\Lambda}\frac{1+a^4r_0^4y^4}{y^{10}\sqrt{y^4-y_c^4}}dy+\cdots-\frac{2qa^4r_0^4}{\sqrt{1-a^4r_0^4q^2}}\Lambda\right]\right|_{\Lambda\to\infty} \qquad (4.40)\end{aligned}$$

When $\Lambda \to \infty$, the above integrals can be evaluated and $\ell(q)$ can be written as a series expansion in inverse powers of y_c as,

$$\ell(q) = \frac{q\sqrt{\pi}y_c}{\sqrt{1-a^4r_0^4q^2}}\left[-2a^4r_0^4\frac{\Gamma\left(\frac{3}{4}\right)}{\Gamma\left(\frac{1}{4}\right)} + (2+a^4r_0^4)\frac{\Gamma\left(\frac{3}{4}\right)}{\Gamma\left(\frac{1}{4}\right)}\frac{1}{y_c^4} + \left(1+\frac{3}{4}a^4r_0^4\right)\frac{\Gamma\left(\frac{7}{4}\right)}{4\Gamma\left(\frac{9}{4}\right)}\frac{1}{y_c^8} + \cdots\right] \tag{4.41}$$

By construction the divergent last term in Eq. 4.40 gets canceled with the divergent term in the first integral when $\Lambda \to \infty$. The other integrals are convergent and makes the expression for $\ell(q)$ finite. By taking the first three terms in the series we can obtain the values of q and y_c which maximize $\ell(q)$ as,

$$\begin{aligned} q^2 &= 2\cosh^2\eta(1-15a^4r_0^4\cosh^2\eta) \\ y_c^4 &= \frac{\cosh^2\eta + q^2}{(1-a^4r_0^4q^2)} = 3\cosh^2\eta(1-8a^4r_0^4\cosh^2\eta). \end{aligned} \tag{4.42}$$

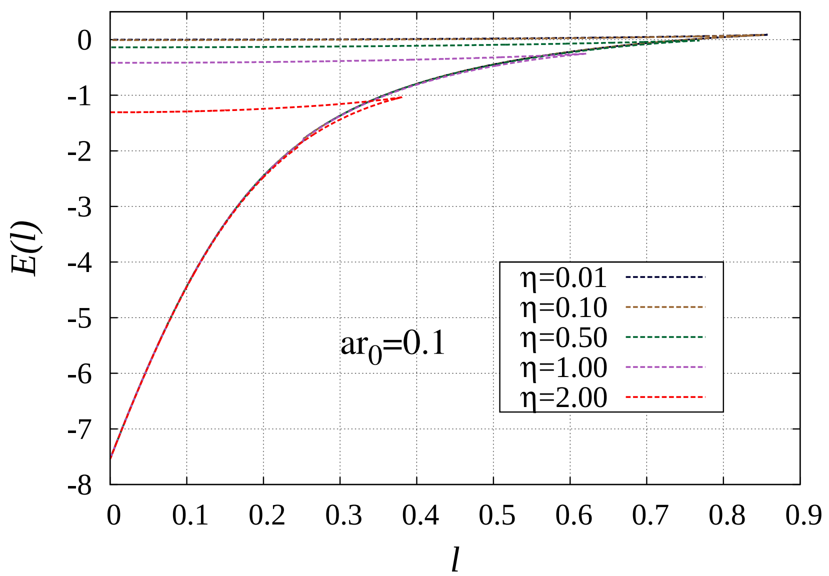

Figure 4.11: Normalized Q-$\bar{Q}$ potential $E(\ell)$ as a function of ℓ for the same set of η (as in Figure 4.10) at $ar_0 = 0.1$

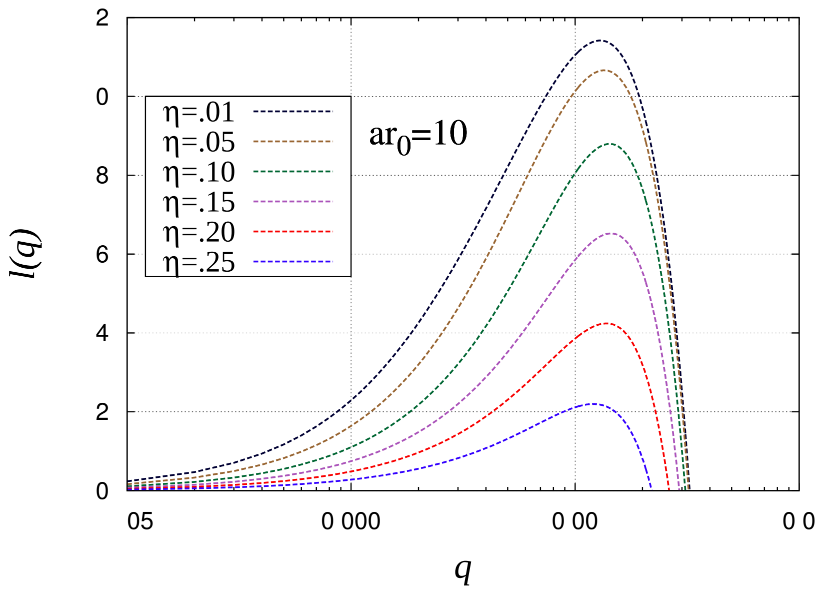

Figure 4.12: Q-$\bar{Q}$ separation $\ell(q)$ as a function of q for different values of η at $ar_0 = 10$

In obtaining the above expressions we have assumed $a^4r_0^4 \ll 1$ and $a^4r_0^4\cosh^2\eta \ll 1$. Using Eq. 4.42 we obtain the maximum value of ℓ up to next to leading order as,

$$\begin{aligned} \ell_{max} &= \frac{2\sqrt{2\pi}\Gamma\left(\frac{3}{4}\right)}{3^{3/4}\Gamma\left(\frac{1}{4}\right)\cosh^{\frac{1}{2}}\eta}\left[1 - \frac{7}{2}a^4r_0^4\cosh^2\eta + \cdots\right] \\ &= \frac{0.74333}{\cosh^{\frac{1}{2}}\eta}\left[1 - \frac{7}{2}a^4r_0^4\cosh^2\eta + \cdots\right]. \end{aligned} \tag{4.43}$$

By using Eqs. 4.20, 4.21 and 4.23 we can rewrite ℓ_{max} in Eq. 4.43 in terms of the gauge theory parameters as,

$$\ell_{max} = 0.74333(1-v^2)^{\frac{1}{4}}\left[1 - \frac{7}{2}\frac{\pi^4\hat{\lambda}T^4\theta^2}{1-v^2} + \cdots\right] \tag{4.44}$$

where we have used $\cosh\eta = \gamma = 1/\sqrt{1-v^2}$, with v being the velocity of the dipole. In Eq. 4.44 the term outside the square bracket is the commutative result (when we put

$\theta = 0$) and represents the usual J/Ψ suppression of the high velocity Q-$\bar{Q}$ pair produced in the QGP in the heavy ion collision observed in RHIC [70, 101]. However, we note that non-commutativity reduces this result due to the second term in the square bracket in Eq. 4.44. The quantity $L_{max} = \ell_{max}/(\pi T)$ can be thought of as the screening length of the dipole since this is the maximum value of L beyond which we have two dissociated quark and antiquark or two disjoint world-sheet for which $E(\ell) = 0$. As the screening length gets smaller less and less dipoles will be created and there will be more suppression of quark-antiquark bound states like J/Ψ. Non-commutativity makes the interaction between the quark and the antiquark weaker due to non-locality and that is the reason it makes the screening length shorter. Note that the velocity of the dipole has an opposite effect in the correction term due to non-commutativity, i.e., higher the velocity, lower would be the correction term due to non-commutativity. Also the correction term is more pronounced

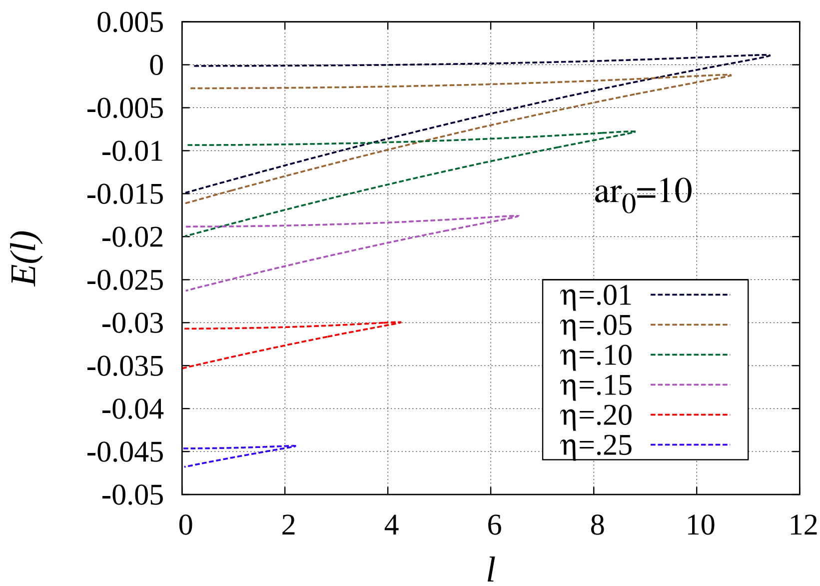

Figure 4.13: Normalized Q-$\bar{Q}$ potential $E(\ell)$ as a function of ℓ for the same set of η (as in Figure 4.12) at $ar_0 = 10$

at higher temperature. We would also like to remark that non-commutativity gives a range for the temperature. Eq. 4.44 is valid when $a^4 r_0^4 \cosh^2\eta \ll 1$ which, in turn, gives a range for the temperature as,

$$T \ll \left(\frac{1}{\pi^4 \hat{\lambda}(1-v^2)\theta^2}\right)^{\frac{1}{4}}. \tag{4.45}$$

When the temperature is above this value the expansion in Eq. 4.43 will break down and the screening length will no longer be given by Eq. 4.44. In that case the screening length has to be computed in the opposite limit where $a^4 r_0^4 \cosh^2\eta \gg 1$. However, in this limit we have not been able to write a closed form analytic expression for the screening length.

4.4.3 Jet quenching parameter - another look

In the previous section we alluded to the two different regimes in which we can compute the Wilson loops. In the regime discussed just now, the rapidity η remains finite and $\sqrt{\cosh\eta} < \Lambda$. So, the velocity of the background is in the range $0 < v < 1$ and the Wilson loop is time-like. Here we discuss the other regime where $\sqrt{\cosh\eta} > \Lambda$ whence, the Wilson loop becomes light-like. Now we can recover the expression for the jet quenching parameter $\hat{q}_{\rm NCYM}$ which we had already obtained in §4.3. Here we rederive the result just for the sake of completeness. This also provides us the excuse to be brief in our discussion here.

Note that as $\cosh^2\eta$ is now greater than Λ^4, where Λ is the upper limit of y, the factor $(y^4 - \cosh^2\eta)$ appearing in the action (Eqs. 4.30 and 4.31) is negative and the action becomes imaginary. So, we rewrite the action in Eq. 4.30 as,

$$\mathcal{S} = \frac{i\mathcal{T} r_0}{\pi\alpha'}\int_0^{\ell/2} d\sigma \mathcal{L} = i\mathcal{T} T\sqrt{\hat{\lambda}}\int_0^{\ell/2} d\sigma \mathcal{L} \tag{4.46}$$

where

$$\mathcal{L} = \sqrt{\left(\cosh^2\eta - y^4\right)\left(\frac{1}{1+a^4r_0^4y^4} + \frac{y'^2}{y^4-1}\right)}. \tag{4.47}$$

which supplies the equation of motion

$$y' = \frac{\sqrt{1+a^4r_0^4q_0^2}\sqrt{(y^4-1)(y_m^4-y^4)}}{q_0(1+a^4r_0^4y^4)} \tag{4.48}$$

where

$$y_m^4 = \frac{\cosh^2\eta - q_0^2}{1+a^4r_0^4q_0^2} \tag{4.49}$$

and q_0 is the constant of motion. On integration, Eq. 4.4.3 gives us,

$$\ell = 2\int_0^{\ell/2} d\sigma = \frac{2q_0}{\sqrt{1+a^4r_0^4q_0^2}}\int_1^{\Lambda}\frac{1+a^4r_0^4y^4}{\sqrt{(y^4-1)(y_m^4-y^4)}}dy. \tag{4.50}$$

Substituting the value of y' from Eq. 4.4.3 into the action (Eq. 4.47), we simplify it as,

$$\mathcal{S}(\ell) = \frac{i\mathcal{T}T\sqrt{\hat{\lambda}}}{\sqrt{1+a^4r_0^4q_0^2}}\int_1^{\Lambda}\frac{\cosh^2\eta - y^4}{\sqrt{(y^4-1)(y_m^4-y^4)}}dy. \tag{4.51}$$

Now since ℓ is very small compared to other length scales in the theory from Eq. 4.50 it is evident that q_0 is also a small parameter whence one has

$$q_0 = \frac{\ell\cosh\eta}{2}\left[\int_1^{\Lambda}\frac{1+a^4r_0^4y^4}{\sqrt{y^4-1}}dy\right]^{-1}. \tag{4.52}$$

In this limit $\mathcal{S}(\ell)$ in Eq. 4.51 can be expanded as,

$$\mathcal{S}(\ell) = \mathcal{S}^{(0)} + q_0^2\mathcal{S}^{(1)} + \mathcal{O}(q_0^4) \tag{4.53}$$

where

$$
\begin{aligned}
\mathcal{S}^{(0)} &= i\mathcal{T}T\sqrt{\hat{\lambda}}\int_1^{\Lambda}\frac{\sqrt{\cosh^2\eta - y^4}}{\sqrt{y^4-1}}dy \\
q_0^2\mathcal{S}^{(1)} &= \frac{i\mathcal{T}T\sqrt{\hat{\lambda}}}{2}q_0^2\int_1^{\Lambda}\frac{1+a^4r_0^4y^4}{\sqrt{\cosh^2\eta - y^4}\sqrt{y^4-1}}dy.
\end{aligned} \tag{4.54}
$$

It can be shown [74, 75] that as $q_0 \to 0$, $\mathcal{S}^{(0)}$ above is equal to $\mathcal{S}_0$, the self-energy of the dissociated quark and antiquark or area of the two disjoint world-sheets. So, subtracting the self-energy we obtain the action as

$$
\mathcal{S} - \mathcal{S}_0 = q_0^2\mathcal{S}^{(1)} = \frac{i\mathcal{T}T\sqrt{\hat{\lambda}}}{4}\ell^2\cosh\eta\left[\int_1^{\Lambda}\frac{1+a^4r_0^4y^4}{\sqrt{y^4-1}}dy\right]^{-1} \tag{4.55}
$$

where we have used Eq. 4.52 and have taken $\eta \to \infty$. Now $\mathcal{T}\cosh\eta$ in Eq. 4.55 can be identified as $L^-/\sqrt{2}$, where L^- is the length of the Wilson loop in the light-like direction. Using the relation in Eq. 3.46, we get

$$
\hat{q}_{\text{NCYM}} = \pi^2\sqrt{\hat{\lambda}}T^3\left[\int_1^{\Lambda}\frac{1+a^4r_0^4y^4}{\sqrt{y^4-1}}dy\right]^{-1}. \tag{4.56}
$$

As expected the above integral diverges as $\Lambda \to \infty$ and hence, needs to be regularized. Here we just furnish the expression for the regularized integral,

$$
\int_1^{\infty}\frac{1+a^4r_0^4y^4}{\sqrt{y^4-1}}dy = \left(1+\frac{a^4r_0^4}{3}\right)a_3, \qquad \text{with,} \quad a_3 = \frac{\sqrt{\pi}\,\Gamma\left(\frac{5}{4}\right)}{\Gamma\left(\frac{3}{4}\right)}. \tag{4.57}
$$

Substituting Eq. 4.57 in Eq. 4.56 and expressing $a^4r_0^4$ in terms of the gauge theory parameters from Eqs. 4.20, 4.21 and 4.23 we obtain,

$$\hat{q}_{\text{NCYM}} = \frac{\pi^{\frac{3}{2}}\Gamma\left(\frac{3}{4}\right)}{\Gamma\left(\frac{5}{4}\right)}\sqrt{\hat{\lambda}}T^3\left(1+\frac{\pi^4T^4\hat{\lambda}\theta^2}{3}\right)^{-1}. \tag{4.58}$$

So, for small non-commutativity, $\theta \ll 1$, the jet quenching parameter is given as,

$$\hat{q}_{\text{NCYM}} = \frac{\pi^{\frac{3}{2}}\Gamma\left(\frac{3}{4}\right)}{\Gamma\left(\frac{5}{4}\right)}\sqrt{\hat{\lambda}}T^3\left(1-\frac{\pi^4T^4\hat{\lambda}\theta^2}{3}+\mathcal{O}(\theta^4)\right) \tag{4.59}$$

whereas, for large non-commutativity, $\theta \gg 1$, the jet quenching parameter takes the form,

$$\hat{q}_{\text{NCYM}} = \frac{3\Gamma\left(\frac{3}{4}\right)}{\pi^{\frac{5}{2}}\Gamma\left(\frac{5}{4}\right)}\frac{1}{\sqrt{\hat{\lambda}}T\theta^2}\left(1-\frac{3}{\pi^4T^4\hat{\lambda}\theta^2}+\mathcal{O}(\frac{1}{\theta^4})\right). \tag{4.60}$$

This is in perfect agreement with our findings in §4.3. For small non-commutativity we have $a^4r_0^4 \ll 1$, which yields a range for the temperature due to non-commutativity,

$$T \ll \left(\frac{1}{\pi^4\hat{\lambda}\theta^2}\right)^{\frac{1}{4}}. \tag{4.61}$$

When the temperature is above this value, the jet quenching expression will no longer be given by Eq. 4.59. In that case we have to use the expression Eq. 4.60 which is valid when the temperature is given by the limit

$$T \gg \left(\frac{1}{\pi^4\hat{\lambda}\theta^2}\right)^{\frac{1}{4}}. \tag{4.62}$$

4.5 Conclusion

In this concluding section let us recapitulate the results of this chapter. In this chapter we considered the first of our anisotropic models - the non-commutative Yang-Mills theory at finite temperature. We took the non-commutativity parameter θ as a measure of anisotropy that breaks the $SO(3)$ symmetry of the gauge theory living on the Minkowski space $\mathbb{R}^{1,3}$ at the boundary to a $SO(2)$ symmetry in the non-commutative Moyal plane $\mathbb{R}^2_\theta$. The four-dimensional space-time now decomposes as $\mathbb{R}^{1,1} \times \mathbb{R}^2_\theta$. The presence of anisotropy thus singles out a particular direction, in this case x^1, in space which should have qualitative effects on the experimental observables in the heavy ion colliders. Translated into the language of the heavy ion colliders we thus have a special direction in the thermal medium, which we can reasonably take as the direction along which the collisions take place. We studied the propagation of heavy Q-$\bar{Q}$ bound states in this anisotropic thermal medium. First, we computed the jet quenching parameter and found out how it picks up corrections arising from a non-zero value of θ. Then we considered two limits when θ is very small or very high and found analytical expression for the jet quenching parameter. We also explored any possibility of whether any signature of non-commutativity can be detected in the present collider experiments. Using some benchmark values of θ available in the literature we computed the correction to the jet quenching parameter coming from the presence of non-commutativity and concluded that even if non-commutativity is present, its existence is too weak to have any appreciable effect on the heavy quark observables in the accessible range of energies. Its presence can only be felt in higher energy domain that may be reached in some future collider. Next we evaluated the expectation values of time-like Wilson loops using the standard recipe and from there extracted information about the bound state interaction potential. To keep the discussion simple, we considered only the case when the dipole is aligned along a non-commutative direction and moves along the commutative direction. We found out how the potential varies with the separation between the quark and the antiquark with the dipole velocity and the non-commutativity as parameters. We explored various regimes of this parameter space and plotted the results.

While the details vary, we observed that generically, introduction of non-commutativity aka anisotropy makes the bound state prone to dissociation. We were also successful in obtaining an analytical expression of the screening length in a restricted domain of the parameter space. Finally, by considering the limit $v \to 1$ we considered light-like Wilson loop and from there recovered the form of the jet quenching parameter calculated in an earlier section. In the case of jet quenching parameter also, we found that turning on a small non-commutativity leads to a decrease in the value of $\hat{q}_{\text{NCYM}}$. A plausible explanation of this decrease can be attributed to the intrinsic non-locality of the underlying non-commutative theory that rules out point-like interactions among the partons. The underlying fuzziness of the theory is thus responsible for an increase in suppression of the yield of quarkonia like J/Ψ.

CHAPTER 5

MASSIVE QUARKS IN HOT DEFORMED SUPER YANG-MILLS PLASMA

5.1 Introduction

The present chapter deals with the second model of anisotropic SYM plasma at finite temperature*. We consider a deformed $\mathcal{N} = 4, SU(N_c)$ thermal SYM theory where the deformation introduces the effect of anisotropy. The gravity dual to this gauge theory was first proposed in [104, 105] inspired by an earlier work [106]. In this medium, we evaluate expectation values of time-like Wilson loops to extract information about how the bound state Q-$\bar{Q}$ potential V varies with the quarkonia size $\sim L$ and the screening length L_{max} of heavy quarkonia. We examine in detail how the presence of anisotropy affects these quantities. In chapter 4 we had already found out the bound state observables like the potential, the screening length and also the jet quenching parameter when the medium

*The chapter is based on [102, 103].

is hot NCYM theory. Carrying out similar computations in a different model enables us to pit the two models against one another and directly compare the anisotropy-induced modifications in the two models. We take into account various orientations of the dipole and make a comparative study among these cases. The static Q-$\bar{Q}$ potential and L_{max} for heavy quarkonia in this medium were considered in [107]. Here we extend the analysis to the velocity-dependent case by considering a heavy Q-$\bar{Q}$ pair moving through the plasma with a velocity v. While we have not restricted the value to be taken by v, we consider only small values of the anisotropy parameter, in which case the dual gravity solution is known perturbatively. To compute $V(L)$ we take recourse to the standard algorithm described in chapter 3 and faithfully followed in chapter 4. We plot the the potential $V(L)$ against the Q-$\bar{Q}$ separation L for various values of v and the anisotropy parameter $\tilde{a}$ and study how the introduction of a small anisotropy influences the potential. Unlike in the static case (described in [107]) where there were only two possible configurations of the dipole, here we shall see that introduction of the velocity parameter gives rise to a plethora of possibilities. We further probe the effect of anisotropy on L and consequently, the screening length L_{max}. We are able to obtain an analytic expression for L_{max} in the anisotropic plasma in a special domain of the parameter space spanned by v and $\tilde{a}$. Although the static Q-$\bar{Q}$ potential has been provided in [107], we reproduce it here since it is recovered naturally in the $v = 0$ limit of our analysis and nicely complements our results for the static Q-$\bar{Q}$ separation. In [108] the authors analyze the screening length when the infinitely massive Q-$\bar{Q}$ pair moves in hot, anisotropic plasma. In our work, one can read off the screening length from the plot of the Q-$\bar{Q}$ separation. Wherever the results overlap, they are in perfect agreement with those obtained in [108].

In addition to studying the heavy quark bound states, we further investigate the dynamics of a massive quark in the background of deformed SYM plasma. The motion of a heavy quark through QGP is reminiscent of the Brownian motion. Based on a simple phenomenological model, encoded in the Langevin equation, we study various quantities related to the propagation of heavy quarks in QGP, like the drag force, the diffusion constant, the relaxation time, the random force auto-correlator, etc. from a holographic perspective.

The present chapter is organized as follows. In §5.2, we review the model and the dual geometry and discuss the general set-up. In §5.3 we compute the Q-$\bar{Q}$ potential and provide numerical results. We also calculate the screening length analytically in a special case. §5.3 is divided into five subsections corresponding to the different cases we consider. In §5.4 we compare our results for the different cases considered and also with some other models available in the literature. §5.5 concerns studying the dynamics of a single massive quark in the same background. The section is split into three subsections. In §5.5.1 we introduce and define the problem that we wish to address and discuss the field-theoretic background of the problem. In §5.5.2 and §5.5.3 we address the problem using the techniques of the gauge/string duality. Finally, in §5.6 we summarize our work and conclude.

5.2 The Dual Geometry

In this section we elaborate upon the gravity dual of the gauge theory we are interested in following [104] and discuss the general set-up of the problem. We will take the gauge theory as a deformed version of $\mathcal{N} = 4, SU(N_c)$ SYM at large 't Hooft coupling λ where the deformation is achieved by introducing a θ-term in the action as

$$\mathcal{S} = \mathcal{S}_{\text{SYM}} + \frac{1}{8\pi^2}\int \theta(x^3)\text{Tr}F \wedge F \tag{5.1}$$

where $\theta(x^3) \propto x^3$ (we take $\{t, x^1, x^2, x^3\}$ as the gauge theory coordinates). The presence of the non-zero θ-term breaks the $SO(3)$ rotational symmetry down to a $SO(2)$ symmetry in the x^1-x^2 plane and makes the theory anisotropic. In the context of heavy ion collisions, x^3 will correspond to the direction of beam whereas the x^1 and x^2 directions span the transverse plane. On the supergravity side the starting point is to consider ten-dimensional type IIB supergravity. Following [106] one can seek a solution where only the metric, the dilaton, the axion and the R-R five-form are excited. The solutions can be obtained consistently from the equations of motion which are furnished by the action,

$$\mathcal{S}^{(10)} = \frac{1}{2\kappa_{10}^2}\int d^{10}x\sqrt{-g}\left(e^{-2\phi}\left(\mathcal{R}+4\partial_M\phi\partial^M\phi\right)-\frac{1}{2}F_1^2-\frac{1}{4!5!}F_5^2\right). \tag{5.2}$$

Here, as usual, $M = 0, 1, 2, ...9$ is the ten-dimensional space-time index, $2\kappa_{10}^2 = 16\pi G_{10}$ is the ten-dimensional gravitational coupling, ϕ and χ are the dilatonic and the axionic excitations respectively and $F_1 = d\chi$ is the axion-strength. g is the determinant of the ten-dimensional metric and $\mathcal{R}$ is the ten-dimensional Ricci scalar. The dilaton is governed by the equation of motion,

$$\mathcal{R} + 4g^{MN}\left(\nabla_M\phi\nabla_N\phi - \partial\phi_M\partial\phi_N\right) = 0 \tag{5.3}$$

while the Einstein equations read,

$$\mathcal{R}_{MN} + 2\nabla_M\nabla_N\phi + \frac{1}{4}g_{MN}e^{2\phi}\partial_P\chi\partial^P\chi - \frac{1}{2}e^{2\phi}\left(F_MF_N + \frac{1}{48}F_{MABCD}F_N^{\ ABCD}\right). \tag{5.4}$$

The form fields obey the equations of motion, Bianchi identities and the self-duality condition,

$$d*F_1 = 0 = d*F_5, \qquad dF_1 = 0 = dF_5, \qquad F_5 = *F_5. \tag{5.5}$$

Here $*$ is the ten-dimensional Hodge dual operator. To consider an anisotropic solution we assume the following form of the ansatz,

$$ds^2 = r^2\left(-\mathcal{F}\mathcal{B}dt^2 + (dx^1)^2 + (dx^2)^2 + \mathcal{H}(dx^3)^2 + \frac{dr^2}{r^4\mathcal{F}}\right) + \mathcal{Z}d\Omega_5^2. \tag{5.6}$$

Here the boundary is located at $r \to \infty$ and $d\Omega_5^2$ is the metric on the five-sphere S^5. We have exploited reparametrization invariance to set g_{11} and g_{22} as in Eq. 5.6. Once this is done, it is not possible to get rid of $\mathcal{B}$ in general, still we can use the scaling symmetry to set $\mathcal{B}$ at the boundary, i.e., $\mathcal{B}_{r\to\infty} = 1$. Similarly, one also sets $\mathcal{H}_{r\to\infty} = 1$ using the scaling symmetry in x^3. $\mathcal{F}, \mathcal{B}, \mathcal{H}, \mathcal{Z}$ and ϕ are considered to be functions of the radial coordinate r alone. $\mathcal{F}$ is the 'blackening factor' which vanishes at the horizon r_h, i.e., $\mathcal{F}_{r=r_h} = 0$. The magnetic part of the five-form is proportional to the volume form of the five-sphere, i.e.,

$$F_5 = \alpha(\Omega_{S^5} + *\Omega_{S^5}). \tag{5.7}$$

where $\alpha = 4$ [104]. Moreover the axion χ is taken to be linearly proportional to x^3,

$$\chi = ax^3. \tag{5.8}$$

We further set,

$$\mathcal{H} = e^{-\phi}, \qquad \text{and} \qquad \mathcal{Z} = e^{\frac{1}{2}\phi}. \tag{5.9}$$

With the choices as discussed above, the ten-dimensional metric factorizes in Einstein frame into a five-sphere S^5 and an asymptotically AdS_5 space, i.e., now we seek solutions of the form $\mathcal{M} \times S^5$. In such a scenario, the action (Eq. 5.2) reduces to the action of five-dimensional axion-dilaton AdS gravity given by,

$$\mathcal{S}^{(5)} = \frac{1}{2\kappa_5^2}\int_{\mathcal{M}}\sqrt{-g}\left[\mathcal{R} + 12 - \frac{1}{2}(\partial\phi)^2 + \frac{1}{2}e^{2\phi}(\partial\chi)^2\right] + \frac{1}{2\kappa^2}\int_{\partial\mathcal{M}}\sqrt{-\gamma}2K \tag{5.10}$$

Here $2\kappa_5^2 = 16\pi G_5$ is the five-dimensional gravitational coupling and now g and $\mathcal{R}$ denote the metric and the Ricci scalar in five dimensions. The five-form flux F_5 gives rise to the cosmological constant $\Lambda = -6/R^2$ with R being set to unity here. Further, the last term, defined on the boundary $\partial\mathcal{M}$ of the manifold, is the usual Gibbons-Hawking boundary term with γ being the metric on $\partial\mathcal{M}$. The dual gravity solution is given in the string frame,

$$ds^2 = r^2\left(-\mathcal{F}\mathcal{B}dt^2 + (dx^1)^2 + (dx^2)^2 + \mathcal{H}(dx^3)^2 + \frac{dr^2}{r^4\mathcal{F}}\right). \tag{5.11}$$

In the above solution anisotropy is introduced through the axion, the dual to the gauge theory θ-term. The anisotropy parameter a turns out to be [104] $a = \lambda n_{\mathrm{D7}}/4\pi N_c$ where n_{D7} is the density of D7-branes (which act as the magnetic source of the axion) along the x^3 direction. The D7-branes wrap around S^5 and extend along the transverse directions, x^1, x^2. Thus in the gravity dual the presence of anisotropy can be attributed to the existence of anisotropic extended objects. Note that the D7-branes do not extend along the radial direction. Hence, they do not reach the boundary and do not contribute any new degrees of freedom to the theory. The fact that the D7-branes wrap around S^5 also leads to significant simplification of the problem since it implies that the $SO(6)$ symmetry of the undeformed theory is preserved. Consequently, none of the Kaluza-Klein modes on S^5 are excited which permits us to find the solution working in five-dimensional supergravity coupled with a few matter fields. $\mathcal{F}, \mathcal{B}$ and $\mathcal{H}$ are all functions of the radial coordinate r and are known analytically only in the limiting cases when the temperature is very high or low.

Otherwise, they are known numerically in the intermediate range. The degree of anisotropy can be controlled by tuning the parameter a. In this work, we shall be concerned with weakly anisotropic plasma (the small a or high temperature T limit, such that $a/T \ll 1$) in which case the functions $\mathcal{F}, \mathcal{B}$ and $\mathcal{H}$ can be expanded to leading order in a around the black D3-brane solution,

$$\begin{aligned} \mathcal{F}(y) &= 1 - \frac{1}{y^4} + a^2 \mathcal{F}_2(y) + \mathcal{O}(a^4), \\ \mathcal{B}(y) &= 1 + a^2 \mathcal{B}_2(y) + \mathcal{O}(a^4), \\ \mathcal{H}(y) &= e^{-\phi(y)} \qquad \text{with} \qquad \phi(y) = a^2 \phi_2(y) + \mathcal{O}(a^4) \end{aligned} \tag{5.12}$$

where

$$\begin{aligned} \mathcal{F}_2(y) &= \frac{1}{24 r_h^2 y^4}\left[8(y^2-1) - 10\log 2 + (3y^4+7)\log\left(1+\frac{1}{y^2}\right)\right], \\ \mathcal{B}_2(y) &= -\frac{1}{24 r_h^2}\left[\frac{10}{1+y^2} + \log\left(1+\frac{1}{y^2}\right)\right], \\ \phi_2(y) &= -\frac{1}{4 r_h^2}\log\left(1+\frac{1}{y^2}\right) \end{aligned} \tag{5.13}$$

and we have defined the dimensionless quantity $y = r/r_h$. The temperature is given by

$$T = \frac{r_h}{\pi} + \frac{a^2}{r_h}\frac{(5\log 2 - 2)}{48\pi} + \mathcal{O}(a^4) \tag{5.14}$$

which can be inverted to yield the horizon position in terms of the temperature, which, in the limit $a/T \ll 1$, reads

$$r_h \sim \pi T\left[1 - a^2 \frac{5\log 2 - 2}{48\pi^2 T^2}\right]. \tag{5.15}$$

The entropy density is simply obtained from the horizon area. The area element at a $t =$ constant, $r = r_h$ hypersurface is

$$dA_h = e^{-\frac{5}{4}\phi_h} r_h^3 dx^1 dx^2 dx^3 \tag{5.16}$$

from which one finds the entropy density s to be ,

$$s = \frac{A_h}{4GV_3} = \frac{1}{2\pi} N_c^2 \times e^{-\frac{5}{4}\phi_h} r_h^3. \tag{5.17}$$

In the small anisotropy regime this yields,

$$s = \frac{\pi^2 N_c^2 T^3}{2} + \frac{N_c^2 T}{16} a^2 + \mathcal{O}(a)^4. \tag{5.18}$$

To compute the quarkonium potential we follow the usual procedure of introducing a fundamental string in this background and evaluate the Nambu-Goto action $\mathcal{S}$. By extremizing this action we find the expectation value of the relevant Wilson loop. Assuming the string to move along x^i with a velocity v and the string end-points to lie along x^j, separated by a distance L (which in the dual gauge theory translates to the Q-$\bar{Q}$ separation), the Wilson loop so formed is a rectangle with a short side L along x^j and a long side $\mathcal{T}$ along any time-like direction in the t-x^i plane. For the static Q-$\bar{Q}$ separation and potential one needs to consider only two possibilities: the dipole lying along the anisotropic direction x^3 or in the transverse plane. However, introduction of the velocity opens up the following possibilities:

1. Dipole in transverse plane, aligned perpendicular to velocity.

2. Dipole along x^3, velocity in transverse plane.

3. Dipole in transverse plane, velocity along x^3.

4. Dipole aligned parallel to velocity in transverse plane.

5. Dipole aligned parallel to velocity along anisotropic direction.[†]

5.3 Q-$\bar{Q}$ Separation and Q-$\bar{Q}$ Potential

In this section we discuss the different cases, alluded to above, one in each subsection, and for each case we numerically study the Q-$\bar{Q}$ separation L with varying values of the rapidity η and the anisotropy parameter a and see how L and hence, the screening length L_{max} gets affected when we turn on a small value of a. We also compute the Q-$\bar{Q}$ potential $V(L)$ (both velocity-dependent and static) and observe the modifications brought about by anisotropy. Further, we provide an analytic expression for L_{max} in a special case.

5.3.1 Dipole in transverse plane, perpendicular to velocity

In the first case that we consider the motion is wholly contained in the transverse plane spanned by x^1 and x^2 and the dipole presents itself perpendicular to the direction of its motion. Without any loss of generality, we first set our axes such that the dipole moves along x^1 while itself being aligned along x^2. Then we go to the rest frame $(t', x^{1\prime})$ of the Q-$\bar{Q}$ pair *via* the following coordinate transformation,

$$
\begin{aligned}
dt &= \cosh\eta dt' - \sinh\eta dx^{1\prime}, \\
dx^1 &= -\sinh\eta dt' + \cosh\eta dx^{1\prime}.
\end{aligned}
\tag{5.19}
$$

[†]Of course, there exist other possibilities where the dipole can have any arbitrary orientation with respect to its velocity, which, itself, can be in any arbitrary direction. However, we do not consider these cases here.

Now the Q-$\bar{Q}$ pair and hence, the Wilson loop can be regarded as static in a plasma that is moving with a velocity v along $-x^{1\prime}$ direction. This implies that the Wilson loop spans t' (since $x^{1\prime}$ is fixed in this rest frame) and x^2 directions with sides $\mathcal{T}$ and L respectively. In terms of the boosted coordinates the metric in Eq. 5.11 can be rewritten as

$$\begin{aligned} ds^2 &= -A(r)dt^2 - 2B(r)dtdx^1 + C(r)(dx^1)^2 + r^2\left((dx^2)^2 + \mathcal{H}(dx^3)^2 + \frac{dr^2}{r^4\mathcal{F}}\right) + e^{\frac{1}{2}\phi}d\Omega_5^2 \\ &\equiv \; G_{MN}dx^M dx^N \end{aligned} \tag{5.20}$$

where

$$\begin{aligned} A(y) &= (yr_h)^2\left[1 - \frac{\cosh^2\eta}{y^4} + a^2\cosh^2\eta\left\{\mathcal{F}_2 + \mathcal{B}_2\left(1 - \frac{1}{y^4}\right)\right\}\right], \\ B(y) &= (yr_h)^2\sinh\eta\cosh\eta\left[\frac{1}{y^4} - a^2\left\{\mathcal{F}_2 + \mathcal{B}_2\left(1 - \frac{1}{y^4}\right)\right\}\right], \\ C(y) &= (yr_h)^2\left[1 + \frac{\sinh^2\eta}{y^4} - a^2\sinh^2\eta\left\{\mathcal{F}_2 + \mathcal{B}_2\left(1 - \frac{1}{y^4}\right)\right\}\right]. \end{aligned} \tag{5.21}$$

(Note that since we shall be using the primed coordinates from now on, we have got rid of the primes for simplicity. Also, we have suppressed the y-dependence of the quantities $\mathcal{F}_2, \mathcal{B}_2$. Further, we have expressed A, B and C as functions of the scaled radial coordinate y.) In this background we evaluate the Nambu-Goto string world-sheet action (Eq. 2.11) using Eq. 2.10, with G_{MN} given by Eq. 5.20 and the gauge choice, $\tau = t, \sigma = x^2$ where $-L/2 \leq x^2 \leq +L/2$ and $r = r(\sigma), x^1(\sigma), x^3(\sigma) =$ constant. We wish to determine the string embedding $r(\sigma)$ supplemented by the boundary condition $r\left(x^2 = \pm L/2\right) \to \infty$. Equipped with the above parametrization, the Nambu-Goto action (Eq. 2.11) becomes,

$$\mathcal{S} = \frac{\mathcal{T}}{2\pi\alpha'}\int_{-L/2}^{L/2} d\sigma\sqrt{A\left(G_{22} + G_{rr}(\partial_\sigma r)^2\right)}. \tag{5.22}$$

Defining the dimensionless quantities, $\tilde{\sigma} = \sigma/r_h$ and $\ell = L/r_h$, we can rewrite the above action as

$$\mathcal{S} = \frac{\mathcal{T} r_h}{2\pi\alpha'} \int_{-\ell/2}^{\ell/2} d\tilde{\sigma} \mathcal{L} \tag{5.23}$$

where

$$\mathcal{L} = \sqrt{A\left(G_{22} + G_{rr} y'^2\right)} \tag{5.24}$$

is the Lagrangian density and $\partial_{\tilde{\sigma}} y = y'$. Note that $\mathcal{L}$ does not have any explicit $\tilde{\sigma}$-dependence which at once allows us to extract the conserved quantity,

$$\mathcal{L} - y' \frac{\partial \mathcal{L}}{\partial y'} = \frac{A G_{22}}{\sqrt{A(G_{22} + G_{rr} y'^2)}} = K \tag{5.25}$$

which, in turn, yields,

$$y' = \frac{1}{K} \sqrt{\frac{G_{22}}{G_{rr}}} \sqrt{A G_{22} - K^2}. \tag{5.26}$$

Upon integration we obtain

$$\ell = 2 \int_0^{\ell/2} d\tilde{\sigma} = 2K \int_{y_t}^{\infty} dy \sqrt{\frac{G_{rr}}{G_{22}}} \frac{1}{\sqrt{A G_{22} - K^2}}. \tag{5.27}$$

The limits in the second integration require a little explanation. Recall that y is the scaled radial coordinate and the string hangs down starting from $y = \infty$ (where the boundary gauge theory lives) up to y_t (which we shall find shortly), where it turns back and rises again up to $y = \infty$. Plugging in the explicit expressions for the metric components, we arrive at,

$$\ell = \frac{2\tilde{K}}{r_h^2} \int_{y_t}^{\infty} dy \frac{1}{\sqrt{\left(y^4 - 1 + \frac{\tilde{a}^2}{24}\Sigma(y)\right)\left(y^4 - y_c^4 + \frac{\tilde{a}^2}{24}\Lambda(y)\cosh^2\eta\right)}} \tag{5.28}$$

where we have defined,

$$\Sigma(y) = 8(y^2-1) - 10\log 2 + (3y^4+7)\log\left(1+\frac{1}{y^2}\right), \tag{5.29}$$

$$\Lambda(y) = 2(1-y^2) - 10\log 2 + 2(y^4+4)\log\left(1+\frac{1}{y^2}\right), \tag{5.30}$$

and $\tilde{a} = a/r_h(\sim a/\pi T)$, $\tilde{K} = K/r_h^2$, $y_c^4 = \cosh^2\eta + \tilde{K}^2$. Using Eq. 5.15 one can now find the actual Q-$\bar{Q}$ separation as

$$L = \frac{2\tilde{K}}{\pi T}\left(1+\frac{\tilde{a}^2}{48}(5\log 2 - 2)\right)\int_{y_t}^{\infty} dy \frac{1}{\sqrt{\left(y^4-1+\frac{\tilde{a}^2}{24}\Sigma(y)\right)\left(y^4-y_c^4+\frac{\tilde{a}^2}{24}\Lambda(y)\cosh^2\eta\right)}}. \tag{5.31}$$

As mentioned earlier, to perform the integration, one needs to specify y_t. The turning point is found out by demanding that the terms in the denominator vanish separately (which is equivalent to demanding that y' vanishes at these points) and accepting the larger one among them. As one can easily verify, the first term in the denominator vanishes at $y=1$, since $\Sigma(1) = 0$, thereby, furnishing a turning point at $y_{t1} = 1$ up to $\mathcal{O}(a^2)$. To find the turning point y_{t2} arising from the second term, we assume the anisotropy parameter $\tilde{a}$[‡] to be small and we need to find a solution to

$$y_{t2}^4 - y_c^4 + \frac{\tilde{a}^2}{24}\Lambda(y_c)\cosh^2\eta = 0. \tag{5.32}$$

Note that we have evaluated Λ at $y = y_c$ since the term is already at $\mathcal{O}(\tilde{a}^2)$ and consequently, the error incurred is $\sim \mathcal{O}(\tilde{a}^4)$. This has a solution

[‡]Since in our analysis a always appears in the form $a^2/r_h^2 \equiv \tilde{a}^2$, we shall, henceforth, call $\tilde{a}$ the anisotropy parameter.

$$y_{t2} = y_c \left(1 - \frac{\tilde{a}^2}{24 y_c^4}\Lambda(y_c)\cosh^2\eta\right)^{1/4}. \tag{5.33}$$

It can be shown that $y_{t2} > 1$ always, so that we take it to be the actual turning point y_t. As expected, by setting $\tilde{a} = 0$ we recover the turning point y_c in the isotropic case. Now Eq. 5.31 gives L as a function of the constant $\tilde{K}$. We shall later show how L is affected by the presence of anisotropy for various values of the rapidity parameter η and the anisotropy parameter $\tilde{a}$. Further, by setting $\eta = 0$ we obtain the static Q-$\bar{Q}$ separation. We postpone the discussion of our numerical results till we give the Q-$\bar{Q}$ potential.

Changing the integration variable from $\tilde{\sigma}$ to y we can rewrite the action (Eq. 5.23) as

$$\mathcal{S} = \frac{\mathcal{T} r_h}{\pi\alpha'}\int_{y_t}^{\infty} dy A\sqrt{\frac{G_{22}G_{rr}}{AG_{22} - K^2}}. \tag{5.34}$$

Putting the explicit expression for the metric components one finally has

$$\begin{aligned}\mathcal{S} &= \frac{\mathcal{T} r_h}{\pi\alpha'}\int_{y_t}^{\infty} dy \frac{y^4 - \cosh^2\eta + \frac{\tilde{a}^2}{24}\Lambda(y)\cosh^2\eta}{\sqrt{\left(y^4 - 1 + \frac{\tilde{a}^2}{24}\Sigma(y)\right)\left(y^4 - y_c^4 + \frac{\tilde{a}^2}{24}\Lambda(y)\cosh^2\eta\right)}} \\ &\equiv \frac{\mathcal{T} r_h}{\pi\alpha'}\int_{y_t}^{\infty} dy \hat{\mathcal{S}}^{ani}.\end{aligned} \tag{5.35}$$

Finally, the potential $V(L)$ is obtained from Eq. 3.17 where $\mathcal{S}_0$ is the diverging part of the action corresponding to two free strings. To compute $\mathcal{S}_0$ we employ the static gauge condition, $\tau = t, \sigma = r, x^1 = x^1(\sigma)$ and x^2, x^3 are independent of τ, σ to have,

$$\mathcal{S}_0 = \frac{\mathcal{T}}{\pi\alpha'}\int_{r_0}^{\infty} dr\sqrt{AG_{rr} + (x^{1\prime})^2(AC + B^2)} \equiv \frac{\mathcal{T}}{\pi\alpha'}\int_{r_0}^{\infty} dr\mathcal{L}_0. \tag{5.36}$$

As before, $\mathcal{S}_0$ too does not have any explicit x^1-dependence implying that there exists a conserved quantity,

$$\frac{\partial \mathcal{L}_0}{\partial x^{1\prime}} = \left(AC + B^2\right) \frac{x^{1\prime}}{\mathcal{L}_0} = \text{constant} = K_0 \tag{5.37}$$

which yields,

$$\begin{aligned}(x^{1\prime})^2 &= K_0^2 \frac{AG_{rr}}{(AC+B^2)(AC+B^2-K_0^2)} \\ &= \frac{\tilde{K}_0^2}{r_h^4} \frac{\left(y^4 - \cosh^2\eta + \frac{\tilde{a}^2}{24}\Lambda(y)\cosh^2\eta\right)}{\left(y^4 - 1 + \frac{\tilde{a}^2}{24}\Lambda\right)\left(y^4 - 1 + \frac{\tilde{a}^2}{24}\Sigma\right)\left(y^4 - 1 - \tilde{K}_0^2 + \frac{\tilde{a}^2}{24}\Lambda\right)}\end{aligned} \tag{5.38}$$

(we have used the scaling $\tilde{K}_0 = K_0/r_h^2$ and omitted the functional-dependence of Σ and Λ on y). Note that in the expression for $\mathcal{S}_0$ we have not specified the lower limit of the integration r_0 (or y_0 after scaling), which we shall now determine. For a string (corresponding to a free quark/antiquark) hanging down we expect it to extend all the way to the horizon at $y = 1$. This is the case when the string moves through the isotropic background. In particular, this implies that the string can not encounter a turning point before $y = 1$. In our case, the possible turning points can be found out from Eq. 5.38 by demanding that $x^{1\prime} = \infty$ at those points. Now the first two terms in the denominator of Eq. 5.38 give the turning point $y_0 = 1$ up to $\mathcal{O}(\tilde{a}^2)$ since $\Sigma(1) = \Lambda(1) = 0$. However, the third term (which contains the unspecified constant $\tilde{K}_0$) gives a turning point $y_0^4 \sim 1 + \tilde{K}_0^2 + \mathcal{O}(\tilde{a}^2)$ which is greater than zero even for the isotropic case. Taking cue from the isotropic case we eliminate this possibility by constraining the value of $\tilde{K}_0$ such that the zero of this term coincides with the zero of the numerator. This at once provides us an expression for $\tilde{K}_0$ as

$$\tilde{K}_0^2 = \sinh^2\eta\left(1 - \frac{\tilde{a}^2}{24}\Lambda\left(y = \sqrt{\cosh\eta}\right)\right). \tag{5.39}$$

Thus we conclude that even in the presence of anisotropy the string extends right up to the horizon (like in the isotropic case) without picking up any correction at least to $\mathcal{O}(\tilde{a}^2)$. We can now recast the action as

$$\begin{aligned}
\mathcal{S}_0 &= \frac{\mathcal{T}}{\pi\alpha'}\int_{r_h}^{\infty} dr\sqrt{AG_{rr}}\sqrt{\frac{AC+B^2}{AC+B^2-K_0^2}} \\
&= \frac{\mathcal{T}r_h}{\pi\alpha'}\int_1^{\infty} dy\frac{\sqrt{\left(y^4-\cosh^2\eta+\frac{\tilde{a}^2}{24}\Lambda(y)\cosh^2\eta\right)\left(y^4-1+\frac{\tilde{a}^2}{24}\Lambda(y)\right)}}{\sqrt{\left(y^4-1+\frac{\tilde{a}^2}{24}\Sigma(y)\right)\left(y^4-\cosh^2\eta+\frac{\tilde{a}^2}{24}\left(\Lambda(y)+\Lambda\big|_{y=\sqrt{\cosh\eta}}\sinh^2\eta\right)\right)}} \\
&\equiv \frac{\mathcal{T}r_h}{\pi\alpha'}\int_1^{\infty} dy\hat{\mathcal{S}}_0^{ani}.
\end{aligned} \tag{5.40}$$

Inserting Eqs. 5.35 and 5.40 in Eq. 3.17 and then using Eq. 5.15 we can now write

$$\frac{V}{T} = \sqrt{\lambda}\left(1 - \frac{\tilde{a}^2}{48}(5\log 2 - 2)\right)\left(\int_{y_t}^{\infty} dy\hat{\mathcal{S}}^{ani} - \int_1^{\infty} dy\hat{\mathcal{S}}_0^{ani}\right) \tag{5.41}$$

where we have used the standard AdS/CFT dictionary $R^4 = \lambda\alpha'^2$ (with R set to unity here) to express our final result in terms of quantities pertaining to the gauge theory. Evaluating Eq. 5.41 involves performing integrals which can not be handled analytically. We, therefore, fall back upon numerical means to perform these integrals and numerically show our results. We compute L for various values of η and $\tilde{a}$ as a function of the constant $\tilde{K}$, numerically invert Eq. 5.31 to express $\tilde{K}$ in terms of L and plug it in Eq. 5.35 to finally obtain $V(L)$ as a function of L. Here we shall provide our numerical results for both the Q-$\bar{Q}$ separation and the Q-$\bar{Q}$ potential. In particular, by setting $\eta = 0$ we recover the static

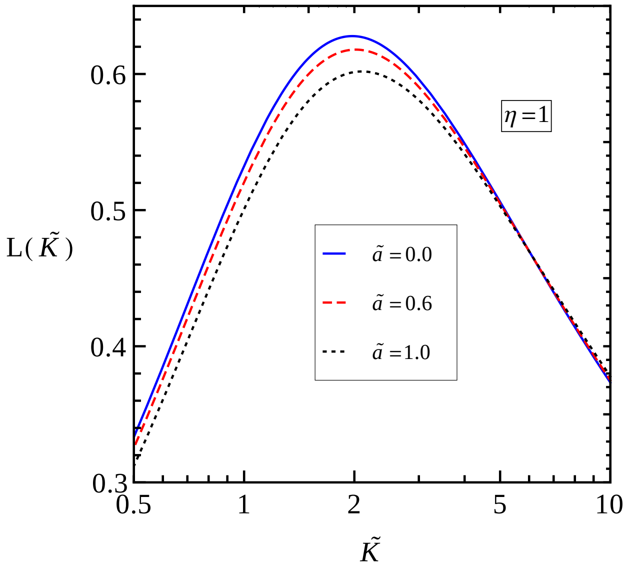

Figure 5.1: Q-$\bar{Q}$ separation L (normalized) as a function of $\tilde{K}$ with $\eta = 1$ for different values of $\tilde{a}$ when dipole lies in transverse plane perpendicular to its velocity

Q-$\bar{Q}$ potential, which was found earlier in [107]. In Figures 5.1-5.4 we have provided the plots for $L(\tilde{K})$-$\tilde{K}$ and $V(L)$-L for $\eta = 1$ $(v = 0.76)$ and $\eta = 4$ $(v = 0.99)$ respectively. While the qualitative pattern of the $L(\tilde{K})$-$\tilde{K}$ and the $V(L)$-L plots are the same for both the values of v, the details differ. So we shall take Figures 5.1 and 5.2 as the prototype case and discuss the results. First of all, we find from Figure 5.1 that as $\tilde{K}$ increases the separation $L(\tilde{K})$ increases till it reaches a maximum L_{max} after which it again falls off. L_{max} is interpreted as the screening length[§] of the dipole, i.e., beyond this critical value of L the screening effect of the plasma is sufficient to break the dipole. We observe that the effect of anisotropy is to suppress the screening length thereby encouraging the melting of the dipole. In particular, the degree of suppression of L_{max} is more for stronger anisotropy. The deviation from the isotropic curve is more pronounced for lower $\tilde{K}$ (before L_{max} is

[§]Note that our definition of the screening length differs slightly from that used in [108].

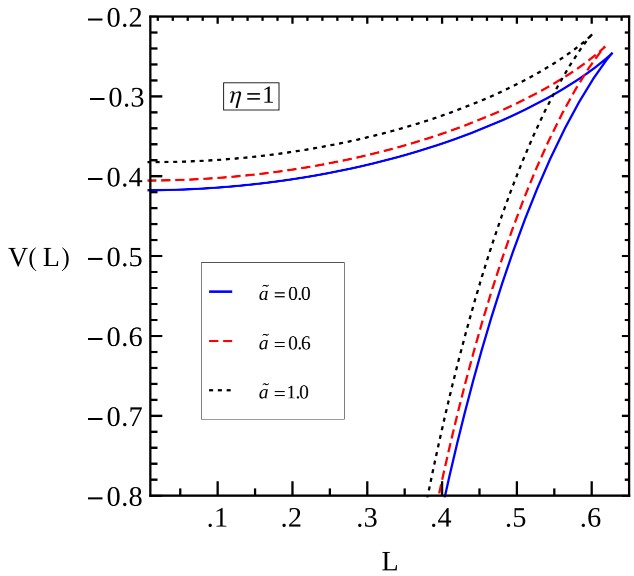

Figure 5.2: Normalized Q-$\bar{Q}$ potential V as a function of L with $\eta = 1$ for the same set of $\tilde{a}$ and same orientation (as in Figure 5.1)

attained) than for higher $\tilde{K}$ (after L_{max}). For $L < L_{max}$ there can be two dipoles at a fixed L for two different values of $\tilde{K}$. To understand at which one of the $\tilde{K}$ values the dipole will actually exist we need to analyze the $V(L)$-L plot. The Q-$\bar{Q}$ potential has two branches corresponding to two different values of $\tilde{K}$. The upper branch corresponds to smaller value of $\tilde{K}$ whereas the lower branch corresponds to higher value of $\tilde{K}$. Of course, the lower branch has lower energy and consequently, it is the preferred state of the dipole. So, even if a dipole is in the upper branch it will not be in a stable configuration and the dipole will make a transition to the lower branch. As we turn on a small anisotropy both the branches of the potential shift slightly upwards. Since the upper branch is physically insignificant, corresponding to an unstable state, we shall confine our discussion to the lower branch only. The marginal upward shift in the potential indicates that the dipole is now loosely bound, the shift being more prominent for higher values of the anisotropy pa-

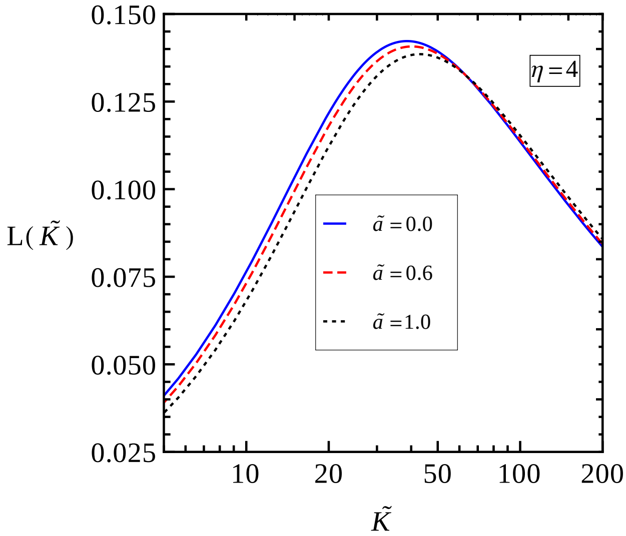

Figure 5.3: Q-$\bar{Q}$ separation L (normalized) as a function of $\tilde{K}$ with $\eta = 4$ for different values of $\tilde{a}$ when dipole lies in transverse plane perpendicular to its velocity

rameter $\tilde{a}$. This fits in with our conclusion from the $L(\tilde{K})$-$\tilde{K}$ plot that anisotropy enhances the screening effect of the medium. Further notice that in both cases the potential is always negative. In Figures 5.5 and 5.6 the plots for the static case are shown. Since the basic nature is the same, we shall not elaborate upon our results and briefly mention the salient features of the plots emphasizing the differences from the velocity-dependent cases. First of all, notice that unlike the moving dipole case, now the deviation from the isotropic curve in the $L(\tilde{K})$-$\tilde{K}$ plot is appreciable on either side of L_{max}. Also note that now L_{max} is much higher for the $\eta = 0$ case and steadily decreases as we increase $\tilde{a}$. In the $V(L)$-L plot the lower branch suffers a small elevation whereas, the insignificant upper branch is largely insensitive to changes in $\tilde{a}$. The new feature that now emerges is that the static potential crosses zero and becomes positive at a particular value $L = L_p$. In the presence of the medium the potential has two parts - the Coulomb part (varying inversely with L) and the

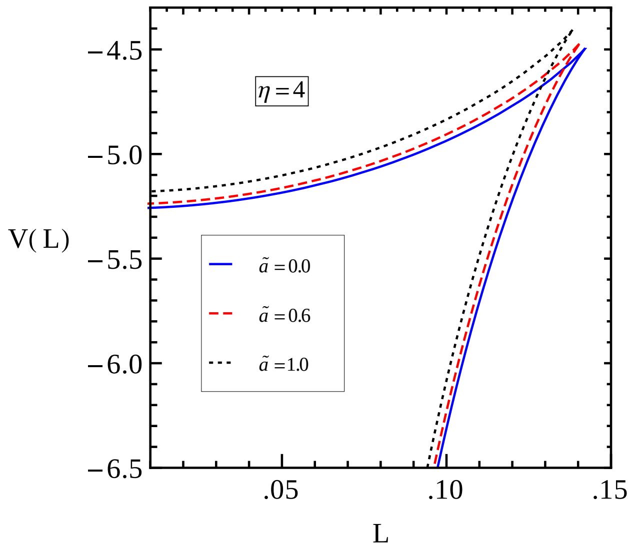

Figure 5.4: Normalized Q-$\bar{Q}$ potential V as a function of L with $\eta = 4$ for the same set of $\tilde{a}$ and same orientation (as in Figure 5.3)

confining part (which goes as L)

$$V(L) = -\frac{\alpha}{L} + \sigma L. \tag{5.42}$$

L_p denotes the separation beyond which the confining part starts to dominate. This feature is nicely captured in the plot here in a qualitative manner. In fact, there will be a critical velocity $v_p = \tanh \eta_p$ (whose value will, in general, also depend upon $\tilde{a}$) beyond which the potential will not contain any positive piece.

We shall now obtain an analytical expression for the screening length, albeit in a special case. The Q-$\bar{Q}$ separation L has already been given in Eq. 5.31. We have mentioned earlier that, in general, the integration appearing in Eq. 5.31 can not be done analytically. Of course, this is not to be thought of as an artifact of our anisotropic background. Rather,

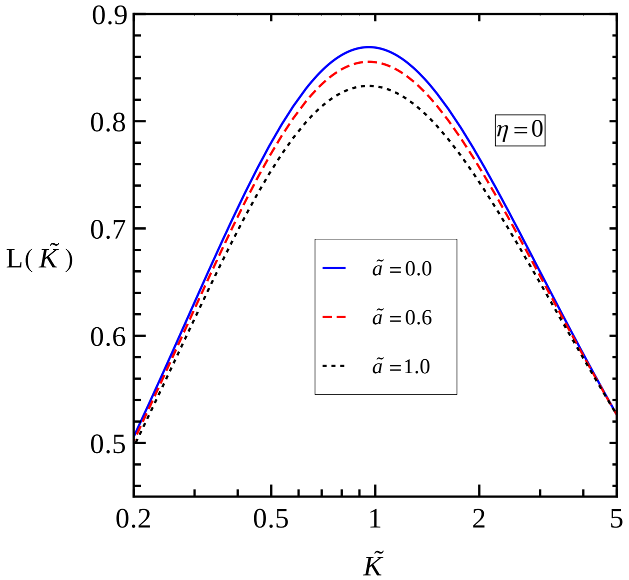

Figure 5.5: Q-$\bar{Q}$ separation L (normalized) as a function of $\tilde{K}$ with $\eta = 0$ for different values of $\tilde{a}$ when dipole lies in transverse plane

it is a handicap present in the isotropic case, too. Here, to facilitate analytical manipulation, we shall confine ourselves to the ultra-relativistic regime where η is large, in which case the turning point y_t also becomes very large but assume the product $\tilde{a}^2 \cosh^2 \eta$ is sufficiently small. In this special case the first term in the denominator in Eq. 5.31 lends itself to a binomial expansion. Here, for the sake of simplicity, we shall consider only the leading order term in the afore-said expansion in which case one can write

$$L = \frac{2\tilde{K}}{\pi T}\left(1 + \frac{\tilde{a}^2}{48}(5\log 2 - 2)\right)\int_{y_t}^{\infty} dy \frac{1}{y^2\sqrt{\left(y^4 - y_c^4 + \frac{\tilde{a}^2}{24}\Lambda(y)\cosh^2\eta\right)}} + \cdots . \quad (5.43)$$

Also, in the limit η becoming very large, $\Lambda(y)$ reduces to $\Lambda(y) = 1 - 10\log 2$, which is, in fact, independent of y. In this simplified scenario, the integral can be handled analytically

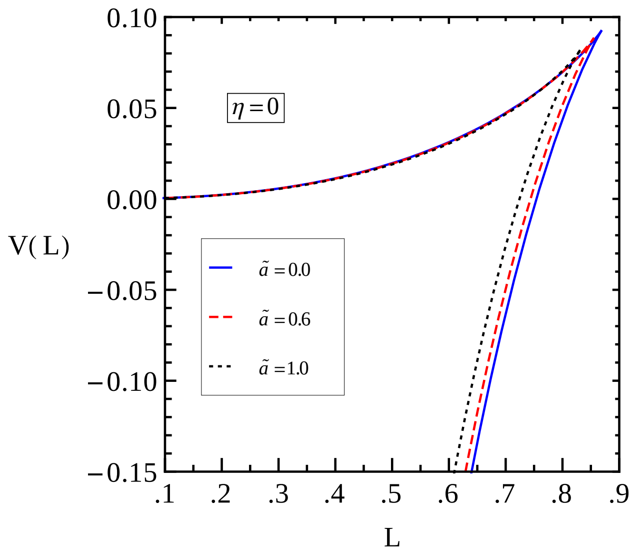

Figure 5.6: Normalized Q-$\bar{Q}$ potential V as a function of L with $\eta = 0$ for the same set of $\tilde{a}$ and same orientation (as in Figure 5.5)

and we have,

$$L = \frac{2\tilde{K}}{\pi T}\left(1 + \frac{\tilde{a}^2}{48}(5\log 2 - 2)\right)\frac{\sqrt{\pi}}{y_t^3}\frac{\Gamma(3/4)}{\Gamma(1/4)}. \tag{5.44}$$

It is now a straight forward exercise to compute the value of $\tilde{K}$ and hence, y_t which maximize L as

$$\begin{aligned} \tilde{K}^2 &= 2\cosh^2\eta + \frac{\tilde{a}^2\cosh^2\eta\,(10\log 2 - 1)}{12} \\ y_t &= y_c\left(1 + \frac{\tilde{a}^2\,(10\log 2 - 1)}{96}\cosh^2\eta\right). \end{aligned} \tag{5.45}$$

Incorporating these values we arrive at the final expression for the screening length L_{max},

$$L_{max} = \frac{1}{\sqrt{\pi}T}\frac{\Gamma(3/4)}{\Gamma(1/4)}\frac{2\sqrt{2}}{3^{3/4}}\frac{1}{\sqrt{\cosh\eta}}\left(1 - \frac{\tilde{a}^2}{16}(2.96\cosh^2\eta - 0.48)\right)$$

$$= \frac{1}{\sqrt{\pi}T}\frac{\Gamma(3/4)}{\Gamma(1/4)}\frac{2\sqrt{2}}{3^{3/4}}(1-v^2)^{1/4}\left(1-\frac{\tilde{a}^2}{16}\left(\frac{2.96}{(1-v^2)}-0.48\right)\right). \quad (5.46)$$

The proportional change brought by anisotropy is,

$$\frac{\Delta L_{max}}{L_{max}\big|_{\tilde{a}=0}} = -\frac{\tilde{a}^2}{16}(2.96\cosh^2\eta - 0.48). \quad (5.47)$$

Having deduced the analytical expression for L_{max}, a few comments are in order here. First, as expected, by setting $\tilde{a} = 0$ here one recovers the usual screening length in an isotropic plasma [27,70]. Second, it is obvious that the correction factor is always negative so that L_{max} decreases in the presence of anisotropy. Third, when $\tilde{a}$ increases, the fall in L_{max} is greater. Again, keeping $\tilde{a}$ fixed, if η increases, L_{max} falls. These conclusions drawn from the analytic expression in Eq. 5.46 are in agreement with all our numerical results in the $L(\tilde{K})$-$\tilde{K}$ plots discussed earlier. Observe that the correction in the screening length arising due to the presence of anisotropy depends on the rapidity parameter as well. One also finds that L_{max} depends inversely upon the temperature and scales with velocity as $(1-v^2)^{1/4}$. The velocity-scaling obtained here is in agreement with that found in [108], where, of course, arbitrary orientation of the dipole with respect to its velocity was allowed and the analysis was not restricted only to weak anisotropy. One infers from Eq. 5.45 that the value of $\tilde{K}$ which maximizes L increases when we turn on the anisotropy parameter. This is also nicely exposed in the $L(\tilde{K})$-$\tilde{K}$ plot in Figures 5.1 and 5.3 where the peaks gradually shift towards right as the anisotropy gets larger. With this we close our discussion of this configuration and move over to the next case.

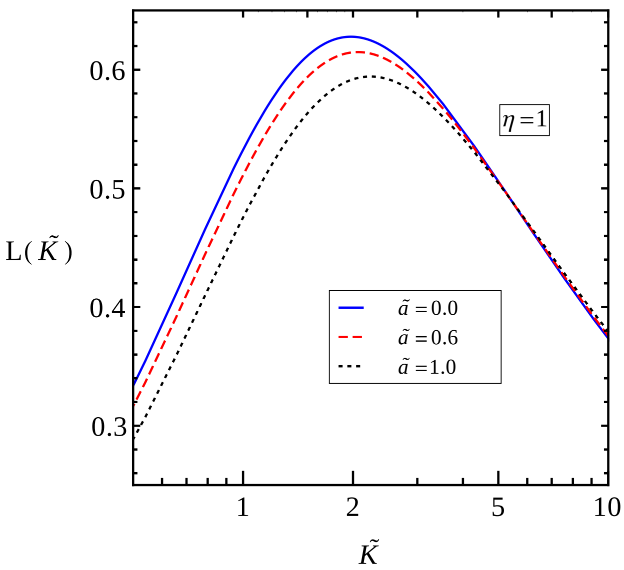

Figure 5.7: Q-$\bar{Q}$ separation L (normalized) as a function of $\tilde{K}$ with $\eta = 1$ for different values of $\tilde{a}$ when velocity is in transverse plane and dipole along anisotropic direction

5.3.2 Dipole along x^3, velocity in transverse plane

In this case the dipole lies along the anisotropic direction x^3 and moves in the transverse plane with a velocity v. Without any loss of generality, we can take the direction of motion to be along x^1. The calculation in this case proceeds in pretty much the same way. So we shall be brief in this section, pointing out only the differences that crops up in the calculations as we go along. Firstly, note that the choice of the static gauge is slightly altered. Now we take $\tau = t, \sigma = x^3, r = r(\sigma)$ with $x^{1,2}$ being independent of τ or σ. Enforcing this choice of gauge in the Nambu-Goto action (Eq. 2.11) results in the following form of the action

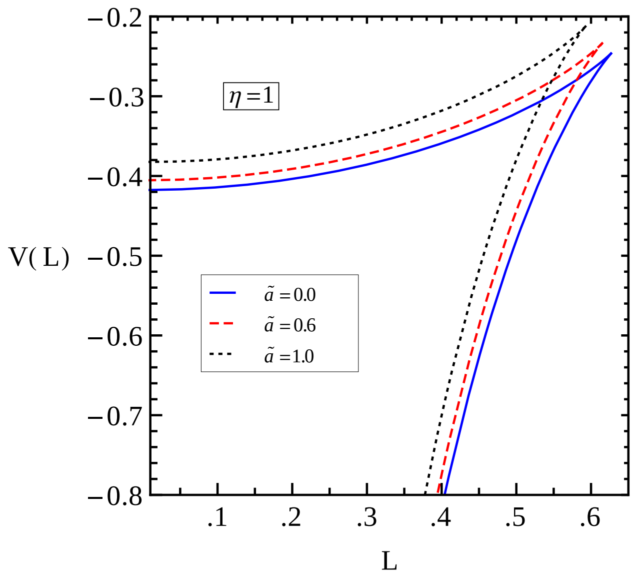

Figure 5.8: Normalized Q-$\bar{Q}$ potential V as a function of L with $\eta = 1$ for the same set of $\tilde{a}$ and same orientation (as in Figure 5.7)

$$\mathcal{S} = \frac{\mathcal{T} r_h}{2\pi\alpha'} \int_{-\ell/2}^{+\ell/2} d\tilde{\sigma} \sqrt{(A\,(G_{33} + G_{rr} y'^2))}. \tag{5.48}$$

As before, the absence of any explicit $\tilde{\sigma}$-dependence leads to the conserved quantity,

$$K = \frac{A G_{33}}{\sqrt{A\,(G_{33} + G_{rr} y'^2)}} \tag{5.49}$$

and the scaled Q-$\bar{Q}$ separation assumes the form,

$$\ell = 2K \int_{y_t}^{\infty} dy \sqrt{\frac{G_{rr}}{G_{33}}} \frac{1}{\sqrt{A G_{33} - K^2}}. \tag{5.50}$$

Plugging in the explicit expressions of the metric components, we finally obtain L as

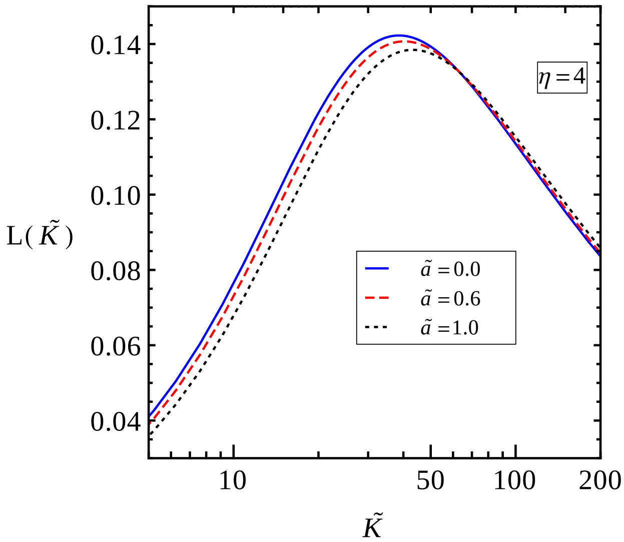

Figure 5.9: Q-$\bar{Q}$ separation L (normalized) as a function of $\tilde{K}$ with $\eta = 1$ for different values of $\tilde{a}$ when velocity is in transverse plane and dipole along anisotropic direction

$$L = \frac{2\tilde{K}}{\pi T}\left(1 + \frac{\tilde{a}^2(5\log 2 - 2)}{48}\right)\int_{y_t}^{\infty} dy \frac{\mathcal{H}^{-1}}{\sqrt{\left(y^4 - 1 + \frac{\tilde{a}^2}{24}\Sigma\right)\left(y^4 - (1 - \frac{\tilde{a}^2}{24}\Lambda)\cosh^2\eta - \tilde{K}^2\mathcal{H}^{-1}\right)}} \tag{5.51}$$

where we have suppressed the explicit y-dependence of $\Sigma(y), \Lambda(y)$ and $\mathcal{H}(y)$ for convenience. The turning point y_t is then found out by demanding that the second term in the denominator vanishes at y_t, i.e., y_t is obtained as a solution to,

$$y_t^4 - \cosh^2\eta + \frac{\tilde{a}^2}{24}\Lambda(y_t)\cosh^2\eta - \tilde{K}^2\mathcal{H}(y_t)^{-1} = 0. \tag{5.52}$$

Using Eq. 5.49, the action is given by

$$\mathcal{S} = \frac{\mathcal{T} r_h}{\pi\alpha'}\int_{y_t}^{\infty} dy A\sqrt{\frac{G_{33}G_{rr}}{AG_{33} - K^2}} \tag{5.53}$$

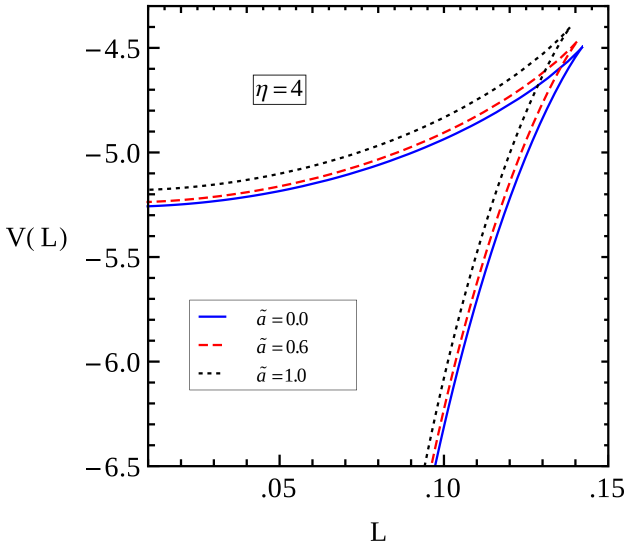

Figure 5.10: Normalized Q-$\bar{Q}$ potential V as a function of L with $\eta = 4$ for the same set of $\tilde{a}$ and same orientation (as in Figure 5.9)

which can be rewritten as

$$\begin{aligned}\mathcal{S} &= \frac{\mathcal{T}r_h}{\pi\alpha'}\int\limits_{y_t}^{\infty} dy \frac{y^4 - \cosh^2\eta + \frac{\tilde{a}^2}{24}\Lambda\cosh^2\eta}{\sqrt{\left(y^4 - 1 + \frac{\tilde{a}^2}{24}\Sigma\right)\left(y^4 - (1 - \frac{\tilde{a}^2}{24}\Lambda)\cosh^2\eta - \tilde{K}^2\mathcal{H}^{-1}\right)}} \\ &\equiv \frac{\mathcal{T}r_h}{\pi\alpha'}\int\limits_{y_t}^{\infty} dy\hat{\mathcal{S}}^{ani}. \end{aligned} \tag{5.54}$$

To evaluate the Q-$\bar{Q}$ potential one also needs to subtract the self-energy term $\mathcal{S}_0$. It is easy to convince oneself that in this case the expression for $\mathcal{S}_0$ as given in Eq. 5.40 remains unaltered and the Q-$\bar{Q}$ potential will be given by Eq. 5.41 with $\hat{\mathcal{S}}^{ani}$ now taken to be as in Eq. 5.54. We have given the $L(\tilde{K})$-$\tilde{K}$ and the $V(L)$-L plots in Figures 5.7-5.10 for $\eta = 1$ and $\eta = 4$ respectively. Figures 5.11 and 5.12 show the static Q-$\bar{Q}$ separation and the static

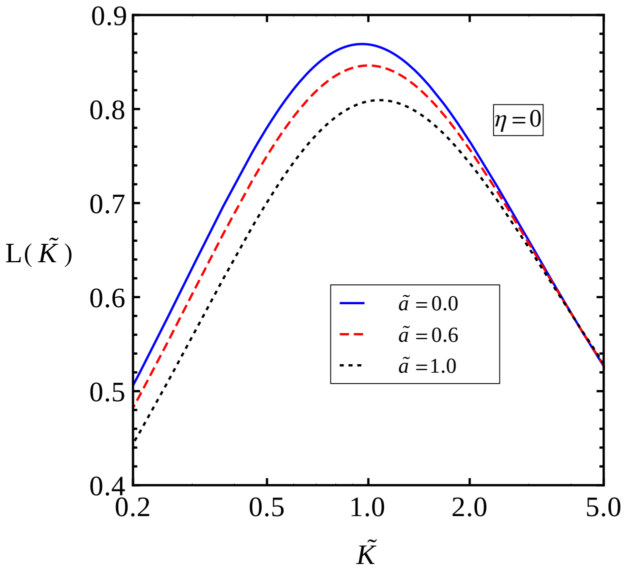

Figure 5.11: Q-$\bar{Q}$ separation L (normalized) as a function of $\tilde{K}$ with $\eta = 0$ for different values of $\tilde{a}$ when dipole lies along anisotropic direction

Q-$\bar{Q}$ potential respectively. We observe that in all the cases the general pattern of the plots (like the rightwards shift of the peak in the $L(\tilde{K})$ curves, attenuation of L_{max} and rise in the $V(L)$ plots with increasing $\tilde{a}$) mimic those obtained earlier in §5.3.1 and hence does not merit a separate discussion.

5.3.3 Dipole in transverse plane, velocity along x^3

Third in our list is the case where the dipole is aligned in the transverse plane and it has a velocity along the anisotropic direction. For the sake of simplicity we have taken the dipole to lie along x^1. While we shall proceed along the same line as in the previous cases, this time the calculations will be a little different since we now need to give a boost along the anisotropic direction, x^3. First of all, we go to the rest frame $(t', x^{3\prime})$ of the Q-$\bar{Q}$ pair by

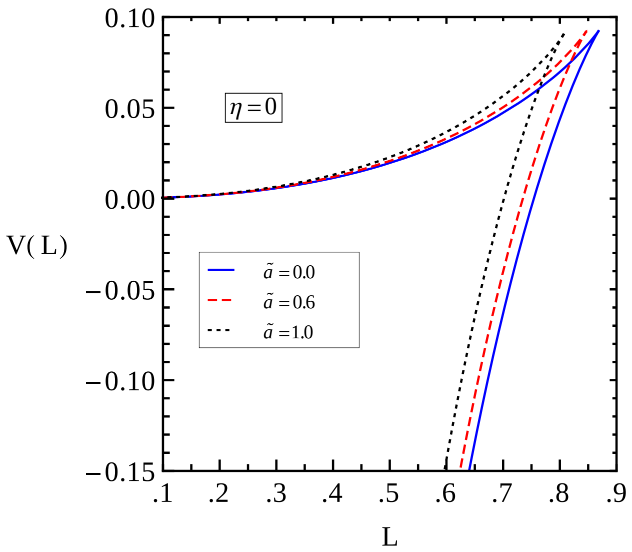

Figure 5.12: Normalized Q-$\bar{Q}$ potential V as a function of L with $\eta = 0$ for the same set of $\tilde{a}$ and same orientation (as in Figure 5.11)

inflicting the boost

$$
\begin{aligned}
dt &= \cosh\eta dt' - \sinh\eta dx^{3\prime}, \\
dx^3 &= -\sinh\eta dt' + \cosh\eta dx^{3\prime}.
\end{aligned}
\tag{5.55}
$$

The Wilson loop so formed spans the t' and x^1 directions. In terms of the boosted coordinates the metric (Eq. 5.11) can be rewritten as

$$
\begin{aligned}
ds^2 &= -\tilde{A}(r)dt^2 - 2\tilde{B}(r)dtdx^3 + \tilde{C}(r)(dx^3)^2 + r^2\left((dx^1)^2 + (dx^2)^2 + \frac{dr^2}{r^4\mathcal{F}}\right) + e^{\frac{1}{2}\phi}d\Omega_5^2 \\
&\equiv \tilde{G}_{MN}dx^M dx^N
\end{aligned}
\tag{5.56}
$$

where

$$
\tilde{A}(y) = \left(\frac{r_h}{y}\right)^2\left[y^4 - \cosh^2\eta + \frac{\tilde{a}^2}{24}\Lambda\cosh^2\eta + y^4\sinh^2\eta(1-\mathcal{H})\right], \tag{5.57}
$$

$$\tilde{B}(y) = \left(\frac{r_h}{y}\right)^2 \sinh\eta\cosh\eta\left[1-\frac{\tilde{a}^2}{24}\Lambda+y^4(\mathcal{H}-1)\right], \tag{5.58}$$

$$\tilde{C}(y) = \left(\frac{r_h}{y}\right)^2 \left[y^4+\sinh^2\eta-\frac{\tilde{a}^2}{24}\Lambda\sinh^2\eta+y^4\cosh^2\eta(\mathcal{H}-1)\right]. \tag{5.59}$$

To evaluate the Nambu-Goto string world-sheet action we employ the following choice of gauge: $\tau = t, \sigma = x^1, r = r(\sigma)$ with $x^{2,3}$ having no τ- or σ-dependence. The action (Eq. 2.11) can now be written as

$$\mathcal{S} = \frac{\mathcal{T}r_h}{2\pi\alpha'}\int_{-\ell/2}^{+\ell/2} d\tilde{\sigma}\sqrt{\tilde{A}\left(\tilde{G}_{11}+\tilde{G}_{rr}y'^2\right)}. \tag{5.60}$$

Again the absence of any explicit σ-dependence furnishes the conserved quantity,

$$K = \frac{\tilde{A}\tilde{G}_{11}}{\sqrt{\tilde{A}\left(\tilde{G}_{11}+\tilde{G}_{rr}y'^2\right)}}. \tag{5.61}$$

Proceeding in the same way as before we get the scaled Q-$\bar{Q}$ separation,

$$\ell = 2K\int_{y_t}^{\infty} dy\sqrt{\frac{\tilde{G}_{rr}}{\tilde{G}_{11}}}\frac{1}{\sqrt{\tilde{A}\tilde{G}_{11}-K^2}} \tag{5.62}$$

from which one can read off the actual Q-$\bar{Q}$ separation

$$L = \frac{2\tilde{K}}{\pi T}\left(1+\frac{\tilde{a}^2(5\log 2-2)}{48}\right)\int_{y_t}^{\infty} dy\frac{1}{\sqrt{\left(y^4-1+\frac{\tilde{a}^2}{24}\Sigma\right)}}\times \frac{1}{\sqrt{y^4-y_c^4+\frac{\tilde{a}^2}{24}\Lambda\cosh^2\eta+y^4\sinh^2\eta(1-\mathcal{H})}}. \tag{5.63}$$

The turning point y_t is found from the solution of

$$y_t^4 - y_c^4 + \frac{\tilde{a}^2}{24}\Lambda(y_t)\cosh^2\eta + y_t^4\sinh^2\eta(1-\mathcal{H}) = 0. \tag{5.64}$$

The factor $(1-\mathcal{H})$ goes as $\frac{\tilde{a}^2}{4}\log\left(1+\frac{1}{y^2}\right)$ up to $\mathcal{O}(\tilde{a}^2)$ and for large y its contribution to the second factor in the denominator is $\frac{\tilde{a}^2}{4}y^2\sinh^2\eta$. This is greater than the other anisotropic term by $\mathcal{O}(y^2)$ for large y. Since, the integration over y extends up to $y=\infty$, the contribution from this term can be quite large. Hence, unlike in the previous cases, this time we do not expect the turning point y_t to appear in the form of a correction to the isotropic value y_c since the presence of this $\mathcal{O}(y^2)$ term renders the applicability of perturbative methods to solve the above equation futile. Thus, one has to depend solely upon numerical techniques to solve Eq. 5.64 in order to extract y_t. In fact, numerical evaluation shows y_t to be markedly different from y_c, particularly for low values of $\tilde{K}$. Once we have obtained y_t, we use it in Eq. 5.63 to numerically study the Q-$\bar{Q}$ separation. The string world-sheet action is

$$\mathcal{S} = \frac{\mathcal{T}r_h}{\pi\alpha'}\int_{y_t}^{\infty} dy\tilde{A}\sqrt{\frac{\tilde{G}_{11}\tilde{G}_{rr}}{\tilde{A}\tilde{G}_{11}-K^2}} \tag{5.65}$$

which, written explicitly, assumes the following form,

$$\begin{aligned}\mathcal{S} &= \frac{\mathcal{T}r_h}{\pi\alpha'}\int_{y_t}^{\infty} dy\frac{y^4-\cosh^2\eta+\frac{\tilde{a}^2}{24}\Lambda\cosh^2\eta+y^4\sinh^2\eta(1-\mathcal{H})}{\sqrt{\left(y^4-1+\frac{\tilde{a}^2}{24}\Sigma\right)\left(y^4-y_c^4+\frac{\tilde{a}^2}{24}\Lambda\cosh^2\eta+y^4\sinh^2\eta(1-\mathcal{H})\right)}}\\ &\equiv \frac{\mathcal{T}r_h}{\pi\alpha'}\int_{y_t}^{\infty} dy\hat{\mathcal{S}}^{ani}. \end{aligned}\tag{5.66}$$

As in the preceding cases, this action is divergent which is cured by taking away the self-energy contribution $\mathcal{S}_0$ of the Q-$\bar{Q}$ pair. To compute $\mathcal{S}_0$ we consider an open string hanging down the radial direction in the following gauge, $\tau = t, \sigma = r, x^3 = x^3(\sigma)$ and x^1, x^2 are independent of τ, σ. Repeating the same exercise as in §5.3.1 one finds $\mathcal{S}_0$ to be

$$\begin{aligned}
\mathcal{S}_0 &= \frac{\mathcal{T}}{\pi\alpha'}\int_{r_h}^{\infty} dr\sqrt{\tilde{A}\tilde{G}_{rr}}\sqrt{\frac{\tilde{A}\tilde{C}+\tilde{B}^2}{\tilde{A}\tilde{C}+\tilde{B}^2-K_0^2}} \\
&= \frac{\mathcal{T}r_h}{\pi\alpha'}\int_1^{\infty} dy\frac{\sqrt{y^4-\cosh^2\eta+\frac{\tilde{a}^2}{24}\Lambda\cosh^2\eta+y^4\sinh^2\eta(1-\mathcal{H})}}{\sqrt{y^4-1-\tilde{K}_0^2+\frac{\tilde{a}^2}{24}\Lambda\mathcal{H}+(\mathcal{H}-1)(y^4-1)}}\times \\
&\qquad\qquad\qquad\qquad\frac{\sqrt{y^4-1+\frac{\tilde{a}^2}{24}\Lambda\mathcal{H}+(\mathcal{H}-1)(y^4-1)}}{\sqrt{y^4-1+\frac{\tilde{a}^2}{24}\Sigma}} \\
&\equiv \frac{\mathcal{T}r_h}{\pi\alpha'}\int_1^{\infty} dy\hat{\mathcal{S}}_0^{ani}
\end{aligned} \tag{5.67}$$

where K_0 is the conserved quantity owing its origin to the absence of any explicit x^3-dependence in the action. The second terms each in the numerator and the denominator separately vanish at $y = 1$ providing a potential turning point $y_t = 1$. The first term in the denominator can contribute another turning point $y_t > 1$ but that possibility is ruled out by judiciously choosing the constant $\tilde{K}_0$ such that the zero of the first term in the numerator coincides with that of the first term in the denominator. We are now in a position to finally compute the Q-$\bar{Q}$ potential (Eq. 5.41) with $\hat{\mathcal{S}}^{ani}$ provided in Eq. 5.66 and the corresponding self-energy term $\hat{\mathcal{S}}_0^{ani}$ in Eq. 5.67. Using the above information we have plotted the Q-$\bar{Q}$ separation and the Q-$\bar{Q}$ potential in Figures 5.13-5.16 ¶. While the gross features of the plots remain almost unaltered, observe that all the signatures of the presence of anisotropy are far more pronounced (particularly in the high rapidity regime) than in either of the preceding cases. This has its roots in the presence of the $\mathcal{O}(y^2)$ term in the anisotropic

¶Note that we have not given the static Q-$\bar{Q}$ separation and the static Q-$\bar{Q}$ potential in this case since these will be the same as in §5.3.1.

contribution to the Q-$\bar{Q}$ separation and the Q-$\bar{Q}$ potential as mentioned earlier. The heavy Q-$\bar{Q}$ potential for this configuration has also been found in [108], using different values of the parameters and we find that our results tally with those presented in [108].

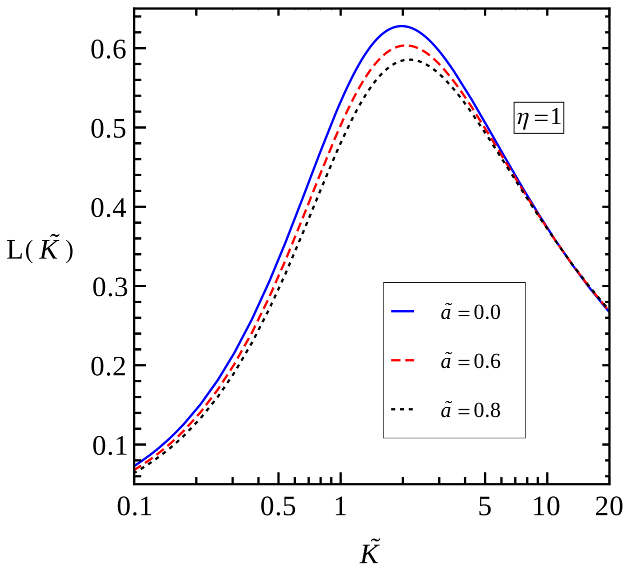

Figure 5.13: Q-$\bar{Q}$ separation L (normalized) as a function of $\tilde{K}$ with $\eta = 1$ for different values of $\tilde{a}$ when velocity is along anisotropic direction and dipole lies in transverse plane

5.3.4 Dipole parallel to velocity in transverse plane

We now come to the case where the dipole is aligned parallel to its direction of motion. This common direction can be in the transverse plane or along the anisotropic direction. We consider the former case in this subsection. For simplicity we shall take this common direction to be along x^1. Boosting to the rest frame, choosing the static gauge, $\tau = t, \sigma =$

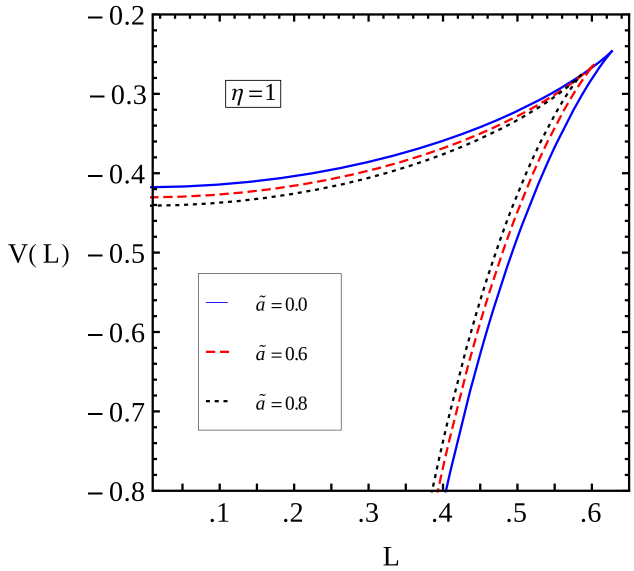

Figure 5.14: Normalized Q-$\bar{Q}$ potential V as a function of L with $\eta = 1$ for the same set of $\tilde{a}$ and same orientation (as in Figure 5.13)

$x^1, r = r(\sigma)$ and $x^2 = x^3 =$ constant leads us to the action,

$$\mathcal{S} = \frac{\mathcal{T} r_h}{2\pi\alpha'} \int_{-l/2}^{l/2} d\tilde{\sigma} \sqrt{A\left(C + G_{rr} y'^2\right) + B^2} \tag{5.68}$$

which, in turn, supplies the constant of motion,

$$K = \frac{AC + B^2}{\sqrt{A\left(C + G_{rr} y'^2\right) + B^2}}. \tag{5.69}$$

Proceeding along the lines of the earlier cases, we compute,

$$y' = \frac{r_0^2}{\tilde{K}} \frac{\sqrt{\left(y^4 - 1 + \frac{\tilde{a}^2}{24}\Sigma\right)\left(y^4 - 1 + \frac{\tilde{a}^2}{24}\Lambda\right)\left(y^4 - 1 - \tilde{K}^2 + \frac{\tilde{a}^2}{24}\Lambda\right)}}{\sqrt{y^4 - \cosh^2\eta + \frac{\tilde{a}^2}{24}\Lambda\cosh^2\eta}} \tag{5.70}$$

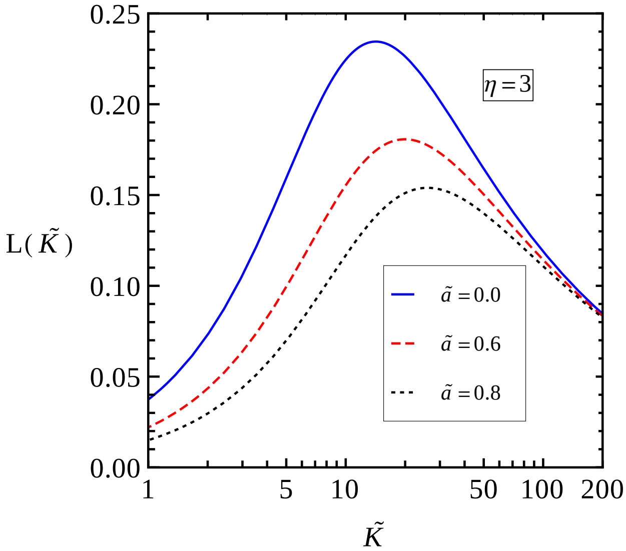

Figure 5.15: Q-$\bar{Q}$ separation L (normalized) as a function of $\tilde{K}$ with $\eta = 3$ for different values of $\tilde{a}$ when velocity is along anisotropic direction and dipole lies in transverse plane

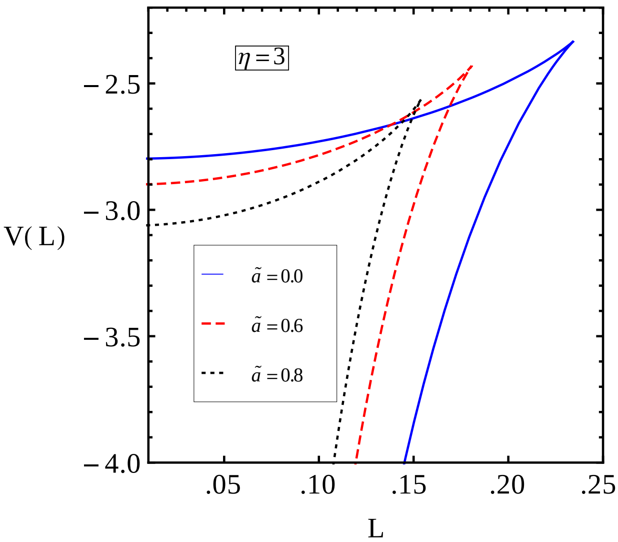

Figure 5.16: Normalized Q-$\bar{Q}$ potential V as a function of L with $\eta = 3$ for the same set of $\tilde{a}$ and same orientation (as in Figure 5.15)

from which we find the Q-$\bar{Q}$ separation to be

$$L = \frac{2\tilde{K}}{\pi T}\left(1+\frac{\tilde{a}^2(5\log 2-2)}{48}\right)\int_{y_t}^{\infty} dy \frac{\sqrt{y^4-\cosh^2\eta+\frac{\tilde{a}^2}{24}\Lambda\cosh^2\eta}}{\sqrt{\left(y^4-1+\frac{\tilde{a}^2}{24}\Sigma\right)\left(y^4-1+\frac{\tilde{a}^2}{24}\Lambda\right)}} \times \frac{1}{\sqrt{y^4-1-\tilde{K}^2+\frac{\tilde{a}^2}{24}\Lambda}}. \tag{5.71}$$

The turning point y_t is obtained from Eq. 5.70 which satisfies

$$y_t^4-1-\tilde{K}^2+\frac{\tilde{a}^2}{24}\Lambda\left(y_t\right)=0. \tag{5.72}$$

At the same time, note that y' now encounters a singularity at y_s, given by,

$$y_s^4-\cosh^2\eta+\frac{\tilde{a}^2}{24}\Lambda(y_s)\cosh^2\eta=0. \tag{5.73}$$

Further, it is evident that for $y<y_s$, the numerator in Eq. 5.71 becomes imaginary. So any potential turning point has to satisfy

$$y_t^4-\cosh^2\eta+\frac{\tilde{a}^2}{24}\Lambda(y_t)\cosh^2\eta>0 \tag{5.74}$$

which imposes a lower bound on $\tilde{K}$ that turns out to be[‖],

$$\tilde{K}^2>\tilde{K}^2_{min}=\sinh^2\eta\left(1-\frac{\tilde{a}^2}{24}\Lambda\left(y=\sqrt{\cosh\eta}\right)\right). \tag{5.75}$$

Incidentally, note that this lower bound turns out to be the same as the constant $\tilde{K}_0$ that appeared in §5.3.1. Upon simplification the action boils down to,

[‖]The existence of this lower bound is found in the isotropic case too as given in [74].

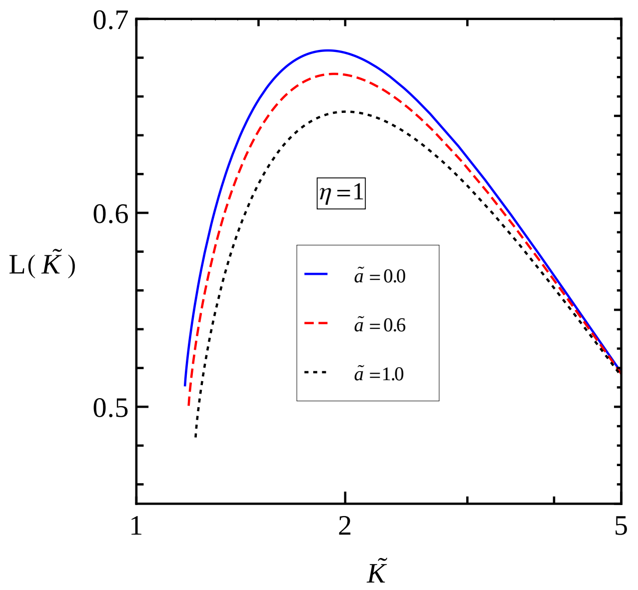

Figure 5.17: Q-$\bar{Q}$ separation L (normalized) as a function of $\tilde{K}$ with $\eta = 1$ for different values of $\tilde{a}$ when the dipole is parallel to its velocity and both lie in the transverse plane

$$\begin{aligned}
\mathcal{S} &= \frac{\mathcal{T}r_h}{\pi\alpha'}\int_{y_t}^{\infty} dy\sqrt{AG_{rr}}\sqrt{\frac{AC+B^2}{AC+B^2-K^2}} \\
&= \frac{\mathcal{T}r_h}{\pi\alpha'}\int_{y_t}^{\infty} dy\frac{\sqrt{\left(y^4-\cosh^2\eta+\frac{\tilde{a}^2}{24}\Lambda\cosh^2\eta\right)\left(y^4-1+\frac{\tilde{a}^2}{24}\Lambda\right)}}{\sqrt{\left(y^4-1+\frac{\tilde{a}^2}{24}\Sigma\right)\left(y^4-1-\tilde{K}^2+\frac{\tilde{a}^2}{24}\Lambda\right)}} \\
&\equiv \frac{\mathcal{T}r_h}{\pi\alpha'}\int_{y_t}^{\infty} dy\hat{\mathcal{S}}^{ani}
\end{aligned} \tag{5.76}$$

with $\tilde{K}$ respecting the inequality in Eq. 5.75. The self-energy contribution $\mathcal{S}_0$ is also given by Eq. 5.76 but now with $\tilde{K}$ saturating the bound in Eq. 5.75 so that $\mathcal{S}_0$ becomes identical with that given in Eq. 5.40. We can now compute the Q-$\bar{Q}$ potential using Eqs. 5.40 and 5.76 in Eq. 5.41 with Eq. 5.15. The Q-$\bar{Q}$ separation and the potential have been plotted in Figures 5.17-5.20 for $\eta = 1$ and $\eta = 4$ respectively. The $L(\tilde{K})$-$\tilde{K}$ plots show that curves

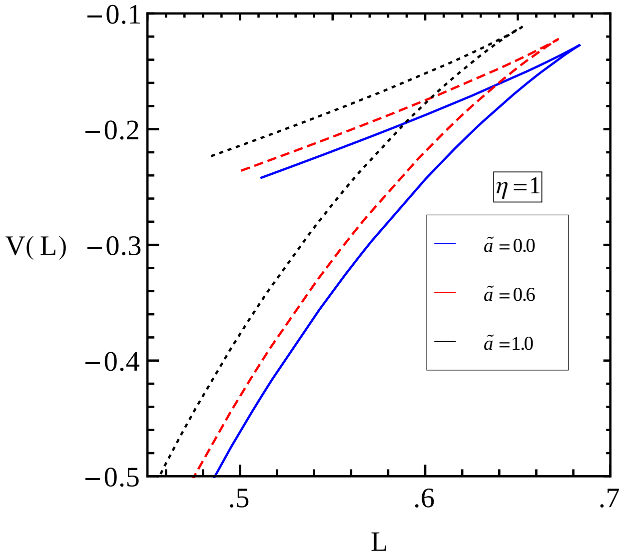

Figure 5.18: Normalized Q-$\bar{Q}$ potential V as a function of L with $\eta = 1$ for the same set of $\tilde{a}$ and same orientation (as in Figure 5.17)

for higher value of $\tilde{K}$ (after L_{max} is attained) exhibit the same pattern as in the earlier cases but for lower values of $\tilde{K}$ there is an inaccessible region for $\tilde{K} \leq \tilde{K}_{min}$ for which there is no solution to the dipole separation. This is reflected in the $V(L)$-L plot where the upper branch of the potential terminates abruptly at $L = L_{min}$ whereas the lower branch shows the usual behavior . A closer scrutiny of the figures suggest that $\tilde{K}_{min}$ increases with increasing $\tilde{a}$ and concomitantly, L_{min} decreases. However, this is manifested only in the unstable, high energy branch, which, in any case, is devoid of much physical significance, being energetically unfavorable.

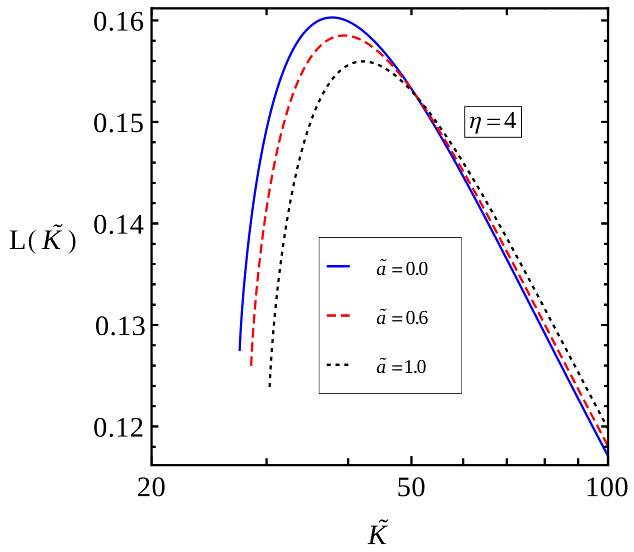

Figure 5.19: Q-$\bar{Q}$ separation L (normalized) as a function of $\tilde{K}$ with $\eta = 4$ for different values of $\tilde{a}$ when dipole is parallel to its velocity and both lie in transverse plane

5.3.5 Dipole parallel to velocity along x^3

Finally, we take up the case where the dipole is oriented along the anisotropic direction x^3 and it moves in the same direction. This time we shall make use of the metric (Eq. 5.56) as obtained in §5.3.3 and use the gauge choice of §5.3.2. All the calculations proceed in identically the same fashion as in §5.3.4 and we end up with the Q-$\bar{Q}$ separation

$$L = \frac{2\tilde{K}}{\pi T}\left(1+\frac{\tilde{a}^2(5\log 2-2)}{48}\right)\int_{y_t}^{\infty} dy \frac{\sqrt{y^4-\cosh^2\eta+\frac{\tilde{a}^2}{24}\Lambda\cosh^2\eta+y^4\sinh^2\eta(1-\mathcal{H})}}{\sqrt{y^4-1-\tilde{K}^2+\frac{\tilde{a}^2}{24}\Lambda\mathcal{H}+(\mathcal{H}-1)(y^4-1)}}\times$$
$$\frac{1}{\sqrt{\left(y^4-1+\frac{\tilde{a}^2}{24}\Sigma\right)\left(y^4-1+\frac{\tilde{a}^2}{24}\Lambda\mathcal{H}+(\mathcal{H}-1)(y^4-1)\right)}}. \quad (5.77)$$

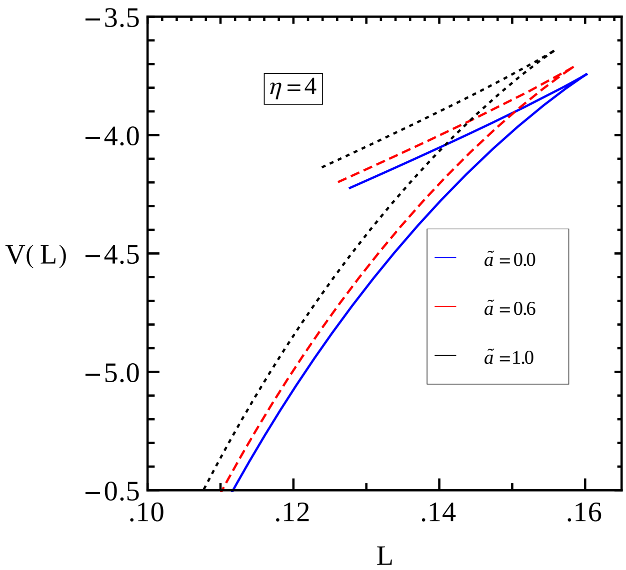

Figure 5.20: Normalized Q-$\bar{Q}$ potential V as a function of L with $\eta = 4$ for the same set of $\tilde{a}$ and same orientation (as in Figure 5.19)

The first term in the denominator provides the turning point y_t which, in turn, is constrained by the condition that the numerator must be real. This results in a lower cut-off on the value of $\tilde{K}$. We can read off this lower bound by demanding that the zeros of the numerator and the first factor in the denominator occur at the same value of y. As was the case in §5.3.3 due to the presence of the $y^4 \sinh^2 \eta(1 - \mathcal{H})$ term here we do not expect the effect of anisotropy to be small enough so as to employ perturbative methods. Hence, we have evaluated the lower limit $\tilde{K}_{min}$ and y_t completely numerically. Finally, the action becomes,

$$\mathcal{S} = \frac{\mathcal{T} r_h}{\pi\alpha'} \int_{y_t}^{\infty} dy \frac{\sqrt{y^4 - \cosh^2\eta + \frac{\tilde{a}^2}{24}\Lambda\cosh^2\eta + y^4\sinh^2\eta(1-\mathcal{H})}}{\sqrt{y^4 - 1 - \tilde{K}^2 + \frac{\tilde{a}^2}{24}\Lambda\mathcal{H} + (\mathcal{H}-1)(y^4-1)}} \times \frac{\sqrt{y^4 - 1 + \frac{\tilde{a}^2}{24}\Lambda\mathcal{H} + (\mathcal{H}-1)(y^4-1)}}{\sqrt{y^4 - 1 + \frac{\tilde{a}^2}{24}\Sigma}}$$

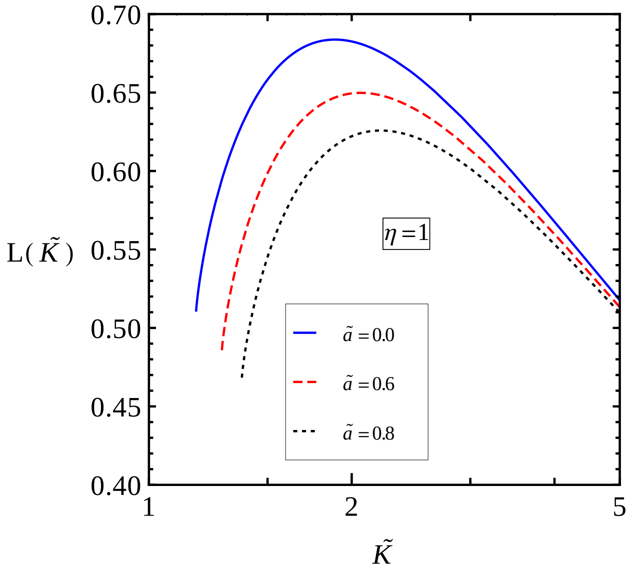

Figure 5.21: Q-$\bar{Q}$ separation L (normalized) as a function of $\tilde{K}$ with $\eta = 1$ for different values of $\tilde{a}$ when dipole is parallel to its velocity and both lie along anisotropic direction

$$\equiv \frac{\mathcal{T} r_h}{\pi\alpha'} \int\limits_{y_t}^{\infty} dy \hat{\mathcal{S}}^{ani}. \tag{5.78}$$

In similar fashion, one finds the self-energy contribution $\mathcal{S}_0$ to be the same as in Eq. 5.67 (and, in fact, Eq. 5.78 with $\tilde{K}$ replaced by its minimum value $\tilde{K}_{min}$). Equipped with this much information we can now obtain the plots for the dipole separation and the potential which are given in Figures 5.21-5.24 for $\eta = 1$ and $\eta = 2$ (corresponding to $v = 0.96$) respectively. The plots are very similar to those in §5.3.4 and so we refrain from giving a detailed description. However, note that now the effect of anisotropy is made more conspicuous by the significant deviation of the curves from the corresponding isotropic ones. Here too, we observe the appearance of a minimal value of the dipole separation for the upper unstable branch arising out of the lower bound that was clamped upon $\tilde{K}$.

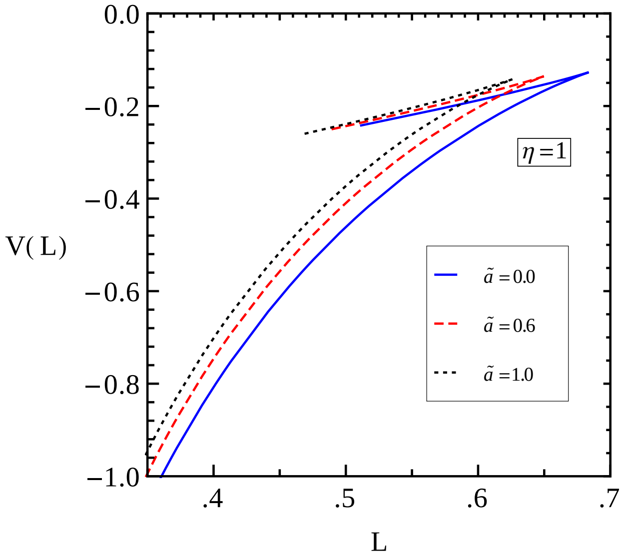

Figure 5.22: Normalized Q-$\bar{Q}$ potential V as a function of L with $\eta = 1$ for the same set of $\tilde{a}$ and same orientation (as in Figure 5.21)

5.4 Comparison Among the Different Cases

In the previous section we have computed the Q-$\bar{Q}$ separation and the Q-$\bar{Q}$ potential for different orientations of the dipole and its velocity. Before concluding, let us do a comparative study of the effects of anisotropy in all the cases. In Figures 5.25 and 5.26 we have given the $L(\tilde{K})$-$\tilde{K}$ and the $V(L)$-L plots for the three surviving cases** for $\eta = 0$ and $\tilde{a} = 0.6$. The legend in the figure needs a little explanation. While the blue line indicates the isotropic curve, 'perp' indicates the dipole is lying in the transverse plane, perpendicular to the direction of anisotropy and 'para' denotes the case where the dipole presents itself along the anisotropic direction. While the presence of anisotropy makes itself felt

** A little deliberation shows that in the static limit many of the cases collapse into each other and need not be considered separately.

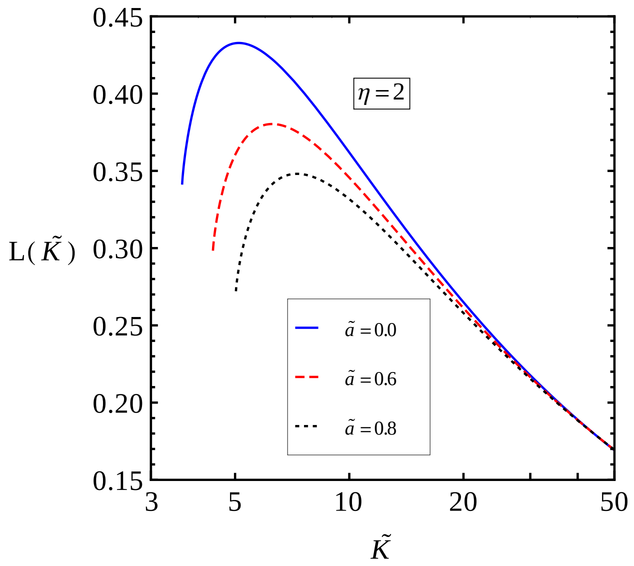

Figure 5.23: Q-$\bar{Q}$ separation L (normalized) as a function of $\tilde{K}$ with $\eta = 2$ for different values of $\tilde{a}$ when dipole is parallel to its velocity and both lie along anisotropic direction

in both the cases, the dipole is more affected when it is aligned parallel to the direction of anisotropy so that one can write, $L_{max}(para) < L_{max}(perp) < L_{max}(isotropic)$ and $V_{isotropic} < V_{perp} < V_{para}$. This observation corroborates the findings in [107]. In Figures 5.27 and 5.28 we have plotted the same quantities, now for $\eta = 2$ and for all the configurations considered. Before delving into the details of the plots, let us again clarify the legend used. Note that now there are two isotropic plots, denoted by 'perp' and 'para' indicating the cases where the dipole lies perpendicular and parallel to the direction of motion respectively. (ij) denotes the configuration where the dipole moves along x^i and is aligned along x^j. Basically, one can distinguish between two sectors: one in which the dipole is perpendicular to its velocity (this contains 'perp', (12), (13), (31)) and the one where it is parallel to its velocity (comprising of 'para', (11), (33)). The general observation is that the screening length diminishes and the potential is weaker for all the cases (ij) shown

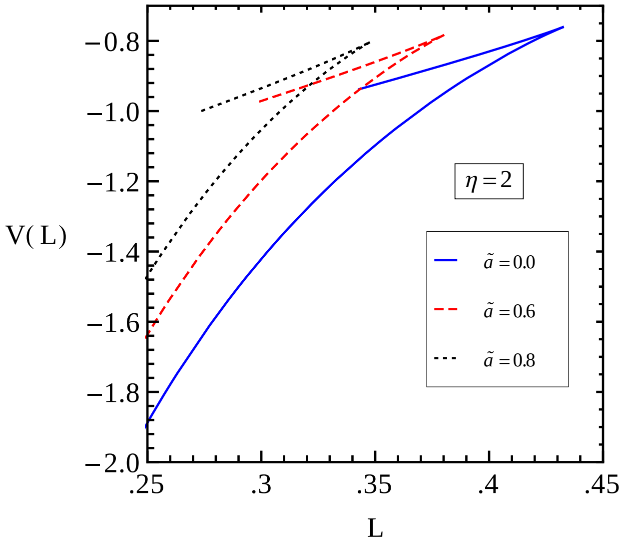

Figure 5.24: Normalized Q-$\bar{Q}$ potential V as a function of L with $\eta = 2$ for the same set of $\tilde{a}$ and same orientation (as in Figure 5.23)

compared to the corresponding isotropic cases. The cases (12) and (31) which merged in the static case now splits up and we find that (31) is severely affected when the combined effects of velocity and anisotropy are taken into account. This is evident both from the $L(\tilde{K})$-$\tilde{K}$ and the $V(L)$-L plots. For this configuration L_{max} drops drastically and also the rise in $V(L)$ is appreciable. As discussed earlier too, this is accounted for by the presence of the $\mathcal{O}(y^2)$ term in the anisotropic contribution, which makes the effect of anisotropy quite pronounced in this configuration. Both (13) and (12) cases are mildly affected when effects of velocity and anisotropy act in conjunction. For these cases L is slightly suppressed from the isotropic value whereas $V(L)$ registers a small increase. Turning to the other sector, we see that in (11), L decreases marginally which is accompanied by a corresponding small increase in the interaction potential when we introduce the anisotropy and the velocity parameter together. However, the (33) plots show a significant departure

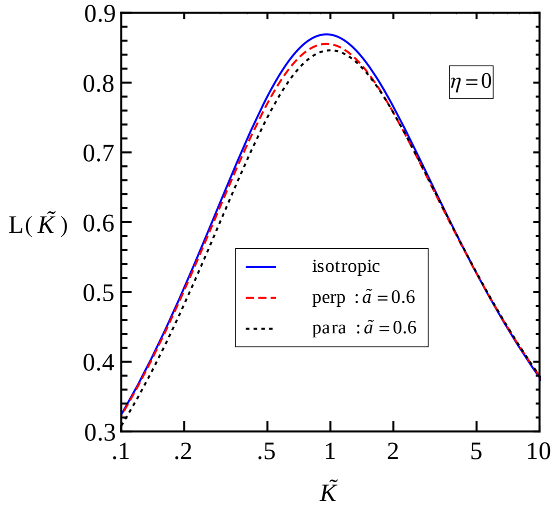

Figure 5.25: Q-$\bar{Q}$ separation L (normalized) as a function of $\tilde{K}$ with $\eta = 0, \tilde{a} = 0.6$ for different orientations of dipole and its velocity

from the isotropic case. For the unstable high energy branch of the potential, the minimum allowed separation L_{min} decreases in the order, $L_{min}(33) < L_{min}(11) < L_{min}(isotropic)$. On the whole, the plots suggest that the dipole separation and the potential are affected the most when the dipole moves along the anisotropic direction (both for the perpendicular and the parallel orientation and we hope, it will hold true for an other orientation in between these two extreme cases), and irrespective of the configuration, the presence of anisotropy makes the dipole more susceptible to dissociation.

In this context, it will be interesting to compare our observations with those extracted from other models of anisotropic plasma. In [109] the heavy quark-antiquark static potential was computed in an anisotropic plasma employing the hard thermal loop approach. It was found out that the presence of anisotropy reduces the screening so that the potential, in general gets strengthened and approaches the vacuum potential. The deviation from the isotropic potential increases as the value of the anisotropy parameter is increased. Further,

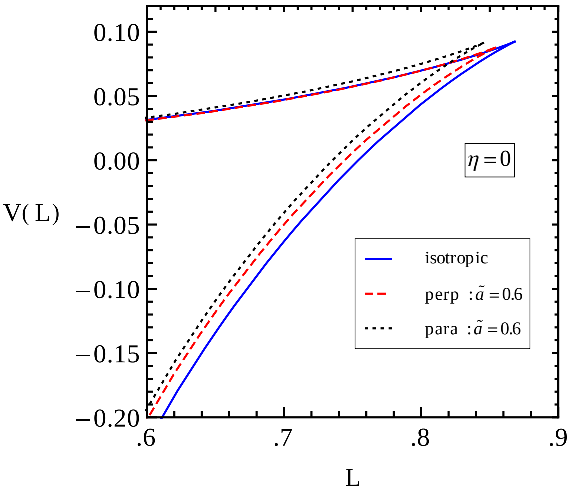

Figure 5.26: Normalized V as a function of L with $\eta = 0, \tilde{a} = 0.6$ for the same set of orientations and velocity

the effects are strongest when the dipole is aligned along the direction of anisotropy (this is in agreement with our findings here). However, the direction of the shift in potential (i.e., decrease or increase from the isotropic case) are opposite here (and in [107]) and what was found in [109]. By introducing the velocity, we have shown here that for sufficiently large velocity the effects of anisotropy on the dipole moving along the anisotropic direction will be the strongest. It might be interesting to attempt a similar study in the perturbative approach and see if introduction of the dipole velocity leads to results similar to that presented here. Another difference is that the results of [109] hold for length scales $\sim \lambda_D = 1/m_D$ where m_D is the Debye mass. At this length scale the Coulomb part of the potential dominates over the linear confining part. However, our analysis here is not constrained in this aspect and in fact, in the static case we have identified a range $L_p < L < L_{max}$ where the confining part dominates over the Coulomb one. Of course, it will be naive on our part to read too much into these comparisons, since the physical

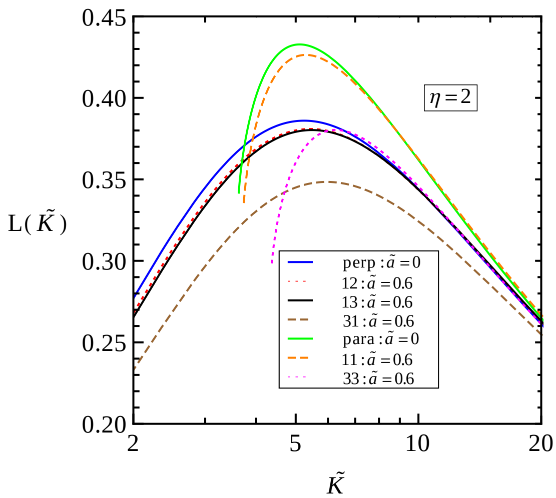

Figure 5.27: L (normalized) as a function of $\tilde{K}$ with $\eta = 2, \tilde{a} = 0.6$ for different orientations of the dipole and directions of velocity

models in the two cases are completely different, the primary difference being that our analysis holds for strongly coupled theories whereas the perturbative calculations are valid only in the weak coupling limit. Another curious comparison can be drawn with the results obtained in chapter 4 for the case of NCYM plasma. The presence of non-commutativity breaks the isotropy and this is reflected in the background metric, where the x^1 direction is taken to be the anisotropic one. The configuration considered in chapter 4 corresponds to that in §5.3.3 here. Surprisingly, we find that the gross characteristics of the results are the same in both models. In NCYM, too, increasing the non-commutativity parameter leads to a depreciation of the screening length and a weakening of the interaction potential. This entices us to think that the two models of anisotropic plasma do show qualitative similarity and there might be some universal features in holographic models of anisotropic plasma. Of course, there were some additional features in NCYM (like the presence of a cut-off) not encountered here.

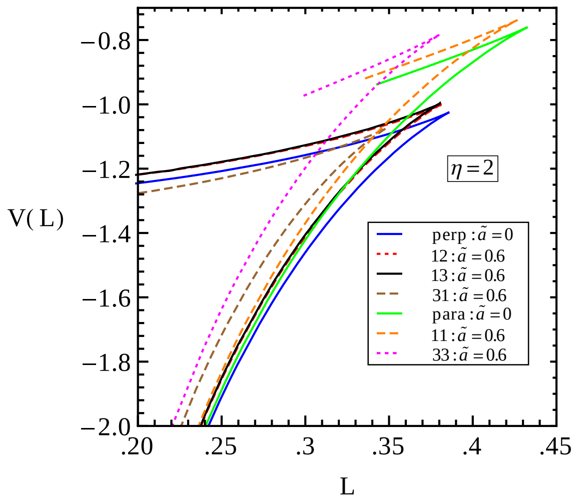

Figure 5.28: Normalized V as a function of L with $\eta = 2, \tilde{a} = 0.6$ for the same set of orientations and velocity

With this we close our discussion of heavy quark bound states in deformed SYM and move over to examining the motion of a heavy quark in strongly coupled QGP in the next section.

5.5 Heavy Quark Dynamics in Anisotropic Background

A particle immersed in a hot fluid exhibits an incessant, random dynamics known as the Brownian motion. Brownian motion originates from the collisions experienced by the particle with the constituents of the fluid undergoing a random thermal motion. The consideration of these random collisions requires the fact that the fluid medium is not a continuum but made of finite-size constituents. Hence, Brownian motion actually offers a better understanding of the underlying microscopic physics of the medium. The random dynamics of a Brownian particle is encoded in the Langevin equation describing the total force acting on the particle as a sum of dissipative and random forces. Although both of these forces have the same microscopic origin, phenomenologically the dissipative force describes the in-medium frictional effect and the random force stands for a source of random kicks from the medium. Brownian motion is a universal phenomenon for all finite temperature systems. Therefore, a heavy probe quark immersed in QGP undergoes the same thermal motion [110]. Recently, Brownian motion of a probe particle has been successfully studied using the framework of the AdS/CFT correspondence [111, 112]. The bulk interpretation of Brownian motion of a heavy probe quark immersed in a $SU(N_c)$ Yang-Mills theory with $\mathcal{N} = 4$ supersymmetries emerges from the consideration of a probe fundamental string in the dual AdS-black hole background, stretching between the AdS boundary and the horizon. The end-point of the string attached to the boundary is holographically mapped to the boundary probe quark. The transverse modes of the probe string are thermally excited by the black hole environment. This excitation propagates up to the boundary and holographically incorporates the Brownian motion of the boundary quark. In an intuitive way, the fact that, semi-classically, the traverse string modes are thermally excited by Hawking radiation reflects the bulk interpretation of random force in the boundary Langevin equation. On the other hand, the fact that the string excitation is absorbed by the black hole environment stands for the bulk realization of boundary frictional force. In the detailed course of computation, we need to quantize the transverse string modes. As explained in [113], the Hawking radiation associated with the string excitations occurs upon quantizing these modes. Once these modes are quantized, using holographic prescription, the erratic motion of string end-point attached to the boundary can be realized as Brownian motion. There are two independent approaches available in the literature to obtain these results. In the first approach, the state of the quantized scalar fields are identified with the Hartle-Hawking vacuum representing the black hole at thermal equilibrium [111]. In the second approach, the GKPW prescription [2, 3] of computing retarded Green's function is utilized. The computation of Langevin equation is done by exploring the correspondence between Kruskal extension of the AdS-black hole geometry and the Schwinger-Keldysh formalism [112]. The detailed comparison between the two independent approaches is given in [114]. There are further generalizations in this direction. Holographic Brownian motion has been studied in the case of charged plasma [115], rotating plasma [116–118], non-Abelian SYM plasma [119], non-conformal plasma [120] and $(1+1)$-dimensional strongly coupled CFT at finite temperature [121]. It has also been studied in the low temperature domain (near criticality) [122, 123]. The relativistic formulation of holographic Langevin dynamics has been successfully addressed in [124]. Moreover, some important universality related issues regarding the Langevin coefficients computed along the longitudinal as well as the transverse directions to the probe quark's motion has been studied in [125]. Here, we study the holographic Brownian motion of a heavy probe quark moving in a strongly coupled anisotropic plasma at finite temperature. For simplicity, we only consider the non-relativistic limit, i.e., we take $v \ll 1$ where v is the velocity of the heavy quark that undergoes Brownian motion. We also take the medium to have small anisotropy and consider only the low-lying modes of the string fluctuations. These conditions are imposed only to facilitate analytical computation. With the gravity background described in §5.2, following [111], we study the bulk interpretation of the boundary Brownian motion. In particular, we explicitly compute the friction coefficient, the diffusion constant and the random force correlator from a holographic perspective when the thermal background has an inherent anisotropy and verify the fluctuation-dissipation theorem and the Einstein-Sutherland relation. In our bulk analysis, we include fluctuations of the probe string modes along both isotropic and anisotropic directions and systematically study the effect of anisotropy in the low frequency limit of the thermal fluctuations.

5.5.1 Brownian motion in the boundary theory

We begin by presenting a brief review of the field-theoretic aspect of the problem following [111,115,119]. The simplest phenomenological model which attempts to explain Brownian motion of a non-relativistic particle of mass m immersed in a thermal bath is given by the Langevin equation along the i-th spatial direction[††],

$$\dot{p}_i(t) = -\gamma_o^{(i)} p_i(t) + R_i(t), \tag{5.79}$$

where $p_i(t) = m\dot{x}_i$ is the non-relativistic momentum of the Brownian particle along the i-th direction. The model, though simple, is capable of capturing the salient features of a particle undergoing Brownian motion. The particle is acted upon by a random force $R_i(t)$ arising out of its interaction with the thermal bath and, at the same time, it is suffering energy dissipation due to the presence of the frictional term with $\gamma_0^{(i)}$ being the friction coefficient. Under the effect of these two competing forces the particle undergoes random thermal motion. The interaction between the Brownian particle and the fluid particles at a temperature T allows for an exchange of energy between the Brownian particle and the fluid leading to the establishment of a thermal equilibrium. In an isotropic medium the friction coefficient does not depend upon the particular space direction under consideration. However, if the medium in which the particle is immersed has an anisotropy then we expect the drag coefficient along the anisotropic direction $\gamma_0^{||}$ to be different from that in the isotropic plane $\gamma_0^{\perp}$. The random force $R_i(t)$ can be approximated by a sequence of independent impulses, each of random sign and magnitude, such that the average vanishes. Each such impulse is an independent random event, i.e., $R_i(t)$ is independent of $R_i(t')$ for

[††]We shall explicitly keep track of the direction index i in our discussion since we need to distinguish between the anisotropic direction and the directions transverse to it.

$t \neq t'$. Such a noise source goes by the name of white noise. These considerations imply

$$\langle R_i(t) \rangle = 0, \qquad \langle R_i(t) R_j(t') \rangle = \kappa_0^{(i)} \delta_{ij} \delta(t - t') \tag{5.80}$$

where we call $\kappa_0^{(i)}$ the Langevin coefficient. Again, the presence of anisotropy inflicts a direction-dependence upon $\kappa_0^{(i)}$. Note that, in particular, the random forces at two different instants are not correlated. The two parameters $\gamma_0^{(i)}$ and $\kappa_0^{(i)}$ completely characterize the Langevin equation (Eq. 5.79). As we shall see, $\gamma_0^{(i)}$ and $\kappa_0^{(i)}$ are not independent, which is not unexpected since they are related by the fluctuation-dissipation theorem,

$$\gamma_0^{(i)} = \frac{\kappa_0^{(i)}}{2mT}. \tag{5.81}$$

The relation between the two quantities has its root in the fact that both the frictional force and the random force have the same origin - microscopically, they arise due to the interaction of the particle with the thermal medium. In this sense, the separation of the R.H.S. of Eq. 5.79 in two parts is *ad hoc* from the microscopic point of view, being only dictated by considerations of phenomenological simplicity. Assuming the theorem of equipartition of energy which states that each degree of freedom contributes $\frac{1}{2}T$ to the energy (T being the temperature and we have set the Boltzmann constant $k_B = 1$), it is possible to derive the the temporal variation of the displacement squared of the particle [111]

$$\langle s^i(t)^2 \rangle = \langle (x^i(t) - x^i(0))^2 \rangle = \frac{2D^{(i)}}{\gamma_0^{(i)}} \left(\gamma_0^{(i)} t - 1 + e^{-\gamma_0^{(i)} t} \right) \tag{5.82}$$

where $D^{(i)}$ is defined to be the diffusion constant. It is related to the friction coefficient $\gamma_0^{(i)}$ through the Einstein-Sutherland relation,

$$D^{(i)} = \frac{T}{\gamma_0^{(i)} m}. \tag{5.83}$$

The solution to Eq. 5.79 has a homogeneous part determined by the initial conditions and an inhomogeneous part proportional to the random force. The homogeneous part will decay to zero in a time of order $t^{(i)}_{\text{relax}} = 1/\gamma_0^{(i)}$ and the long-time dynamics will be governed entirely by the inhomogeneous part, independent of the initial conditions. Based on these considerations, one can distinguish between two different temporal domains: $t \ll 1/\gamma_0^{(i)}$ whence $s^i \sim \sqrt{T/m}\, t$ showing that the particle moves under inertia as if no force is acting upon it. The speed in this case is fixed by the equipartition theorem. In the opposite regime $t \gg 1/\gamma_0^{(i)}$ one obtains $s^i \sim \sqrt{2D^{(i)} t}$ which is reminiscent of the random walk problem. In this time domain, Brownian particle loses its memory of the initial value of the velocity. The transition from one regime to another occurs at the critical value of

$$t^{(i)}_{\text{relax}} \sim \frac{1}{\gamma_0^{(i)}} \tag{5.84}$$

which represents a characteristic time-scale of the theory, called the relaxation time, beyond which the system thermalizes.

The model we have considered above is based on two assumptions: i) the friction to be instantaneous and ii) the random forces at two different instants to be uncorrelated. The validity of these assumptions holds good only when the Brownian particle is very heavy compared to the constituents of the medium. However, this does not give the correct picture when the Brownian particle and the constituents of the medium have comparable masses. To overcome these pitfalls the Langevin equation is generalized such that the friction now depends upon the past history of the particles and also the random forces at different instants are correlated. To incorporate these effects we modify Eq. 5.79 to the generalized

$$\mu^{(i)}(\omega) \equiv \frac{1}{-i\omega + \gamma[\omega]} \tag{5.91}$$

is called the admittance and since it depends upon γ it inherits the anisotropic effect. The admittance is a measure of the response of the Brownian particle to external perturbations. In particular, if the external force is taken as

$$K_i(t) = K_i^{(0)} e^{-i\omega t} \tag{5.92}$$

then the response is,

$$\langle p_i(t) \rangle = \mu^{(i)}(\omega) K_i^{(0)} e^{-i\omega t}. \tag{5.93}$$

If the memory kernel $\gamma(t-t')$ is sharply peaked around $t' = t$ then

$$\int_0^\infty dt' \gamma^{(i)}(t-t') p_i(t') \approx \int_0^\infty dt' \gamma^{(i)}(t') p_i(t) = \frac{1}{t^{(i)}_{\text{relax}}} p_i(t). \tag{5.94}$$

Thus, for the generalized Langevin equation, described by Eq. 5.85, the generalization of the relaxation time is

$$t^{(i)}_{\text{relax}} \sim \left(\int_0^\infty dt \gamma(t) \right)^{-1} = \frac{1}{\gamma[\omega = 0]} = \mu^{(i)}(\omega = 0). \tag{5.95}$$

The Wiener-Khintchine theorem relates the power spectrum $I_{\mathcal{O}}(\omega)$ of any quantity $\mathcal{O}$ with its two-point function as follows,

$$\langle \mathcal{O}(\omega) \mathcal{O}(\omega') \rangle = 2\pi \delta(\omega + \omega') I_{\mathcal{O}}(\omega) \tag{5.96}$$

where the power spectrum $I_{\mathcal{O}}(\omega)$ is defined as

$$I_{\mathcal{O}}(\omega) = \int_{-\infty}^{\infty} dt \langle \mathcal{O}(t_0)\mathcal{O}(t_0+t)\rangle e^{i\omega t}. \tag{5.97}$$

For stationary systems this does not depend upon the choice of t_0 and hence, we can as well set $t_0 = 0$. Now if we turn off the external force $K_i(t)$ then from Eq. 5.87 we get,

$$p_i(\omega) = \frac{R_i(\omega)}{-i\omega + \gamma[\omega]} = \mu^{(i)}(\omega) R_i(\omega) \tag{5.98}$$

which leads to the obvious result

$$I_{p_i}(\omega) = \frac{I_{R_i}(\omega)}{|\gamma[\omega] - i\omega|^2} = |\mu^{(i)}(\omega)|^2 I_{R_i}(\omega). \tag{5.99}$$

Making use of Eqs. 5.86 and 5.99 we are lead to the result,

$$\kappa^{(i)} = I_{R_i} = \frac{I_{p_i}(\omega)}{|\mu^{(i)}(\omega)|^2}. \tag{5.100}$$

The random force correlator $\kappa^{(i)}$ provides yet another time scale involved in Brownian motion. If we take $\kappa^{(i)}$ to be of the form,

$$\kappa^{(i)}(t) = \kappa^{(i)}(0) e^{-\frac{t}{t_{\text{col}}}} \tag{5.101}$$

then t_{col} is the width of the correlator. It is the temporal span over which the random forces are correlated and gives the time scale for the duration of a collision.

In the next subsection, following holographic techniques prescribed in [111], we investigate the bulk realization of the boundary Brownian motion of a heavy probe moving in an anisotropic thermal plasma. In doing so, we first describe the profile of the probe string stretching between the AdS boundary and the horizon. Then we describe how to compute bulk correlators of the transverse fluctuations of the probe string.

5.5.2 The holographic story

To incorporate heavy dynamical probe quark in the boundary theory, one introduces N_f D7-flavor branes located at $r = r_m$. We work within probe approximation meaning $N_f \ll N_c$ and neglect the backreaction of the flavor brane on the background (for simplicity we take $N_f = 1$). On the gauge theory side this is tantamount to working in the quenched approximation. The probe string stretches from the boundary at $r = r_m$ to the black hole horizon $r = r_h$. The flavor brane spans the four gauge theory directions, the radial direction and also a three-sphere $S^3 \subset S^5$. We take the boundary gauge theory to live at the radial coordinate $r = r_m$. We assume that the source of the fluctuations of the string modes is purely Hawking radiation. Moreover, keeping the string coupling g_s small ensures that we can ignore the interaction between the transverse fluctuation modes and the closed string modes in the bulk.

5.5.3 Bulk view of Brownian motion

To study the dynamics of the fundamental string in the background given by Eq. 5.11 we need to evaluate the Nambu-Goto string world-sheet action provided in Eq. 2.11. We choose the static gauge for evaluating Eq. 2.11 as $\tau = t, \sigma = r$. The trivial solution that satisfies the equation of motion obtained by variation of $\mathcal{S}$ is given by $X^m = \{t, \vec{0}, r\}$. This corresponds to a quark that is in equilibrium in a thermal bath and in the bulk picture to a string hanging straight down radially. We now wish to consider fluctuations around this classical solution. We want to see the effects of anisotropy both along the anisotropic direction as well as in the isotropic plane. To this end we consider fluctuations of the form: $X^m = \{t, X_1(t,r), 0, X_3(t,r), r\}$ where $X_1(t,r)$ is a fluctuation along an isotropic direction while $X_3(t,r)$ is a perturbation along the anisotropic direction. The position of the quark is given by, $x^\mu = \{t, X_1(t, r_m), 0, X_3(t, r_m)\}$. Using this parametrization we find out the components of the world-sheet metric as,

$$
\begin{aligned}
g_{\tau\tau} &= r^2 \left(-\mathcal{F}\mathcal{B} + (\dot{X}_1)^2 + \mathcal{H}(\dot{X}_3)^2\right), \\
g_{\sigma\sigma} &= r^2 \left((X_1')^2 + \mathcal{H}(X_3')^2 + \frac{1}{r^4\mathcal{F}}\right), \\
g_{\tau\sigma} &= r^2 \left(\mathcal{H}\dot{X}_1 X_3' + \mathcal{H} X_1' \dot{X}_3\right)
\end{aligned}
\tag{5.102}
$$

where $X_i' \equiv \partial_\sigma X_i$ and $\dot{X}_i \equiv \partial_\tau X^i$. From now on, we suppress the explicit r-dependence of the metric elements $\mathcal{F}, \mathcal{B}, \mathcal{H}$. If we restrict ourselves to small perturbation around the classical solution we can safely leave out terms higher than quadratic order in the fluctuations whence the action reduces to [‡‡]

$$
\mathcal{S} = \frac{1}{4\pi\alpha'} \int d\tau d\sigma \sqrt{\mathcal{B}} \left[\mathcal{F} r^4 \left((X_1')^2 + \mathcal{H}(X_3')^2\right) - \frac{1}{\mathcal{F}\mathcal{B}} \left((\dot{X}_1)^2 + \mathcal{H}(\dot{X}_3)^2\right)\right]. \tag{5.103}
$$

While writing Eq. 5.103 we have omitted a constant factor that is independent of X_i. Variation of the above action yields the equation of motion for the fluctuation X_3

$$
\ddot{X}_3 - \frac{\mathcal{F}\sqrt{\mathcal{B}}}{\mathcal{H}} r_h^2 \partial_y \left(\sqrt{\mathcal{B}}\mathcal{H}\mathcal{F} y^4 X_3'\right) = 0 \tag{5.104a}
$$

where we have used the new scaled coordinate, $y = r/r_h$ and now the prime ($'$) denotes derivative with respect to y. The equation of motion for X_1 is obtained in a similar fashion,

[‡‡]This essentially means that we are in the regime $|\partial_t X_i| \ll 1$ which, in turn, implies taking the non-relativistic limit. Hence, on the gauge theory side, the dual picture will also be non-relativistic.

$$\ddot{X}_1 - \mathcal{F}\sqrt{\mathcal{B}}r_h^2\partial_y\left(\sqrt{\mathcal{B}}\mathcal{F}y^4X_1'\right) = 0 \tag{5.104b}$$

which is the same as Eq. 5.104a with $\mathcal{H} = 1$. Later on, we shall also consider forced motion of the quark under the effect of an electromagnetic field. This is simply achieved by switching on a $U(1)$ electromagnetic field on the flavor D7-brane. Since the string end-point on the boundary represents a quark, it is charged, and hence will couple to the electromagnetic field. Consequently, we need to incorporate this effect at the level of the action. The action $\mathcal{S}$ is then generalized to $\mathcal{S}_{total} = \mathcal{S} + \mathcal{S}_b$ where

$$\mathcal{S}_b = \int_{\partial\Sigma}\left(A_t + A_i\dot{X}_i\right)dt. \tag{5.105}$$

Since it is just a boundary term it will not affect the dynamics of the string in the bulk. However, it will modify the boundary conditions that we need to impose upon the string end-point. We need to find solutions to Eqs. 5.104a and 5.104b near the boundary which we shall do by employing the matching technique. The solutions are, in general, quite complicated. However, they are readily obtained near the horizon. So before finding out the actual solutions let us see how these solutions behave in the vicinity of $y \to 1$. First of all, we inflict a coordinate transformation $r \to r_*$ which takes us to the tortoise coordinates so that

$$\frac{d}{dr} = \frac{1}{r^2\mathcal{F}\sqrt{\mathcal{B}}}\frac{d}{dr_*} \tag{5.106}$$

and

$$dr = r^2\mathcal{F}\sqrt{\mathcal{B}}dr_*. \tag{5.107}$$

In this new coordinate system, the Nambu-Goto action assumes the form,

$$\mathcal{S} = \frac{1}{4\pi\alpha'} \int d\tau dr_* r^2 \left[\left((\partial_{r_*} X_1)^2 - (\dot{X}_1)^2 \right) + \mathcal{H} \left((\partial_{r_*} X_3)^2 - (\dot{X}_3)^2 \right) \right]. \tag{5.108}$$

Near the horizon it simplifies to,

$$\mathcal{S} = \frac{1}{4\pi\alpha'} r_h^2 \int d\tau dr_* \left[\left((\partial_{r_*} X_1)^2 - (\dot{X}_1)^2 \right) + \mathcal{H}(r_h) \left((\partial_{r_*} X_3)^2 - (\dot{X}_3)^2 \right) \right]. \tag{5.109}$$

The equation of motion for both X_1 and X_3 obtained by varying this action turns out to be the same,

$$\left(\partial_{r_*}^2 - \partial_\tau^2 \right) X_{1,3} = 0. \tag{5.110}$$

So near the boundary, the fluctuations are governed by a Klein-Gordon equation for massless scalars. From now on, in this section, we shall refer to the fluctuations as X_i, it being understood that everything we discuss here holds true for both X_1 as well as X_3. From Eq. 5.11 it is clear that t is an isometry of the background and hence we can try solutions of the form,

$$X_i(t, r) \sim e^{-i\omega t} g_\omega(r). \tag{5.111}$$

Eq. 5.110 has two independent solutions corresponding to ingoing and outgoing waves respectively which we write as,

$$X_i^{\text{out}}(r) = e^{-i\omega t} g_i^{\text{out}}(r) \sim e^{-i\omega(t - r_*)} \tag{5.112a}$$

$$X_i^{\text{in}}(r) = e^{-i\omega t} g_i^{\text{in}}(r) \sim e^{-i\omega(t + r_*)}. \tag{5.112b}$$

To find r_* we need to solve Eq. 5.107 which yields,

$$r_* = \frac{1}{4r_h} \log\left(\frac{r}{r_h} - 1\right)\left[1 - \frac{\tilde{a}^2}{48}(5\log 2 - 2)\right] \tag{5.113}$$

where we have defined $\tilde{a} = \frac{a}{r_h} \sim \frac{a}{\pi T}$. Hence,

$$g_i^{\text{out/in}}(r) = \left(\frac{r}{r_h} - 1\right)^{\pm\frac{i\nu}{4}\left(1 - \frac{\tilde{a}^2}{48}(5\log 2 - 2)\right)} \tag{5.114}$$

where $\nu = \frac{\omega}{r_h}$. One thus finds that, $g_i^{\text{out}} = (g_i^{\text{in}})^*$.

Following standard quantization techniques of scalar fields in curved space-time we can perform a mode expansion of the fluctuations as

$$X_i(t,r) = \int_0^\infty \frac{d\omega}{2\pi}[a_\omega u_\omega(t,r) + a_\omega^\dagger u_\omega(t,r)^*]. \tag{5.115}$$

Here $u_\omega(t,r)$ is a set of positive frequency basis. These modes can in turn be expressed as a linear combination of the ingoing and the outgoing waves

$$u_\omega(t,r) = A[g^{\text{out}}(r) + Bg^{\text{in}}(r)]e^{-i\omega t}. \tag{5.116}$$

The constant B is determined by imposing boundary condition at $r = r_m$. However, as we shall later see, B turns to be a pure phase. This implies that the outgoing and the ingoing modes have the same amplitude. This signifies that the black hole environment which can emit Hawking radiation is in a state of thermal equilibrium. One is then left with determining the constant A which is fixed by demanding normalization of the modes through the conventional Klein-Gordon inner product defined *via*,

$$(f_i, g_j)_\sigma = -\frac{i}{2\pi\alpha'}\int_\sigma \sqrt{\tilde{g}} n^\mu G_{ij}(f_i \partial_\mu g_j^* - \partial_\mu f_i g_j^*). \tag{5.117}$$

Here, σ defines a Cauchy surface in the (t, r) subspace of the ten-dimensional space-time metric, $\tilde{g}$ is the induced metric on the surface σ and n^μ denotes a unit normal to σ in the future direction. Without any loss of generality we can take the surface σ to be a constant t surface since the inner product does not depend upon the exact choice of the surface in the (t, r)-plane. Following [115] we argue that the primary contribution to the above integral arises from the IR region. Of course, regions away from the horizon do contribute but since the horizon is semi-infinite in the tortoise coordinate, the normalization is completely fixed by the near-horizon regime. For the anisotropic direction this gives,

$$(f_i, g_j)_\sigma = -\frac{i\delta_{ij} r_h^2 \mathcal{H}(r_h)}{2\pi\alpha'} \int\limits_{r_* \to -\infty} dr_* (f_i \dot{g}_j{}^* - \dot{f}_i g_j^*) \tag{5.118}$$

from which we can extract A to be,

$$A = \sqrt{\frac{\pi\alpha'}{\omega r_h^2 \mathcal{H}(r_h)}}. \tag{5.119}$$

On the other hand, for fluctuations along the isotropic direction we have,

$$(f_i, g_j)_\sigma = -\frac{i\delta_{ij} r_h^2}{2\pi\alpha'} \int\limits_{r_* \to -\infty} dr_* (f_i \dot{g}_j{}^* - \dot{f}_i g_j^*) \tag{5.120}$$

which fixes A as,

$$A = \sqrt{\frac{\pi\alpha'}{\omega r_h^2}}. \tag{5.121}$$

The normalisation ensures that the inner product $(u_\omega, u_\omega) = 1$ which, in turn, guarantees that the canonical commutation relations are satisfied,

$$[a_\omega, a_{\omega'}] = [a_\omega^\dagger, a_{\omega'}^\dagger] = 0, \qquad [a_\omega, a_{\omega'}^\dagger] = 2\pi\delta(\omega + \omega'). \tag{5.122}$$

In the semi-classical approximation the string modes are thermally excited by the Hawking radiation of the world-sheet horizon and obey the Bose-Einstein distribution,

$$\langle a_\omega a^\dagger_\omega \rangle = \frac{2\pi\delta(\omega+\omega')}{e^{\beta\omega}-1}. \tag{5.123}$$

Equipped with this much machinery we are now ready to compute the displacement squared for the test quark in the boundary. This is required if we wish to find out an expression for the diffusion constant. Recalling that the position of the Brownian particle is specified by $x_i(t) = X_i(t, r_m)$, we have

$$\langle x_i(t)x_i(0)\rangle = \int_0^\infty \frac{d\omega d\omega'}{(2\pi)^2}[\langle a_\omega a^\dagger_{\omega'}\rangle u_\omega(t,r_m)u_{\omega'}(0,r_m)^* + \langle a^\dagger_\omega a_{\omega'}\rangle u_\omega(t,r_m)^* u_{\omega'}(0,r_m)]. \tag{5.124}$$

However, this is afflicted by a divergence that can be attributed to the zero point energy which persists even we go to the zero temperature limit. The way to bypass this catastrophe is to invoke the normal ordering of products

$$\langle : x_i(t)x_i(0) : \rangle = \int_0^\infty \frac{d\omega}{2\pi}\frac{2|A|^2\cos\omega t}{e^{\beta\omega}-1}|g^{\text{out}}(r_m) + Bg^{\text{in}}(r_m)|^2. \tag{5.125}$$

Finally, after a little algebra we arrive at the expression for displacement squared,

$$s_i^2(t) \equiv \langle : [x_i(t)-x_i(0)]^2 : \rangle = \frac{4}{\pi}\int_0^\infty d\omega |A|^2 \frac{\sin^2\omega t/2}{e^{\beta\omega}-1}|g^{\text{out}}(r_m) + Bg^{\text{in}}(r_m)|^2. \tag{5.126}$$

With the general formalism in place, we are now in a position to take up the problem of analyzing Brownian motion in an anisotropic strongly coupled plasma from the holographic point of view.

Brownian motion along anisotropic direction

To analyze Brownian motion along the anisotropic direction our first task will be to solve Eq. 5.104a in the asymptotic limit. To achieve this, we recast Eq. 5.104a making use of Eq. 5.111 as,

$$\nu^2 g(y) + \frac{\mathcal{F}\sqrt{\mathcal{B}}}{\mathcal{H}}\partial_y\left(\sqrt{\mathcal{B}}\mathcal{H}\mathcal{F}y^4 g'(y)\right) = 0. \tag{5.127}$$

Inserting the explicit expressions of the various functions, this can be written as,

$$g''(y) + 4\frac{y^3}{y^4-1}\left[1+\tilde{a}^2\Psi(y)\right]g'(y) + \frac{y^4\nu^2}{(y^4-1)^2}\left[1+\tilde{a}^2\Upsilon(y)\right]g(y) = 0 \tag{5.128}$$

where

$$\begin{aligned}\Psi(y) &= \frac{1}{96y^4(y^4-1)}\left[3-9y^2-23y^6+y^4(29+40\log 2)-40y^4\log\left(1+\frac{1}{y^2}\right)\right]\\ \Upsilon(y) &= \frac{1}{24(y^4-1)}\left[6-6y^2+20\log 2-5(3+y^4)\log\left(1+\frac{1}{y^2}\right)\right].\end{aligned} \tag{5.129}$$

We need to find a solution to this equation. However, as it turns out, obtaining an analytic solution is a notoriously difficult problem for any arbitrary frequency ν. To circumvent this difficulty we work only in the low frequency approximation and then attempt to solve the equation by the ‘matching technique’. Since we only require the solution near the boundary, we just give here the expression of the required solution. The interested reader is referred to appendix for the details of the solution. We shall have two solutions corresponding to the ingoing and the outgoing waves

$$g^{\text{out/in}} = k_1^{\text{out/in}}\left[1+\frac{\nu^2}{2y^2}+\mathcal{O}\left(\frac{1}{y^4}\right)\right] + k_3^{\text{out/in}}\left[\frac{1}{y^3}+\mathcal{O}\left(\frac{1}{y^5}\right)\right] \tag{5.130}$$

where

$$
\begin{aligned}
k_1^{\text{out/in}} =& 1 \mp \frac{i\nu}{8}(\pi - 2\log 2) \pm \frac{i\nu\tilde{a}^2}{768}\left[28 - 16\beta(2) - 20(\log 2)^2\right. \\
& \left. + \pi(-8 + \pi + 14\log 2) + 8\log 2\right] + \mathcal{O}(\nu^2) \\
k_3^{\text{out/in}} =& \mp \frac{i\nu}{3}(1 + \frac{\tilde{a}^2}{4}\log 2) + \mathcal{O}(\nu^2)
\end{aligned} \tag{5.131}
$$

where $\beta(s)$ is the Dirichlet beta function given by $\beta(s) = \sum_{n=0}^{\infty} \frac{(-1)^n}{(2n+1)^s}$ and $\beta(2) \sim 0.915966$. We find that the relation, $g^{\text{out}} = g^{\text{in}*}$, obtained earlier in the near-horizon analysis, continues to hold true in the asymptotic limit. We can now use these solutions, supplemented by the appropriate boundary conditions to find out various quantities of interest. However, before going into the intricacies of the actual computation, let us digress a little bit to clarify the boundary conditions involved in the problem. Although we are interested in the world-sheet theory of the probe string, the choice of the static gauge implies that the characteristics of the background space-time is encoded in the induced metric. Hence, we can exploit the rules of the AdS/CFT correspondence to understand the boundary conditions. When working in the Lorentzian AdS/CFT it is customary to choose normalisable boundary conditions [126] for the modes. In the present scenario this amounts to pushing the boundary all the way up to $y \to \infty$. However, the AdS/CFT dictionary tells us that the radial distance is mapped holographically to the mass of the probe quark so that placing the boundary at $y \to \infty$ essentially means that we are considering our probe quark to be infinitely massive. Of course, this at once rules out any possibility of the quark undergoing Brownian motion. The problem can be solved if, instead, we impose a UV cut-off in our theory. More specifically, we introduce a UV cut-off surface and identify it with the boundary where the gauge theory lives. In fact, this is exactly the location of the flavor brane y_m to which the end-point of the string is attached. The relation between the position of the UV cut-off and the mass of the probe can be read off easily as,

$$m = \frac{1}{2\pi\alpha'} \int_{r_h}^{r_m} dr \sqrt{-g_{tt} g_{rr}} = \frac{1}{2\pi\alpha'} \left[y_m - 1 + \frac{\tilde{a}^2}{24} (\log 2 - 3\pi) \right] \tag{5.132}$$

and the world-sheet metric elements g_{tt}, g_{rr} are written for the classical string configuration, i.e., omitting the contribution arising out of the fluctuations. On this surface we can impose Neumann boundary condition, $\partial_r X_i = 0$. One can not impose Dirichlet condition since it implies no fluctuation on the boundary at all. However, this works only when we consider the free Brownian motion of the particle in the absence of any external force. In the case of forced motion this is modified to,

$$\Pi_i^y \big|_{\partial\Sigma} \equiv \frac{\partial \mathcal{L}}{\partial X_i'} = K_i = K_i^{(0)} e^{-i\omega t} \tag{5.133}$$

where we have assumed a fluctuating external force. Now the general solution X_i is a linear combination of the outgoing and the ingoing modes at the horizon,

$$X_i = A^{\text{out}} X_i^{\text{out}} + A^{\text{in}} X_i^{\text{in}}. \tag{5.134}$$

where $X_i^{\text{out/in}} = e^{-i\omega t} g^{\text{out/in}}$ and $g^{\text{out/in}}$ is given in Eq. 5.130. In the semi-classical approximation the outgoing modes are thermally excited by the Hawking radiation emanating from the black hole whereas the ingoing modes can be arbitrary. Since the Hawking radiation is a random phenomena the phase of A^{out} takes random values and and its average $\langle A^{\text{out}} \rangle$ vanishes. So we can omit the first term in Eq. 5.134 and consider only the ingoing wave. When one plugs in the form of the Lagrangian in Eq. 5.133 one finds that, like the equations of motion, the boundary conditions along the anisotropic direction and the isotropic directions decouple which allows us to treat each direction separately. Coming back to the particular case of the anisotropic direction, the boundary condition given in Eq. 5.133 assumes the form,

$$\frac{1}{2\pi\alpha'}\mathcal{H}\mathcal{F}\sqrt{\mathcal{B}}y^4 r_h^3 X_3'\big|_{y=y_m} = K_3 = K_3^{(0)}e^{-i\omega t}. \tag{5.135}$$

This yields

$$A^{\text{in}} = \frac{2\pi\alpha' K_3^{(0)}}{\mathcal{H}\mathcal{F}\sqrt{\mathcal{B}}y^4 r_h^3 g'(y)}\Bigg|_{y=y_m}. \tag{5.136}$$

where $g(y)$ represents the ingoing solution in Eq. 5.130. So, on the boundary the average position of Brownian quark is given by,

$$\langle x_3(t)\rangle = \langle X_3(t, y_m)\rangle = K_3^{(0)}e^{-i\omega t}\frac{2\pi\alpha' g}{\mathcal{H}\mathcal{F}\sqrt{\mathcal{B}}y^4 r_h^3 g'}\Bigg|_{y=y_m}. \tag{5.137}$$

The average momentum is,

$$\langle p_3(t)\rangle = m\langle \dot{x_3}\rangle = -K_3\frac{2i\pi\alpha' m\nu g}{\mathcal{H}\mathcal{F}\sqrt{\mathcal{B}}y^4 r_h^2 g'}\Bigg|_{y=y_m}. \tag{5.138}$$

Comparison with Eq. 5.90 results in,

$$\mu^{||}(\nu) \equiv \mu^{(3)}(\nu) = -\frac{2i\pi\alpha' m\nu g}{\mathcal{H}\mathcal{F}\sqrt{\mathcal{B}}y^4 r_h^2 g'}\Bigg|_{y=y_m}. \tag{5.139}$$

Here we have used the superscript "||" to denote quantities along the anisotropic direction (the x_3 direction). Reinstating the expressions for the various functions and expanding up to $\mathcal{O}(\tilde{a}^2)$ in the low frequency regime we obtain the relaxation time for heavy quark diffusing along the anisotropic direction,

$$\mu^{||}(0) = t^{||}_{\text{relax}} = \frac{2m}{\pi\sqrt{\lambda}T^2}\left[1 - \frac{a^2}{24\pi^2 T^2}(2 + \log 2)\right] \tag{5.140}$$

from which one gets the drag coefficient along the anisotropic direction

$$\gamma^{||}[0] = \frac{\pi\sqrt{\lambda}T^2}{2m}\left[1 + \frac{a^2}{24\pi^2 T^2}(2 + \log 2)\right] = \gamma_{iso}\left[1 + \frac{a^2}{24\pi^2 T^2}(2 + \log 2)\right] \tag{5.141}$$

where γ_{iso} represents the drag coefficient when the quark moves in an isotropic SYM plasma. Here we have used the standard AdS/CFT dictionary, $R^4 = (\alpha')^2\lambda$ with $R = 1$ in our convention. Our expression for the friction coefficient $\gamma^{||}$ matches exactly with that obtained in [127] in the non-relativistic limit $v \ll 1$ along the anisotropic direction. Note that the drag force increases compared to its isotropic counterpart when the quark moves along the anisotropic direction.

Next we turn towards computing the displacement squared for the Brownian particle from which we can extract the expression for the diffusion constant $D^{||}$. We have already provided a generic expression for s_i^2 in Eq. 5.126. The details of the calculation will depend upon the background metric. Let us again return to the boundary condition Eq. 5.133, but now with the gauge fields turned off. Eq. 5.133 then reads for the anisotropic direction,

$$\frac{\partial\mathcal{L}}{\partial X_3'} = \frac{1}{2\pi\alpha'}\mathcal{H}\mathcal{F}\sqrt{\mathcal{B}}y^4 r_h^3 X_3'\Big|_{y=y_m} = 0 \tag{5.142}$$

which translates to $X_3' = 0$ at the boundary. The fluctuations $X_i(t, y)$ can be expressed as a sum of the outgoing and the ingoing modes as,

$$X_i(t, y) = A[g^{\text{out}}(y) + Bg^{\text{in}}(y)]e^{-i\omega t}. \tag{5.143}$$

It then easily follows that, $X_3' = 0$ implies

$$B = -\frac{g^{\text{out}\prime}}{g^{\text{in}\prime}}\bigg|_{y=y_m} = 1 + \mathcal{O}(\nu) \tag{5.144}$$

which gives,

$$|g^{\text{out}}(y_m) + Bg^{\text{in}}(y_m)|^2 = 4 + \mathcal{O}(\nu). \tag{5.145}$$

Using Eqs. 5.119 and 5.145 in Eq. 5.126 one then has,

$$s_3^2 = \frac{4t}{\pi T\sqrt{\lambda}}\left[1 - \frac{a^2}{24\pi^2 T^2}(2 + \log 2)\right]. \tag{5.146}$$

Hence, the diffusion constant along the anisotropic direction is,

$$D^{||} = \frac{2}{\pi T\sqrt{\lambda}}\left[1 - \frac{a^2}{24\pi^2 T^2}(2 + \log 2)\right] = \frac{T}{m\gamma^{||}}. \tag{5.147}$$

This is nothing but the Einstein-Sutherland relation (Eq. 5.83) mentioned earlier. We have thus performed an explicit verification of the relation from the bulk point of view.

Finally, we proceed to verify the fluctuation-dissipation theorem for which we need to know the random force correlator. First of all, we compute the two-point correlator of the momentum along the i-th direction,

$$\begin{aligned}\langle : p_i(t)p_i(0) : \rangle &\equiv -m^2\partial_t^2\langle : x_i(t)x_i(0) : \rangle \\ &= \int_0^\infty \frac{d\omega}{2\pi}\frac{2m^2\omega^2|A|^2\cos\omega t}{e^{\beta\omega} - 1}|g^{\text{out}}(y_m) + Bg^{\text{in}}(y_m)|^2.\end{aligned} \tag{5.148}$$

Invoking the Wiener-Khintchine theorem (Eq. 5.96), and the expression for A (Eq. 5.119) and specialising to the anisotropic direction we find,

$$I_{p_3}(\omega) = 4\frac{m^2\pi}{r_h^2\alpha'\mathcal{H}(y=1)\beta}\frac{\beta\omega}{e^{\beta\omega}-1}. \tag{5.149}$$

Expanding in ω and keeping only the leading order term one has

$$I_{p_3}(\omega) = \frac{4m^2}{\sqrt{\lambda}\pi T}\left(1+\frac{a^2}{24\pi^2T^2}(5\log 2-2)\right)\left(1-\frac{a^2}{4\pi^2T^2}\log 2\right)+\mathcal{O}(\omega). \tag{5.150}$$

Now, the Langevin coefficient along the direction of anisotropy is

$$\begin{aligned}\kappa^{||} = I_{R_3} &= \frac{I_{p_3}(\omega)}{|\mu^{||}(\omega)|^2} \\ &= 2mT\frac{\pi\sqrt{\lambda}T^2}{2m}\left[1+\frac{a^2}{24\pi^2T^2}(2+\log 2)\right] = 2mT\gamma^{||} \\ &= \kappa_{iso}\left[1+\frac{a^2}{24\pi^2T^2}(2+\log 2)\right]\end{aligned} \tag{5.151}$$

(where κ_{iso} is the Langevin coefficient in isotropic plasma) which is nothing but the statement of the fluctuation-dissipation theorem. We thus observe that the strength of the auto-correlator along the anisotropic direction increases in the presence of anisotropy. Thus, we explicitly check the validity of the fluctuation-dissipation theorem for a heavy test quark executing Brownian motion in a strongly coupled, anisotropic plasma when the fluctuations are aligned with the direction of anisotropy.

Brownian motion transverse to the anisotropic direction

Next we discuss the case of Brownian motion in the isotropic plane. For definiteness, we take the motion to be along X_1 direction. The calculations in this case proceeds in almost the same way as in the preceding case. As is evident upon comparing Eqs. 5.104a and 5.104b the equation of motion in the isotropic direction can be simply obtained by setting

Langevin equation,

$$\dot{p}_i(t) = -\int_{-\infty}^{t} dt' \gamma^{(i)}(t-t') p_i(t') + R_i(t) + K_i(t). \tag{5.85}$$

Note that now the history of the particle is encoded in the function $\gamma(t-t')$ and we have also included the possibility of an external force impressed upon the particle through the term $K_i(t)$. $R_i(t)$ now obeys,

$$\langle R_i(t) \rangle = 0, \qquad \langle R_i(t) R_i(t') \rangle = \kappa^{(i)}(t-t'). \tag{5.86}$$

At this stage it is convenient to go over to the Fourier space representation of the generalized Langevin equation

$$p_i(\omega) = \frac{R_i(\omega) + K_i(\omega)}{-i\omega + \gamma[\omega]} \tag{5.87}$$

where $p_i(\omega)$, $R_i(\omega)$ and $K_i(\omega)$ are the Fourier transforms of $p_i(t)$, $R_i(t)$ and $K_i(t)$ respectively, i.e.,

$$p_i(\omega) = \int_{-\infty}^{\infty} dt\, p_i(t) e^{i\omega t} \tag{5.88}$$

and so on. On the other hand, causality restricts $\gamma(t) = 0$ for $t < 0$ so that $\gamma[\omega]$ is the Fourier-Laplace transform

$$\gamma[\omega] = \int_{0}^{\infty} dt \gamma(t) e^{i\omega t}. \tag{5.89}$$

Upon taking statistical average in Eq. 5.87, one finds,

$$\langle p_i(\omega) \rangle = \mu^{(i)}(\omega) K_i(\omega) \tag{5.90}$$

where we have made use of Eq. 5.86.

$\mathcal{H} = 1$ in the anisotropic case. This can also be understood by looking at the metric in Eq. 5.11. So we shall be brief in our discussion here. The equation to solve is

$$\nu^2 g(y) + \mathcal{F}\sqrt{\mathcal{B}}\partial_y \left(\sqrt{\mathcal{B}}\mathcal{F} y^4 g'(y)\right) = 0 \tag{5.152}$$

which can be recast as,

$$g''(y) + 4\frac{y^3}{y^4-1}\left[1+\tilde{a}^2\tilde{\Psi}(y)\right]g'(y) + \frac{y^4\nu^2}{(y^4-1)^2}\left[1+\tilde{a}^2\tilde{\Upsilon}(y)\right]g(y) = 0 \tag{5.153}$$

where

$$\begin{aligned}\tilde{\Psi}(y) &= \frac{1}{96y^4(y^4-1)}\left[15-21y^2-11y^6+y^4(17+40\log 2)-40y^4\log\left(1+\frac{1}{y^2}\right)\right]\\ \tilde{\Upsilon}(y) &= \frac{1}{24(y^4-1)}\left[6-6y^2+20\log 2-5(3+y^4)\log\left(1+\frac{1}{y^2}\right)\right].\end{aligned} \tag{5.154}$$

As in the anisotropic version, here, too, we look for solutions by resorting to the matching technique. Here we present only the final form of the solution in the asymptotic limit,

$$g^{\text{out/in}} = \tilde{k}_1^{\text{out/in}}\left[1+\frac{\nu^2}{2y^2}+\mathcal{O}\left(\frac{1}{y^4}\right)\right] + \tilde{k}_3^{\text{out/in}}\left[\frac{1}{y^3}+\mathcal{O}\left(\frac{1}{y^5}\right)\right] \tag{5.155}$$

where

$$\begin{aligned}\tilde{k}_1^{\text{out/in}} =& 1 \mp \frac{i\nu}{8}(\pi - 2\log 2) \mp \frac{i\nu\tilde{a}^2}{768}[-80\beta(2)\\ &+\pi(8+5\pi) - 4(7+2\log 2) + 10(\pi+2\log 2)\log 2] + \mathcal{O}(\nu^2)\\ \tilde{k}_3^{\text{out/in}} =& \mp\frac{i\nu}{3}.\end{aligned} \tag{5.156}$$

We thus find that the y-dependence is the same as in the anisotropic counterpart, only the coefficients $\tilde{k}_1$ and $\tilde{k}_3$ are different. Note that in particular, the coefficient $\tilde{k}_3$ does not pick up any contribution from anisotropy. The boundary condition now reads in the presence of the gauge field on the boundary

$$\frac{1}{2\pi\alpha'}\mathcal{F}\sqrt{\mathcal{B}}y^4 r_h^3 X_1'\Big|_{y=y_m} = K_1 = K_1^{(0)} e^{-i\omega t} \tag{5.157}$$

which fixes the normalisation factor

$$A^{\text{in}} = \left.\frac{2\pi\alpha' K_1^{(0)}}{\mathcal{F}\sqrt{\mathcal{B}}y^4 r_h^3 g'}\right|_{y=y_m} . \tag{5.158}$$

One can now easily obtain expressions for the position and hence, the momentum of the Brownian quark from which follows the expression for the admittance,

$$\mu^{\perp}(\nu) = -\left.\frac{2i\pi\alpha'\nu m g}{\mathcal{F}\sqrt{\mathcal{B}}y^4 r_h^2 g'}\right|_{y=y_m} \tag{5.159}$$

with $g(y)$ now being the ingoing solution in Eq. 5.155. Here we denote the direction transverse to the anisotropic one as "$\perp$". Reinstating the expressions for the various functions and expanding upto $\mathcal{O}(\tilde{a}^2)$ in the low frequency domain we obtain the relaxation time for fluctuations in the transverse plane.

$$\mu^{\perp}(0) = t^{\perp}_{\text{relax}} = \frac{2m}{\pi\sqrt{\lambda}T^2}\left[1 + \frac{a^2}{24\pi^2 T^2}(5\log 2 - 2)\right] \tag{5.160}$$

from which one gets the drag coefficient along the isotropic direction

$$\gamma^{\perp}[0] = \frac{\pi\sqrt{\lambda}T^2}{2m}\left[1 - \frac{a^2}{24\pi^2T^2}(5\log 2 - 2)\right] = \gamma_{iso}\left[1 - \frac{a^2}{24\pi^2T^2}(5\log 2 - 2)\right]. \tag{5.161}$$

This expression for the friction coefficient $\gamma^{\perp}$ in the isotropic direction agrees with that obtained in [127] in the non-relativistic limit $v \ll 1$. It is to be observed, that the isotropic direction also picks up correction from anisotropy, i.e., even the isotropic plane can "feel" the presence of anisotropy in the normal direction. Moreover, while the presence of anisotropy increases the drag force along the anisotropic direction it leads to a suppression in the drag force in the isotropic plane.

The computation for the displacement squared for the Brownian particle proceeds in exactly similar fashion as in the previous case. Switching off the external field we impose the free Neumann condition,

$$\frac{\partial \mathcal{L}}{\partial X_i'} = \frac{1}{2\pi\alpha'}\mathcal{F}\sqrt{\mathcal{B}}y^4 r_h^3 X_1'\bigg|_{y=y_m} = 0 \tag{5.162}$$

which translates to $X_1' = 0$ at the boundary that furnishes,

$$B = -\frac{g^{\text{out}\prime}}{g^{\text{in}\prime}}\bigg|_{y=y_m} = 1 + \mathcal{O}(\nu) \tag{5.163}$$

which implies,

$$|g^{\text{out}}(y_m) + Bg^{\text{in}}(y_m)|^2 = 4 + \mathcal{O}(\nu). \tag{5.164}$$

Using Eqs. 5.164 and 5.121 in Eq. 5.126 one then has,

$$s_1^2 = \frac{4t}{\pi T\sqrt{\lambda}}\left[1 + \frac{a^2}{24\pi^2T^2}(5\log 2 - 2)\right]. \tag{5.165}$$

We can now easily read off the diffusion constant to be,

$$D^{\perp} = \frac{2}{\pi T\sqrt{\lambda}}\left[1 + \frac{a^2}{24\pi^2 T^2}(5\log 2 - 2)\right]. \tag{5.166}$$

A comparison of Eqs. 5.161 and 5.166 reveals the relation,

$$D^{\perp} = \frac{T}{m\gamma^{\perp}} \tag{5.167}$$

which verifies the validity of the Einstein-Sutherland relation in the isotropic plane.

Next we find the random force correlator $\kappa^{\perp}$ along the isotropic direction. We have,

$$\begin{aligned} I_{p_1}(\omega) &= 4\frac{m^2\pi}{r_h^2\alpha'\beta}\frac{\beta\omega}{e^{\beta\omega}-1} \\ &= \frac{4m^2}{\sqrt{\lambda}\pi T}\left(1 + \frac{a^2}{24\pi^2 T^2}(5\log 2 - 2)\right) + \mathcal{O}(\omega). \end{aligned} \tag{5.168}$$

Now,

$$\begin{aligned} \kappa^{\perp} = I_{R_1} &= \frac{I_{p_1}(\omega)}{|\mu^{\perp}(\omega)|^2} \\ &= 2mT\frac{\pi\sqrt{\lambda}T^2}{2m}\left[1 - \frac{a^2}{24\pi^2 T^2}(5\log 2 - 2)\right] = 2mT\gamma^{\perp} \\ &= \kappa^{iso}\left[1 - \frac{a^2}{24\pi^2 T^2}(5\log 2 - 2)\right]. \end{aligned} \tag{5.169}$$

Hence, we find that the fluctuation-dissipation theorem continues to hold true in the isotropic plane too and also the random forces are less correlated in the isotropic plane due to the presence of anisotropy in the perpendicular direction.

5.6 Conclusion

Finally, we conclude with a brief review of the results obtained in the chapter. In the first part, we found the velocity-dependent Q-$\bar{Q}$ separation L and the Q-$\bar{Q}$ potential V in a strongly coupled, anisotropic SYM plasma at finite temperature *via* the gauge/string duality. The gauge theory we took is a deformation of $\mathcal{N} = 4$ SYM theory whose gravity dual has been proposed in [104, 105]. Barring the screening length L_{max} in a special case, in all other cases we presented numerical results. The general observation is that when we turn on a small value of the anisotropy parameter $\tilde{a}$, the screening length decreases and the Q-$\bar{Q}$ interaction becomes weaker so that the dipole becomes more prone to dissociation. We considered five different cases, depending upon the direction of velocity of the dipole and the direction along which it is aligned. While the generic features are the same in all the cases, the minute details vary from case to case. In particular, when the dipole lies along the direction of anisotropy the effects are manifested more prominently in the static case. However, for finite velocity v, it is the dipole moving along the anisotropic direction that is affected the most. We also set the rapidity parameter $\eta = 0$ and recovered the static Q-$\bar{Q}$ separation and the static Q-$\bar{Q}$ potential. In these cases, our observations are consistent with those recently obtained in [107]. So our calculations suggest that in the initial stages of QGP formation, presence of anisotropy can act as an agent for quarkonium dissociation. Finally, we also compared the results obtained in this model *vis-a-vis* some other models. In particular, all our results are remarkably similar with those obtained for hot NCYM theory where the presence of non-commutativity can be seen as a source of anisotropy. In the next stage we studied holographic Brownian motion of a non-relativistic heavy probe quark in the same thermal medium. Our computation in the bulk theory involved an explicit solution of the transverse fluctuation modes of the probe string in the low frequency regime along anisotropic as well as isotropic directions. The above restrictions were imposed to have an analytic handle upon the computations. One might try to relax some of these restrictions, like considering general values of the parameter a/T. For large values of a/T or, small values of T, the gravity background is known analytically and one might try to perform a similar computation. However, in that regime of the parameter space, quantum fluctuations will dominate over random fluctuations. For intermediate values of a/T no analytical results are available and one will have to fall back upon numerical means right from the outset. It might also be possible that some of the results obtained in this paper, get modified away from these limits we have considered. Hence, it might be interesting to investigate Brownian motion in more general scenarios. In this context one might refer to the recent paper [128], where the authors study relativistic Langevin diffusion of a heavy quark in strongly coupled, anisotropic Yang-Mills plasma for both small and large values of the anisotropy parameter. It is important to note that if we could precisely measure Brownian dynamics in the boundary, it would have been a very promising step towards learning the quantum dynamics of black hole physics. However, that requires the knowledge of non-perturbative gauge theory correlators which is beyond the scope of this paper. In this work, using the holographic prescription, we have computed the drag coefficient, the diffusion constant and the strength of the random force in low frequency as well as non-relativistic limits. The expressions for the drag coefficient and the Langevin coefficient along the anisotropic direction clearly signify an enhancement over the corresponding isotropic counterparts. The fluctuations along the isotropic direction also respond to the anisotropy in the bulk. As a result, in the boundary theory, we observe that both the drag coefficient and the coefficient of auto-correlator take lower value compared to the case of ordinary SYM plasma. We also find that even in the presence of anisotropy, the fluctuation-dissipation theorem is still valid for random variation along both isotropic and anisotropic directions. Moreover, we compute the diffusion constant and reproduce the Einstein-Sutherland relation in a holographic sense. We observe an interesting qualitative agreement of our results with those obtained in the case of NCYM plasma. In [119] the drag force, the diffusion constant and the Langevin coefficient were holographically computed for strongly coupled NCYM theory. In the case of NCYM plasma, an unbroken $SO(2)$ symmetry is confined to the non-commutative plane whereas for spatially deformed anisotropic SYM plasma, the unbroken $SO(2)$ symmetry lives on the isotropic plane (x_1-x_2 plane). Therefore, it is reasonable to compare the result in the isotropic plane in the present work with the NCYM result. Within the small anisotropy approximation, it is observed that in both cases, the drag force coefficient is weaker than the one computed in the context of ordinary SYM plasma. This observation is also true for the relevant Langevin coefficient. It is important to check the validity of this comparison for arbitrary strength of anisotropy. However, this is beyond the scope of analytic computation and is left for a future work.

CHAPTER 6

EPILOGUE

In this concluding chapter we summarize the main results of the thesis. The primary goal of the present thesis was to investigate the effects of anisotropy upon various heavy quark observables in quark-gluon plasma that may be relevant to heavy ion collisions. Recently, there has accumulated a large body of experimental findings indicating that the plasma produced in the collider is dominated by strong coupling effects. This requires that our formalism to probe the plasma should be reliable at strong coupling. This made us take recourse to the gauge/string duality which is tailor-made to suit strong coupling situations. In particular, we focused on those issues where we expect the duality to provide precious information in the strongly coupled regime where perturbative tools may not work well. We examined two specific models of anisotropic plasma - in one model anisotropy is sourced by the presence of space-space non-commutativity while in another model anisotropy is achieved by deforming its isotropic version *via* a topological term. Most of our analysis was based upon computing the expectation values of various types of Wilson loops in the gauge theory, which, by the gauge/string dictionary is mapped to evaluating the string world-sheet action supplemented by proper boundary conditions. As a warm-up exercise we thus evaluated expectation values of Wilson loops in $(p+1)$-dimensional $\mathcal{N}=4$ super Yang-Mills theory at finite temperature and strong 't Hooft coupling from which we could extract information about the heavy quark potential, the screening length and the jet quenching. Then in the non-commutative Yang-Mills theory we studied the heavy quark potential, the jet quenching and the screening length. An added motivation to consider non-commutative theories was to explore the possibility if any signature of non-commutativity can be obtained in the present day collider experiments. To this end we also made some estimates of the correction picked up by the jet quenching parameter due to non-commutativity and concluded that at the energy scale reached in the current collider experiments the presence of non-commutativity, if any at all, can not be detected. In the deformed Yang-Mills theory we studied the quarkonia potential for various orientations of the dipole with respect to the direction of anisotropy and also the stochastic motion of a heavy quark which supplied information about the drag force, the diffusion coefficient and the random force auto-correlator. Quite intriguingly, it was found that the effects of anisotropy are qualitatively very similar on the bound state potential and the drag force in both these models. This is an important step forward towards our understanding of anisotropic QGP since in the absence of a string dual to real world QCD the toy models are our best source of information about the strongly coupled domain of QGP.

As a concluding note, let us also point to some future directions based on the work done in the thesis. In p-p collisions, a large fraction of the observed yield of J/Ψ mesons arises from the production of excited states, Ψ' and χ_c, which subsequently decay to J/Ψ. In a nucleus-nucleus collision, one expects the suppression of the excited states to be triggered at a lower temperature since they are larger in size than the ground state J/Ψ. In fact, it has been even proposed that the observed suppression of the J/Ψ mesons at RHIC and at the SPS may arise solely from the dissociation of the more loosely bound Ψ' and χ_c states, with the J/Ψ's themselves remaining bound in the quark-gluon plasma produced [44]. Irrespective of whether this proposal is correct or not, it is clear that in the absence of separate measurements of the production of the excited states, any conclusions about the observed J/Ψ suppression require careful modeling of, and inferences about, the contribution of the decays of excited states. An interesting line of research can be to study the *decay of excited states*. A distinguishing feature of the excited states is that they are endowed with a non-zero angular momentum. Holographically, such states can be realized *via* rotating strings where the rotation imparts a non-zero angular momentum to the string and hence the quark-antiquark pair.

We had mentioned earlier that in the time domain that we focus upon the plasma is anisotropic but in equilibrium. An obvious question that crops up is what happens when the plasma is away from equilibrium. While recently there have been advances in studying the far-from-equilibrium dynamics of the plasma, an important issue to answer is how the presence of anisotropy affects this temporal evolution.

While we have found tantalizing similarities between the effects of anisotropy upon various quantities computed in the two models of anisotropic plasma, this is not enough to establish the existence of a universality class. To make any robust statement along such lines, one needs to see how far these similarities survive while computing other quantities of interest. In the same spirit it is also necessary to see if these qualitative features hold in other holographic models of anisotropic plasma. Exploring these issues can make for interesting topics of future studies.

Another line of progress will be to try to understand the effects of anisotropy in more detail. The possibility of the presence of a sizable anisotropy has prompted developing field-theoretic models of anisotropic hydrodynamics. A very important as well as interesting direction of research will be to try to study anisotropic hydrodynamics in the framework of the gauge/string duality. A possible starting point can be to borrow the idea of fluid/gravity correspondence [129, 130] and try to generalize to the anisotropic scenario. While this will be highly challenging, nevertheless, it is worthwhile to attempt such a study as it can potentially teach us valuable lessons on anisotropic hydrodynamics from a holographic perspective. Once such a model is in place a possible avenue of future explorations will be to study the signatures of QGP like quarkonia melting, heavy quark energy loss, excess photon and dilepton production, etc. in such a hydrodynamic model.

It is hoped that pursuing these lines of investigation can hopefully teach us important lessons about strongly coupled QGP and empower us to obtain a better understanding of the rich physics underlying QCD.

APPENDIX A

SOLUTION ALONG ANISOTROPIC DIRECTION

In this appendix we present the details of the solution (Eq. 5.130). We employ the so-called matching technique. The solution to Eq. 5.128 is extremely difficult to obtain analytically for any frequency. To make the problem tractable we focus only on the behavior of the solution in the low frequency domain. In this frequency domain we resort to the matching technique whereby we find the solutions in three different regimes and then match these solutions to leading order in the frequency at the interface of two domains. To be more specific, we find solutions to Eq. 5.128 in the following three limiting cases: (A) Near the horizon, i.e., $y \to 1$ for arbitrary frequency and then take the low frequency limit. (B) Throughout the bulk (i.e., arbitrary y) but for low frequency $\nu \ll 1$ and then take the near-horizon limit. We match this solution with the low frequency limit of the solution obtained in (A). Finally, in (C) we solve the equation in the asymptotic limit $(y \to \infty)$ for arbitrary ν. Then taking the low frequency limit we match it with the solution of (B). Below we elucidate the details of the solutions for each regime.

A.1 Near-horizon limit

In this regime we solve Eq. 5.128 near the horizon, i.e., in the limit $y \to 1$ whence, Eq. 5.128 simplifies to,

$$g''_A(y) + \frac{1}{y-1} g'_A(y) + \frac{\nu^2}{16(y-1)^2}\left[1 + \frac{\tilde{a}^2}{24}(5\log 2 - 2)\right] g_A(y) = 0. \tag{A.1}$$

This has a solution,

$$g_A(y) = A^{\text{out}}(y-1)^{\frac{i\nu}{4}\left[1-\frac{\tilde{a}^2}{48}(5\log 2-2)\right]} + A^{\text{in}}(y-1)^{-\frac{i\nu}{4}\left[1-\frac{\tilde{a}^2}{48}(5\log 2-2)\right]} \tag{A.2}$$

where the coefficients $A^{\text{out/in}}$ correspond to outgoing and ingoing modes respectively. We normalize these modes according to Eq. 5.114 and expand for low frequencies to obtain,

$$g_A^{\text{out/in}}(y) \sim 1 \pm \frac{i\nu}{4}\log(y-1)\left[1 - \frac{\tilde{a}^2}{48}(5\log 2 - 2)\right] + \mathcal{O}(\nu^2). \tag{A.3}$$

A.2 Low frequency limit

Next we attempt to solve Eq. 5.128 in the low frequency limit but for arbitrary y, i.e., throughout the bulk. We can perform a series expansion in powers of ν to write the solution in the generic form,

$$g_B(y) = g_0(y) + \nu g_1(y) + \nu^2 g_2(\nu) + ... \tag{A.4}$$

Inserting this ansatz in Eq. 5.128, setting the coefficient of each power of ν to zero and solving the resulting equations we can find g_0, g_1, g_2. At the zeroth order, the equation to solve is,

$$g_0''(y) + \frac{4y^3}{y^4-1}\left[1+\tilde{a}^2\Psi(y)\right] g_0'(y) = 0 \tag{A.5}$$

with $\Psi(y)$ being given in Eq. 5.129. The solution to the equation for general y is quite complicated and is given by,

$$\begin{aligned}
g_0(y) = {} & \frac{1}{2}C_1(\tan^{-1} y + \tanh^{-1} y) + C_2 + \frac{\tilde{a}^2}{768(y^4-1)}C_1\Bigg\{ -16y + 16y^3 + 80y\log 2 \\
& + \log\left(1+\frac{1}{y^2}\right)(-80y - 51(y^4-1)\log(1-y) - 9(y^4-1)\log(y-1) \\
& + 60(y^4-1)\log(1+y)) - (y^4-1)\Bigg[\log(y-1)\big[-17 - 9\log\left(1+\frac{1}{y^2}\right)\big] \\
& + \log(1-y)(25 + 102\log y + 17\log(y^2+1)) \\
& - 8(1+17\log y)\log(1+y) - 8\log(y^2+1)\log(1+y) \\
& + 4\log(-i+y)\left[2i\log(1-iy) + 2\log\left(i\frac{y+1}{y-1}\right) - i\log(4(-i+y))\right] \\
& + 4\log(i+y)\left[-2i\log(1+iy) + 2\log\left(i\frac{y+1}{1-y}\right) + i\log(4(i+y))\right]\Bigg] \\
& - 8(y^4-1)\tanh^{-1} y(15\log 2 + 17\log(1+y^2)) \\
& + 8(y^4-1)\tan^{-1} y(4 - 15\log 2 + 4\log y) \\
& + 8(y^4-1)\Bigg[2\mathrm{Li}_2(1-y) - i\mathrm{Li}_2\left(\frac{1}{2}(1+iy)\right) + 2\mathrm{Li}_2(-y) - 2i\mathrm{Li}_2(-iy) \\
& + 2i\mathrm{Li}_2(iy) - \mathrm{Li}_2\left(\frac{1}{2}(-1+i)(y-i)\right) + \mathrm{Li}_2\left(\frac{1}{2}(1+i)(-i+y)\right) \\
& - \mathrm{Li}_2\left(\frac{1}{2}(-1-i)(i+y)\right) + i\mathrm{Li}_2\left(\frac{1}{2}(1-iy)\right) + \mathrm{Li}_2\left(\frac{1}{2}(1-i)(i+y)\right)\Bigg]\Bigg\} + \mathcal{O}(\tilde{a}^4)
\end{aligned} \tag{A.6}$$

with C_1 and C_2 being the constants of integration and $\mathrm{Li}_n(z)$ is the Polylogarithm function. Upon taking the near-horizon limit it reduces to *

$$\begin{aligned} g_0(y) = C_2 + C_1 &\left[\left(\frac{1}{8} - \frac{i}{4}\right)\pi + \frac{\log 2}{4} - \frac{\log(y-1)}{4}\right] \\ &+ \frac{\tilde{a}^2 C_1}{2304}\left[84 - 48\beta(2) + (24 - 75i - \pi)\pi - 90(1-2i)\pi\log 2\right. \\ &\left.-204(\log 2)^2 + 24\log 2 - 24\log(y-1) + 204\log 2\log(y-1)\right]. \end{aligned} \tag{A.7}$$

Upon comparison with Eq. A.3 we can extract the coefficients C_1 and C_2 as,

$$C_1 = 0, \qquad C_2 = 1 \tag{A.8}$$

for both outgoing and ingoing waves. Next we proceed to find $g_1(y)$. Now note that $g_1(y)$ satisfies the same equation as g_0 and so has the same solution (Eqs. A.6 and A.7) albeit with different constants of integration, but now the matching has to be done with the coefficient of ν in Eq. A.3. Replacing C_1 and C_2 in Eq. A.7 with $\tilde{C}_1$ and $\tilde{C}_2$ respectively and comparing with Eq. A.3 we can extract the constants for both outgoing and ingoing waves as

$$\begin{aligned} \tilde{C}_1^{\text{out/in}} &= \mp i\left[1 + \frac{\tilde{a}^2}{4}\log 2\right] + \mathcal{O}(\tilde{a}^4), \\ \tilde{C}_2^{\text{out/in}} &= \pm\left(\frac{1}{4} + \frac{i}{8}\right)\pi \pm \frac{1}{4}i\log 2 \mp i\frac{\tilde{a}^2}{2304}\left[-84 + 48\beta(2) - (24 - 75i - \pi)\pi\right. \\ &\quad \left.+ (18(1-2i)\pi + 60\log 2 - 24)\log 2\right] + \mathcal{O}(\tilde{a}^4). \end{aligned} \tag{A.9}$$

*While taking the near-horizon limit we have let $y \to 1 + \epsilon$ and used the following expansion

$$\mathrm{Li}_n\left(z + (a+ib)\epsilon\right) = \mathrm{Li}_n(z) + \epsilon\frac{a+ib}{z}\mathrm{Li}_{n-1}(z) + \mathcal{O}(\epsilon^2)$$

The constants so evaluated can now be used in the full solution for $g_B(y)$ and not just in the near-horizon limit (the restriction to low frequency regime still holds, though), which now reads

$$
\begin{aligned}
g_B(y) = {} & 1 + \nu\left[\frac{1}{2}\tilde{C}_1(\tan^{-1} y + \tanh^{-1} y) + \tilde{C}_2\right] + \frac{\nu\tilde{a}^2}{768(y^4-1)}\tilde{C}_1\Bigg\{ -16y + 16y^3 \\
& + 80y\log 2 + \log\left(1+\frac{1}{y^2}\right)(-80y - 51(y^4-1)\log(1-y) - 9(y^4-1)\log(y-1) \\
& + 60(y^4-1)\log(1+y)) - (y^4-1)\Bigg[\log(y-1)\big[-17 - 9\log\left(1+\frac{1}{y^2}\right)\big] \\
& + \log(1-y)(25 + 102\log y + 17\log(y^2+1)) \\
& - 8(1+17\log y)\log(1+y) - 8\log(y^2+1)\log(1+y) \\
& + 4\log(-i+y)\big[2i\log(1-iy) + 2\log\left(i\frac{y+1}{y-1}\right) - i\log(4(-i+y))\big] \\
& + 4\log(i+y)\big[-2i\log(1+iy) + 2\log\left(i\frac{y+1}{1-y}\right) + i\log(4(i+y))\big]\Bigg] \\
& - 8(y^4-1)\tanh^{-1} y(15\log 2 + 17\log(1+y^2)) \\
& + 8(y^4-1)\tan^{-1} y(4 - 15\log 2 + 4\log y) \\
& + 8(y^4-1)\Bigg[2\mathrm{Li}_2(1-y) - i\mathrm{Li}_2\left(\frac{1}{2}(1+iy)\right) + 2\mathrm{Li}_2(-y) - 2i\mathrm{Li}_2(-iy) \\
& + 2i\mathrm{Li}_2(iy) - \mathrm{Li}_2\left(\frac{1}{2}(-1+i)(y-i)\right) + \mathrm{Li}_2\left(\frac{1}{2}(1+i)(-i+y)\right) \\
& - \mathrm{Li}_2\left(\frac{1}{2}(-1-i)(i+y)\right) + i\mathrm{Li}_2\left(\frac{1}{2}(1-iy)\right) + \mathrm{Li}_2\left(\frac{1}{2}(1-i)(i+y)\right)\Bigg]\Bigg\} + \mathcal{O}(\tilde{a}^4).
\end{aligned}
\tag{A.10}
$$

Next we can take the asymptotic limit of the full solution to arrive at,

$$
\begin{aligned}
g_B^{\text{out/in}} \sim & 1 \mp \frac{i\nu}{8}(\pi - 2\log 2) \\
& \pm \frac{i\nu\tilde{a}^2}{768}\left[28 - 16\beta(2) - 20(\log 2)^2 + \pi(-8 + \pi + 14\log 2) + 8\log 2\right] + \mathcal{O}(\nu^2) \\
& \mp \frac{1}{y^3}\left[\frac{i\nu}{3}\left(1 + \frac{\tilde{a}^2}{4}\log 2\right) + \mathcal{O}(\nu^2)\right] + \mathcal{O}(1/y^4).
\end{aligned}
\tag{A.11}
$$

A.3 Asymptotic limit

Finally, we are to solve Eq. 5.128 in the asymptotic limit, i.e., near the boundary where the gauge theory lives. We attempt a power series in the form,

$$
g_C(y) = k_0 + k_1/y + k_2/y^2 + k_3/y^3. \tag{A.12}
$$

It turns out that only the constants k_0 and k_3 are independent and the solution assumes the form,

$$
g_C(y) = k_0\left[1 + \frac{\nu^2}{2y^2} + \mathcal{O}(1/y^4)\right] + k_3\left[\frac{1}{y^3} + \mathcal{O}(1/y^5)\right]. \tag{A.13}
$$

Matching the coefficients with Eq. A.11 in the low frequency limit furnishes the two undetermined constants k_0 and k_3 as follows,

$$
\begin{aligned}
k_0^{\text{out/in}} =& 1 \mp \frac{i\nu}{8}(\pi - 2\log 2) \\
& \pm \frac{i\nu\tilde{a}^2}{768}\left[28 - 16\beta(2) - 20(\log 2)^2 + \pi(-8 + \pi + 14\log 2) + 8\log 2\right] + \mathcal{O}(\nu^2) \\
k_3^{\text{out/in}} =& \mp\left[\frac{i\nu}{3}\left(1 + \frac{\tilde{a}^2}{4}\log 2\right) + \mathcal{O}(\nu^2)\right].
\end{aligned}
\tag{A.14}
$$

The final result is then given in Eq. 5.130.

BIBLIOGRAPHY

[1] J. M. Maldacena, *The Large N limit of superconformal field theories and supergravity*, *Adv. Theor. Math. Phys.* **2** (1998) 231–252, [hep-th/9711200].

[2] S. Gubser, I. R. Klebanov, and A. M. Polyakov, *Gauge theory correlators from noncritical string theory*, *Phys. Lett.* **B428** (1998) 105–114, [hep-th/9802109].

[3] E. Witten, *Anti-de Sitter space and holography*, *Adv. Theor. Math. Phys.* **2** (1998) 253–291, [hep-th/9802150].

[4] O. Aharony, S. S. Gubser, J. M. Maldacena, H. Ooguri, and Y. Oz, *Large N field theories, string theory and gravity*, *Phys. Rept.* **323** (2000) 183–386, [hep-th/9905111].

[5] **PHENIX** Collaboration, K. Adcox et al., *Formation of dense partonic matter in relativistic nucleus-nucleus collisions at RHIC: Experimental evaluation by the PHENIX collaboration*, *Nucl. Phys.* **A757** (2005) 184–283, [nucl-ex/0410003].

[6] **STAR** Collaboration, J. Adams et al., *Experimental and theoretical challenges in the search for the quark gluon plasma: The STAR Collaboration's critical assessment of the evidence from RHIC collisions*, *Nucl. Phys.* **A757** (2005) 102–183, [nucl-ex/0501009].

[7] E. V. Shuryak, *What RHIC experiments and theory tell us about properties of quark-gluon plasma?*, *Nucl. Phys.* **A750** (2005) 64–83, [hep-ph/0405066].

[8] G. Policastro, D. T. Son, and A. O. Starinets, *The Shear viscosity of strongly coupled N=4 supersymmetric Yang-Mills plasma*, *Phys. Rev. Lett.* **87** (2001) 081601, [hep-th/0104066].

[9] P. Kovtun, D. T. Son, and A. O. Starinets, *Holography and hydrodynamics: Diffusion on stretched horizons*, *JHEP* **0310** (2003) 064, [hep-th/0309213].

[10] D. Teaney, *The Effects of viscosity on spectra, elliptic flow, and HBT radii*, *Phys. Rev.* **C68** (2003) 034913, [nucl-th/0301099].

[11] N. Iqbal and H. Liu, *Universality of the hydrodynamic limit in AdS/CFT and the membrane paradigm*, *Phys. Rev.* **D79** (2009) 025023, [arXiv:0809.3808].

[12] M. Martinez and M. Strickland, *Dissipative Dynamics of Highly Anisotropic Systems*, *Nucl. Phys.* **A848** (2010) 183–197, [arXiv:1007.0889].

[13] M. Martinez and M. Strickland, *Non-boost-invariant anisotropic dynamics*, *Nucl. Phys.* **A856** (2011) 68–87, [arXiv:1011.3056].

[14] M. Martinez and M. Strickland, *Constraining relativistic viscous hydrodynamical evolution*, *Phys.Rev.* **C79** (2009) 044903, [arXiv:0902.3834].

[15] Y. V. Kovchegov, *Early Time Dynamics in Heavy Ion Collisions from CGC and from AdS/CFT*, *Nucl.Phys.* **A830** (2009) 395C–402C, [arXiv:0907.4938].

[16] T. Lappi, *Energy density of the glasma*, *Phys.Lett.* **B643** (2006) 11–16, [hep-ph/0606207].

[17] K. Fukushima, *Initial fields and instability in the classical model of the heavy-ion collision*, *Phys.Rev.* **C76** (2007) 021902, [arXiv:0704.3625].

[18] Y. V. Kovchegov, *Can thermalization in heavy ion collisions be described by QCD diagrams?*, *Nucl.Phys.* **A762** (2005) 298–325, [hep-ph/0503038].

[19] A. Krasnitz, Y. Nara, and R. Venugopalan, *Gluon production in the color glass condensate model of collisions of ultrarelativistic finite nuclei*, *Nucl.Phys.* **A717** (2003) 268–290, [hep-ph/0209269].

[20] W. Florkowski, *Anisotropic fluid dynamics in the early stage of relativistic heavy-ion collisions*, *Phys. Lett.* **B668** (2008) 32–35, [arXiv:0806.2268].

[21] W. Florkowski and R. Ryblewski, *Dynamics of anisotropic plasma at the early stages of relativistic heavy-ion collisions*, *Acta Phys. Polon.* **B40** (2009) 2843–2863, [arXiv:0901.4653].

[22] R. Ryblewski and W. Florkowski, *Early anisotropic hydrodynamics and the RHIC early-thermalization and HBT puzzles*, *Phys. Rev.* **C82** (2010) 024903, [arXiv:1004.1594].

[23] W. Florkowski and R. Ryblewski, *Highly-anisotropic and strongly-dissipative hydrodynamics for early stages of relativistic heavy-ion collisions*, *Phys. Rev.* **C83** (2011) 034907, [arXiv:1007.0130].

[24] R. Ryblewski and W. Florkowski, *Non-boost-invariant motion of dissipative and highly anisotropic fluid*, *J. Phys.* **G38** (2011) 015104, [arXiv:1007.4662].

[25] R. Ryblewski and W. Florkowski, *Highly anisotropic hydrodynamics – discussion of the model assumptions and forms of the initial conditions*, *Acta Phys. Polon.* **B42** (2011) 115–138, [arXiv:1011.6213].

[26] R. Ryblewski and W. Florkowski, *Highly-anisotropic and strongly-dissipative hydrodynamics with transverse expansion*, *Eur. Phys. J.* **C71** (2011) 1761, [arXiv:1103.1260].

[27] J. Casalderrey-Solana, H. Liu, D. Mateos, K. Rajagopal, and U. A. Wiedemann, *Gauge/String Duality, Hot QCD and Heavy Ion Collisions*, arXiv:1101.0618.

[28] D. J. Gross and F. Wilczek, *Ultraviolet Behavior of Nonabelian Gauge Theories*, *Phys. Rev. Lett.* **30** (1973) 1343–1346.

[29] H. D. Politzer, *Reliable Perturbative Results for Strong Interactions?*, *Phys. Rev. Lett.* **30** (1973) 1346–1349.

[30] N. Brambilla, S. Eidelman, P. Foka, S. Gardner, A. Kronfeld, et al., *QCD and strongly coupled gauge theories: challenges and perspectives*, `arXiv:1404.3723`.

[31] E. Witten, *Cosmic Separation of Phases*, *Phys. Rev.* **D30** (1984) 272–285.

[32] K. A. Olive, *The Thermodynamics of the Quark - Hadron Phase Transition in the Early Universe*, *Nucl. Phys.* **B190** (1981) 483.

[33] H. Satz, *The SPS heavy ion programme*, *Phys. Rept.* **403-404** (2004) 33–50, [`hep-ph/0405051`].

[34] B. Zakharov, *Radiative energy loss of high-energy quarks in finite size nuclear matter and quark - gluon plasma*, *JETP Lett.* **65** (1997) 615–620, [`hep-ph/9704255`].

[35] R. Baier, Y. L. Dokshitzer, A. H. Mueller, S. Peigne, and D. Schiff, *Radiative energy loss and p(T) broadening of high-energy partons in nuclei*, *Nucl.Phys.* **B484** (1997) 265–282, [`hep-ph/9608322`].

[36] M. Gyulassy and X.-n. Wang, *Multiple collisions and induced gluon Bremsstrahlung in QCD*, *Nucl.Phys.* **B420** (1994) 583–614, [`nucl-th/9306003`].

[37] U. A. Wiedemann, *Gluon radiation off hard quarks in a nuclear environment: Opacity expansion*, *Nucl. Phys.* **B588** (2000) 303–344, [`hep-ph/0005129`].

[38] M. Gyulassy, P. Levai, and I. Vitev, *Reaction operator approach to nonAbelian energy loss*, *Nucl.Phys.* **B594** (2001) 371–419, [`nucl-th/0006010`].

[39] X.-f. Guo and X.-N. Wang, *Multiple scattering, parton energy loss and modified fragmentation functions in deeply inelastic e A scattering*, *Phys.Rev.Lett.* **85** (2000) 3591–3594, [hep-ph/0005044].

[40] J. Casalderrey-Solana and C. A. Salgado, *Introductory lectures on jet quenching in heavy ion collisions*, *Acta Phys.Polon.* **B38** (2007) 3731–3794, [arXiv:0712.3443].

[41] F. D'Eramo, H. Liu, and K. Rajagopal, *Jet Quenching Parameter via Soft Collinear Effective Theory (SCET)*, *Int.J.Mod.Phys.* **E20** (2011) 1610–1615, [arXiv:1010.0890].

[42] T. Matsui and H. Satz, *J/ψ Suppression by Quark-Gluon Plasma Formation*, *Phys. Lett.* **B178** (1986) 416.

[43] H. Satz, *Colour deconfinement and quarkonium binding*, *J. Phys.* **G32** (2006) R25, [hep-ph/0512217].

[44] F. Karsch, D. Kharzeev, and H. Satz, *Sequential charmonium dissociation*, *Phys. Lett.* **B637** (2006) 75–80, [hep-ph/0512239].

[45] M. B. Green and J. H. Schwarz, *Supersymmetrical String Theories*, *Phys. Lett.* **B109** (1982) 444–448.

[46] J. H. Schwarz, *Superstring Theory*, *Phys. Rept.* **89** (1982) 223–322.

[47] J. Polchinski, *Dirichlet Branes and Ramond-Ramond charges*, *Phys. Rev. Lett.* **75** (1995) 4724–4727, [hep-th/9510017].

[48] E. Witten, *Bound states of strings and p-branes*, *Nucl. Phys.* **B460** (1996) 335–350, [hep-th/9510135].

[49] L. Brink, J. H. Schwarz, and J. Scherk, *Supersymmetric Yang-Mills Theories*, *Nucl. Phys.* **B121** (1977) 77.

[50] F. Gliozzi, J. Scherk, and D. I. Olive, *Supersymmetry, Supergravity Theories and the Dual Spinor Model*, *Nucl. Phys.* **B122** (1977) 253–290.

[51] R. Leigh, *Dirac-Born-Infeld Action from Dirichlet Sigma Model*, *Mod. Phys. Lett.* **A4** (1989) 2767.

[52] J. L. Petersen, *Introduction to the Maldacena conjecture on AdS / CFT*, *Int. J. Mod. Phys.* **A14** (1999) 3597–3672, [hep-th/9902131].

[53] G. Gibbons and K.-i. Maeda, *Black Holes and Membranes in Higher Dimensional Theories with Dilaton Fields*, *Nucl. Phys.* **B298** (1988) 741.

[54] G. T. Horowitz and A. Strominger, *Black strings and P-branes*, *Nucl. Phys.* **B360** (1991) 197–209.

[55] D. Garfinkle, G. T. Horowitz, and A. Strominger, *Charged black holes in string theory*, *Phys. Rev.* **D43** (1991) 3140.

[56] E. Witten, *Anti-de Sitter space, thermal phase transition, and confinement in gauge theories*, *Adv. Theor. Math. Phys.* **2** (1998) 505–532, [hep-th/9803131].

[57] S. Gubser, I. R. Klebanov, and A. Peet, *Entropy and temperature of black 3-branes*, *Phys. Rev.* **D54** (1996) 3915–3919, [hep-th/9602135].

[58] G. Gibbons and S. Hawking, *Action Integrals and Partition Functions in Quantum Gravity*, *Phys. Rev.* **D15** (1977) 2752–2756.

[59] A. Chamblin, R. Emparan, C. V. Johnson, and R. C. Myers, *Charged AdS black holes and catastrophic holography*, *Phys. Rev.* **D60** (1999) 064018, [hep-th/9902170].

[60] A. Chamblin, R. Emparan, C. V. Johnson, and R. C. Myers, *Holography, thermodynamics and fluctuations of charged AdS black holes*, *Phys. Rev.* **D60** (1999) 104026, [hep-th/9904197].

[61] S. S. Gubser, *Thermodynamics of spinning D3-branes*, *Nucl. Phys.* **B551** (1999) 667–684, [hep-th/9810225].

[62] R.-G. Cai and K.-S. Soh, *Critical behavior in the rotating D-branes*, *Mod. Phys. Lett.* **A14** (1999) 1895–1908, [hep-th/9812121].

[63] M. Cvetic and S. S. Gubser, *Phases of R charged black holes, spinning branes and strongly coupled gauge theories*, *JHEP* **9904** (1999) 024, [hep-th/9902195].

[64] M. Cvetic and S. S. Gubser, *Thermodynamic stability and phases of general spinning branes*, *JHEP* **9907** (1999) 010, [hep-th/9903132].

[65] J. M. Maldacena, *Wilson loops in large N field theories*, *Phys. Rev. Lett.* **80** (1998) 4859–4862, [hep-th/9803002].

[66] S.-J. Rey and J.-T. Yee, *Macroscopic strings as heavy quarks in large N gauge theory and anti-de Sitter supergravity*, *Eur. Phys. J.* **C22** (2001) 379–394, [hep-th/9803001].

[67] S. Chakraborty and S. Roy, *Wilson loops in (p+1)-dimensional Yang-Mills theories using gravity/gauge theory correspondence*, *Nucl. Phys.* **B850** (2011) 463–476, [arXiv:1103.1248].

[68] K. G. Wilson, *Confinement of Quarks*, *Phys. Rev.* **D10** (1974) 2445–2459.

[69] A. Kovner and U. A. Wiedemann, *Gluon radiation and parton energy loss*, hep-ph/0304151.

[70] H. Liu, K. Rajagopal, and U. A. Wiedemann, *An AdS/CFT Calculation of Screening in a Hot Wind*, *Phys. Rev. Lett.* **98** (2007) 182301, [hep-ph/0607062].

[71] E. Caceres, M. Natsuume, and T. Okamura, *Screening length in plasma winds*, *JHEP* **0610** (2006) 011, [hep-th/0607233].

[72] M. Chernicoff, J. A. Garcia, and A. Guijosa, *The Energy of a Moving Quark-Antiquark Pair in an N=4 SYM Plasma*, *JHEP* **0609** (2006) 068, [hep-th/0607089].

[73] S. D. Avramis, K. Sfetsos, and D. Zoakos, *On the velocity and chemical-potential dependence of the heavy-quark interaction in N=4 SYM plasmas*, *Phys. Rev.* **D75** (2007) 025009, [hep-th/0609079].

[74] H. Liu, K. Rajagopal, and U. A. Wiedemann, *Wilson loops in heavy ion collisions and their calculation in AdS/CFT*, *JHEP* **0703** (2007) 066, [hep-ph/0612168].

[75] H. Liu, K. Rajagopal, and U. A. Wiedemann, *Calculating the jet quenching parameter from AdS/CFT*, *Phys. Rev. Lett.* **97** (2006) 182301, [hep-ph/0605178].

[76] N. Itzhaki, J. M. Maldacena, J. Sonnenschein, and S. Yankielowicz, *Supergravity and the large N limit of theories with sixteen supercharges*, *Phys. Rev.* **D58** (1998) 046004, [hep-th/9802042].

[77] H. Satz, *Quarkonium Binding and Dissociation: The Spectral Analysis of the QGP*, *Nucl. Phys.* **A783** (2007) 249–260, [hep-ph/0609197].

[78] S. Chakraborty and S. Roy, *Calculating the jet quenching parameter in the plasma of NCYM theory from gauge/gravity duality*, *Phys. Rev.* **D85** (2012) 046006, [arXiv:1105.3384].

[79] S. Chakraborty, N. Haque, and S. Roy, *Wilson loops in noncommutative Yang-Mills theory using gauge/gravity duality*, *Nucl. Phys.* **B862** (2012) 650–670, [arXiv:1201.0129].

[80] W. Heisenberg and W. Pauli, *On Quantum Field Theory. (In German)*, *Z. Phys.* **56** (1929) 1–61.

[81] H. S. Snyder, *Quantized space-time*, *Phys. Rev.* **71** (1947) 38–41.

[82] A. H. Chamseddine and A. Connes, *Universal formula for noncommutative geometry actions: Unification of gravity and the standard model*, *Phys. Rev. Lett.* **77** (1996) 4868–4871.

[83] N. Seiberg and E. Witten, *String theory and noncommutative geometry*, *JHEP* **9909** (1999) 032, [hep-th/9908142].

[84] J. M. Maldacena and J. G. Russo, *Large N limit of noncommutative gauge theories*, *JHEP* **9909** (1999) 025, [hep-th/9908134].

[85] A. Hashimoto and N. Itzhaki, *Noncommutative Yang-Mills and the AdS / CFT correspondence*, *Phys. Lett.* **B465** (1999) 142–147, [hep-th/9907166].

[86] A. Connes, M. R. Douglas, and A. S. Schwarz, *Noncommutative geometry and matrix theory: Compactification on tori*, *JHEP* **9802** (1998) 003, [hep-th/9711162].

[87] S. M. Carroll, J. A. Harvey, V. A. Kostelecky, C. D. Lane, and T. Okamoto, *Noncommutative field theory and Lorentz violation*, *Phys. Rev. Lett.* **87** (2001) 141601, [hep-th/0105082].

[88] D. E. Kharzeev, L. D. McLerran, and H. J. Warringa, *The Effects of topological charge change in heavy ion collisions: 'Event by event P and CP violation'*, *Nucl. Phys.* **A803** (2008) 227–253, [arXiv:0711.0950].

[89] V. Skokov, A. Y. Illarionov, and V. Toneev, *Estimate of the magnetic field strength in heavy-ion collisions*, *Int. J. Mod. Phys.* **A24** (2009) 5925–5932, [arXiv:0907.1396].

[90] J. Breckenridge, G. Michaud, and R. C. Myers, *More D-brane bound states*, *Phys. Rev.* **D55** (1997) 6438–6446, [hep-th/9611174].

[91] R.-G. Cai and N. Ohta, *Noncommutative and ordinary superYang-Mills on (D(p - 2), D p) bound states*, *JHEP* **0003** (2000) 009, [hep-th/0001213].

[92] J. Lu and S. Roy, *((F, D1), D3) bound state and its T dual daughters*, *JHEP* **0001** (2000) 034, [hep-th/9905014].

[93] F. Ardalan, H. Arfaei, and M. Sheikh-Jabbari, *Dirac quantization of open strings and noncommutativity in branes*, *Nucl. Phys.* **B576** (2000) 578–596, [hep-th/9906161].

[94] A. Dhar and Y. Kitazawa, *Wilson loops in strongly coupled noncommutative gauge theories*, *Phys. Rev.* **D63** (2001) 125005, [hep-th/0010256].

[95] A. Anisimov, T. Banks, M. Dine, and M. Graesser, *Comments on noncommutative phenomenology*, *Phys. Rev.* **D65** (2002) 085032, [hep-ph/0106356].

[96] I. Mocioiu, M. Pospelov, and R. Roiban, *Low-energy limits on the antisymmetric tensor field background on the brane and on the noncommutative scale*, *Phys. Lett.* **B489** (2000) 390–396, [hep-ph/0005191].

[97] S. Doplicher, K. Fredenhagen, and J. E. Roberts, *The Quantum structure of space-time at the Planck scale and quantum fields*, *Commun. Math. Phys.* **172** (1995) 187–220, [hep-th/0303037].

[98] M. Alishahiha, Y. Oz, and M. Sheikh-Jabbari, *Supergravity and large N noncommutative field theories*, *JHEP* **9911** (1999) 007, [hep-th/9909215].

[99] D. Bigatti and L. Susskind, *Magnetic fields, branes and noncommutative geometry*, *Phys. Rev.* **D62** (2000) 066004, [hep-th/9908056].

[100] S. S. Haque and A. Hashimoto, *Mass-spin relation for quark anti-quark bound states in non-commutative Yang-Mills theory*, *Nucl. Phys.* **B829** (2010) 555–572, [arXiv:0903.4841].

[101] S. Digal, P. Petreczky, and H. Satz, *String breaking and quarkonium dissociation at finite temperatures*, *Phys. Lett.* **B514** (2001) 57–62, [hep-ph/0105234].

[102] S. Chakraborty and N. Haque, *Holographic quark-antiquark potential in hot, anisotropic Yang-Mills plasma*, *Nucl. Phys.* **B874** (2013) 821–851, [arXiv:1212.2769].

[103] S. Chakrabortty, S. Chakraborty, and N. Haque, *Brownian motion in strongly coupled, anisotropic Yang-Mills plasma: A holographic approach*, *Phys.Rev.* **D89** (2014) 066013, [arXiv:1311.5023].

[104] D. Mateos and D. Trancanelli, *Thermodynamics and Instabilities of a Strongly Coupled Anisotropic Plasma*, *JHEP* **1107** (2011) 054, [arXiv:1106.1637].

[105] D. Mateos and D. Trancanelli, *The anisotropic N=4 super Yang-Mills plasma and its instabilities*, *Phys. Rev. Lett.* **107** (2011) 101601, [arXiv:1105.3472].

[106] T. Azeyanagi, W. Li, and T. Takayanagi, *On String Theory Duals of Lifshitz-like Fixed Points*, *JHEP* **0906** (2009) 084, [arXiv:0905.0688].

[107] D. Giataganas, *Probing strongly coupled anisotropic plasma*, *JHEP* **1207** (2012) 031, [arXiv:1202.4436].

[108] M. Chernicoff, D. Fernandez, D. Mateos, and D. Trancanelli, *Quarkonium dissociation by anisotropy*, *JHEP* **1301** (2013) 170, [arXiv:1208.2672].

[109] A. Dumitru, Y. Guo, and M. Strickland, *The Heavy-quark potential in an anisotropic (viscous) plasma*, *Phys. Lett.* **B662** (2008) 37–42, [arXiv:0711.4722].

[110] R. Rapp and H. van Hees, *Heavy Quarks in the Quark-Gluon Plasma*, arXiv:0903.1096.

[111] J. de Boer, V. E. Hubeny, M. Rangamani, and M. Shigemori, *Brownian motion in AdS/CFT*, *JHEP* **0907** (2009) 094, [arXiv:0812.5112].

[112] D. T. Son and D. Teaney, *Thermal Noise and Stochastic Strings in AdS/CFT*, *JHEP* **0907** (2009) 021, [arXiv:0901.2338].

[113] A. E. Lawrence and E. J. Martinec, *Black hole evaporation along macroscopic strings*, *Phys. Rev.* **D50** (1994) 2680–2691, [hep-th/9312127].

[114] V. E. Hubeny and M. Rangamani, *A Holographic view on physics out of equilibrium*, *Adv. High Energy Phys.* **2010** (2010) 297916, [arXiv:1006.3675].

[115] A. N. Atmaja, J. de Boer, and M. Shigemori, *Holographic Brownian Motion and Time Scales in Strongly Coupled Plasmas*, *Nucl. Phys.* **B880** (2014) 23–75, [arXiv:1002.2429].

[116] A. N. Atmaja, *Holographic Brownian Motion in Two Dimensional Rotating Fluid*, *JHEP* **1304** (2013) 021, [arXiv:1212.5319].

[117] A. N. Atmaja, *Effective Mass of Holographic Brownian Particle in Rotating Plasma*, arXiv:1308.3014.

[118] J. Sadeghi, F. Pourasadollah, and H. Vaez, *Holograghic Brownian motion in three dimensional Gödel black hole*, *Adv. High Energy Phys.* **2014** (2014) 762151, [arXiv:1308.2483].

[119] W. Fischler, J. F. Pedraza, and W. Tangarife Garcia, *Holographic Brownian Motion in Magnetic Environments*, *JHEP* **1212** (2012) 002, [arXiv:1209.1044].

[120] U. Gursoy, E. Kiritsis, L. Mazzanti, and F. Nitti, *Langevin diffusion of heavy quarks in non-conformal holographic backgrounds*, *JHEP* **1012** (2010) 088, [arXiv:1006.3261].

[121] P. Banerjee and B. Sathiapalan, *Holographic Brownian Motion in 1+1 Dimensions*, *Nucl. Phys.* **B884** (2014) 74–105, [arXiv:1308.3352].

[122] D. Tong and K. Wong, *Fluctuation and Dissipation at a Quantum Critical Point*, *Phys. Rev. Lett.* **110** (2013), no. 6 061602, [arXiv:1210.1580].

[123] M. Edalati, J. F. Pedraza, and W. Tangarife Garcia, *Quantum Fluctuations in Holographic Theories with Hyperscaling Violation*, *Phys. Rev.* **D87** (2013), no. 4 046001, [arXiv:1210.6993].

[124] G. Giecold, E. Iancu, and A. Mueller, *Stochastic trailing string and Langevin dynamics from AdS/CFT*, *JHEP* **0907** (2009) 033, [arXiv:0903.1840].

[125] D. Giataganas and H. Soltanpanahi, *Universal Properties of the Langevin Diffusion Coefficients*, *Phys. Rev.* **D89** (2014) 026011, [arXiv:1310.6725].

[126] V. Balasubramanian, P. Kraus, and A. E. Lawrence, *Bulk versus boundary dynamics in anti-de Sitter space-time*, *Phys. Rev.* **D59** (1999) 046003, [hep-th/9805171].

[127] M. Chernicoff, D. Fernandez, D. Mateos, and D. Trancanelli, *Drag force in a strongly coupled anisotropic plasma*, *JHEP* **1208** (2012) 100, [arXiv:1202.3696].

[128] D. Giataganas and H. Soltanpanahi, *Heavy Quark Diffusion in Strongly Coupled Anisotropic Plasmas*, *JHEP* **1406** (2014) 047, [arXiv:1312.7474].

[129] S. Bhattacharyya, V. E. Hubeny, S. Minwalla, and M. Rangamani, *Nonlinear Fluid Dynamics from Gravity*, *JHEP* **0802** (2008) 045, [arXiv:0712.2456].

[130] N. Banerjee, J. Bhattacharya, S. Bhattacharyya, S. Dutta, R. Loganayagam, et al., *Hydrodynamics from charged black branes*, *JHEP* **1101** (2011) 094, [arXiv:0809.2596].